CITY, UNIVERSITY OF LONDON

SCHOOL OF MATHEMATICS, COMPUTER SCIENCE AND ENGINEERING

The Effect of Multi-Angle Spatially Variable Ground Motions on the Seismic Behaviour of Cable-Stayed Bridges

Doctoral Thesis

by

Eleftheria-Anthi Efthymiou

Submitted in partial fulfilment of the requirements for the award of
DOCTOR OF PHILOSOPHY

London, July 2019

Contents

List of Figures

List of Tables

Acknowledgements

Conducting doctoral research is a long journey filled with new knowledge and learning outcomes, observations and conclusions... The contribution to this 4-year long journey of several people has been invaluable and I would like to take the chance to acknowledge and thank them.

First and foremost, I would like to thank my supervisor Dr. Alfredo Camara. His continuous guidance and support throughout the period of the research has contributed to the successful submission of the present PhD thesis. His insightful comments have challenged me continuously to learn more not only about my research topic but also about myself.

I would also like to acknowledge the financial support provided to me by City, University of London and by the Research Centre for Civil Engineering Structures in particular, who have allowed me to participate in international conferences and discuss my work and progress with very knowledgeable academics and industry representatives.

I am very grateful to my fellow PhD candidates and friends who have supported me and I am also grateful for the new friends I made during this period.

Most importantly, I would like to thank from the bottom of my heart my beloved parents Anna and Christos, and my partner Kostas for their continuous support and for believing in me during the good and the bad times of this journey. This work is dedicated to them.

Declaration

I grant powers of discretion to the University Librarian to allow this dissertation to be copied in whole or in part without further reference to me. This permission covers only single copies made for study purposes, subject to normal conditions of acknowledgements.

Abstract

The definition of the Spatial Variability of the Ground Motion (SVGM) is a complex and multi-parametric problem that has caught the attention of the research community since the first accelerometer arrays were installed. The effect of this phenomenon on the seismic response of long and multiply supported structures in general, and on cable-stayed bridges, in particular, has been studied by many researchers who have emphasised the significance of considering this phenomenon in the seismic analysis, but have also agreed that the SVGM is a multi-component phenomenon that needs more research.

This work examines the effect of the multi-support excitation on the seismic response of cable-stayed bridges by means of the time delay of the earthquake at different supports and of the loss of coherency of the seismic waves. The focus herein is the effect of the SVGM on cable-stayed bridges with various configurations in terms of their length and in terms of design parameters, such as the pylon shape and the pylon-cable system configuration, combined with the influence of the incidence angle of the seismic waves. Furthermore, the SVGM is examined at higher levels of earthquake intensity in order to assess the vulnerability of the bridge when subjected to lower probability ground motions.

The aim of this research is to provide general conclusions that are applicable to a wide range of cable-stayed bridges and to contribute to the ongoing effort to interpret and predict the effect of the SVGM.

It has been found that the influence of the multi-support excitation on the seismic response of the bridges is strongly affected by the shape of the pylons, by the pylon-cable system configuration and by and the seismic incidence angle. The SVGM also excites vibration modes that do not contribute to the seismic response when identical support motions are considered and it increases the probability of failure in the constituent components of the bridge.

List of Abbreviations

AASHTO	**A**merican **A**ssociation of **S**tate **H**ighway and **T**ransportation **O**fficials
AD-LCP	Bridge model with '**A**'-shaped pylons with lower **D**iamond configurations and two **L**ateral **C**able **P**lanes
A-LCP	Bridge model with '**A**'-shaped pylons and two **L**ateral **C**able **P**lanes
ATC	**A**pplied **T**echnology **C**ouncil
at	**at**tenuation effect of the SVGM
CDF	**C**umulative **D**istribution **F**unction
CSABAC	**C**altrans **S**eismic **A**dvisory **B**oard *Ad-hoc* **C**ommittee on Soil-Foundation-Structure Interaction
DFT	**D**iscrete **F**ourier **T**ransform
DHA, DHB	**D**ownhole **A**ccelerometers **A**, **B**
DRHA	**D**irect **R**esponse-**H**istory **A**nalysis
FFFF	**F**irm soil conditions at the foundations of all the supports of the bridges
FN, FP	**F**ault **N**ormal, **F**ault **P**arallel earthquake components
FSSF	Variable soil conditions among the different supports of the bridges; **F**irm soil at the end supports and **S**oft soil at the intermediate supports
HHT	**H**ilber **H**ughes **T**aylor algorithm
H-LCP	Bridge model with '**H**'-shaped pylons and two **L**ateral **C**able **P**lanes
H&V	**H**arichandran **&** **V**anmarcke coherency model
H&W	**H**arichandran **&** **W**ang

inc	**inc**oherence effect of the SVGM
is	***i***ntermediate transverse ***s***truts of the pylons
JRA	**J**apan **R**oad **A**ssociation
ll	***l***ateral ***l***egs of the pylons
ls	***l***ower transverse ***s***truts of the pylons
LSST	**L**arge **Sc**ale **S**eismic **T**est
L&W	**L**uco **&** **W**ong coherency model
MCEER	**M**ultidisciplinary **C**enter for **E**arthquake **E**ngineering **R**esearch
MDoF	**M**ulti **D**egree **o**f **F**reedom
MSRS	**M**ultiple **S**upport **R**esponse **S**pectrum
NL-RHA	**N**on**L**inear **R**esponse-**H**istory **A**nalysis
PDF	**P**robability **D**ensity **F**unction
PEER	**P**acific **E**arthquake **E**ngineering **R**esearch Center
PGA	**P**eak **G**round **A**cceleration
PSD	**P**ower **S**pectral **D**ensity
RHA	**R**esponse-**H**istory **A**nalysis
RS	**R**esponse **S**pectrum
SD	**S**tandard **D**eviation
SDoF	**S**ingle **D**egree **o**f **F**reedom
SMA	**S**trong **M**otion **A**ccelerograph
SMART-1	**S**trong **M**otion **AR**ray in **T**aiwan
SPC	**S**eismic **P**erformance **C**ategory
sr	**s**ite **r**esponse effect of the SVGM
SSI	**S**oil-**S**tructure **I**nteraction
SSSS	**S**oft soil conditions at the foundations of all the supports of the bridges

SVGM	**S**patial **V**ariability of the **G**round **M**otion
SYNC	**SYNC**hronous motion
us	***u***pper transverse ***s***truts of the pylons
wp	**w**ave **p**assage effect of the SVGM
Y-CCP	Bridge model with inverted '**Y**'-shaped pylons and one **C**entral **C**able **P**lane
Y-LCP	Bridge model with inverted '**Y**'-shaped pylons and two **L**ateral **C**able **P**lanes
YD-CCP	Bridge model with inverted '**Y**'-shaped pylons with lower **D**iamond configurations and one **C**entral **C**able **P**lane
YD-LCP	Bridge model with inverted '**Y**'-shaped pylons with lower **D**iamond configurations and two **L**ateral **C**able **P**lanes

List of Symbols

Note: Several symbols are repeated along the thesis to maintain their classical notation. However, they do not interfere with each other and the distinction is clear. Symbol * in the units means that the parameter can adopt any form of the response. Only the most relevant symbols are listed here.

Greek Symbols

Symbol	Description	SI Unit
α, β	Distance dependent angles that define the incoherence effect	rad
a_g	Design ground acceleration on type A ground	m/s^2
a_{LW}	Parameter of Luco and Wong (1986) coherency model	s/m
a_m, a_n	Effective influence factors	dimensionless
a_R, β_R	Coefficients for Rayleigh's damping	dimensionless
α_s	Skew angle	$^\circ$
β_i	Angle that the i^{th} cable forms with the axis of the deck	rad
β_r	Factor for the magnitude of ground displacements that take place in opposite directions at consequent supports	dimensionless
γ	Coherency function	dimensionless
γ_{jk}^{M}	Smoothed coherency of signals recorded at stations j and k	dimensionless
$\gamma_{mn}^{\text{inc, wp, sr, at}}$	Coherency of signals recorded at stations m and n due to the incoherence, wave passage, site response and attenuation effects, respectively	dimensionless
$\Delta_{D,P}$	Distance between cables on the deck in the main span	m
$\Delta_{D,S}$	Distance between cables on the deck in the side span	m

Symbol	Description	SI Unit
Δt_d	Time difference in damage initiation between pylons P1 and P2	s
ε	Normal total deformation	dimensionless
$\dot{\boldsymbol{\varepsilon}}^{pl}$	Plastic strain rate	dimensionless
ε_{crack}	Deformation marking concrete cracking initiation	dimensionless
$\varepsilon_{c,t}^{\max}$	Maximum deformation of concrete under tension	dimensionless
$\varepsilon_{cu,c}$	Ultimate deformation of confined concrete under compression	dimensionless
ε_{cy}	Elastic limit deformation of concrete under compression	dimensionless
ε_{su}	Ultimate deformation of reinforcing steel	dimensionless
ε_{sy}	Elastic limit deformation of reinforcing steel	dimensionless
η	Damping correction factor for design spectra	dimensionless
θ	Incidence angle of the seismic waves	$^\circ$
θ_{mn}	Frequency-dependent phase angle between signals at stations m and n	rad
θ_{mn}^{wp}, θ_{mn}^{sr}	Frequency-dependent phase angles between signals at stations m and n from the wave passage and site response effects, respectively	rad
μ	Mean response	*
μ_{ar}, μ_{med}	Arithmetic mean and median response, respectively	*
μ_X, μ_Y	Mean value of variables X and Y, respectively	*
ν_c, ν_s	Poisson's ratios of concrete and steel, respectively	dimensionless
ξ	Fraction of critical damping	dimensionless
ξ_f	Damping of the soil layer that is considered equivalent to a SDoF oscillator (Clough and Penzien 2015)	dimensionless
ξ_g	Damping of the soil layer that is considered equivalent to a SDoF oscillator (Kanai 1957, Tajimi 1960)	dimensionless
ξ_i	Damping of the i^{th} oscillator	dimensionless

Symbol	Description	SI Unit
ρ^*	Fictional density for the complete composite deck section	kg/m^3
ρ_a , ρ_c, ρ_s	Density of asphalt, concrete and steel, respectively	kg/m^3
ρ_c^*	Increased density of concrete	kg/m^3
ρ_j	Response ratio for response quantity j	dimensionless
$\rho_{s_{mi}s_{nj}}$	Cross-correlation coefficient for the i^{th} and j^{th} oscillator responses at stations m and n, respectively	dimensionless
$\rho_{u_m s_{nj}}$	Cross-correlation coefficient between the ground displacement at support m and the oscillator response at n for the j^{th} mode	dimensionless
$\rho_{u_m u_n}$	Cross-correlation coefficient for ground displacements at m and n	dimensionless
σ	Normal stress	N/m^2
σ	Standard deviation of the response	*
$\boldsymbol{\sigma}^c$	Normal stress derived from the constitutive equation, ignoring any viscous dissipation effects	N/m^2
$\sigma_{T,i}$	Tensile stress of the i^{th} cable	N/m^2
τ	Difference between two time instances	s
τ	Time instance during the duration of the earthquake	s
ϕ_k	Phase angles for signal generation uniformly distributed over the range [0, 2π)	rad
Ω	Damage ratio j	dimensionless
ω	Circular frequency	rad/s
ω_f	Circular frequency of the soil layer that is considered equivalent to a SDoF oscillator (Clough and Penzien 2015)	rad/s
ω_g	Circular frequency of the soil layer that is considered equivalent to a SDoF oscillator (Kanai 1957, Tajimi 1960)	rad/s
ω_i	Circular frequency of the i^{th} mode	rad/s
ω_k, ω_n	Discrete circular frequency of the k^{th} and n^{th} frequency steps, respectively	rad/s

Latin Symbols

Symbol	Description	SI Unit
A	Discrete Fourier transform	*
A1, A2	Abutments of the cable-stayed bridges	dimensionless
A_a, A_c, A_s	Cross-sectional area of the asphalt, concrete and steel parts of the deck section, respectively	m^2
A_i	Area of the deck that is assigned to the i^{th} cable	m^2
$A_{T,i}$	Cross-sectional area of the cable	m^2
A^*_{tot}	Cross section of the composite deck section homogenised to steel	m^2
a_{HV}, A	Parameters of Harichandran and Vanmarcke (1986) coherency model	dimensionless
B	Width of the deck	m
b, B	Parameters of Harichandran and Vanmarcke (1986) coherency model	dimensionless
b_{mi}, b_{nj}	Effective modal participation factors at supports m and n for the i^{th} and j^{th} modes, respectively	dimensionless
$\mathbf{C}$	Damping matrix of the structure	Ns/m
$\mathbf{C}_{ff}$	Damping matrix associated with the unconstrained ('f') degrees of freedom of the structure	Ns/m
$\mathbf{C}_{sf}$, $\mathbf{C}_{fs}$	Coupling damping matrices associated with the unconstrained ('f') and with the support ('s') degrees of freedom of the structure	Ns/m
$\mathbf{C}_{ss}$	Damping matrix associated with the support ('s') degrees of freedom of the structure	Ns/m
$\mathrm{cov}\,(X, Y)$	Covariance of variables X and Y	dimensionless
$D_m(\omega_i,\xi_i)$, $D_n(\omega_j,\xi_j)$	Displacement response spectra applied to stations m and n, respectively	m
d_b	Diameter of the longitudinal reinforcement bars	m
d_{g}	Design ground displacement	m

Symbol	Description	SI Unit
d_{LCP}, d_{CCP}	Depth of the deck for the LCP and the CCP bridges, respectively	m
d_{mn}^{L}	Projected distance along the direction of the wave propagation between stations m and n	m
$d_{\mathrm{r}i}$	Foundation displacement of support i under multiple support excitation	m
$\mathrm{d}t$	Time step	s
$E[\cdot]$	Expectation operator	dimensionless
E_c, E_s	Young's moduli of concrete and of reinforcing and structural steel, respectively	N/m^2
E_p	Young's modulus of prestressing steel	N/m^2
E_{Sp}	Total work dissipated in the structure through plasticity	J
E_W	Total work input to the structure by the seismic forces	J
$\mathbf{F}_s$	Vector of the reaction forces at the support ('s') degrees of freedom	N
$F_{T,i}$	Tensile force that the i^{th} cable is required to transfer from the deck to the pylon	N
$F_{T,ult}$	Maximum tensile force that the i^{th} cable can carry	N
F_X	Cumulative Distribution Function of the continuous variable X	dimensionless
$F_{x,main/2}$	Horizontal forces transferred to the pylon from the half main span	N
$F_{x,side}$	Horizontal forces transferred to the pylon from the side span	N
F_v	Site coefficient for the long-period branch of the design response spectrum	dimensionless
F_z	Force that each cable is required to carry	N
f	Frequency	Hz

Symbol	Description	SI Unit
f_0	Frequency parameter of Harichandran and Vanmarcke (1986) coherency model	Hz
f_1	Fundamental vibration frequency	Hz
f_{cm}	Mean elastic compressive stress of concrete	N/m^2
$f_{cm,c}$	Ultimate compressive stress of confined concrete	N/m^2
$f_{c,t}$	Maximum tensile stress of concrete	N/m^2
f_i	Vibration frequency of the i^{th} mode	Hz
$f_{s,t}$	Ultimate tensile stress of reinforcement and structural steel	N/m^2
f_{tl}	Frequency corresponding to the time lag between pylons P1 and P2	Hz
f_X	Probability Density Function of variable X	*
f_{sy}	Yield stress of reinforcement and structural steel	N/m^2
H	Frequency-response function of soil column	rad/s
H	Height of the tallest pier between examined joints	m
H	Height of the pylon above the deck	m
H_A	Length of the anchorage area in the pylon	m
H_i	Height of the lower part of the pylons below the deck	m
H_{tot}	Total height of the pylon	m
I	Intensity modulating function	dimensionless
I_a	Arias intensity	m/s
$\mathrm{Im}[\cdot]$	Imaginary part of complex number	dimensionless
I_T	Distance between cables in the pylon	m
i	Imaginary unit	dimensionless
$\mathbf{K}$	Elastic stiffness matrix of the structure	N/m

Symbol	Description	SI Unit
$\mathbf{K}_{ff}$	Elastic stiffness matrix associated with the unconstrained ('f') degrees of freedom of the structure	N/m
$\mathbf{K}_{sf}$, $\mathbf{K}_{fs}$	Coupling elastic stiffness matrices associated with the unconstrained ('f') and with the support ('s') degrees of freedom of the structure	N/m
$\mathbf{K}_{ss}$	Elastic stiffness matrix associated with the support ('s') degrees of freedom of the structure	N/m
k	Parameter of Harichandran and Vanmarcke (1986) coherency model	m
L	Total length of the bridge	m
L_{elem}	Length of the beam finite element	m
L_{g}	Maximum distance beyond which the ground motions may be considered completely uncorrelated	m
L_{IP}	Distance of the intermediate piers from the end abutments	m
L_{lim}	Limiting length associated with the length of the continuous deck	m
L_P	Main span length of the cable-stayed bridges	m
L_S	Side span length of the cable-stayed bridges	m
l_{mn}	Distance between stations m and n	m
l_p	Plastic hinge length	m
$\mathbf{M}$	Mass matrix of the structure	kg
M	Number of discrete frequencies	dimensionless
M	Smoothing window to reduce variance in the signals	dimensionless
$\mathbf{M}_{ff}$	Mass matrix associated with the unconstrained ('f') degrees of freedom of the structure	kg
M_{jj}	Bending moment along the axis j	Nm
$\mathbf{M}_{sf}$, $\mathbf{M}_{fs}$	Coupling mass matrices associated with the unconstrained ('f') and with the support ('s') degrees of freedom of the structure	kg

Symbol	Description	SI Unit
$\mathbf{M}_{ss}$	Mass matrix associated with the support ('s') degrees of freedom of the structure	kg
M_W	Moment magnitude of the earthquake	dimensionless
N_s	Minimum seating length	cm, mm
N_T	Number of stays per half main span and cable plane	dimensionless
$P(\cdot)$	Probability	dimensionless
g, q	Uniformly distributed dead and live loads, respectively	N/m^2
R	Amplification factor for displacements	dimensionless
$\mathrm{Re}[\cdot]$	Real part of complex number	dimensionless
R_i	Response quantity i	*
R_{xx}	Autocovariance function of a stochastic process	*
S	Amplification factor due to the soil class	dimensionless
S	Power Spectral Density	*
S_1	Spectral acceleration when the period is equal to 1 s	m/s^2
S_a	Spectral acceleration	m/s^2
S_e	Elastic response spectrum	*
S_{jj}	Power Spectral Density at station j	cm^2/s^3
S_{jj}^M	Smoothed Power Spectral Density at station j	cm^2/s^3
S_{jk}	Cross Spectral Density at stations j and k	cm^2/s^3
S_{jk}^M	Smoothed Cross Spectral Density at stations j and k	cm^2/s^3
S_{KT}, S_{CP}	Kanai (1957), Tajimi (1960) and Clough and Penzien (2015) Power Spectra, respectively	cm^2/s^3
S_{o}	Power Spectral Density at bedrock	cm^2/s^3
S_{v}	Velocity Power Spectral Density	cm^2/s

Symbol	Description	SI Unit
S_{d}	Displacement Power Spectral Densities	$\mathrm{cm}^2\mathrm{s}$
T	Vibration period	s
T_1	Fundamental vibration period	s
$T_{1,i}$	Governing vibration period contributing to response quantity i	s
P1, P2	Pylons of the cable-stayed bridges	dimensionless
T_{B}, T_{C}, T_{D}	EC8 corner vibration periods for design spectra	s
t	Time instance	s
t_1, t_2	Consecutive time instances	s
t_{A1}, t_{A2}	Time instance that the delayed earthquake reaches abutments A1 and A2, respectively	s
t_C	Thickness of concrete section in the pylon	m
t_d	Time instance of the damage initiation	s
$t_{d_{\mathrm{P1}}}$, $t_{d_{\mathrm{P2}}}$	Time instance of the damage initiation in pylons P1 and P2, respectively	s
t_{EQ}	Total duration of the earthquake	s
t_{P1}, t_{P2}	Time instance that the delayed earthquake reaches pylons P1 and P2, respectively	s
t_{tl}	Time lag between consequent supports	s
$\mathbf{u}$	Vector of relative displacements	m
$\dot{\mathbf{u}}$	Vector of relative velocities	m/s
$\ddot{\mathbf{u}}$	Vector of relative accelerations	$\mathrm{m/s}^2$
$\mathbf{u}_d$	Vector of dynamic displacements	m
$\mathbf{u}_f$	Vector of total displacements at the unconstrained ('f') degrees of freedom of the structure	m

Symbol	Description	SI Unit
$\dot{\mathbf{u}}_f$	Vector of total velocities at the unconstrained ('f') degrees of freedom of the structure	m/s
$\ddot{\mathbf{u}}_f$	Vector of total accelerations at the unconstrained ('f') degrees of freedom of the structure	m/s^2
u_G	Relative displacement of the ground occurring due to ground deformation between piers	cm
$\ddot{u}_g^{(j)}(t)$	Uniformly modulated, non-stationary accelerations	m/s^2
$\ddot{\mathrm{u}}_{\mathrm{g},\,x}$, $\ddot{\mathrm{u}}_{\mathrm{g},\,y}$	Acceleration histories parallel to the x and y axes of the cable-stayed bridges	m/s^2
$u_{m,\max}$, $u_{n,\max}$	Mean peak ground displacements at stations m and n, respectively	m
$\mathbf{u}_{ps}$	Vector of pseudo-static displacements	m
u_R	Differential displacement between the superstructure and the substructure	cm
$\mathbf{u}_s$	Vector of prescribed support ('s') displacements	m
$\dot{\mathbf{u}}_s$	Vector of prescribed support ('s') velocities	m/s
$\ddot{\mathbf{u}}_s$	Vector of prescribed support ('s') accelerations	m/s^2
V	Volume of the part of the structure that sustains damage	m^3
$\mathbf{v}$	Velocity field vector	m/s
$\mathrm{var}\,(X)$	Variance of X	dimensionless
$\mathrm{v}_{\mathrm{app}}$	Apparent velocity of wave propagation	m/s
v_s	Elastic S-wave velocity	m/s

Chapter 1

Intoduction

Contents

1.1 Background & Motivation

Cable-stayed bridges are landmark structures constituting key parts of transportation networks and they are capable of spanning long distances that seemed impossible in the past. These structures are usually very flexible and light-weight, with long fundamental periods, complex modal couplings among their key structural elements (Abdel-Ghaffar 1991, Abdel-Ghaffar and Khalifa 1991) and reduced damping compared to other types of bridges (Kawashima and Unjoh 1991), making them susceptible to dynamic actions such as seismic and wind actions. The seismic design of the pylons in cable-stayed bridges located in earthquake-prone regions is particularly important given the key role of these members in the global resistance of the structure and it usually governs their design (Gimsing and Georgakis 2012).

One of the most crucial characteristics of earthquakes is that the travelling seismic waves do not remain constant as they pass through various soil media, hence they are altered as they reach successive supports of structures that are extended in length and have multiple supports. Long structures, such as most cable-stayed bridges, are subjected to ground motions with significantly different amplitudes and frequency contents among their supports. The resulting differential movements of the supports modify the seismic response of the structure (Hao *et al.* 1989). The Spatial Variability of the Ground Motion (SVGM), as this phenomenon is referred to, has a significant effect on cable-stayed bridges and research has shown that this effect may be favourable or unfavourable for the response of these structures. Significant scientific work has been conducted on this topic and several pioneering works are available to the engineering community. A number of methodologies are available to the engineers, allowing them to account for this phenomenon in the design, varying from simplified methods to the most rigorous tools. However, the uncertain nature of the SVGM has not allowed for a specific framework to be established on the basis of predicting the effect of the multi-support excitation of the supports on the seismic response. Current codes of practice are usually limited to the proposal of increased seating lengths of the deck to account for the SVGM. It is mainly the European seismic code (Eurocode 8; Part 2 2005) that has defined a more detailed set of guidelines including when and how to consider the SVGM. Although, this has been considered as a step forward methodology to account for the multi-support excitation, there are limitations which have been recognised in the literature.

1.2 Aim & Objectives

The purpose of the present research work is to examine the effect of the SVGM on the seismic response of cable-stayed bridges with variable lengths and pylon-cable system configurations combined with the influence of the velocity of propagation of the earth-

quake, the loss of coherency of the seismic waves, and of the earthquake's incidence angle. Several parameters are examined in this study including a response ratio that quantifies the effect of the SVGM on the structure, a damage factor which addresses the damage induced to structures subjected to multiple excitations of their supports and the probability of failure in the constituent components of the bridges, among others.

This thesis unveils several aspects of the topic that have not attracted sufficient attention. The first point that differentiates this work from the existing ones in the literature, is that the focus is put directly on the effect of the SVGM on the pylons of cable-stayed bridges. The present study takes account of several design decisions, such as the shape of the pylons and the pylon-cable system configuration in a generic manner, which has not been examined in the past. Furthermore, the effect of the incidence angle of the seismic waves in combination with the SVGM has not been extensively examined and this is considered herein by examining the seismic response of the pylons under multi-angle and asynchronous excitations. Finally, the different parameters of the wave propagation have been considered in this work by examining the influence of the loss of coherency of the seismic waves and of the time delay of the earthquake at different supports.

1.3 Thesis Organisation

In order to address the aforementioned research objectives the following chapters are included in this thesis:

Chapter 2 provides a detailed discussion about the state of knowledge on cable-stayed bridges and on the characteristics of the SVGM, accompanied by the effect that this phenomenon has on the seismic response of long, multiply-supported structures. A complete reference is made to the available methodologies to address the SVGM and to code provisions about this phenomenon.

Chapter 3 follows with the description of the cable-stayed bridges that are examined for the purpose of this study. The geometric characteristics of the structures are presented, along with the description of the finite element models that are used for the elastic and the inelastic dynamic analyses. A wide range of cable-stayed bridges are considered with main span lengths of 200, 400 and 600 m and different pylon-cable system configurations, in order to ensure the generality of the conclusions of the research. Specifically, five pylon shapes are adopted with two different configurations of the lower part of the pylon and two different cable system configurations, resulting in seven conceptually different cable-stayed bridges.

Chapter 4 defines the seismic action that is applied to the foundations of the cable-stayed bridges. In order for the effect of the SVGM on the seismic response of the struc-

tures to be predicted in the most accurate way possible, the seismic action must be defined very thoroughly. The seismic action is defined to comply with the prescriptions of Eurocode 8; Part 1 (2004) representing strong earthquakes in seismic active regions worldwide. A computer program is developed in Python (van Rossum 1995) to generate sets of synthetic accelerograms that account for the time delay between the arrival of the earthquake at different supports and for the loss of coherency of the seismic waves, which constitute important components of the SVGM, based on an established generation model. The accelerograms are generated for the horizontal components of the earthquakes and they are rotated in the range of 0°-180° in order to consider the influence of the seismic angle of incidence with respect to the deck of the bridge.

Chapter 5 defines the methodology to analyse the bridges. For the purpose of this study dynamic analyses of the bridges are performed in the linear and nonlinear ranges by means of the response-history analysis.

Chapter 6 presents the results from the elastic dynamic analyses of the bridges by means of the examination of the seismic forces that are developed along the height of the pylons, the comparison of the seismic response obtained from the asynchronous motion of the pylons to the response from the identical support motion and the close link between the effect of the SVGM with the excitation of higher-order and antisymmetric vibration modes of the bridges.

Chapter 7 extends the discussion to the nonlinear range by considering the nonlinear behaviour of the materials (concrete and reinforcement steel) of the bridges. The behaviour of important structures, such as cable-stayed bridges, must be assessed under the effect of very strong earthquakes which might push them beyond the elastic limits. The initiation and propagation of damage in the pylons of the bridges subjected to asynchronous motion is examined and compared to the introduced damage when synchronous motion is considered. Finally, the probability of failure is computed of the constituent components of the bridge.

Chapter 8 summarises the main conclusions of the study and presents the author's recommendations on future work on the topic.

Chapter 2

State of the Art

Contents

2.1 Introduction

The purpose of this chapter is to provide an overview of the state of knowledge on the Spatial Variability of the Ground Motion (SVGM) and its effect on the seismic response of cable-stayed bridges.

The chapter is introduced by a historic review on cable-stayed bridges and it is followed by a detailed reference to their main characteristics and the features that make these structures unique compared to other types of bridges.

The chapter then focuses on the SVGM by defining this phenomenon, describing its main components and presenting the first observations that led to its definition. In order to describe the SVGM analytically, the concepts of the Power Spectral Density of a signal and of the Cross Spectral Density between two signals are presented. Then the link between the two is discussed by means of the coherency function as a fundamental component in the description of the SVGM. The impact of the multi-support excitation on the structural response is then discussed in depth in Section 2.3.5, followed by the combined effect of the SVGM with the soil-structure interaction in Section 2.3.6 and with the earthquake's angle of incidence with respect to the bridge axis in Section 2.3.7. The chapter is concluded with a reference to the suggestions and prescriptions of international codes of practice and guidelines with regard to the SVGM.

2.2 Cable-stayed Bridges

2.2.1 History of Cable-Stayed Bridges

Cable-stayed bridges are landmark structures that constitute key parts of transportation networks and are capable of spanning long distances that seemed impossible in the past. The idea behind them dates back to the early rope bridges and is an adaptation to the guy ropes that were used to secure tent structures and the masts of sailing ships (Parke and Hewson 2008). However, even though this idea was underlying it was not found interesting until the beginning of the 19^{th} century when wrought iron bars, which later led to steel wires, were developed (Gimsing and Georgakis 2012).

The evolution in the concept of cable-stayed bridges is summarised in Fig. 2.1. The initial concept of a beam bridge that was supported by a few stays and its deck worked mainly in bending was gradually replaced by the modern multi-stay cable bridge in which the deck is more slender and works mainly in tension and compression (Leonhardt and Zellner 1980). This new type of bridge allows for more economic and more efficient construction.

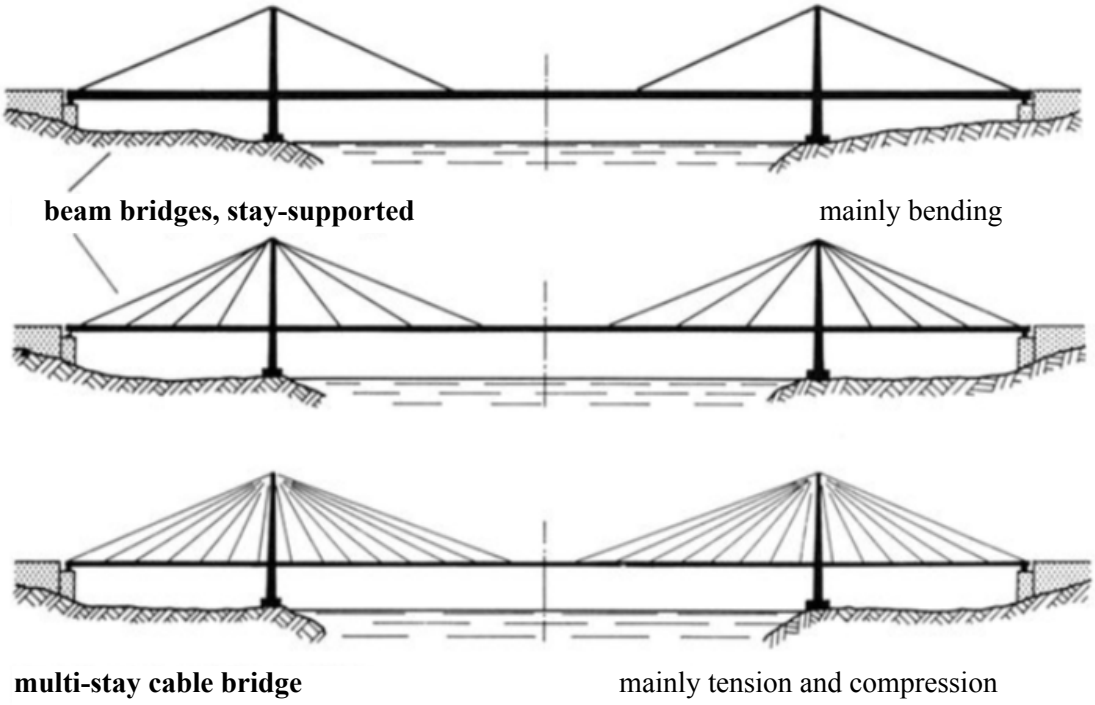

Figure 2.1: Development from stayed beam bridges to the modern multi-stay cable system (*taken from Leonhardt and Zellner (1980)*).

Cable-stayed bridges were originally considered the most feasible solution for spans in the range of approximately 150 m (500 ft) to 600 m (2000 ft) (Abdel-Ghaffar and Nazmy 1991). The first modern cable-stayed bridge, whose construction was completed in 1956, was the Strömsund Bridge in Sweden with a main span of 183 m. The state of knowledge and the new technologies and materials that are available nowadays have allowed for the maximum main span limit to be extended to more than 1000 m in the cases of the Russky Bridge in Russia (1104 m) and of the Sutong Yangtze River Bridge in China (1088 m), (Gimsing and Georgakis 2012, Pipinato 2016).

2.2.2 Geometric Characteristics

Cable-stayed bridges are formed of three principal components (Gimsing and Georgakis 2012):

a. The pylons are the vertical members of a cable-stayed bridge. Their role is to transfer the axial load resulting from the vertical components of the forces from the cable system to the foundations.

b. The cable system is the connecting part between the load bearing deck and the load transferring pylon.

c. The deck is the structural part of the bridge that holds the traffic and is subjected

to the greatest part of the externally induced loading (i.e. dead and live loads and wind actions.)

Pylons

The most commonly adopted pylon shapes vary from 'H'-shaped pylons to inverted 'Y'-shaped ones. The 'H'- shaped pylons consist of two lateral legs connected to each other through transverse (with respect to their axis) struts at different elevations, such as the Jingyue Yangtze River Bridge in China. On the other hand, in the case of 'Y'-shaped pylons the legs start inclined at their base and end up being connected to a single vertical member at the top which accommodates the anchorages of the cable-system, such as the Sutong Yangtze River Bridge also in China. The 'A'-shaped pylons represent a modification of the inverted 'Y'-shaped geometry in which the legs are inclined throughout their height and eventually meet at the top, such as the Russky Bridge in Russia. Finally, there are pylons with one vertical leg that could be described as 'I'-shaped pylons, such as the Millau Viaduct in France. The configuration of the pylon below the deck also varies. The individual legs of the pylons can continue down to the foundation level being separate or they can meet below the deck and form what is most commonly known as the 'lower diamond' configuration, such as the Tatara Bridge in Japan and the Rion-Antirrion Bridge in Greece (Leonhardt and Zellner 1980). The different types of pylons are included in Fig. 2.2.

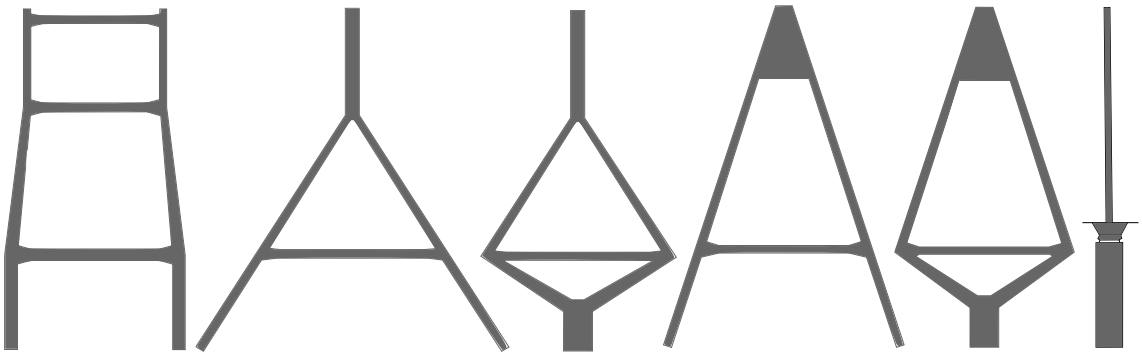

Figure 2.2: Schematic representation of the different pylon configurations. (a) 'H', (b) inverted 'Y', (c) inverted 'Y' with lower diamond, (d) 'A', (e) 'A' with lower diamond and (f) 'I'.

The pylons with individual legs that are connected at the top (i.e. the inverted 'Y'- and 'A'-shaped pylons) are stiffer configurations compared to the 'H'-shaped pylon, because of the inclination of their legs. On the other hand, pylons with lower diamonds are more flexible structures because of the inclination of the individual legs until they meet to a common vertical leg below the deck level which provides certain rotation capacity

(Camara and Astiz 2011, Xiong *et al.* 2013, Camara and Efthymiou 2016).

Cable System

The choice of the cable system is one of the most important aspects of the design of a cable-stayed bridge (Gimsing and Georgakis 2012). There are different configurations, each one having advantages and disadvantages. In order to identify the different characteristics of each cable-system, the following classification has been made:

Longitudinal Configuration

In the longitudinal direction of the cable system (which coincides with the axis of the deck) there are three different configurations namely; 'fan', 'semi-harp' (or 'modified fan') and 'harp', as shown in Fig. 2.3. The difference among the various cable systems is reflected in the anchorages of the cables in the pylon. The fan cable system (Fig. 2.3(a)) supports the total number of cables at the top of the pylon[1]. This configuration is suitable for moderate spans and a relatively small number of cables. The fan arrangement is, conceptually, the most efficient solution because it maximises the longitudinal restraint at the pylon top, however, there have been issues raised with regard to the maintenance and replacement of the cables, as well as fatigue issues raising from the bending of the cables. The other end is the harp configuration of Fig. 2.3(c) in which each cable is individually supported at equally spaced anchors along the height of the pylon in a manner that the cables are placed parallel to each other. The main disadvantage of this cable system is that it is vulnerable against non-symmetric live loading and its structural efficiency relies mostly on the bending stiffness of the pylon and the deck. Finally, the intermediate solution of the semi-harp configuration that is included in Fig. 2.3(b) allows for the individual anchorage of each cable near the top of the pylon (in $1.5-2.5$ m vertical distances) and is the preferred solution in modern cable-stayed bridges. This configuration provides a clear force path in the pylon with the stresses in each anchor point being significantly smaller than the stress at the top of the pylon in the fan configuration and it allows for a larger number of cables to be accommodated by the pylon which, in turn, provides a larger number of supports to the deck allowing it to behave as a continuous elastic supported girder. Furthermore, the individual anchorages allow for easy maintenance and replacement of the cables and finally, the larger number of cables with varying lengths and natural frequencies increases the damping of the bridge (Parke and Hewson 2008).

[1]This approach has been adopted from the concept of the suspension bridge and it was the preferred solution in the first modern cable-stayed bridges, such as the Strömsund Bridge (Parke and Hewson 2008).

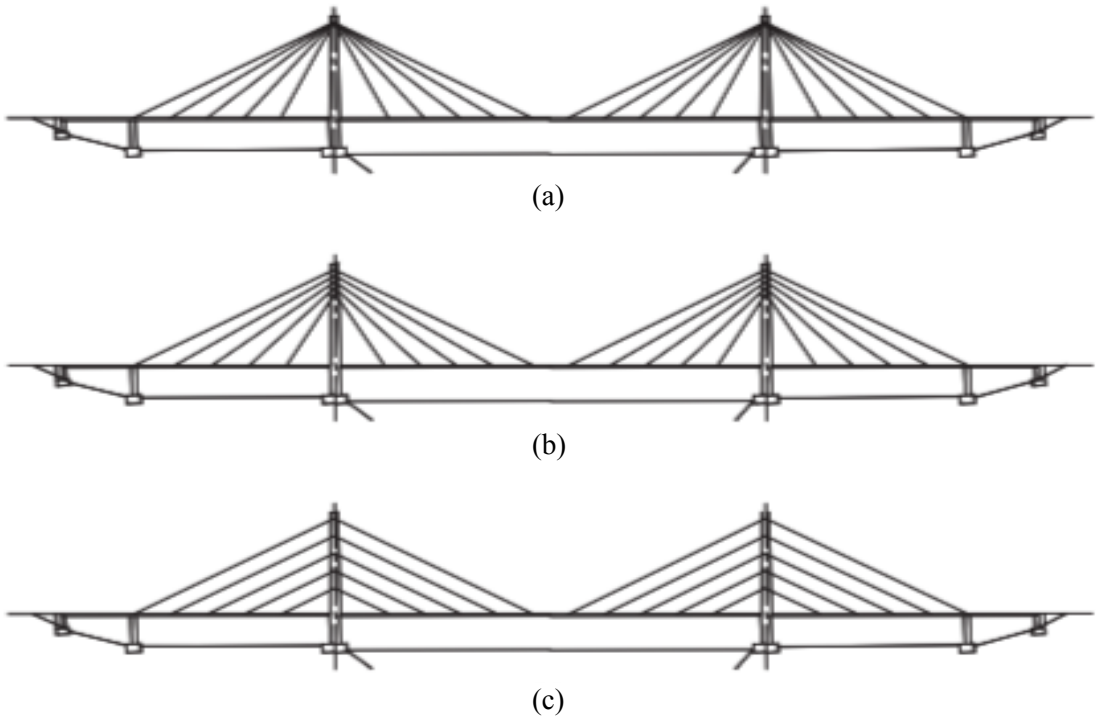

Figure 2.3: Different longitudinal cable system configurations. (a) Fan, (b) semi-harp (or modified fan), (c) harp (*taken from Parke and Hewson (2008)*).

Transverse Configuration

In the transverse direction (perpendicular to the deck axis) there are mainly two different configurations of the cables that are most commonly adopted. Fig. 2.4 shows the 'lateral' and the 'central' cable configurations. The former is composed of two lateral[1] cable planes that are connected at their one end to the pylon anchorage zone and at the other end, to the edges of the deck (Fig. 2.4(a)). The latter cable configuration consists of one centrally anchored cable plane that is connected to the pylon and to the centre of the deck at the other end (Fig. 2.4(b)). The lateral cable configuration can be combined with pylons of 'H', inverted 'Y' and 'A' shapes and even with single-leg 'I'-shaped pylons (as in the case of the Oakland bay Suspension Bridge), as opposed to the central cable system which can be accommodated by an 'I'-shaped or by an inverted 'Y'-shaped pylon. The lateral cable configuration of Fig. 2.4(a) ensures a stiffer connection between the pylons and the deck and allows for an easier erection of the deck during construction, but the central cable plane of Fig. 2.4(b) arguably provides a more aesthetically pleasing outcome and may also result in lower fatigue of the cables[2] (Walther *et al.* 1988).

[1]The lateral cable planes are vertical in the case of 'H'-shaped pylons, whereas they are slightly inclined when 'A'-shaped pylons are adopted (Walther *et al.* 1988)

[2]Provided that the deck has high torsional rigidity, it can spread concentrated loads more efficiently resulting in smaller stress variations in the cables (Walther *et al.* 1988).

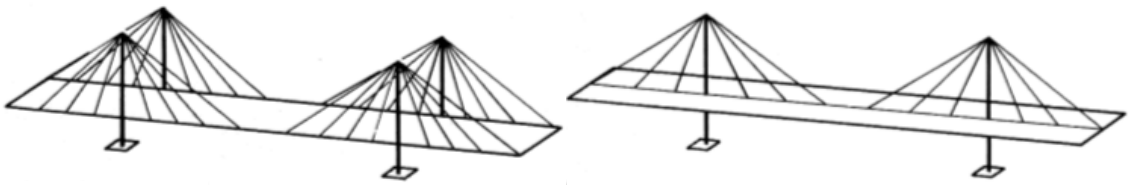

(a) (b)

Figure 2.4: Different transverse cable system configurations. (a) Two lateral cable planes, (b) one central cable plane (*adapted from Walther et al. (1988)*).

Deck

The deck in cable-stayed bridges plays an important role in the structural integrity of the complete structure given that it is subjected to the major part of the external loads[1]. The deck mainly works in bending and in axial compression derived from the horizontal force component of the stays (Parke and Hewson 2008). The shape of the cross section of the deck is determined to a large extent by the configuration of the cable system and by the width of the deck itself which, in turn, depends on the services to be supported (e.g. the number of lanes in road bridges). Fig. 2.5 presents two typical deck cross sections used in the design of cable-stayed bridges. When the deck is suspended by lateral cable planes from its edges the necessary torsional rigidity is provided to the deck by the cable system, hence the solution of an open deck cross section is adequate, as shown in Fig. 2.5(a). On the other hand, central cable system configurations require a torsionally stiffer deck because, as opposed to the case of lateral cable planes, this type of cable system does not provide any torsional rigidity to the deck. For such cases, usually a closed box section is adopted for the deck enabling it to carry eccentric loading (Fig. 2.5(b)) (Leonhardt and Zellner 1980).

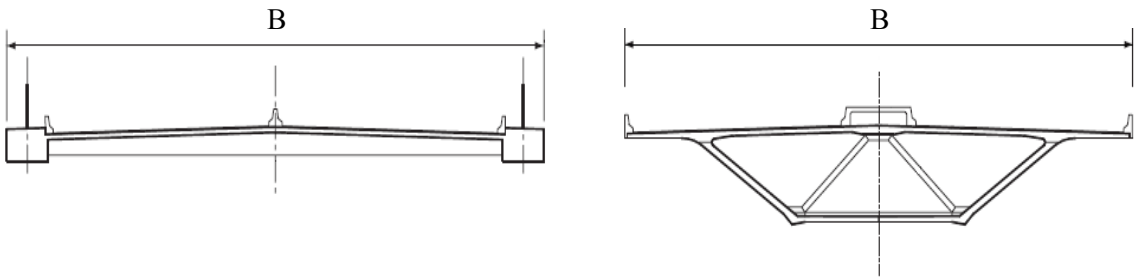

(a) (b)

Figure 2.5: Typical deck cross sections for (a) lateral cable configuration and (b) central cable configuration (*adapted from Parke and Hewson (2008)*).

[1]The total live load from the traffic is directly applied to the deck, and often the dead load and the wind area are larger for the deck than for the cable system (Gimsing and Georgakis 2012).

2.2.3 Nonlinear Behaviour

Fleming (1979) describes a cable-stayed bridge as a nonlinear system whose deck is supported elastically at a number of points (cables) throughout its length. Fig. 2.6 shows the nonlinear behaviour of cable-stayed bridges. The rise of nonlinearities is due to (Fleming 1979, Camara 2018):

a. The nonlinear force-deformation relationships for the cables due to the sagging caused by their self-weight.

b. The nonlinear force-deformation relationships for the bending members of the cable-stayed bridge due to interactions between large bending and axial deformations in the members (second order effects).

c. The large displacements due to the large flexibility of cable-stayed bridges.

These sources of nonlinearity determine the structural response of these bridges and it is essential that they be accounted for in the analysis and in the design process.

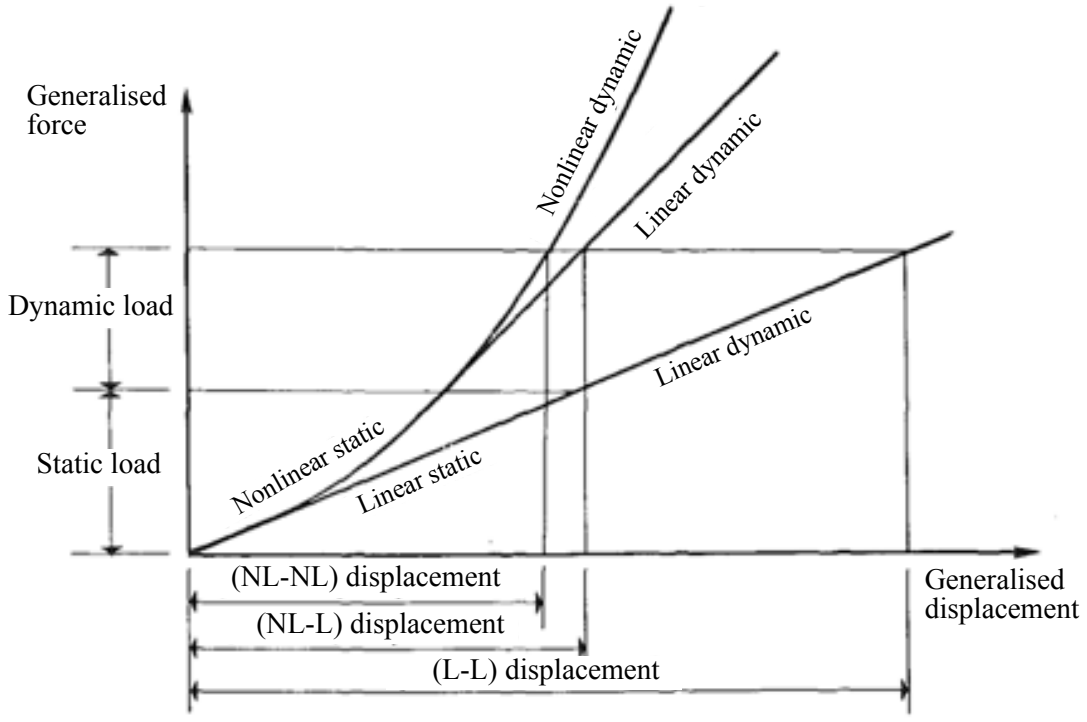

Figure 2.6: Nonlinearities of cable-stayed bridges (*taken from Abdel-Ghaffar and Nazmy (1991)*).

2.2.4 Vibration Modes

From a dynamic point of view, cable-stayed bridges are characterised by the close spacing between vibration modes, which interact with each other. This coupling is the outcome of the combination of structural elements (pylons, deck and cables) that have very different geometric characteristics, mass and stiffness (Abdel-Ghaffar 1991, Camara *et al.* 2014, Chen and Duan 2014).

The first vibration modes have long periods, usually in the range of 2-8 seconds, depending on the main span length (Chen and Duan 2014), and are associated with the deck, followed by modes that excite the cable-system and are coupled with the deck. The pylon modes are usually of higher order and may also be coupled with the deck, depending on the support conditions and on the relative stiffness between the deck and the pylons[1] (Valdebenito and Aparicio 2006, Camara and Efthymiou 2016, Camara 2018). The strong coupling in the vibration modes of cable-stayed bridges highlights the three-dimensional nature of their behaviour (Abdel-Ghaffar and Nazmy 1991).

2.2.5 Seismic Response of Cable-Stayed Bridges

Cable-stayed bridges present features that make them unique compared to other types of bridges. They are more flexible and light-weight structures compared to other bridge types, with longer vibration periods (Abdel-Ghaffar 1991, Abdel-Ghaffar and Khalifa 1991, Chen and Duan 2014), which means that they are subjected to lower spectral accelerations and lower seismic forces than stiffer bridge types. However, they also present lower damping values (less than the 5% of the critical damping that is commonly adopted) than other types of structures and hence, they are susceptible to dynamic actions such as wind and seismic actions (Kawashima and Unjoh 1991). Furthermore, their extended length (which can reach several hundreds of meters in main span) suggests that their end (abutments) and intermediate (pylons) supports are subjected to different ground motions because of the propagation of the earthquake with finite velocity, of the loss of coherency of the ground motion that reaches different supports and of the variable ground conditions that may be met among the abutments and the pylons, which could result in significant damage in the composing members of the bridge (Walther *et al.* 1988). The spatial and temporal variabilities of the ground motions at the supports of cable-stayed bridges and the effect that these have on the seismic response of the pylons, which act as the primary load transferring components of this type of bridges, is the motivation behind this thesis and is discussed in greater detail in Section 2.3.

[1]The transverse flexure of the pylons of cable-stayed bridges with relatively short spans ($\leq$ 300 m) is strongly coupled with the transverse movement of the deck. For longer spans the flexibility of the deck increases faster than the flexibility of the pylons, which seem to remain unaffected by the fundamental transverse mode of the deck (Camara and Efthymiou 2016).

The seismic response of cable-stayed bridges has been studied over the years with significant research works coming from Abdel-Ghaffar and Rubin (1983a, b), Abdel-Ghaffar (1991), Abdel-Ghaffar and Nazmy (1991), Nazmy and Abdel-Ghaffar (1992), among others and more recent ones from Soyluk and Dumanoglu (2000, 2004), Dyke *et al.* (2003), Allam and Datta (2004), Camara and Astiz (2012, 2014), Camara and Efthymiou (2016). The seismic behaviour of these bridges, which is characterised by the contribution of a large number of vibration modes (Abdel-Ghaffar and Nazmy 1991), can be adequately predicted when examined under the effect of the horizontal earthquake components. It has been found that cable-stayed bridges are not particularly vulnerable against the vertical component of the earthquake because the pylons are designed to withstand very large dead and live loads and the deck responds as an elastic girder suspended by multiple support points (Walther *et al.* 1988, Gimsing and Georgakis 2012), however several authors oppose to this simplification and argue that the vertical component can be important when near-fault earthquakes are considered (Valdebenito and Aparicio 2005), which however is not within the scope of this research work.

The large number of cable-stayed bridges that are constructed in seismically active regions worldwide establishes the need to assess the seismic behaviour of these structures and especially of the pylons, which are responsible for the overall structural integrity of the bridge and whose seismic design usually governs their overall design in seismic prone regions Gimsing and Georgakis (2012).

2.3 Spatial Variability of the Ground Motion

2.3.1 Definition

The SVGM or multi-support excitation can be described by the differential movement of the supports of structures that are extended in length such as long bridges, tunnels, pipelines, dams and large rigid foundations, among others. Eurocode 8; Part 2 (2005) defines the SVGM in bridges as a '*situation in which the ground motion at different supports of the bridge differs and, hence, the seismic action cannot be based on the characterisation of the motion at a single point*'. According to Abdel-Ghaffar (1991), the multiple support excitation begins when the structure is long with respect to the wavelengths of the input motion in the frequency range of importance to its earthquake response and consequently different supports may be subjected to different excitations. The SVGM introduces differential movements to the supports of multiply supported structures that modify their seismic response (Hao *et al.* 1989).

The SVGM is the outcome of the combination of four important components, as described by Der Kiureghian and Neuenhofer (1992) and Der Kiureghian (1996), namely:

a. **Wave passage effect**. This component refers to the difference in the arrival times of the ground motion to different stations. It is expressed by considering a finite value for the propagation velocity of the seismic waves, which will be discussed in detail in Chapter 4.

b. **Incoherence effect**. It refers to the loss of coherency of the ground motion due to consequent reflections and refractions of the seismic waves in heterogeneous soil media. It is accounted for through the coherency function, γ, which will be discussed in detail in Section 2.3.4.

c. **Site response effect**. This component reflects the modification of the amplitudes and the frequency contents of the ground motions at different supports due to changes in the soil conditions along the deck. It is described by considering different power or response spectra at different supports that are appropriate for the different soil types (Shinozuka *et al.* 2000).

d. **Attenuation effect**. This component describes the gradual decrease of the amplitudes of the seismic waves with distance as they travel away from the fault. It is expressed as a function of frequency[1] and distance from the fault (Der Kiureghian 1996). This effect is deemed insignificant for the scale of typical man-made structures and it is often ignored.

2.3.2 Early Observations

The SVGM has been extensively studied by various researchers; Abdel-Ghaffar (1991), Abdel-Ghaffar and Nazmy (1991), Zerva (1991), Der Kiureghian and Neuenhofer (1992), Soyluk and Dumanoglu (2000), Sextos (2001), Sextos *et al.* (2004) and Burdette *et al.* (2006), among others. The phenomenon started being examined more closely as soon as the first dense instrument arrays were installed and started recording. Arrays such as the linear El Centro Differential Array which recorded the 1979 Imperial Valley earthquake (Spudich and Cranswick 1984), the two-dimensional Strong Motion ARray in Lotung, Taiwan (SMART-1) (Bolt *et al.* 1982) and the three-dimensional Large Scale Seismic Test (LSST) also in Lotung (Abrahamson *et al.* 1991a, b) have provided engineers and seismologists with invaluable information on the SVGM.

Fig. 2.7 includes the configurations of the three seismic arrays that provided the first observations of the SVGM. The El Centro Differential Array in California (Fig. 2.7(a)) consisted of six stations, each one equipped with a three-component set of force-balanced accelerometers. The distance of the various stations from the reference one (Station 1) varied from approximately 18 m to 305 m. Another array element, Station A1, was

[1]Usually higher frequency waves tend to decay faster (Der Kiureghian 1996).

installed south of Station 1 featuring an analog-recording SMA-1 accelerometer. As a historic reference, it is interesting to note that the installation of the array was completed just in time to record the 1979 Imperial Valley earthquake (Bycroft 1982). The El Centro array was located at a distance of 24 km away from the epicentre of the earthquake.

The SMART-1 array's operation began at the end of 1982. Installed in the North-East corner of Taiwan, in the city of Lotung, the two-dimensional accelerometer array recorded numerous seismic motions during its lifespan (1980-1991). Many empirical and semi-empirical models that account for spatially variable motions have been developed based on those records. It consisted of 37 stations that were arranged in three concentric circles, as can be seen in Figure 2.7(b), covering an area of about 12 km^2. Each circle ring namely 'Inner', 'Middle' and 'Outer' circles, respectively, was formed of 12 equally spaced triaxial accelerometers numbered from 1 to 12 following the first letter of the ring they belonged to (i.e. I10 for Inner circle, 10$^{\text{th}}$ station). There was also a central station named C00. The radii of the three circle rings were equal to 200 m for the Inner circle and increased to 1000 m and 2000 m for the Middle and Outer circles, respectively. The distances between different stations varied from 105 m to 4000 m.

The LSST also in Lotung was operational between 1985 and 1991. This smaller scale and three-dimensional array was an addition to the existing SMART-1 array and it was installed within the latter's southwest quadrant, between the Middle and Outer circles, in close proximity to Station O08. This array was added in an attempt to obtain spatially variable motions in distances as short as a few meters apart. It consisted of 15 free-surface triaxial accelerometers arranged radially in three arms at 120° intervals, as it can be observed in Fig. 2.7(c). In the centre of the surface configuration two models of a reactor containment vessel at 1/4 and 1/12 scales were installed and instrumented with 14 accelerometers and 20 strain gauges (Abrahamson *et al.* 1987). The three-dimensional LSST consisted of eight downhole triaxial accelerometers (Fig. 2.7(d)) noted as DHA and DHB in Fig. 2.7(c) that reached a total depth of 47 m.

2.3.3 Power Spectral Density

The Power Spectral Density (PSD), $S_{xx}(\omega)$, of a random process is the Fourier Transform of its autocovariance function $R_{xx}(\omega)$ (Vanmarcke 1983). A detailed discussion on stochastic processes is included in Appendix A. The definition of the PSD is expressed in Eq. (2.1):

$$S_{xx}(\omega) = \frac{1}{2\pi} \int_{-\infty}^{\infty} R_{xx}(\tau) \exp\left(-\,\mathrm{i}\,\omega\tau\right) \;\; \mathrm{d}\tau \tag{2.1}$$

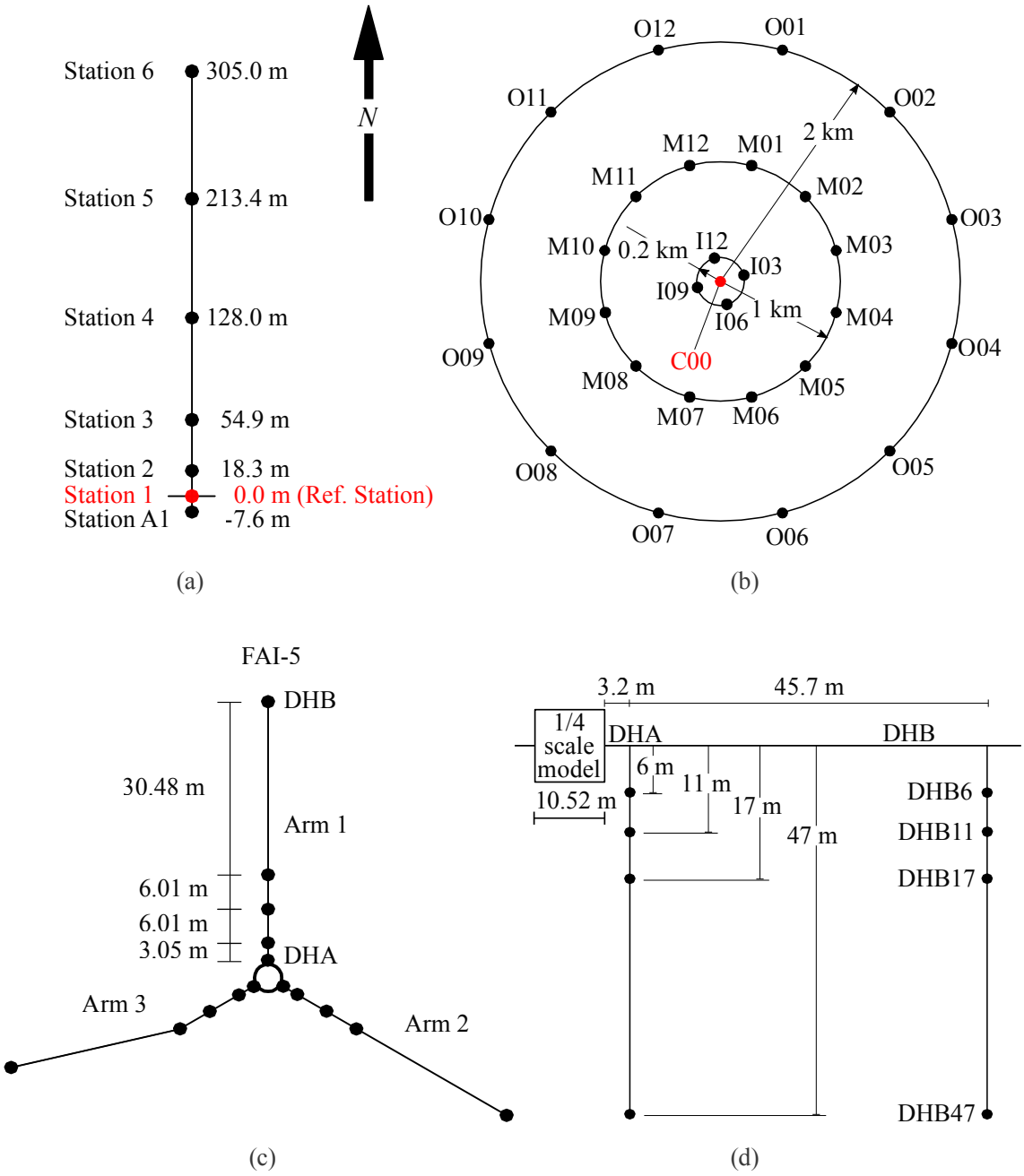

Figure 2.7: Configurations of (a) the El Centro Differential Array (*taken from Spudich and Cranswick (1984)*), (b) the SMART-1 (taken from Bolt *et al.* (1982)), (c) the surface configuration of the LSST array and (d) the downhole configuration of the LSST array ((c), (d) *taken from Abrahamson et al. (1991b)*).

in which ω is the circular frequency of the random process in [rad/s], τ represents the time lag and $\mathrm{i} = \sqrt{-1}$ is the imaginary unit.

There exist parametric models developed to describe the PSD of the ground motions based on recorded data. The most widely accepted model is the Kanai & Tajimi spectrum (Kanai 1957, Tajimi 1960) and its extension by Clough and Penzien (2015). The Kanai & Tajimi spectrum (S_{KT}) is based on the observation that the spectral density of the earthquake is constant at bedrock (S_{o}) while at the ground surface it can be modified by the vibrational properties of the soil layer. In this case, the soil layer is considered equivalent to a Single-Degree-of-Freedom (SDoF) oscillator with frequency ω_g and damping ξ_g. It is essentially a white process[1], S_{o}, passed through a filter with properties ω_g and ξ_g of the following form:

$$S_{\mathrm{KT}}(\omega) = S_{\mathrm{o}} \frac{1 + 4\xi_g^2 \left(\frac{\omega}{\omega_g}\right)^2}{\left[1 - \left(\frac{\omega}{\omega_g}\right)^2\right]^2 + 4\xi_g^2 \left(\frac{\omega}{\omega_g}\right)^2} \tag{2.2}$$

For a stationary process, the velocity (S_{v}) and displacement (S_{d}) PSD's are defined, respectively, as:

$$S_{\mathrm{v}} = \frac{1}{\omega^2}\ S(\omega) \quad \text{and} \quad S_{\mathrm{d}} = \frac{1}{\omega^4}\ S(\omega) \tag{2.3}$$

Later, Clough and Penzien (2015) introduced a second filter to the spectrum in order to attenuate the very low frequencies which would otherwise lead to infinite ground velocities and displacements[2]:

$$S_{\mathrm{CP}}(\omega) = S_{\mathrm{o}} \frac{1 + 4\xi_g^2 \left(\frac{\omega}{\omega_g}\right)^2}{\left[1 - \left(\frac{\omega}{\omega_g}\right)^2\right]^2 + 4\xi_g^2 \left(\frac{\omega}{\omega_g}\right)^2} \frac{\left(\frac{\omega}{\omega_f}\right)^2}{\left[1 - \left(\frac{\omega}{\omega_f}\right)^2\right]^2 + 4\xi_f^2 \left(\frac{\omega}{\omega_f}\right)^2} \tag{2.4}$$

in which ω_f and ξ_f are parameters appropriately selected to filter out the very low fre-

[1] A white process can be defined as a process with uniform PSD over the specified frequency range, $-\infty < \omega < \infty$ (Clough and Penzien 2015).

[2] It can be seen in Eq. (2.3) that as $\omega \to 0$, $S_{\mathrm{v}} \to \infty$ and $S_{\mathrm{d}} \to \infty$.

quencies. Fig. 2.8(a) presents the two acceleration PSD spectra, normalised with respect to the white bedrock excitation spectrum ($S_o = 1.0$ cm^2/s^3). It is obvious that the revised form of Clough and Penzien (2015) (S_{CP}) only modifies the Kanai & Tajimi spectrum in the lower frequency range ($\omega \leq 1$ rad/s). Fig. 2.8(b) presents the normalised displacement PSD that is obtained with Eq. (2.3). The displacement PSD is the one that controls the parameters of the Clough & Penzien filter (2015). It can be observed that the low frequencies affect significantly the displacement spectrum hence the filtering must be done carefully. To this end, Der Kiureghian and Neuenhofer (1992) investigated the filter parameters and proposed appropriate values for firm, medium and soft soil conditions.

Soil Type	ω_g [rad/s]	ξ_g	ω_f [rad/s]	ξ_f
soft	5.0	0.2	0.5	0.6
medium	10.0	0.4	1.0	0.6
firm	15.0	0.6	1.5	0.6

Table 2.1: Proposed parameters by Der Kiureghian and Neuenhofer (1992) for the Clough & Penzien spectrum (Clough and Penzien 2015).

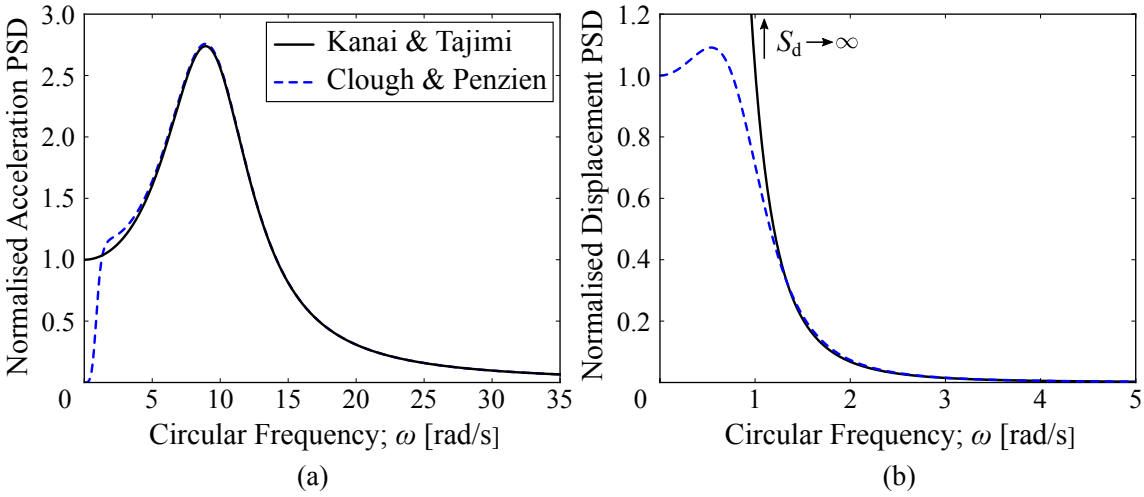

Figure 2.8: Normalised Kanai & Tajimi (1957, 1960) and Clough & Penzien (2015) (a) acceleration and (b) displacement PSD spectra. Values for the parameters are adopted from Der Kiureghian and Neuenhofer (1992) for medium soil conditions equal to $\omega_g = 10.0$ rad/s, $\omega_f = 1.0$ rad/s, $\xi_g = 0.4$ and $\xi_f = 0.6$. Assumed $S_o = 1.0$ cm^2/s^3. The change in the scales of the horizontal and the vertical axes should be noted.

2.3.4 Coherency Function

The coherency, γ_{mn}, of two signals recorded at two different stations 'm' and 'n' is expressed through the coherency function. It is essentially the cross spectral density (S_{mn}) of the signals at stations m and n normalised by their power spectra as follows:

$$\gamma_{mn}(\omega) = \frac{S_{mn}(\omega)}{\sqrt{S_{mm}(\omega) S_{nn}(\omega)}} \tag{2.5}$$

in which S_{mm} and S_{nn} are the PSD's of the records at stations m and n, respectively and ω is the circular frequency in [rad/s]. The coherency is complex valued and can be defined as a frequency based model to describe the SVGM (Abrahamson *et al.* 1991b). The absolute value of the coherency is termed 'lagged coherency' and it has real values ranging between $0 \leq |\gamma_{mn}(\omega)| \leq 1$.

$$0 \leq \frac{|S_{mn}(\omega)|}{\sqrt{S_{mm}(\omega)S_{nn}(\omega)}} \leq 1 \tag{2.6}$$

When $|\gamma_{mn}(\omega)|$ reaches unity the signals are completely correlated but as the lagged coherency tends to zero the signals gradually become less correlated. The lowest bound is $|\gamma_{mn}(\omega)| = 0$, for which the two signals are completely uncorrelated and can be considered completely independent. The real part of the coherency focuses on the loss of coherency whereas the imaginary part expresses the wave passage and the site response effects (Abrahamson *et al.* 1991b, Der Kiureghian 1996), which will be also demonstrated at a later stage of this section. Under the assumption that the seismic waves propagate from station m to station n and that the wave propagation velocity remains constant through various soil media, the complex coherency can be expressed as a function of the lagged coherency as:

$$\gamma_{mn}(\omega) = |\gamma_{mn}(\omega)| \exp\left[\mathrm{i}\,\theta_{mn}(\omega)\right] \tag{2.7}$$

in which ω is the circular frequency in [rad/s] and $\theta_{mn}(\omega)$ is a frequency-dependent phase angle defined as:

$$\theta_{mn}(\omega) = \tan^{-1}\frac{\mathrm{Im}\left[\gamma_{mn}(\omega)\right]}{\mathrm{Re}\left[\gamma_{mn}(\omega)\right]} \tag{2.8}$$

$\mathrm{Im}[\cdot]$ and $\mathrm{Re}[\cdot]$ denote the imaginary and real parts of the complex coherency γ_{mn}, respectively.

Several models for the estimation of the coherency have been proposed in the past based on the information provided from the SMART-1 array. Some models are characterised as 'empirical' because they are based only on observations from the available records. Other models are defined as 'semi-empirical' because their form is based on analytical work but the parameters that they employ are defined from actual observations.

Harichandran and Vanmarcke (1986) proposed one of the most employed empirical coherency models. Its formulation is based on the lagged coherencies from four events

recorded at the SMART-1 and on the assumption of ergodicity[1] of the recorded signals. The authors also observed that the loss of coherency with frequency and distance was independent of the direction of the propagation (isotropy of the signals) and proposed the sum of two exponentials as follows:

$$|\gamma(l_{mn},f)| = A\exp\left[\frac{-2Bl_{mn}}{a_{\mathrm{HV}}v(f)}\right] + (1-A)\exp\left[\frac{-2Bl_{mn}}{v(f)}\right] \tag{2.9}$$

$$v(f) = k\left[1+\left(\frac{f}{f_0}\right)^{b}\right]^{-1/2} \quad \text{and} \quad B = (1-A+a_{\mathrm{HV}}A)$$

where: l_{mn} is the separation distance between stations m and n in [m], f is the frequency in [Hz] and $v(f)$ is the frequency-dependent spatial scale of fluctuation. For the lagged coherency, Harichandran and Vanmarcke (1986) initially performed a least-squares fit of the above model to the unsmoothed real part of the coherency of the aligned signals of Event 20 in the radial direction (recorded at SMART-1 array). The values of the model parameters were obtained as:

$$A = 0.736; \quad a_{\mathrm{HV}} = 0.147; \quad k = 5120 \text{ m}$$
$$f_0 = 1.09 \text{ Hz}; \quad b = 2.78$$

Later, the same authors proposed revised values for the above parameters by examining again the recorded signals from Event 20 but this time in the radial and tangential directions. The resulting coherency model is not greatly modified when compared to the original model. A different study on the same model, by Harichandran and Wang (1990), introduced the following values for the same parameters based on Event 24 recorded at the SMART-1 array:

$$A = 0.626; \quad a_{\mathrm{HV}} = 0.022; \quad k = 19700 \text{ m}$$
$$f_0 = 2.02 \text{ Hz}; \quad b = 3.47$$

Another widely used coherency model is the semi-empirical model proposed by Luco and Wong (1986):

$$|\gamma(l_{mn},\omega)| = \exp\left[-\left(a_{\mathrm{LW}}\omega l_{mn}\right)^2\right] \tag{2.10}$$

[1]Ergodicity in a stochastic stationary process is the assumption that the ensemble averages of the process are identical to the averages taken along any realisation of this process along its infinite duration. The assumption of stationarity may be adopted in the case of seismic records if the strong motion window of the signals is considered a segment of a stationary process with no beginning and no end.

$$a_{\text{LW}} = \frac{v}{v_s} \quad \text{and} \quad v = \mu \left(\frac{R}{r_0} \right)^{1/2}$$

in which v_s is the elastic S-wave velocity in [m/s] in the random medium, R is the distance in [m] travelled by the wave in a random medium, r_0 is the scale length of random inhomogeneities along the wave's path and μ^2 is a measure of the relative variations of the elastic properties within the random medium. The parameter a_{LW} in [s/m] in Eq. (2.10) controls the decay of the coherency model. Higher values of a_{LW} result in a more abrupt loss of coherency with increasing separation distance and frequency. Finally, ω is the circular frequency in [rad/s] and l_{mn} is the distance in [m] between two supports m and n.

Later, Abrahamson *et al.* (1991a, b) assumed that the coherency is not affected by the magnitude of the earthquake and the source-to-site distance. To this end they obtained the non-parametric coherencies from 15 events recorded at the LSST array and based on the assumption that those can be grouped together (because they are obtained from the same site), they proposed a single non-parametric coherency model. Their coherency model is more applicable between points that are relatively closely spaced (below 100 m apart):

$$|\gamma\left(l_{mn},f\right)| = \tanh\left\{ \left(2.54 - 0.012 l_{mn}\right) \left[\exp\left[\left(-0.115 - 0.00084 l_{mn}\right) f\right] + \frac{f^{-0.878}}{3} \right] + 0.35 \right\} \tag{2.11}$$

in which l_{mn} is the distance between stations m and n in [m] and f is the frequency in [Hz].

Finally, a very important model for the estimation of the coherency was proposed by Der Kiureghian (1996), which was the first one to account for the wave passage, incoherence, site response and attenuation effects of the SVGM at the same time. The general form of the proposed coherency model for two signals at stations m and n has the following form:

$$\gamma_{mn}(\omega) = \gamma_{mn}^{\text{inc}}(\omega) \cdot \gamma_{mn}^{\text{wp}}(\omega) \cdot \gamma_{mn}^{\text{sr}}(\omega) \cdot \gamma_{mn}^{\text{at}}(\omega) \tag{2.12}$$

a. The component of the coherency function referring to the incoherence effect ('inc') is defined as follows:

$$\gamma_{mn}^{\text{inc}}(\omega) = \cos\left[\beta\left(l_{mn},\omega\right)\right] \exp\left[-\frac{1}{2}\alpha^2\left(l_{mn},\omega\right)\right] \tag{2.13}$$

It is real-valued and is described as a function of angles α and β, that are dependent on the distance l_{mn} between stations m and n in [m], and on the circular frequency ω in [rad/s].

b. The wave passage effect ('wp') is expressed as a function of ω in [rad/s], of the distance d_{mn}^{L} between m and n along the direction of the wave propagation projected on the ground surface in [m], and of the apparent wave propagation velocity v_{app} in [m/s].

$$\gamma_{mn}^{\text{wp}}(\omega) = \exp\left[-\,\text{i}\,\frac{\omega d_{mn}^{\text{L}}}{\text{v}_{\text{app}}(\omega)}\right] \tag{2.14}$$

The wave propagation velocity in Eq. (2.14) depends on ω. By assuming plane waves and an infinite elastic medium, the velocity remains constant and it is independent of the frequency, resulting in the following:

$$\gamma_{mn}^{\text{wp}}(\omega) = \exp\left[-\,\text{i}\,\frac{\omega d_{mn}^{\text{L}}}{\text{v}_{\text{app}}}\right] \tag{2.15}$$

The term in the right-hand side of Eq. (2.14) reflects a deterministic phase shift between the ground motions at stations m and n that is created by the finite value of the wave propagation velocity and depends on the circular frequency ω:

$$\theta_{mn}^{\text{wp}}(\omega) = -\frac{\omega d_{mn}^{\text{L}}}{\text{v}_{\text{app}}(\omega)} \tag{2.16}$$

c. The consideration of the site response effect ('sr') is based on the assumption that even if the motions at the level of the bedrock underneath two different stations m and n are identical[1], the corresponding motions at the surface will be different due to the different filtering properties of the soil columns[2] around m and n. This component of the coherency model is described by the frequency-response functions $H_j(\omega)$ (with $j = m, n$) of the soil columns at m and n, which represent the amplitude of the harmonic motion at the ground surface triggered by a harmonic of

[1] This assumption was originally made by Kanai (1957) and is actually the basis for the Kanai & Tajimi Spectrum, as described in Eq. (2.2).

[2] A soil 'column' is adopted by Der Kiureghian (1996) to develop the coherency model that refers to the site response effect by assuming a one-dimensional shear wave propagating vertically from the bedrock to the station under consideration. This soil column can be represented as a linear (or linearised) system with known properties.

exponential form $\exp[\mathrm{i}\,\omega t]$ at the bedrock level:

$$\gamma_{mn}^{\mathrm{sr}}(\omega) = \exp\left[-\mathrm{i}\,\theta_{mn}^{\mathrm{sr}}(\omega)\right] \tag{2.17}$$

The site response effect causes a phase shift of the surface motions at m and n, which depends on ω and is defined as:

$$\theta_{mn}^{\mathrm{sr}}(\omega) = \tan^{-1}\frac{\mathrm{Im}\left[H_m(\omega)H_n(-\omega)\right]}{\mathrm{Re}\left[H_m(\omega)H_n(-\omega)\right]} \tag{2.18}$$

The phase angles $\theta_{mn}^{\mathrm{wp}}$ and $\theta_{mn}^{\mathrm{sr}}$ in Eqs. (2.16) and (2.18) are the two components of the total phase angle θ_{mn} in Eq. (2.8), proving that the imaginary part of the complex coherency depends on the wave passage and site response effects.

d. Finally, the attenuation effect ('at') is described by considering, for each station m and n, decreasing functions of the form $f_j(\omega,r_j)$, with $j = m, n$. These are functions of the circular frequency ω in [rad/s] and of the source-to-station distance r_j in [m], with $j = m, n$.

$$\gamma_{mn}^{\mathrm{at}}(\omega) = \frac{E\left[f_m(\omega,r_m)f_n(\omega,r_n)\right]}{\sqrt{E\left[f_m^2(\omega,r_m)f_n^2(\omega,r_n)\right]}} \tag{2.19}$$

in which $0 \leq f_j(\omega,r_j) \leq 1$ with $j = m, n$ and $E[\cdot]$ denotes the expectation operator.

Der Kiureghian (1996) proved in his study that the attenuation of the seismic waves is usually not significant for the scale of typical man-made structures by examining multiple cases of statistical dependence between the functions at the pairs of stations m and n. The author concluded that the waves remain practically unaffected by this type of attenuation, especially when the case of bridges is considered. Hence in the following equation that describes the complete multi-component coherency model no term accounting for the attenuation effect is included. Eq. (2.12) is then re-written as the combination of Eqs. (2.13), (2.15) and (2.17):

$$\begin{aligned}\gamma_{mn}(\omega) &= \gamma_{mn}^{\mathrm{inc}}(\omega)\cdot\gamma_{mn}^{\mathrm{wp}}(\omega)\cdot\gamma_{mn}^{\mathrm{sr}}(\omega)\\ &= \cos\left[\beta\left(l_{mn},\omega\right)\right]\exp\left[-\tfrac{1}{2}\alpha^2\left(l_{mn},\omega\right)\right]\exp\left\{\mathrm{i}\left[\theta_{mn}^{\mathrm{wp}}(\omega)+\theta_{mn}^{\mathrm{sr}}(\omega)\right]\right\}\end{aligned} \tag{2.20}$$

where $\theta_{mn}^{\mathrm{wp}}(\omega)$ and $\theta_{mn}^{\mathrm{sr}}(\omega)$ are defined in Eqs. (2.16) and (2.18), respectively.

Fig. 2.9 demonstrates the difference among several coherency models. For exam-

ple, the model proposed by Luco and Wong (1986) assumes completely coherent waves at low frequencies (<1 Hz) regardless of the adopted value for the coherency drop parameter, whereas the proposed model from Harichandran and Vanmarcke (1986) accepts that there is significant loss of coherency between the signals even at very low frequencies, which is dependent on the adopted model parameters and on the separation distance between the stations. Zerva (2009) compared various coherency models and observed that the models that do not assume completely correlated motions at low frequencies (in this case the models of Harichandran and Vanmarcke (1986) and Harichandran and Wang (1990)) result in higher differential ground displacements even at short separation distances and hence they have a more pronounced effect on the pseudo-static response of the structure.

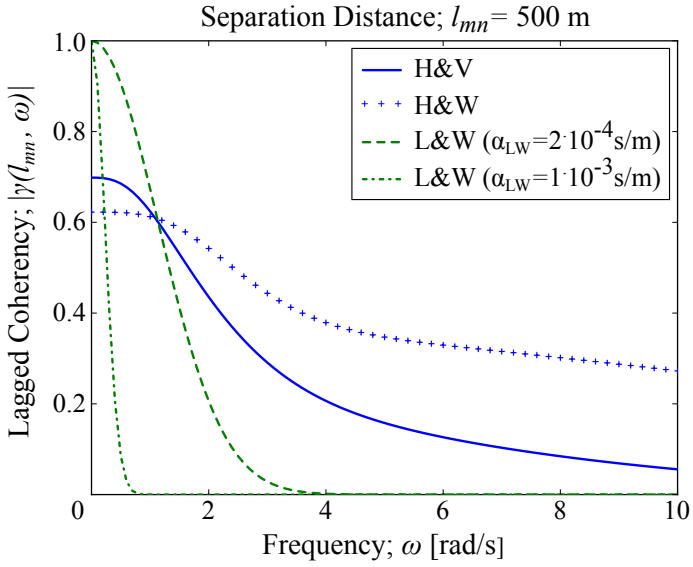

Figure 2.9: Comparison of different coherency models. 'H&V' stands for Harichandran and Vanmarcke (1986), 'H&W' for Harichandran and Wang (1990) and 'L&W' for Luco and Wong (1986); parameter a_{LW} in the 'L&W' model controls the decay in the coherency, as described in Eq. (2.10).

2.3.5 Effect of the SVGM on the Structural Response

The effect of the SVGM on the structural response depends on a number of factors including the amplitude of the seismic motion, the angle of incidence of the seismic waves relatively to the axis of the structure, the geometric characteristics of the structure and the stiffness of the surrounding soil, as it will be discussed in detail in the following sections. The effect of the SVGM has been examined in multiply-supported structures and structures that are extended in length. Examples of such structures are pipelines (Hindy and Novak 1980, Lee and Penzien 1983, Papadopoulos *et al.* 2017), ideal beam models (Zerva 1990, 1991, Hao 1997), frame structures (Bi *et al.* 2010), highway bridges (Shinozuka *et al.* 2000, Tzanetos *et al.* 2000), curved bridges (Sextos *et al.* 2004, Sextos and Kappos 2009), cable-stayed and suspension bridges (Abdel-Ghaffar and Rubin 1983a,

Abdel-Ghaffar and Nazmy 1991, Soyluk and Dumanoglu 2000, 2004, Allam and Datta 2004, Sextos *et al.* 2014), rigid foundations (Luco and Wong 1986) and dams (Chen and Harichandran 2001).

The SVGM induces differential movements among the supports of multiply supported structures which modify their seismic response (Hao *et al.* 1989). The multi-support excitation results in the decrease of the inertia-generated forces in a structure when compared to the resulting forces from the identical motion of the supports and at the same time it generates pseudo-static forces that are not present when identical support motion is considered (Priestley *et al.* 1996), which can be proven by distinguishing between the dynamic and the pseudo-static displacements in a structure. The equation of motion of a linear Multi-Degree-of-Freedom (MDoF) system with N unconstrained ('f') and R restrained (at the supports; 's') degrees of freedom can be written in the following form (Clough and Penzien 2015):

$$\begin{bmatrix} \mathbf{M}_{ff} & \mathbf{M}_{fs} \\ \mathbf{M}_{sf} & \mathbf{M}_{ss} \end{bmatrix} \begin{Bmatrix} \ddot{\mathbf{u}}_f \\ \ddot{\mathbf{u}}_s \end{Bmatrix} + \begin{bmatrix} \mathbf{C}_{ff} & \mathbf{C}_{fs} \\ \mathbf{C}_{sf} & \mathbf{C}_{ss} \end{bmatrix} \begin{Bmatrix} \dot{\mathbf{u}}_f \\ \dot{\mathbf{u}}_s \end{Bmatrix} + \begin{bmatrix} \mathbf{K}_{ff} & \mathbf{K}_{fs} \\ \mathbf{K}_{sf} & \mathbf{K}_{ss} \end{bmatrix} \begin{Bmatrix} \mathbf{u}_f \\ \mathbf{u}_s \end{Bmatrix} = \begin{Bmatrix} \mathbf{0} \\ \mathbf{F}_s \end{Bmatrix} \quad (2.21)$$

in which $\mathbf{u}_f = \left[\mathbf{u}_{f,1}, \ldots, \mathbf{u}_{f,N}\right]^{\mathrm{T}}$ is the N-vector of total displacements at the unconstrained ('f') degrees of freedom, $\mathbf{u}_s = \left[\mathbf{u}_{s,1}, \ldots, \mathbf{u}_{s,R}\right]^{\mathrm{T}}$ is the R-vector of the prescribed support ('s') displacements, $\dot{\mathbf{u}}$ and $\ddot{\mathbf{u}}$ are velocity and acceleration vectors, respectively with dimensions similar to the displacement vector $\mathbf{u}$ ($N \times 1$ and $R \times 1$ for the 'f' and 's' degrees of freedom, respectively), $\mathbf{M}_{ff}$, $\mathbf{C}_{ff}$ and $\mathbf{K}_{ff}$ are the $N \times N$ mass, damping and stiffness matrices, respectively, associated with the unconstrained ('f') degrees of freedom, $\mathbf{M}_{ss}$, $\mathbf{C}_{ss}$ and $\mathbf{K}_{ss}$ are the $R \times R$ matrices associated with the supports ('s' degrees of freedom), $\mathbf{M}_{fs}$, $\mathbf{C}_{fs}$ and $\mathbf{K}_{fs}$ are the $N \times R$ coupling matrices associated with both sets of degrees of freedom (with $\mathbf{M}_{sf}$, $\mathbf{C}_{sf}$ and $\mathbf{K}_{sf}$ being the transpose of $\mathbf{M}_{fs}$, $\mathbf{C}_{fs}$ and $\mathbf{K}_{fs}$, respectively) and $\mathbf{F}_s$ is the R-vector of the reaction forces at the support degrees of freedom of a structure subjected to multi-support seismic excitation.

The free displacement vector $\mathbf{u}_f$ can be decomposed into a pseudo-static component ($\mathbf{u}_f^{ps}$) resulting from the differential displacements at the support points and a dynamic component ($\mathbf{u}_f^{d}$) resulting from the dynamic response of the structure against the input inertial forces, as follows:

$$\mathbf{u}_f = \mathbf{u}_f^{ps} + \mathbf{u}_f^{d} \quad (2.22)$$

The pseudo-static displacement vector can be obtained from Eq. (2.21) by excluding the inertial and the damping terms:

$$\mathbf{u}_f^{ps} = -\mathbf{K}_{ff}^{-1}\mathbf{K}_{fs}\mathbf{u}_s \tag{2.23}$$

By substituting Eqs. (2.22) and (2.23) in Eq. (2.21) the formulation to obtain the dynamic displacements vector is obtained:

$$\mathbf{M}_{ff}\ddot{\mathbf{u}}_f^d + \mathbf{C}_{ff}\dot{\mathbf{u}}_f^d + \mathbf{K}_{ff}\mathbf{x}_f^d = \left(\mathbf{M}_{ff}\mathbf{K}_{ff}^{-1}\mathbf{K}_{fs} - \mathbf{M}_{fs}\right)\ddot{\mathbf{u}}_s + \left(\mathbf{C}_{ff}\mathbf{K}_{ff}^{-1}\mathbf{K}_{fs} - \mathbf{C}_{fs}\right)\dot{\mathbf{u}}_s \tag{2.24}$$

which is reduced to:

$$\mathbf{M}_{ff}\ddot{\mathbf{u}}_f^d + \mathbf{C}_{ff}\dot{\mathbf{u}}_f^d + \mathbf{K}_{ff}\mathbf{u}_f^d = \left(\mathbf{M}_{ff}\mathbf{K}_{ff}^{-1}\mathbf{K}_{fs} - \mathbf{M}_{fs}\right)\ddot{\mathbf{u}}_s \tag{2.25}$$

because the damping forces are considered significantly lower compared to the inertial forces leading to $\left(\mathbf{C}_{ff}\mathbf{K}_{ff}^{-1}\mathbf{K}_{fs} - \mathbf{C}_{fs}\right)\dot{\mathbf{u}}_s \approx 0$.

Components of the SVGM

The wave propagation velocity strongly influences the effect that the SVGM has on the response of a long structure. Typically lower values of the propagation velocity, c, tend to increase the structural response by increasing the pseudo-static forces induced under the SVGM (Eq. (2.23)) and by decreasing their dynamic counterpart (Abdel-Ghaffar and Nazmy 1991, Zerva 1991, Soyluk and Dumanoglu 2000, Wang *et al.* 2003, Soyluk and Dumanoglu 2004, Bi *et al.* 2010). With increasing values of the wave propagation velocity the pseudo-static forces that result from the differential movement of the supports are reduced. In the limit of an infinite value of the velocity of propagation ($c \rightarrow \infty$) the problem is reduced to the synchronous motion for which the pseudo-static effects are eliminated[1] and the response is completely represented by the dynamic component (Soyluk and Dumanoglu 2000). The interplay between the dynamic and pseudo-static components of the structural response may determine whether the overall influence of the SVGM on the structure will be favourable or unfavourable (Mezouer *et al.* 2010). Recent research on highway bridges (Wang *et al.* 2009) has shown that when the wave propagation velocity is higher than 1000 m/s the dynamic component usually dominates the response of those structures, whereas for velocities lower than 300 m/s the pseudo-static component becomes dominant. Abdel-Ghaffar and Nazmy (1991) proposed a threshold wave propagation velocity below which the pseudo-static forces dominate the overall re-

[1] It is obvious that when there is no time delay in the arrival of the ground motion at different stations, there are no differential displacements between consequent supports and, as a result there are no pseudo-static displacements (Priestley *et al.* 1996).

sponse in cable-stayed bridges and is defined as the ratio of the main span length over the fundamental vibration period of the bridge, if the wavelength is in the same order as the main span and the period of the wave is the same as the fundamental model of the bridge. In fact, the contribution of the fundamental mode in the seismic response depends on the value of the wave propagation velocity, at least in highway bridges (Wang *et al.* 2003). However, when the fundamental frequency of the structure is significantly higher than the dominant frequencies of the ground motion the SVGM might not influence the response significantly (Zerva 1991).

Zerva (1991) investigated the impact of the incoherence and wave passage effects on the response of multiply supported structures by analysing two- and three- span continuous symmetric beams. The author concluded that the incoherence effect is more important than the wave passage effect, which can be neglected, in cases where the seismic waves are highly incoherent. However, as the ground motion tends to become more coherent, the delay in the arrival times of the waves at different supports can amplify the response of the structure. Shinozuka *et al.* (2000) verified that the incoherence effect is usually more important than the wave passage effect in highway bridges, but for longer spans the time delay of the seismic motion at different supports can become critical. Zerva (1992) found that there exists a critical value of the apparent velocity beyond which the incoherence effect is the dominant component of the SVGM. This critical velocity reaches 1000 m/s for lifelines such as buried pipelines and above-ground structures with multiple supports. Above this critical velocity the incoherence effect is more pronounced than the wave passage effect. However, this finding has derived from research on these particular types of structures and hence the proposed velocity threshold cannot be generalised to the case of cable-stayed bridges, which is the focus of this thesis. Although extensive research has been performed on the effect of the SVGM on such structures, no threshold velocity has been established to distinguish between the relative importance of the wave passage and the incoherence effects.

The specific soil conditions at the support points of multiply supported structures (site response effect) can affect the impact of the SVGM on the structure and in some cases they can be critical to the seismic response (Der Kiureghian 1996). The effect of the differential motion of the supports on the overall seismic behaviour of the structure has been found to be beneficial when the supports are founded on stiff soil whereas it is detrimental in the case of soft soil conditions (Mezouer *et al.* 2010). Adanur *et al.* (2017) extended the research on the effect of the local soil conditions at the foundations of each support by assuming different soil conditions at the anchorage blocks and the pylons of the Bosphorus Suspension Bridge in Turkey with a main span of 1074 m. They considered different soil scenarios among which only one represented uniform foundation soil conditions (i.e. firm soil under the four supports), whereas the remaining cases represented combinations of soft, medium and firm foundation soils. The authors concluded

that the cases which assumed soft foundation soil resulted in the highest seismic response. Generally, the more different the foundation soil conditions among the different supports of extended structures, the higher the effect of the SVGM on the seismic response (Ates *et al.* 2006) and usually the response is maximised when the structure resonates with the fundamental frequencies of the soils (Bi *et al.* 2010).

Cable-Supported Bridges

Abdel-Ghaffar and Rubin (1983a) studied the lateral response of the 2737-m long Golden Gate suspension Bridge in California, accounting for the wave passage and incoherence effects of the SVGM. They concluded that neglecting the influence of the SVGM did not represent the worst seismic response of the suspension bridge and that this simplification would be unconservative. Later, Soyluk and Dumanoglu (2000) examined the structural response of Jindo Bridge, a cable-stayed bridge located in South Korea with a total length of 484 m, when subjected to asynchronous motion caused by the wave passage effect, which was defined only by different values for the velocity of wave propagation. The authors compared the results with the respective structural response from the synchronous excitation, which they considered as the reference case. It was found that both the deck and the pylons of this bridge were affected by the multiple support excitation in an unfavourable way.

Abdel-Ghaffar and Nazmy (1991) examined the effect of the asynchronous and three-directional ground motion on the seismic behaviour of two cable-stayed bridges with moderate and long main spans equal to 335.5 m (1100 ft) and 671 m (2200 ft), respectively. The results showed that the consideration of the out-of-phase motion of the pylons altered significantly the seismic response quantities compared to the respective ones obtained when synchronous motion of the supports was considered. The authors noticed that the SVGM could be either favourable or unfavourable for the seismic response compared to the seismic response from the synchronous motion. The unpredictable nature of the SVGM regarding the seismic response was later echoed by Der Kiureghian (1996). However, the effect of the SVGM seems to be more important on stiff structures and, typically, it does not significantly affect the response of longer and more flexible structures (Nazmy and Abdel-Ghaffar 1992). The pseudo-static component of the structural response is responsible for the increased influence of the SVGM on stiff structures (Priestley *et al.* 1996, Zerva 2009). Generally, the stiffer the structure, the more dominant is the pseudo-static component of the response, as opposed to flexible structures in which the total response is dominated by the dynamic component (Bi *et al.* 2010). This statement can be extended in the sense that the stiffer components of a structure composed of elements with very different flexibilities, such as a cable-stayed bridge, are more vulnerable to the multi-support excitation. Similarly, the components that are controlled

predominantly by higher-order modes are susceptible to the effect of the SVGM because the pseudo-static response becomes important in lower frequencies (Abdel-Ghaffar and Nazmy 1991, Nazmy and Abdel-Ghaffar 1992, Soyluk and Dumanoglu 2004, Sextos and Kappos 2008).

In a cable-stayed bridge the pylons are usually spaced at distances of hundreds of meters apart. In this sense, and depending on the value of the wave propagation velocity, the ground motion may reach the pylons seconds apart (Soyluk and Dumanoglu 2000). In a time-domain analysis of a cable-stayed bridge, if the acceleration time-histories are applied to the supports at the base of the pylons with a time delay differential displacement will occur causing the pylons to move relatively towards each other or in the opposite direction (Walther *et al.* 1988, Soyluk and Dumanoglu 2000). This will reportedly affect the deck and the pylons, as has been also seen in the experimental study of the effect of the asynchronous motion on cable-stayed bridges (Quan *et al.* 2008, Yang and Cheung 2011). In fact, the vertical displacement of the deck is increased considerably compared to the synchronous motion case and the internal forces in the pylons (i.e. the bending moments and the shear forces) are increased with decreasing values of the wave propagation velocity[1]. In particular, the axial load in the pylons and the shear forces at the base of the pylons are affected, as it was observed in the study of the 1510-m long 2nd Bosphorus Bridge in Turkey by Apaydin *et al.* (2016). The different directions of the multi-support excitation is also an important factor in the understanding of the effect of the SVGM in cable-stayed bridges because of the complex couplings among different directions of the response. Quan *et al.* (2008) examined the effect of the horizontal and vertical components of the multi-support excitation on the 542-m long Quincy Bay-view Bridge spanning over the Mississippi River in Illinois and noticed that when the bridge was subjected to vertical multi-support excitation the pylons oscillated longitudinally and the deck vertically. When the SVGM was considered longitudinally (parallel to the traffic) the pylons oscillated longitudinally again and the deck oscillated both longitudinally and vertically. Finally, under the effect of transversely (with respect to the deck) propagated multi-support excitation, the pylons and the deck oscillated transversely and completely independently from the other two directions, contrary to the vertical and the longitudinal multi-support excitations, which were strongly coupled.

Effect on the Seismic Fragility of Bridges

The probability that a structure will reach or exceed a pre-defined damage state when subjected to different levels of ground motion is estimated by means of the fragility analysis and it is usually expressed in the form of fragility curves. This type of analysis dates back to the seventies when it was originally used to estimate the probabily of failure of a

[1] As the velocity of the wave propagation decreases the delay in the arrival time of the ground motion to the pylons increases.

nuclear power plant against various peak ground accelerations (Kennedy *et al.* 1980, Kim and Feng 2003). Saxena (2000), Deodatis *et al.* (2000) and Saxena *et al.* (2000) worked on the development of fragility curves for the piers of two multi-span highway reinforced concrete bridges[1] in the direction parallel to the structures. They concluded that for the studied bridges the assumption of multi-support excitation provided unconservative results and that the SVGM should be considered. Later Kim and Feng (2003), following the aforementioned work, and based on the findings of Shinozuka *et al.* (2000) that the structural response of the piers of multi-span highway bridges is generally underestimated if the SVGM is ignored, worked towards the development of fragility curves that could account for the differential motion of the supports in the direction perpendicular to the axis of the bridge. The authors also concluded that the ductility demand of the piers of bridges can be underestimated if the differential movement of the supports is neglected. This was later verified by Lupoi *et al.* (2005) who emphasised the need to draw general conclusions and, to a certain extent, identify any underlying trends regarding the effect of the SVGM on the nonlinear structural response of long bridges. To this end, the authors examined a set of 27, 200-m long, prestressed concrete, box-girder highway bridges with four spans (50-m long each), two combinations of deck and pier sections and various pier heights. In terms of the SVGM their work considered the wave passage, incoherence and site response effects. The results showed that the multi-support excitation increased the ductility demand at the base of the piers in the majority of cases. In some cases the probability of failure in a particular bridge varied significantly (by more than one order of magnitude) when compared to the respective failure probability from the identical support motion for specific combinations of the adopted parameters for the SVGM. Very recently, Zhong *et al.* (2017) used the fragility analysis approach to predict the vulnerability of a cable-stayed bridge whose supports were subjected to differential ground motions. They also considered the three important components of the SVGM and concluded that the SVGM increased the fragility of the pylons. More specifically, the site response effect seemed to be more important than the wave passage or the incoherence effects in that study. The authors also concluded that the cable-stayed bridge was more susceptible to damage in the direction perpendicular to the deck rather than in the direction parallel to it.

Multi-Modal Contribution

When Abdel-Ghaffar and Rubin (1983a) studied the lateral response of the Golden Gate suspension bridge in California, they found that in order to capture a sufficiently accurate

[1]Deodatis *et al.* (2000) selected a five-span continuous reinforced concrete bridge with a total length of 245 m, and Saxena (2000) and Saxena *et al.* (2000) analysed the 500-m long, twelve-span Santa Clara Bridge in California.

response of the bridge subjected to lateral multi-support excitations[1] a large number of vibration modes was necessary among which, several were antisymmetric and of higher order.

The SVGM is reportedly responsible for the increased contribution of higher-order and mainly antisymmetric vibration modes to the structural response (Tzanetos *et al.* 2000, Sextos 2001). Symmetric structures do not behave symmetrically when subjected to multiple excitations of their supports. In a symmetric structure the multi-support excitation may excite antisymmetric modes (Zerva 2009) which do not contribute to the structural response of the bridge when identical support excitation is considered (Camara and Efthymiou 2016, Papadopoulos and Sextos 2018). In fact, recent studies on the continuously monitored[2] 395-m long Evripppos cable-stayed bridge in Greece showed that vibration modes that were dominant under the assumption of identical support motion were de-amplified when the SVGM was considered (Sextos *et al.* 2014), which emphasises the unpredictable effect of the SVGM. These findings suggest that the SVGM has a fundamentally different effect on structures from a vibrational viewpoint. Consequently, it has not been possible yet to develop a general pattern to predict the response of the structure under multi-support excitation based on the assumption of identical motion of the supports. However, Sextos and Kappos (2008) proposed an approximate methodology based on the statistical analysis of the seismic response of 27 highway bridges that were subjected to multi-support excitations. The simplified methodology consisted of four steps and it was directly associated with the higher-order modes that are excited when the SVGM was considered:

Step 1. Perform modal analysis to identify the principal vibration modes of the bridge and their participation factors.

Step 2. Identify higher-order modes that are likely to be excited by the SVGM and the structural components that are most affected by those vibration modes.

Step 3. Perform dynamic analysis of the bridge ignoring the multi-support excitation.

Step 4. Increase the resulting displacements and internal forces *only at the sections which*, based on Step 2, *are affected by the identified higher-order modes*.

The increase is estimated through the proposed coefficient R, as defined below:

[1]The authors utilised recorded data from arrays No. 4, 5, 6, 7 and 8 of the Imperial Valley Earthquake in California ($M_w = 6.6$ of October 15th, 1979). Closely spaced arrays such as the ones discussed in Section 2.3.2 provide records that can be used as input motions to the supports of a structure provided that the distance between supports coincides with the distance between array stations and that the soil and earthquake characteristics between the area in which the earthquake was recorded and the area of the structure are similar.

[2]An accelerometer array consisiting of 43 triaxial sensors was installed on the Evripppos bridge in 1994 and has been monitoring the free-field excitation and the response of the superstructure in a series of earthquakes since then (Sextos *et al.* 2014).

$$R = \frac{0.0005 \cdot L}{a \cdot b \cdot c} + 1.0 < 2.0 \tag{2.26}$$

in which L is the total length of the bridge, a is a parameter associated with the response quantity and the structural component under consideration, b is linked with the number of different soil categories that are met at the foundations of the bridge and c denotes whether the bridge is curved or not. The proposed values of a, b and c are listed below:

$$a = \begin{cases} 1.3 & \text{when the displacement of the deck is examined} \\ 1.0 & \text{when the internal forces at the piers' sections are examined} \end{cases}$$

$$b = \begin{cases} 1.0 & \text{for uniform soil conditions (1 soil category)} \\ 0.8 & \text{for soil conditions corresponding to 2 soil categories} \\ 0.5 & \text{for soil conditions corresponding to > 2 soil categories} \end{cases}$$

$$c = \begin{cases} 1.0 & \text{for straight bridges} \\ 0.6 & \text{for curved bridges} \end{cases}$$

Control of the Seismic Response of Structures Subjected to the SVGM

The complex and strongly coupled response of cable-stayed bridges makes the task of controlling them equally complex. Dyke *et al.* (2003) established a benchmark problem whose aim was to develop control strategies and methodologies appropriate for cable-stayed bridges and to provide a benchmark result to help future research works. The authors utilised the 'benchmark' Bill Emerson Memorial Bridge[1] which is presented in Fig. 2.10 and they examined it on the basis of the efficiency of various control strategies on cable-stayed bridges, including passive, active, semiactive control startegies or a combination thereof. More recently, Abdel Raheem *et al.* (2011) extended this research by considering the multi-support excitation. The motivation behind their research was the need to design a control system for cable-stayed bridges that could also account for the pseudo-static component of the structural response when the SVGM is considered. The bridge was found to perform well under the assumption of identical support motion when passive, semi-active and active control devices were adopted. However, the larger contri-

[1]The Bill Emerson Memorial Bridge spans the Mississippi River near Cape Girardeau in Missouri. It has a total length of 1206 m. It has a cable-stayed part with a main span reaching of 350.6 m in length, 142.7-m long side spans, and an approach bridge from one side (from Illinois) that is 570 m long. The cable-stayed bridge is composed of two 'H'-shaped pylons, 128 cables arranged in two planes and in a semi-harp and a 29.3-m wide composite open section deck.

bution of high-order and mainly antisymmetric vibration modes triggered by the SVGM and the pseudo-static component of the structural response could not be efficiently controlled. Therefore, control strategies designed based on the assumption of synchronous motion may prove inadequate when multiple excitation of the supports is considered and according to the authors' opinion codes of practice must be updated to accommodate the SVGM.

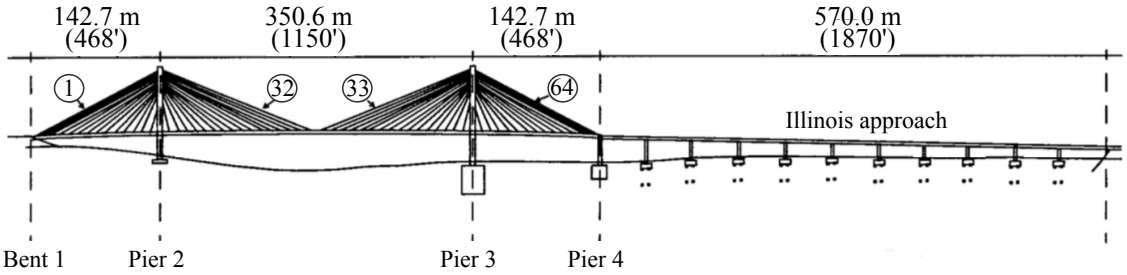

Figure 2.10: The 'Benchmark' Bill Emerson Memorial Bridge.

In this context, Papadopoulos and Sextos (2018) examined, from a vibrational point of view, the effect of the SVGM on the seismic response of the Lissos River Bridge, an 11-span base-isolated reinforced concrete bridge with an overall length of 433 m. They examined the effect of the multi-support excitation on the dynamic component of the response which is the one affecting seismically isolated bridges. They found that when the wave passage effect was examined alone the unfavourable effect of the SVGM was concentrated on the last piers in the direction of the earthquake propagation. On the other hand, when the incoherence component of the SVGM was considered the effect of the asynchronous excitation was more uniformly distributed among the piers. More importantly, they concluded that in most cases wherein SVGM was found to be unfavourable on the response quantity under consideration, an antisymmetric mode involving the vibration of those parts of the bridge that were affected by the SVGM was excited. Nevertheless, the opposite was not verified in the case of the Lissos Bridge.

2.3.6 Effect of the Soil-Structure Interaction

As mentioned in Section 2.3.5, the effect of the SVGM depends on the stiffness of the surrounding soil, among other factors. This effect can be important in bridges that are skewed or curved. Previous studies on these types of bridges by Lou and Zerva (2004), Sextos *et al.* (2004) and Burdette *et al.* (2006) have shown that apart from the geometry of the bridge, the flexibility of the foundation can affect the impact of the seismic waves on the structure. When the fundamental vibration frequency of the structure coincides with the fundamental vibration frequency of the underlying soil layer, the dynamic component of the response is dominant (Bi *et al.* 2010). It is noted that in some cases the multi-support excitation can significantly modify the response of the bridge in terms of displacements,

but whether the effect is beneficial or detrimental to the structural response of the bridge cannot be predicted beforehand.

The SVGM is closely linked with the effect of the interaction of the foundation with the surrounding soil and the structure, most commonly referred to as Soil-Structure Interaction (SSI). The bridge interacts with the surrounding soil during the earthquake imposing soil deformations which, in turn, cause the motion of the interface between the structure and the soil to differ from the respective motion in the free field (Clough and Penzien 2015). The flexibility of the foundation soil allows it to interact with the structure in a way that results in energy dissipation defined as kinematic interaction, and at the same time inertial forces are present due to the vibration of the structure which is defined as inertial interaction (Sextos *et al.* 2004).

The effect of the SSI has gained increasing attention because of the increasing number of structures, bridges in particular, that are constructed on soft soils. The interaction of the structure with the surrounding soil may alter the dynamic response of the structure and hence it is suggested that this interaction is combined with the multi-support excitation (Soyluk and Sicacik 2011). The effect of the SSI on the seismic response of a structure is dependent on the properties of the foundation soil and on the properties of the structure (Kawano and Furukawa 1988). It tends to elongate the fundamental period of the bridge-foundation-surrounding soil system and for this reason it can influence the internal forces in a structure, especially if the foundation soil is characterised by vibration frequencies that are close to the important frequencies of the structure (Spyrakos 1992, Abdel Raheem and Hayashikawa 2003). Given that the elongation of the structural period and the frequency content of the earthquake depend on the surrounding soil conditions, the effect of the SSI in the case of the seismic excitation becomes more complex (Khan *et al.* 2004b).

Sextos *et al.* (2004) identified the effect of the interaction of the bridge foundation with the surroundng soil as the fifth component of the SVGM, along with the wave passage, incoherence, site response and attenuation effects (discussed in Section 2.3.1). The modified (from the SVGM) seismic waves that reach the supports of the bridge can be further altered by the vibration of the foundation relative to the surrounding soil. The effect of the SSI on the seismic response of a bridge is a multi-parametric problem that is dependent on the intensity of the ground motion, the governing frequencies of the surrounding soil and of the structure, the incidence angle of the seismic waves and the stiffness and damping of the soil and of the structure, among others. Unfortunately, this complex problem cannot be generalised and it must be addressed on a case-by-case basis, so that its detrimental or beneficial impact on the seismic response can be evaluated (Pender 1993, Wolf 1994, Gazetas and Mylonakis 1998, Sextos *et al.* 2004). A more practical and simplified approach that falls between the detailed consideration of the SSI and the simplistic consideration of the supports as completely fixed, is to represent the effect of the surrounding

soil with springs and dashpots. However, this hinders the risk of not representing effectively the dynamic stiffness of the soil. Zheng and Takeda (1995) noted that springs are an adequate representation of the surrounding soil if its dominant frequency is relatively low and this would be applicable to cable-stayed bridges that are founded on soft soils, which are typically governed by low fundamental frequencies. In the present thesis the large number of different bridge models that have been employed suggests the use of springs and dashpots to model the SSI, as will be discussed in detail in Chapter 4.

2.3.7 Effect of the Incidence Angle of the Seismic Waves

A number of studies have been conducted on the influence of the angle of incidence of the seismic waves on the structural response of bridges with multiple configurations. The combination of the incidence angle with the SVGM has started to gain the attention of the research community, with different works stating that the maximum value of the response quantity under consideration may not occur when the direction of propagation coincides with the principal axes of the bridge. Allam and Datta (2004) examined a 335-m span cable-stayed bridge with different orientations with respect to the propagation of the earthquake and subjected to ground motions whose rate of correlation depended on the incidence angle of the seismic waves (a). When the ground motion's incidence angle was $a = 0°$ the major horizontal component of the earthquake coincided with the axis of the deck, whereas when $a = 90°$, the moderate horizontal earthquake component was parallel to the deck, as can be observed in Fig. 2.11, and the seismic waves were considered completely correlated ($|\gamma| = 1$). The minor component of the earthquake was considered in the vertical direction regardless of a. They observed that there existed critical orientations of the bridge, which depended on the response quantity of interest and the region of the bridge under consideration, in which the structural response was larger than the obtained one when the ground motion coincided with the principal directions of the bridge. By examining the same cable-stayed bridge, Khan (2012) observed that under the assumption of three-directional and partially correlated seismic motions, the structural reliability[1] of the bridge was minimised when the major earthquake component coincided with the axis of the bridge ($\theta = 0°$) because in this orientation the ground motions at the different supports presented the lowest correlation and the stress in the bridge was maximised.

Sextos *et al.* (2004) examined the effect of the angle of incidence on the curved Kristallopigi Bridge in Greece, which has a curvature radius of 488 m. The authors verified that in terms of displacements at the piers and at the abutments the maximum values where not obtained when the earthquake propagated parallel or perpendicular with re-

[1]The structural reliability of a structure can be viewed as the qualitative assessment of its structural safety within a probabilistic context.

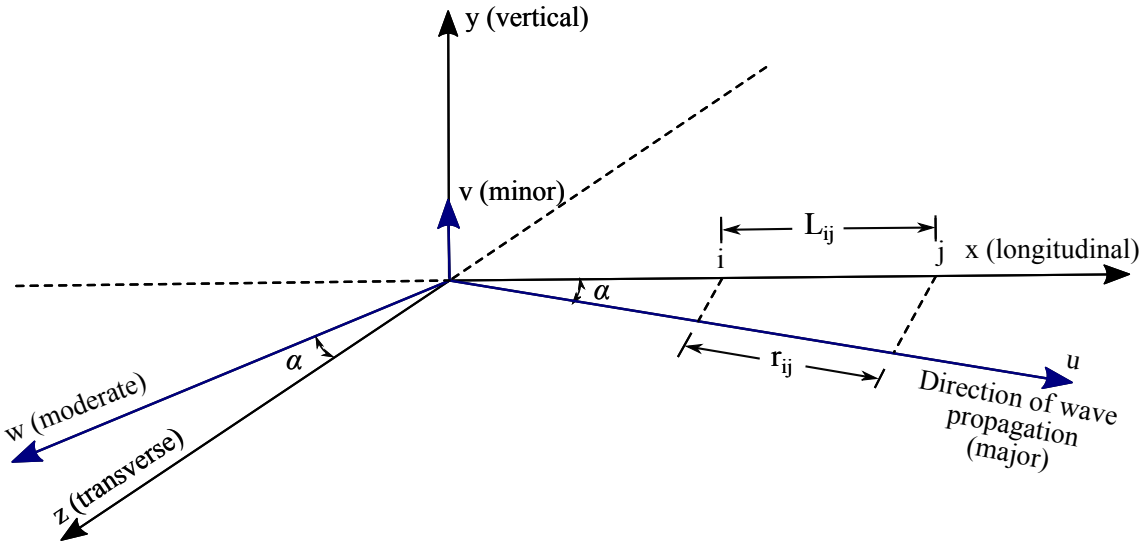

Figure 2.11: Principal axes of the 335-m span cable-stayed bridge (x, y, z) and the principal directions of the ground motion (u, v, w); a is the incidence angle of the seismic waves (*taken from Allam and Datta (2004)*).

spect to the bridge's chord. They pointed out, though, that when the wave passage effect is involved in the assessment of the effect of the SVGM on the seismic response of this particular bridge, the time delay is a more important parameter to address.

Moschonas and Kappos (2012) derived multi-directional pushover curves accounting for the interaction between the axial force and the biaxial bending moments at critical pier sections or the biaxial shear forces at the bearings. The influence of the incidence angle of the earthquake propagation was identified but it was dependent on whether only one or both horizontal earthquake components were considered, as well as on the number of ground motions considered.

Mackie *et al.* (2011), on the other hand, stated that for highway bridges subjected to multi-angle, bi-directional excitations the effect of the angle of incidence of the ground motion may be negligible, at least when assessing the fragility at the individual component level rather than at the bridge-system level. Taskari and Sextos (2015) examined the effect of the multi-angle earthquake propagation on the fragility of a constructed 99-m long, three-span highway bridge and concluded that, contrary to Mackie *et al.* (2011), the seismic performance of this bridge was strongly influenced by its orientation with respect to the fault. In fact, they found that the angle of incidence was an important aspect in the fragility analysis of this bridge because not only it influenced the individual fragilities of different structural components, it was also inherent in cases in which the fragility analysis seemed independent of the angle of incidence. In those cases, the mechanism that produced the damage was dependent on the angle of incidence.

Despite the above, the effect of the incidence angle of the earthquake on the structural response of cable-stayed bridges subjected to multi-support excitation has not gained

sufficient attention yet. To this end, the present research attempts to incorporate this aspect of the ground motions in the seismic analysis of cable-stayed bridges with various pylon, deck and cable-system configurations in an attempt to draw general and practical conclusions regarding the combined effect of the SVGM and the incidence angle of the earthquake, θ.

2.3.8 Existing Analysis Methods Accounting for the SVGM

Up to this point the effect of the multi-angle, multi-support excitation on the seismic response of different types of bridges has been discussed, but a fundamental question remains; When must the SVGM be considered and how should it be accounted for in bridge design? This twofold question this section.

Most international guidelines, such as the American AASHTO (1996) and ATC32 (1996) and the Japanese JRA (2002) only deal with this phenomenon from the viewpoint of seating length criteria and avoid to determine conditions under which the SVGM should be considered in the seismic analysis or not. On the other hand, the European Eurocode 8; Part 2 (2005) includes provisions on the consideration of this effect in the analysis. More specifically, according to Eurocode 8; Part 2 (2005), the SVGM must be considered in the design of bridges with continuous decks when at least one of the following applies:

a. The supports of the bridge are founded on different soils such that they can be categorised as different soil categories based on the soil categorisation of Eurocode 8; Part 1 (2004).

b. The length of the continuous deck exceeds the limiting length $L_{\text{lim}} = L_{\text{g}}/1.5$ depending on the ground type. L_{g} is the maximum distance beyond which, the ground motions may be considered completely uncorrelated as included below:

Ground Type	**A**	**B**	**C**	**D**	**E**
L_{g} [m]	600	500	400	300	500

Table 2.2: Eurocode 8; Part 2 (2005) prescribed values on the distance beyond which ground motions may be considered uncorrelated.

The consideration of the SVGM in the seismic analysis can be approached from a deterministic or from a stochastic point of view (Shinozuka *et al.* 2000). A deterministic approach only accounts for the wave passage effect in terms of delaying the ground motion time-history depending on the distance between different supports and the waves' velocity of propagation. On the other hand, a stochastic approach considers ground motion time histories at different stations to be modelled as stochastic vector processes with prescribed spectral characteristics at each station. Such processes can take account of the

incoherence and the site response effects of the SVGM, by considering a loss of coherency model for the lagged coherency and the wave propagation through an exponential term.

Preliminary Design Method

Priestley *et al.* (1996) proposed a simplified methodology for the consideration of the SVGM in the early stages of the design in order to assess roughly the influence of the out-of-phase motion of the supports of long structures. The methodology is based on the assumption that the seismic waves are completely correlated and hence the asynchronism is only due to the difference in the arrival times of the seismic waves at consequent supports (wave passage effect). Delayed ground displacements are considered that are assumed to first reach the foundation of the support that is closest to the epicentre of the earthquake. The difference in the arrival times between adjacent supports or in other words the time lag Δt in [s], is a function of the distance L between the supports in [m] and of the wave velocity, v_s in [m/s]:

$$\Delta t = \frac{L \cos \theta}{v_s} \tag{2.27}$$

The delay is proportional to the distance between the supports while it is reduced for higher values of v_s, and for infinite velocity the supports are synchronously excited. The delay is also dependent on the orientation of the long structure with respect to the epicentral area by means of the incidence angle θ in a similar manner as the loss of coherency according to Allam and Datta (2004) in Section 2.3.7. When the propagation of the earthquake is parallel to the axis of the structure, and $\theta = 0°$, the delay is maximised but when the structure is rotated by 90°, the ground motion may reach all the supports of the bridge simultaneously:

Multiple Support Response Spectrum Method

Based on the priciples of the random vibration theory, Der Kiureghian and Neuenhofer (1992) developed the Multiple Support Response Spectrum (MSRS) combination rule for the evaluation of the mean maximum response of linear, MDoF structures with multiple supports that are subjected to multi-support excitation. This methodology accounts for the three important components of the SVGM; the wave passage, incoherence and site response effects. It also allows for the cross-correlations between the motions at different supports that arise from the SVGM and between the different vibration modes of the structure and for the combination of the dynamic and pseudo-static components of the response.

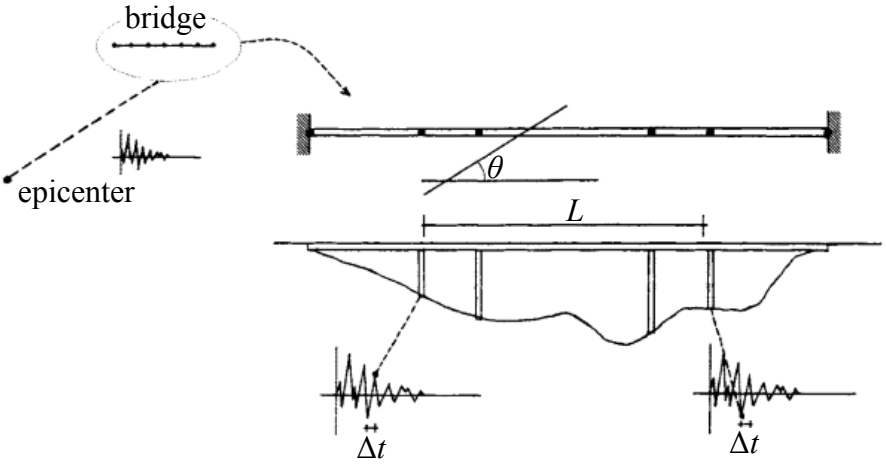

Figure 2.12: Asynchronous motion of the supports of bridges and the effect of the incidence angle (*taken from Priestley et al. (1996)*).

Let m and n represent two supports at a distance l_{mn} apart and that i and j are two oscillators at supports m and n, respectively. Each oscillator has unit mass, circular frequency ω in [rad/s] and damping ξ. The proposed model assumes seismic excitations to be zero-mean, stationary stochastic processes[1] of time. To calculate the expected maximum response ($E[\max|\cdot|]$), displacement response spectra are applied to the different support degrees of freedom of the structure and coherency functions are adopted to describe the variation between support motions:

$$\begin{aligned} E[\max|z(t)|] \approx \Bigg[& \sum_{m=1}^{S}\sum_{n=1}^{R} \alpha_m \alpha_n \rho_{u_m u_n} u_{m,\max} u_{n,\max} \\ & + 2\sum_{m=1}^{R}\sum_{n=1}^{R}\sum_{j=1}^{N} \alpha_m b_{nj} \rho_{u_m s_{nj}} u_{m,\max} D_n(\omega_j,\xi_j) \\ & + \sum_{m=1}^{R}\sum_{n=1}^{R}\sum_{i=1}^{N}\sum_{j=1}^{N} b_{mi} b_{nj} \rho_{s_{mi} s_{nj}} u_{m,\max} D_m(\omega_i,\xi_i)\, D_n(\omega_j,\xi) \Bigg]^{1/2} \end{aligned} \tag{2.28}$$

in which N is the number of the unconstrained degrees of freedom, R is the number of the support degrees of freedom, a_m and a_n are effective influence factors, b_{mi} and b_{nj} are effective modal participation factors at supports m and n for the i^{th} and j^{th} modes, respectively, $\rho_{u_m u_n}$ is the cross-correlation coefficient for the ground displacements, $u_{m,\max}$ and $u_{n,\max}$ are the mean peak ground displacements at m and n, respectively, $\rho_{u_m s_{nj}}$ is the cross-correlation coefficient between the ground displacement at support m and the oscillator response at n for the j^{th} mode, $D_m(\omega_i,\xi_i)$ and $D_n(\omega_j,\xi_j)$ are the displacement

[1]The theory and basic definitions of stationary processes and stochastic processes are presented in Appendix A.

response spectra applied to m and n, expressed as the expected values of the peak absolute response of the assumed oscillators i and j with properties (ω_i, ξ_i) and (ω_j, ξ_j), respectively and $\rho_{s_{mi}s_{nj}}$ is the cross-correlation coefficient for the i^{th} and j^{th} oscillator responses at m and n, respectively. The first term (double-sum term) in the right-hand side of Eq. (2.28) represents the pseudo-static component of the response, the second term (triple-sum term) is a cross-term of the pseudo-static and the dynamic components and the third term (quadruple-sum term) represents the dynamic component of the response.

The MSRS combination rule has proven a reliable method of analysis that captures the response of a structure subjected to multiple support excitations when compared to the response history analysis and, more importantly, it reduces the computational cost compared to the latter analysis method. However, since the response spectrum methods focus on obtaining the maximum seismic response, the history of the response is lost. The combination of modal maxima to obtain the global response may introduce errors because these maximum response values do not occur at the same time. Furthermore, the nonlinear behaviour of the materials cannot be captured in response spectrum methods, limiting their application mainly to linear problems.

Response History Analysis

The response of a structure under any kind of dynamic loading may be evaluated in the time domain by employing the step-by-step integration of the equation of motion. In the simple case of a linear SDoF system with mass m, damping c, and stiffness k, subjected to an earthquake excitation $\mathrm{m}\,\ddot{\mathrm{u}}_{\mathrm{g}}$, the generalised equation of motion at a specific time instance, t_i, can be described by Eq. (2.29), with $\ddot{\mathrm{u}}_i$, $\dot{\mathrm{u}}_i$ and u_i being the acceleration, velocity and displacement of the SDoF system respectively at $t = t_i$:

$$\mathrm{m}\,\ddot{\mathrm{u}}_i + \mathrm{c}\,\dot{\mathrm{u}}_i + \mathrm{k}\,\mathrm{u}_i = -\,\mathrm{m}\,\ddot{\mathrm{u}}_{\mathrm{g}i} \tag{2.29}$$

The excitation force $\mathrm{m}\,\ddot{\mathrm{u}}_{\mathrm{g}i}$ is considered as a sequence of short-duration ($\mathrm{d}t$) pulses, whose individual contributions to the response, when combined, result in the overall response of the structure at any subsequent time increment t_{i+1} (Chen and Duan 2014, Clough and Penzien 2015). Hence, to obtain the overall response of the structure to $\mathrm{m}\,\ddot{\mathrm{u}}_g$, the total of the short-duration pulses can be integrated in the time domain, which leads to a step-by-step integration of the equation of motion (Eq. (2.29)). During each time step the system of dynamics is considered a linear system with the stiffness characteristics that exist at the beginning of the time step. At the end of the time step the system characteristics are re-evaluated to obtain the new tangent stiffness matrix that will be used as initial condition in the next time step ($t_{i+1} = t_i + \mathrm{d}t$) (Clough and Penzien 2015).

In more general MDoF systems, the equation of motion (which has been introduced in Eq. (2.21)) at $t = t_i$ is extended to:

$$[\mathbf{M}]\{\ddot{\mathbf{u}}_i\} + [\mathbf{C}]\{\dot{\mathbf{u}}_i\} + [\mathbf{K}]\{\mathbf{u}_i\} = -[\mathbf{M}]\{\boldsymbol{\iota}\}\{\ddot{\mathbf{u}}_{g,i}\} \tag{2.30}$$

in which $[\mathbf{M}]$, $[\mathbf{C}]$ and $[\mathbf{K}]$ are the mass, damping and stiffness matrices, respectively, $\{\ddot{\mathbf{u}}_i\}$, $\{\dot{\mathbf{u}}_i\}$ and $\{\mathbf{u}_i\}$ are the acceleration, velocity and displacement vectors, respectively, $[\mathbf{M}]\{\boldsymbol{\iota}\}\{\ddot{\mathbf{u}}_{g,i}\}$ is the support excitation and $\{\boldsymbol{\iota}\}$ is the influence vector which defines the degrees of freedom to which the earthquake is applied. To proceed to the next time increment, Eq. (2.30) is solved, resulting in the equation of motion for time instance t_{i+1} and for a time step dt:

$$[\mathbf{M}]\{\ddot{\mathbf{u}}_{i+1}\} + [\mathbf{C}]\{\dot{\mathbf{u}}_{i+1}\} + [\mathbf{K}]\{\mathbf{u}_{i+1}\} = -[\mathbf{M}]\{\boldsymbol{\iota}\}\{\ddot{\mathbf{u}}_{g,i+1}\} \tag{2.31}$$

For the step-by-step integration of Eqs. (2.29) and (2.30), several methodologies have been proposed. Among them, the most commonly used is the one proposed by Newmark (1959) and a later extension proposed by Hilber *et al.* (1977). The Response History Analysis (RHA) is a rigorous tool to evaluate the dynamic response of a structure in the linear and nonlinear ranges by providing time-histories of the response quantities under a specific ground motion. To perform this type of analysis, sets of carefully selected, natural or synthetic acceleration histories must be applied to the supports of the structure. The RHA is an accurate tool to capture the inelastic behaviour of a structure in that it can account for geometric and material nonlinearities. However, the computational cost that is required to perform this type of analysis, combined with the detailed mathematical models necessary to describe the cyclic load-deformation relationships in all structural elements may not justify the application of this method in the early stages of the design process (Priestley *et al.* 1996, Krawinkler and Seneviratna 1998).

Soyluk *et al.* (2004) examined the influence of different types of analysis on a cable-stayed bridge accounting for the multi-support excitation. They compared the results obtained from stochastic and deterministic analyses. Among the stochastic approaches, one was a spectral analysis based on the PSD function of the ground motion. The second approach was the MSRS developed by Der Kiureghian and Neuenhofer (1992) and the third approach was the one proposed by Allam and Datta (2000) based on the relationship between the PSD function and the response spectrum of the input ground motion and the fundamentals of the random vibration theory. Soyluk *et al.* (2004) found that the deterministic method, being based on absolute maximum response quantities, provided a higher structural response compared to the frequency domain analyses which provide mean of absolute maximum values.

2.3.9 International Code Provisions

International Provisions and Guidelines based on Seating-Length

The complex and unpredictable nature of the earthquake in general, and of the SVGM in particular, involves a great amount of uncertainty in considering it in the seismic design and analysis of long structures. Engineers may choose to neglect its effect on the structural response because the uncertainty that arises when trying to model the SVGM is higher than that when ignoring the phenomenon altogether (Sextos 2013). However, it has been proven by now that ignoring the multi-support excitation may underestimate the structural response. International code provisions have addressed this phenomenon by including guidelines with varying complexity among them, but in a manner that would be easily applicable by the engineer.

Sextos and Kappos (2009) performed a detailed study on the different code provisions and guidelines for the SVGM. They found that several current codes of practice such as the American AASHTO (1996) and ATC32 (1996), and the Japanese JRA (2002) deal with the phenomenon only in terms of increased seating lengths. The first and most intuitive cause of failure of a bridge because of the SVGM is the collapse of the superstructure because of the differential movement of the supports, especially in bridges that are composed of simply supported beams (Novak *et al.* 2015), which justifies the emphasis put on increasing the seating length.

AASHTO (1996) defined a minimum seating length N_s for the expansion ends of girders as a function of the length L of the deck in [m], the height H of the pier in [m] and the skew angle α_s of the support in [°] as follows:

$$N_s\,(\text{in mm}) = \begin{cases} (203 + 1.67L + 6.66H)\left(1 + 0.000125\alpha_s^2\right) & \text{for SPC}_{A,B} \\ (305 + 2.50L + 10.0H)\left(1 + 0.000125\alpha_s^2\right) & \text{for SPC}_{C,D} \end{cases} \tag{2.32}$$

in which N_s is estimated based on the Seismic Performance Category (SPC) A, B, C or D as defined in AASHTO (1996).

In a similar manner ATC49/MCEER (2003) proposes a formula for the calculation of the minimum seating length:

$$N_s\,(\text{in mm}) = \left[0.10 + 0.0017L + 0.007H + 0.05\sqrt{H}\cdot\sqrt{1+\left(2\frac{B}{L}\right)^2}\right]\frac{1+1.25F_vS_1}{\cos\alpha_s} \tag{2.33}$$

$$\text{with } \frac{B}{L} \leq \frac{3}{8}$$

in which L is the distance between joints in [m], H is the height of the tallest pier between the considered joints in [m], B is the width of the superstructure in [m], α_s is the skew angle in [°], F_v is the site coefficient for the long-period branch of the design response spectrum and S_1 is the one-second period spectral acceleration. Furthermore if different soil conditions are found at the abutments and the intermediate piers then different response spectra should be defined for the different soil conditions and the envelope spectrum from the individual response spectra should be employed. Although the ATC49/MCEER (2003) does not provide any guidelines for the analysis procedure to account for the SVGM, it is included in the commentary of the document that the displacement demand should be increased by 50% to account for the effect of the SVGM on the demand and the capacity models and on the analysis procedures.

Finally, the JRA (2002) defines the seating length in terms of the differential displacement between the superstructure and the substructure, u_R in [cm], of the relative displacement of the ground that occurs due to ground deformation between piers, u_G in [cm] and of the clear span length, L in [m], as follows:

$$N_s\,(\text{in cm}) = u_R + u_G \geq 70 + \frac{L}{2} \tag{2.34}$$

Eurocode 8: Part 2 Provisions

Eurocode 8; Part 2 (2005) prescribes the use of the coherency functions of Luco and Wong (1986) and of Der Kiureghian (1996), as described in Section 2.3.4, and is in favour of the MSRS combination rule (Der Kiureghian and Neuenhofer 1992) and of the RHA.

Based on the finding that the response of a long structure under multi-support excitation can be divided into a dynamic and a pseudo-static component (Eq. (2.22)) that is caused by the differential motion of the supports (Priestley *et al.* 1996), the code introduces another, yet more simplified, approach to consider the SVGM. The essence of the methodology is to consider the dynamic component of the response by imposing identical input motions at all the supports. The ground motions are defined by means of a single response spectrum or identical acceleration histories at all the supports, that correspond

to the worst soil type among the foundations. Next, the pseudo-static component of the response is obtained by applying two sets of displacements at the supports namely, 'Set A' and 'Set B', as shown in Figs. 2.13 and 2.14, respectively. These two sets are identified as the most critical cases among numerous combinations of relative displacements. Set A (Fig. 2.13) consists of relative displacements that are applied to all supports of the bridge and have the same direction, as follows:

$$d_{ri} = \varepsilon_r L_i \leq d_g \sqrt{2} \tag{2.35a}$$

$$\text{with } \varepsilon_r = \frac{d_g \sqrt{2}}{L_g} \tag{2.35b}$$

where d_g is the design ground displacement corresponding to the ground type of the i^{th} support, in accordance with Eurocode 8; Part 1 (2004), L_i is the projected horizontal distance of support i from the reference support ($i = 0$), which may be selected as one of the end supports, and L_g is the maximum distance beyond which, the ground motions may be considered completely uncorrelated, as presented in Table 2.3.8.

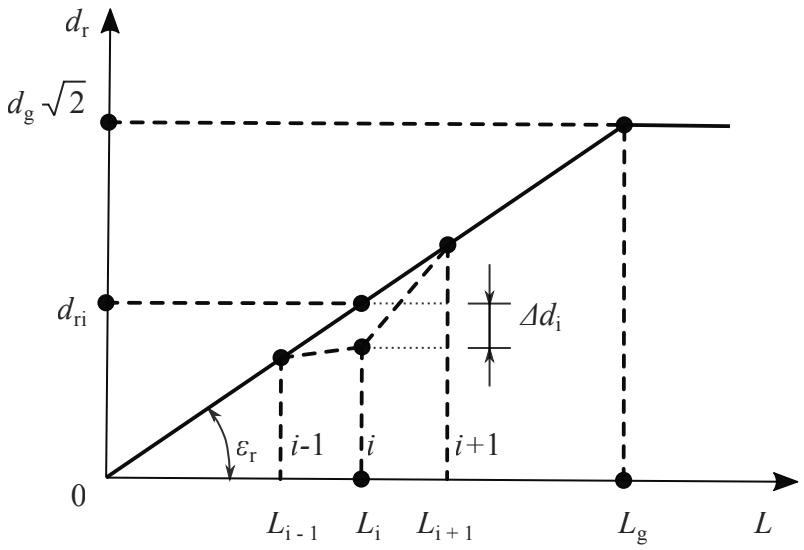

Figure 2.13: Prescribed Displacement Set A (*taken from Eurocode 8; Part 2 (2005)*).

Set B (Fig. 2.14) considers the influence of the ground displacements that take place in opposite directions at consequent supports by assuming the displacements (Δd_i) of any intermediate support i (with $i > 1$) relative to the adjacent supports ($i-1$) and ($i+1$) which are considered to undergo zero displacement:

$$\Delta d_i = \pm \beta_r \, \varepsilon_r \, L_{av,i} \tag{2.36}$$

in which $L_{av,i}$ is the average of the distances between the i^{th} support and the supports adjacent to it, ($i-1$) and ($i+1$) and β_r is a factor for the magnitude of the ground displace-

ments that take place in opposite directions at consequent supports. β_r equals 0.5 when the support under consideration and the two adjacent supports are founded on the same ground and 1.0 if the soil type is different.

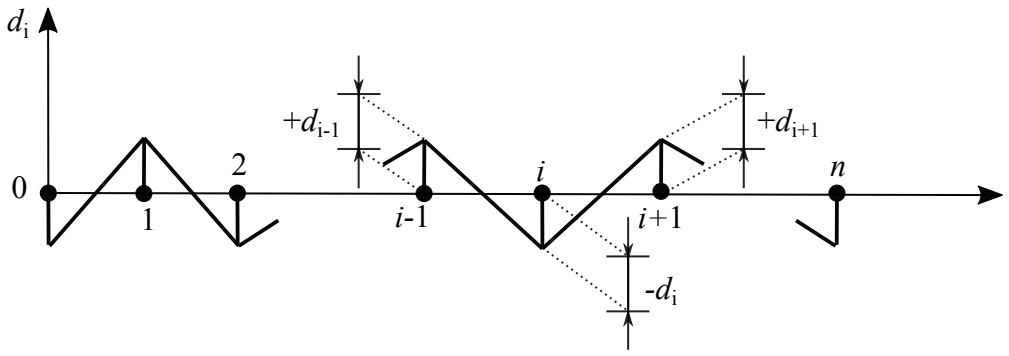

Figure 2.14: Prescribed Displacement Set B (*taken from Eurocode 8; Part 2 (2005)*).

For each direction of the bridge the maximum effects of the dynamic ('d') and pseudo-static ('ps') components of the response quantity r_i, with i representing the response quantity of interest must be combined by using the Square Root of Sum of Squares (SRSS) combination rule to obtain the final value of the response quantity R_i for each direction of the excitation as follows:

$$R_i = \sqrt{r_{i,d}^2 + r_{i,ps}^2} \tag{2.37}$$

This methodology has been deemed a step-forward attempt to consider the effect of the SVGM on bridges, compared to other international codes of practice and guidelines that limit their specifications on the problem to increased seating lengths (JRA 2002, AASHTO 1996, ATC32 1996). On the other hand, due to its essentially static nature, this approach has been criticised because it neglects the dynamic component that arises from the multi-support excitation and hence it cannot capture the influence of higher order vibration modes on the seismic response. This is particularly important in the case of seismically isolated bridges (Sextos and Kappos 2009, Papadopoulos and Sextos 2018). Moreover, the fact that maximum values from the dynamic and the pseudo-static analyses are combined by means of the SRSS combination rule can lead to significant underestimations of the effect of the SVGM, which may be unconservative (Nuti and Vanzi 2005, Sextos and Kappos 2009, Camara 2011). Finally, this approach cannot capture accurately the effect of the multi-support excitation on irregular or curved bridges and further improvements are deemed necessary (Nuti and Vanzi 2005, Sextos and Kappos 2009, Papadopoulos *et al.* 2013). Eurocode 8; Part 2 (2005) inherently assumes that the energy and the frequency content of the ground motion is reflected by the dynamic component and that the waveform of the time-series is accounted for through the static analysis. Based on this and on the previous discussion on the limitations of Eurocode's approach on the

consideration of the SVGM, Falamarz-Sheikhabadi and Zerva (2017) recently proposed a new displacement waveform resulting from the linear combination of three sinusoidal waves that correspond to the predominant ground displacement, velocity and acceleration. This approach can account for the propagation characteristics of the seismic waves, such as the wave passage and the incoherence effects of the SVGM improving the Eurocode's proposed pseudo-static displacement, which cannot account for those characteristics.

2.4 Conclusions

To conclude the discussion on the effect of the SVGM on the seismic response of different structural types, it has been established that the multi-support excitation reportedly affects the response of long structures, particularly if their supports are founded on different soil types, and clearly it cannot be neglected. However, the multi-parametric and complex character of this phenomenon has allowed for different assumptions and considerations to be made by different researchers on the basis of the definition of the SVGM, *per se*, and of the assessment of its effect on long structures. The effect of the SVGM needs to be accounted for in the seismic analysis of bridges because neglecting it might underestimate the response. This effect depends on the span length, the soil conditions at the supports and at the surrounding soils, the rigidity of the structure and the degree of redundancy (Nazmy and Abdel-Ghaffar 1992). Furthermore, its complex nature and the unpredictable effect on the structural response only has allowed to identify various trends without being able to establish a general and robust framework to deal with this phenomenon, not to mention that this uncertainty justifies to a certain extent the observed discrepancy among different approaches and the obtained results (Shinozuka *et al.* 2000).

The effect of the SVGM on the response of cable-stayed bridges has been established and discussed in detail in this chapter. These landmark structures are characterised by their extended length, high flexibility and by the fact that they are composed of elements with very different structural properties. These factors result in cable-stayed bridges having a complex seismic behaviour, which combined with the multi-parametric and uncertain nature of the SVGM, make the prediction of the seismic response of those structures a very difficult task. Furthermore, the pylons of cable-stayed bridges are responsible for the integrity of the complete structure and their integrity must be ensured even under very strong earthquakes. To this end, the aim of this thesis is to examine the seismic response of different pylon shapes with different dimensions against the multiple excitation of the supports and to provide practical conclusions on the basis of the effect of the SVGM on cable-stayed bridges with different configurations. The parameters that are examined herein are the velocity of propagation, the loss of coherency and the incidence angle of the seismic waves. In order to capture the history of the seismic response, the Response-History Analysis (RHA) is adopted to analyse the bridges under the effect of spatially

variable ground motions.

Chapter 3

Numerical Models

Contents

3.1 Introduction

The previous chapter presented an in-depth discussion of the concept of cable-stayed bridges and their unique characteristics compared to other types of bridges, which was accompanied by a detailed reference to the nature of the SVGM and to its effect on the structural response of long structures.

The aim of the this research is to draw general conclusions on the effect of the SVGM on the seismic response of cable-stayed bridges. This work differs from previous studies (introduced in Section 2.3.5) in the sense that it focuses on the response of the pylons, which represent key components of a cable-stayed bridge and are responsible for the structural integrity of the whole structure. However, the focus of this study is not placed upon a particular cable-stayed bridge. Instead, seven different pylon-cable system configurations are considered so that observations can be made on the basis of which configurations are more or less sensitive to the influence of the SVGM.

In order to have the most accurate results possible and to predict the response of the bridges in a way that will prove insightful, the models must be developed and validated with detail. This chapter presents the different aspects of the cable-stayed bridge models that are studied. It is introduced by a description of the geometric definition of the cable-stayed bridges, followed by the properties of the materials that compose each of their different parts and finally, the finite element discretisation of the structures is discussed.

3.2 Description of the Cable-Stayed Bridges

3.2.1 Geometric Considerations

The design of a cable-stayed bridge involves a long process of decision-making regarding the span length, the pylon shape, the cable-system and the geometry of the deck, among others. These decisions are dictated to a great extent, by the span that needs to be bridged, the site features and by environmental factors that will influence the bridge throughout its lifespan.

The bridge models employed in this study are based on previous works from Camara (2011), Camara *et al.* (2014) and Efthymiou and Camara (2015). Although the most important features of the models are discussed in this chapter, a more detailed discussion is included therein. The overall arrangement in each bridge model consists of two symmetric concrete pylons, a composite deck and the cable system. The most important considerations for the definition of the cable-stayed bridges in the present study are summarised in the following:

- **Main span length, L_P.** The length of the span between the centres of the two pylons takes values of 200, 400 and 600 m, representing a short-span, an intermediate-span and a relatively long-span cable-stayed bridge, respectively. The elevations and the side views of the three different bridges are presented in Figs. 3.1 and 3.2, respectively.

- **Pylon shape.** Pylons with conventional 'H'-, inverted 'Y'- and 'A'- shapes are considered, as shown in Fig. 3.3. In this figure the notation of the pylons is included and will be followed hereinafter. The part of the notation before the hyphen corresponds to the shape of the pylon. The letter 'D' stands for the lower diamond configuration which has been considered in the inverted 'Y'- and 'A'- shaped pylons.

- **Cable-system.** In the orientation parallel to the traffic the cables have been arranged in a semi-harp configuration, which constitutes the best solution in terms of structural efficiency and economy (Parke and Hewson 2008). In the transverse direction two different cable configurations have been considered in this research. The case of two Lateral Cable Planes (LCP) for all the pylon geometries and one Central Cable Plane (CCP) only in the inverted 'Y'-shaped[1] pylon with and without the lower diamond. The cable arrangement is included in the second part of the notation, after the hyphen, in Fig. 3.3.

- **Deck.** Two different deck sections have been examined whose shape is associated with the cable system configuration. When two LCP's are considered the cross section of the deck is an open section deck, as opposed to adopting a closed box section for the deck when one CCP is considered. Moreover, the width of the deck is equal to 25 m accommodating four traffic lanes, regardless of the length of the bridge.

A more detailed discussion of the different parameters of the bridges is included in the following sections. Altogether 21 bridge models are considered, with a typical example being included in Fig. 3.4.

[1] Among the pylon shapes proposed in this work the single central plane of cables is only feasible in the inverted 'Y'-shaped pylon, which features a single vertical member at the top.

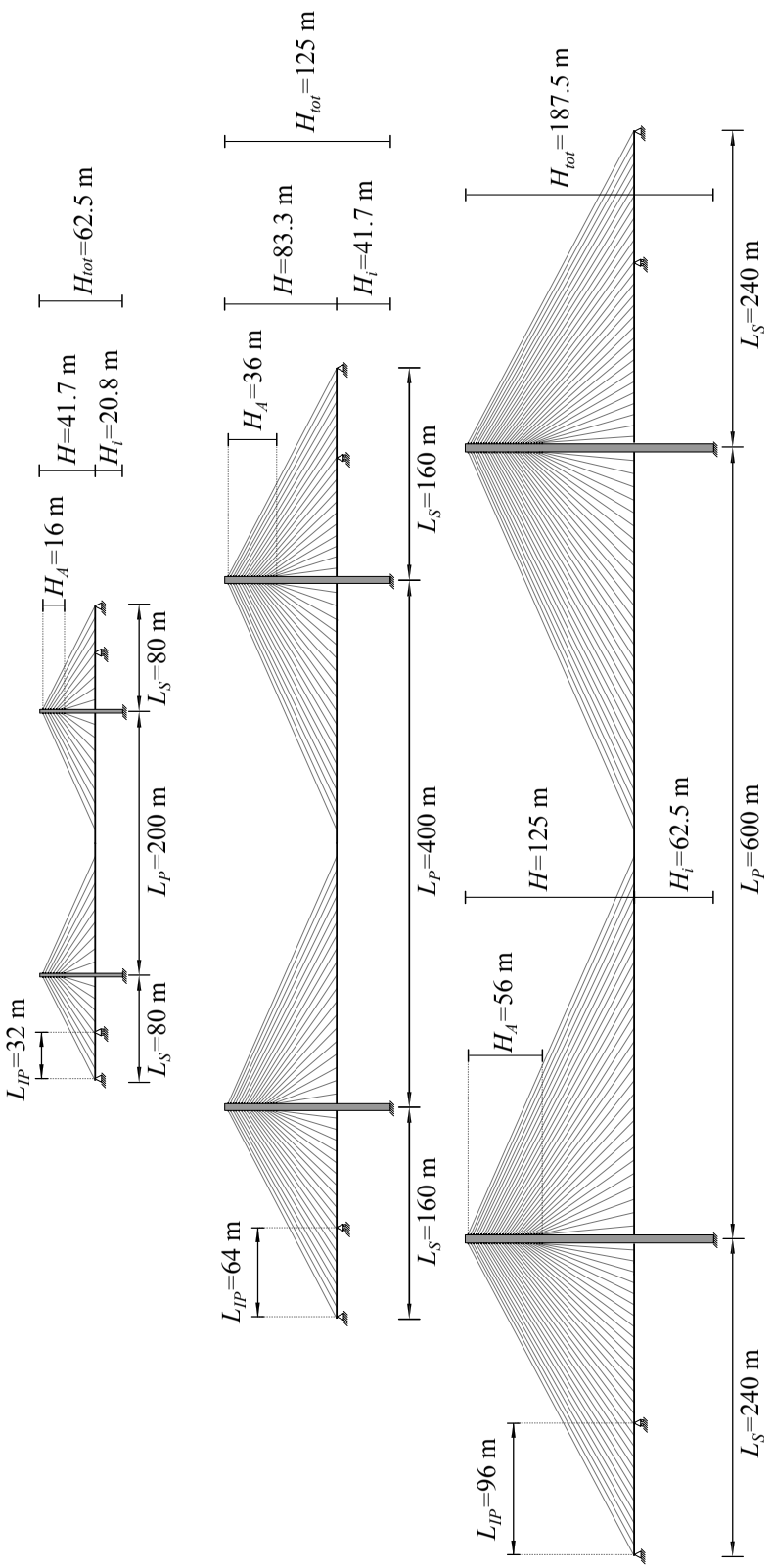

Figure 3.1: Elevations of the different cable-stayed bridge models.

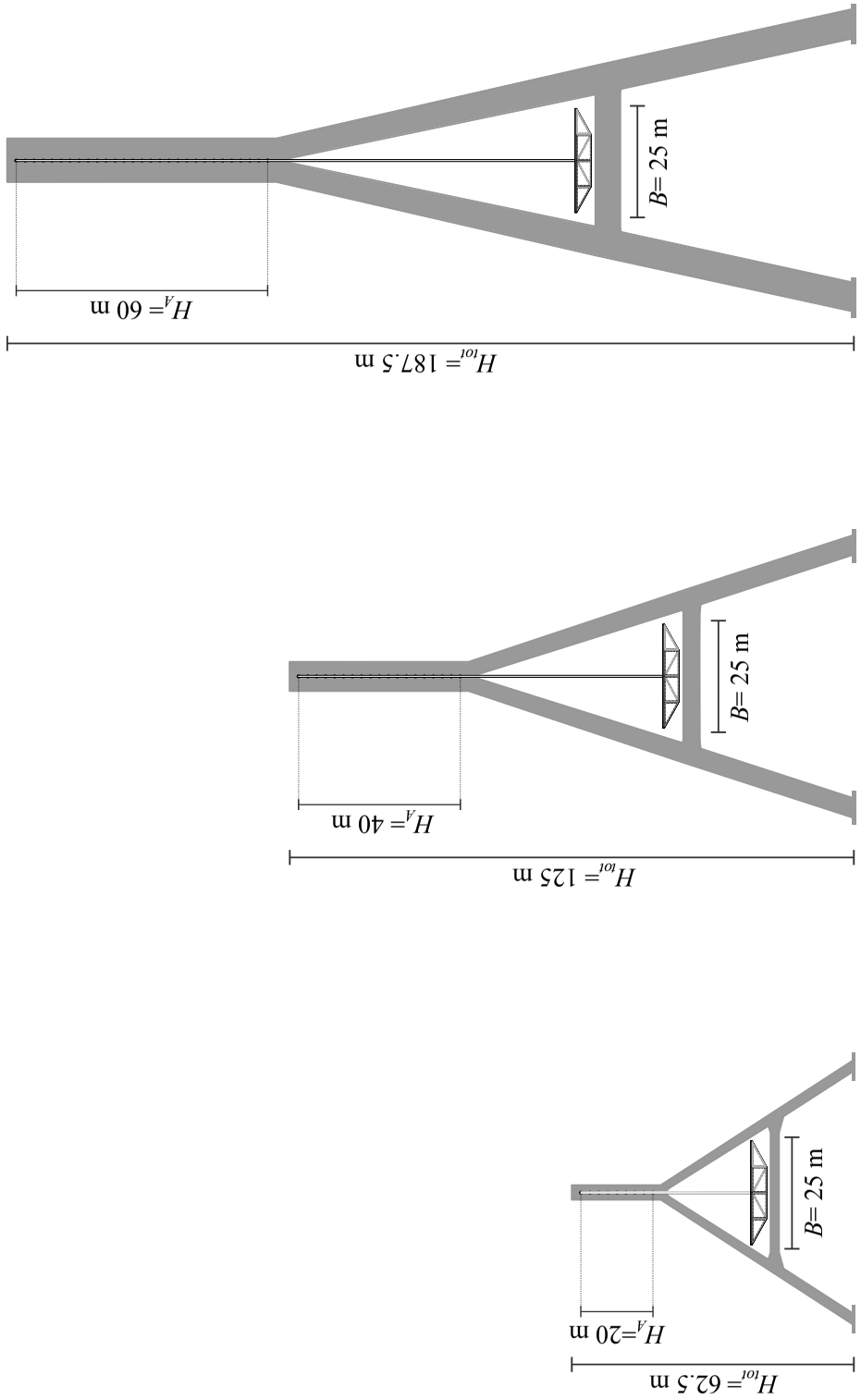

Figure 3.2: View of the inverted 'Y'-shaped pylon of the cable-stayed bridges with $L_P = 200$, 400 and 600 m.

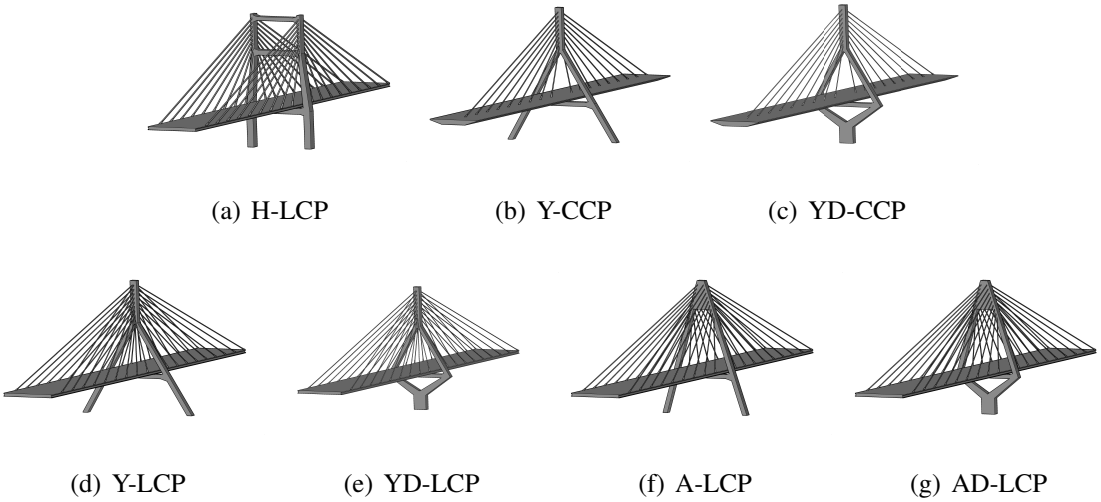

(a) H-LCP (b) Y-CCP (c) YD-CCP

(d) Y-LCP (e) YD-LCP (f) A-LCP (g) AD-LCP

Figure 3.3: Different pylon shapes and cable system arrangements considered in this work, along with the reference keywords.

The distance between the cable anchorages is $I_T = 2$ m in the pylon and approximately $\Delta_D = 10$ m in the deck (further details will be provided in the following sections). The complete structures, as seen in Fig. 3.5, present symmetry along the longitudinal (x, direction of traffic) and the transverse (y) directions. The dimensions of the complete bridges, including the pylons, deck and cable sections, are defined as functions of the main span length (L_P) according to Camara *et al.* (2014). The dimensions of the concrete pylon sections respond to those in constructed cable-stayed bridges. The parametric definition of the general bridge arrangement is shown in Fig. 3.5.

In the side spans vertical piers are considered by fixing the vertical displacement of the deck in order to control the longitudinal displacement of the upper part of the pylon where the cable system is anchored. The main span length defines the length of the side spans (L_S) and the distance from the end abutments where the intermediate piers are placed (L_{IP}), as shown in Fig. 3.5:

$$L_S = \frac{L_P}{2.5} \quad \text{and} \quad L_{IP} = \frac{L_S}{2.5} \tag{3.1}$$

Bridge Dimensions [m]					
L_P	L_S	L_{IP}	L_{tot}	$\Delta_{D,P}$	$\Delta_{D,S}$
200	80	32	360	10	8.9
400	160	64	720	10	8.4
600	240	96	1080	10	8.3

Table 3.1: Geometric characteristics of the considered cable-stayed bridges.

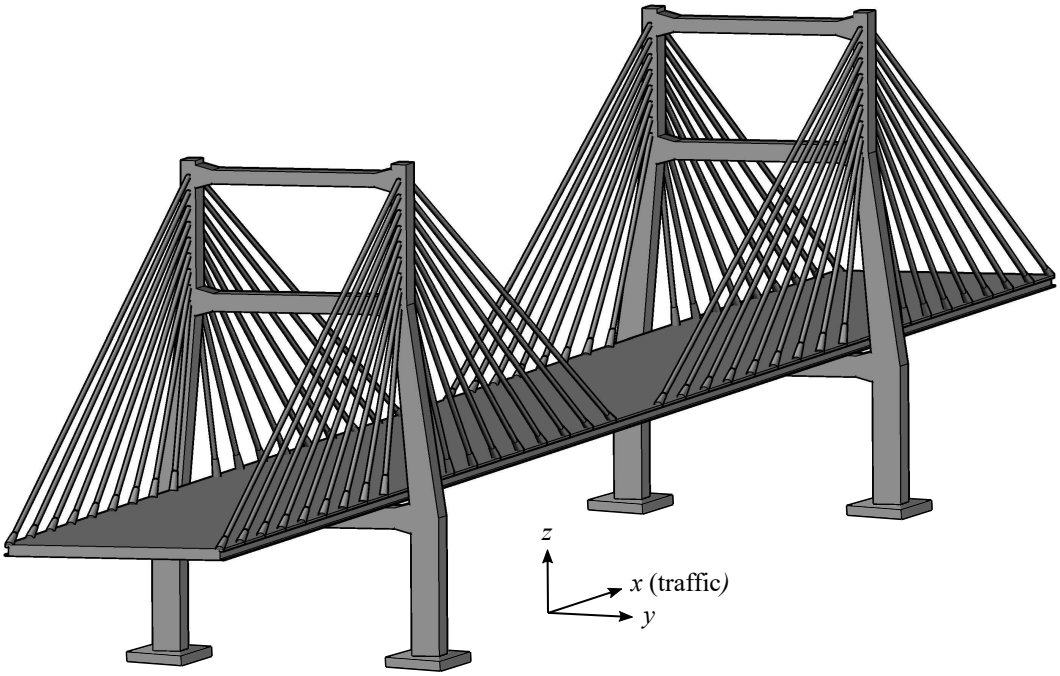

Figure 3.4: Complete 3D model of one of the cable-stayed bridges; H-LCP model.

The main span length also defines the number of cables in each plane[1]. The number of cables N_T in each plane if defined as:

$$N_T = \frac{\frac{L_P}{2} - \Delta_{D,P}}{\Delta_{D,P}} \tag{3.2}$$

where $\Delta_{D,P}$ is the distance between cables in the main span. For the bridges with L_P = 200, 400 and 600 m the number of cables in each plane is $N_T = 9$, 19 and 29, respectively. For the convenience of the reader the main dimensions of the cable-stayed bridges are included in Table 3.1. The notation in the Table is included in Fig. 3.5.

Deck

The width of the deck (B) is fixed at 25 m in all models, accommodating four traffic lanes. In LCP bridges the deck has an open composite cross-section formed of two longitudinal I-shaped steel girders at the edges and a 25-cm thick concrete slab on top. To ensure the overall stability of the deck, transverse I-beams connecting the two longitudinal girders are placed at fixed intervals equal to half the distance between cable anchorages i.e. at $\Delta_{D,P}/2 = 5$ m in the main span and at mid-distance between cable anchorages, $\Delta_{D,S}/2$

[1]The side span accommodates one plane of cables in the direction of traffic (x) and the main span accommodates two cable planes in the same direction.

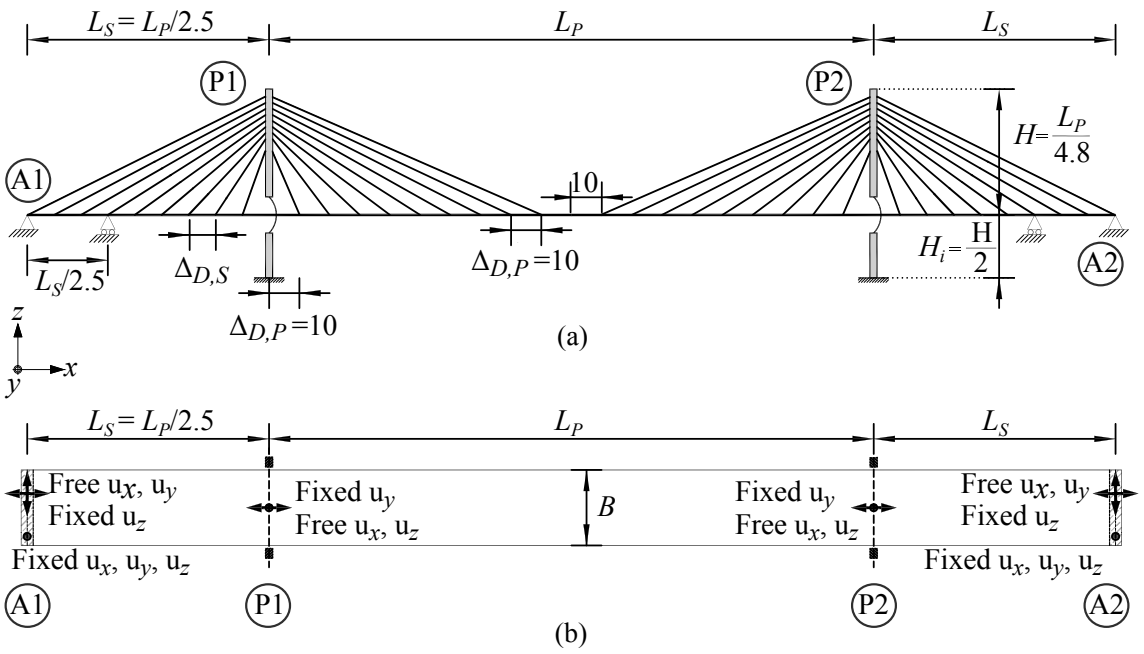

Figure 3.5: Parametric definition of the cable-stayed bridge models. (a) Elevation, (b) plan view. All dimensions are in [m].

in the side spans, as illustrated in Fig. 3.6. In CCP bridges the deck is a composite box girder that provides the bridge with sufficient torsional rigidity by means of a steel U-section closed by a 25-cm thick concrete slab. The composite box section is stiffened with transverse steel diaphragms at the same fixed intervals as in the open deck section of the bridges with two LCP's.

The depth of the deck in the LCP models increases slightly with the main span due to aerodynamic considerations. The depth of the deck in these structures is not significantly affected by the increase in the main span length (L_P) and it is more influenced by the transverse and the longitudinal distance between consecutive anchorages, which in this case coincide with $B = 25$ m and $\Delta_{D,P} = 10$ m, respectively. In conventional composite-deck bridges with these dimensions the depth of the deck can be estimated as (Astiz 2001):

$$d_{LCP} = 0.78 + 0.00302\ L_P \tag{3.3}$$

The depth of the deck in the CCP bridges is defined herein from the recommendations given by Camara (2011) based on constructed cable-stayed bridges with this cable configuration:

$$d_{CCP} = \frac{L_P}{90} \tag{3.4}$$

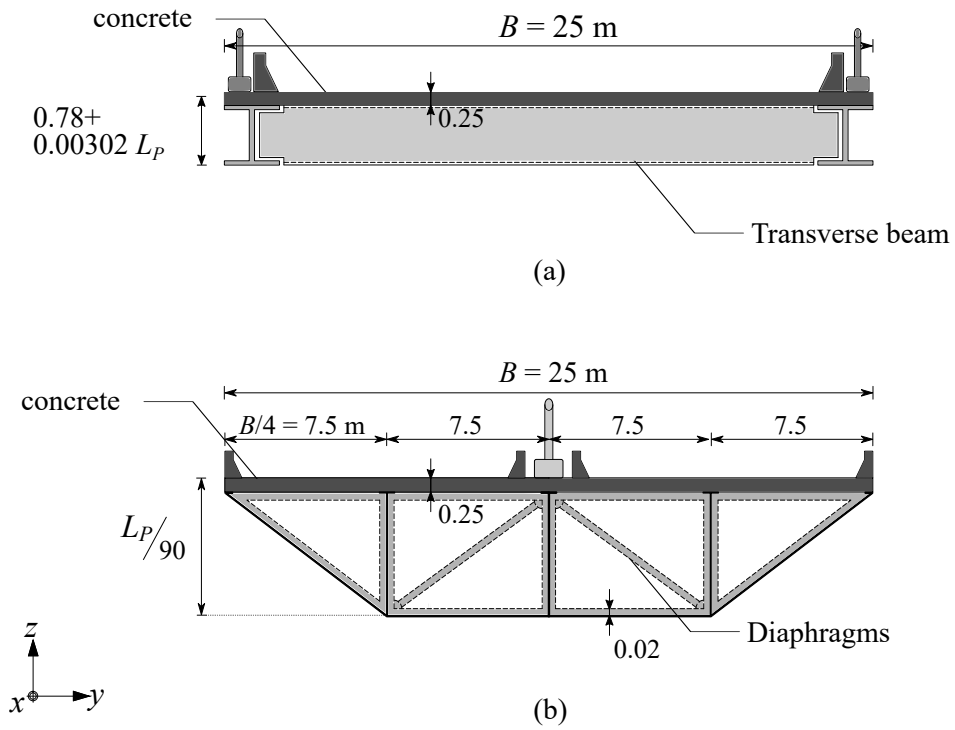

Figure 3.6: Parametric definition of the deck. (a) LCP and (b) CCP. All dimensions are in [m].

Deck Dimensions [m]			
L_P	B	d_{LCP}	d_{CCP}
200	25	1.4	2.2
400	25	2.0	4.4
600	25	2.6	6.7

Table 3.2: Geometric characteristics of the deck sections of the considered cable-stayed bridges.

It is noticed both from Eqs. (3.3), (3.4) and Table 3.2 that the depth of the deck is larger in the bridges with a single CCP. The torsional rigidity that is provided to the deck by the dual planes of cables in LCP bridges is lost in the case of CCP bridges. For this reason the necessary torsional rigidity is provided by the closed box section which is deeper than the open composite section of the LCP deck. Moreover, the rate of increase in the open deck of the LCP bridges is lower than the one of the CCP bridges (Eqs. (3.3) and (3.4)).

Pylons

The dimensions of the pylons are obtained from the study of Camara *et al.* (2014) based on a compiled database of constructed cable-stayed bridges. The large number of cable-stayed bridges considered in the present work prescribes the need for uniformity in the geometric considerations. To this end, the height of the pylons above the level of the

Pylon Dimensions [m]				
L_P	H	H_i	H_{tot}	H_A
200	41.7	20.8	62.5	16
400	83.3	41.7	125.0	36
600	125.0	62.5	187.5	56

Table 3.3: Length of the pylon regions in [m] depending on the main span length of the cable-stayed bridges L_P.

deck's centre of gravity (H) is defined as a function of the main span length (L_P) and it is assumed to be the same for all the pylon shapes.

$$H = \frac{L_P}{4.8} \tag{3.5}$$

The height of the pylons below the deck (H_i) is usually determined by the site characteristics. H_i affects the overall seismic pylon stiffness and therefore also the seismic response of the bridges. However, given the large number of bridges considered in this work, the study of the influence of H_i is not considered and a single value is proposed as a function of H:

$$H_i = \frac{H}{2} \tag{3.6}$$

The total height of the pylons (H_{tot}) is then defined as:

$$H_{tot} = H + H_i \tag{3.7}$$

and it is equal to 62.5, 125 and 187.5 m for the 200-, 400- and 600-m main span bridges, respectively. The length of the anchorage system (H_A) is defined by the number of cables included in each plane:

$$H_A = I_T \cdot (N_T - 1) \tag{3.8}$$

Fig. 3.7 and Table 3.3 present the parametrisation and the overall dimensions of the pylons (in terms of the main span length), respectively.

The section dimensions of the different parts of the pylons are defined as functions of H, based on the dimensions of a range of constructed bridges, and these are listed in Table 3.4. Due to the large number of bridge models in this research the most efficient combination between simplicity and accuracy of the results is preferred. For this reason the pylons, which are the main focus of the research, are modelled in detail. Addition-

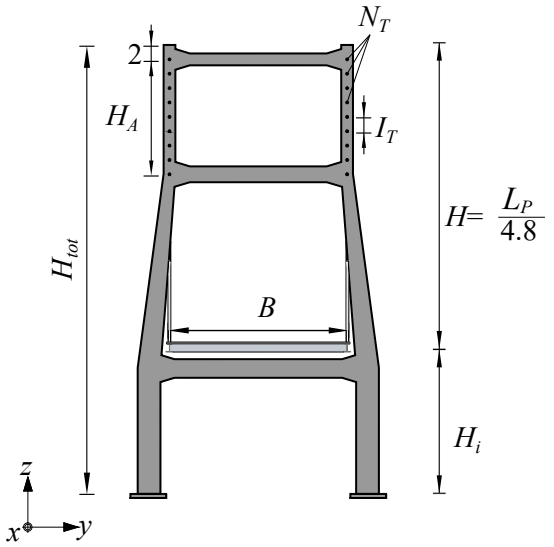

Figure 3.7: Parametric description of the pylon dimensions. The sample 'H'-shaped pylon is presented but the same parametrisation rules are applied to the inverted 'Y'- and 'A'-shaped pylons. All dimensions are in [m].

Pylon	Anchorage Area		Intermediate Part		Lower Piers		Lower Diamond	
	a (x)	b (y)	a (x)	b (y)	a (x)	b (y)	a (x)	b (y)
'H'	$H/15$	$H/25$	$H/14^{(*)}$	$H/19^{(*)}$	$H/13$	$H/13$	-	-
'Y'	$H/18$	$H/13$	$H/18$	$H/16^{(*)}$	$H/18$	$H/20$	$H/15$	$H/6$
'A'	$H/18$	$H/23$	$H/18$	$H/21^{(*)}$	$H/18$	$H/20$	$H/15$	$H/6$

Table 3.4: Section dimensions of the different components of the pylons as functions of the height of the pylon above the deck, H in [m]. The symbol * denotes average section dimensions in the regions of the pylons with variable sections.

ally to the original models proposed by Camara *et al.* (2014), which featured constant sections in the different regions of the pylons, in the present thesis a smooth transition between constant sections of different dimensions is considered. The motivation for this improvement in the models is to reduce the concentration of stresses at the connections of the regions of the pylons with different cross sections, observed in Camara and Astiz (2012). Table 3.4 lists the ratios that define the external dimensions of the sections in each part of the pylons. In areas where a smooth transition is provided and there is not a constant section the average dimensionless ratio is included in the table and is also marked with an asterisk (*). Table 3.5 lists the ratios for the struts in each pylon shape. Although the sections have constant dimensions almost throughout the length of the struts, these increase gradually at the two ends near the connections with the legs at a distance of 2.9-3.6 m, depending on the pylon shape, from the centre of gravity of the pylon cross section.

The pylon sections are hollow and the thickness of the concrete sections (t_C) is kept constant throughout the height of the legs. t_C is estimated so that the maximum compression in the anchorage area, where the stresses are maximum, does not exceed an allowable value of 10 MPa under the effect of the self-weight and the live loads. The

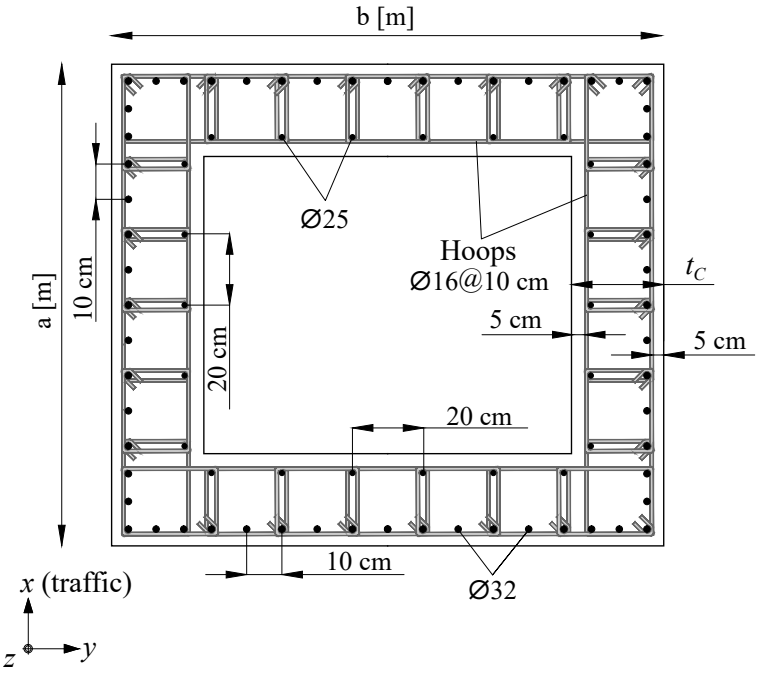

Figure 3.8: Geometric definition of the pylon cross section with the longitudinal and the transverse reinforcement arrangements.

Pylon	Upper Strut		Intermediate Strut		Lower Strut	
	a (x)	h (z)	a (x)	h (z)	a (x)	h (z)
'H'	$H/24$	$H/25$	$H/18$	$H/19$	$H/15$	$H/16$
'Y'	-	-	-	-	$H/18$	$H/23$
'A'	-	-	-	-	$H/18$	$H/23$

Table 3.5: Section dimensions of the transverse struts as functions of the height of the pylon above the deck, H in [m].

constant thickness is justified by the fact that the stresses are lower in the other parts of the pylons and by the need to simplify the modelling process. However, in the pylons with a lower diamond configuration the thickness of the concrete section in this area is increased to 0.45 m regardless of the main span length.

Cable System

For the estimation of the cross sectional area of the cables it has been assumed initially that the stress in each cable should not exceed 40% of the ultimate stress allowed in prestressing steel: $f_{\text{u}} = 1770$ MPa. Having established this stress threshold, the vertical component of the force in each stay should balance out the applied load from the self-weight and the live loads in the area corresponding to the stay under consideration.

Fig. 3.9 shows the areas that correspond to each cable in bridges with dual LCP's and with one single CCP. The analytical estimation of the force in each cable is obtained by considering vertical equilibrium of forces and it is shown in Fig 3.9.

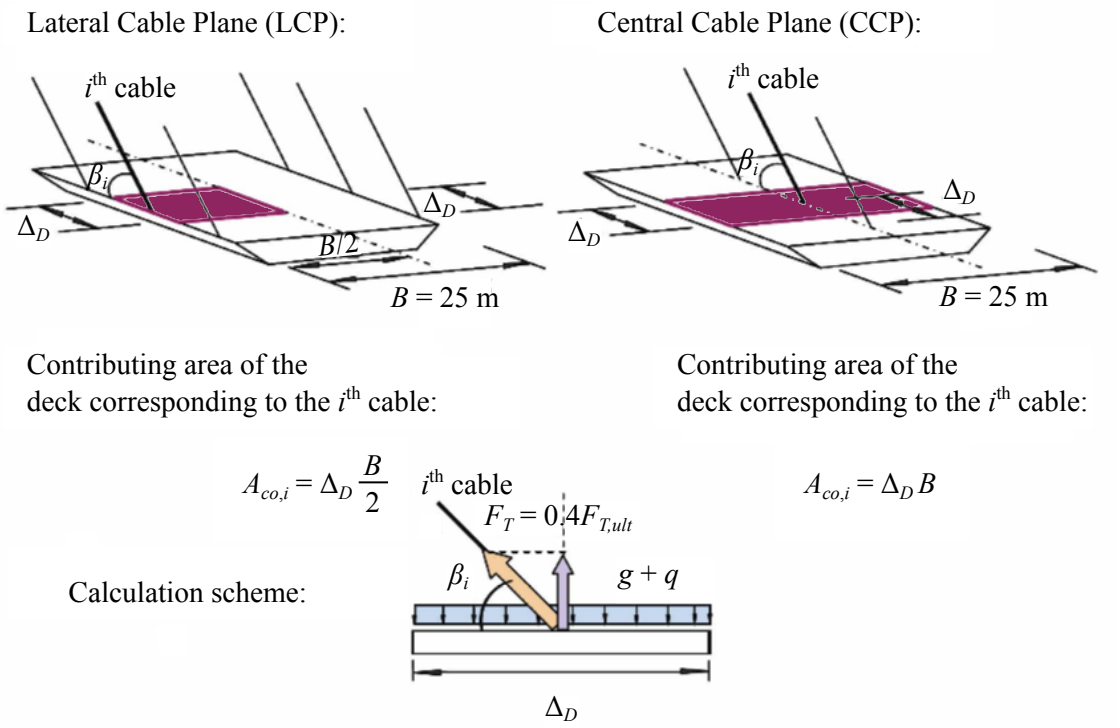

Figure 3.9: Contributing areas of the deck associated with each cable and calculation scheme to obtain their load, both in LCP and CCP models. Dimensions in [m] (*taken from Camara (2011)*).

$$\sum F_z = 0 \quad \Rightarrow \quad F_{T,i} \sin(\beta_i) = (g+q)\, A_i \tag{3.9}$$

in which $F_{T,i} = \sigma_{T,i} A_{T,i}$ is the tensile force that the i^{th} cable is required to transfer from the deck to the pylon, $\sigma_{T,i}$ (with $\sigma_{T,i} = 0.4\ f_u$) and $A_{T,i}$ are the tensile stress and the cross-sectional area of the cable, respectively, β_i is the angle that the cable forms with the deck, g and q are the uniformly distributed dead and live load, respectively and A_i is the area of the deck that is assigned to the i^{th} cable, as shown in Fig. 3.9. The cross-sectional area is estimated as follows:

$$\sigma_{T,i} A_{T,i} \sin(\beta_i) = (g+q)\, A_i \quad \Rightarrow \quad A_{T,i} = \frac{(g+q)\, A_i}{0.4 f_u \sin(\beta_i)} \tag{3.10}$$

Usually, when the cross-sectional area of all the cables is calculated the bridge model is analysed under the effect of the self-weight. This step initiates an iterative procedure which results from the redistribution of forces in the cables. The cables that connect the pylon to the vertically restrained areas of the deck (such as the cables at the abutments and the intermediate piers) receive higher forces $F_{T,i}$ than the remaining cables which may remain relatively unstressed. For this reason larger $A_{T,i}$ is assigned to the former cables and reduced $A_{T,i}$ is assigned to the latter. The iterations are repeated until the ver-

tical deformation of the deck is reduced to an acceptable minimum value and until the longitudinal bending of the pylons is reduced. In other words the sum of the forces that are transferred to the pylon from the cables of the side span ($\sum F_{x,side}$) is equal to the sum of the horizontal forces that is transferred to the same pylon from the corresponding half main span $\left(\sum F_{x,main/2}\right)$ and the pylon is in compression only. In this research the iterative procedure is replaced by a simplified direct method discussed in Camara (2011). This method increases the section in the cables that connect the pylons with the abutments and the intermediate piers and it has been observed to yield results that are admissible in terms of pylon bending and deck displacement under permanent loads. It should be noted that the aim of the present research is to provide the seismic forces distribution among the cables and not to assess the effect of the live-load induced fatigue of the cables, for which a more detailed design of the cable sections should be provided.

3.2.2 Boundary Conditions

In order to have a successful analysis procedure the detailed modelling of the structures must be accompanied by an adequate representation of the boundary conditions.

Fig. 3.5 shows that in this study the abutments constrain the displacements of the deck in the vertical (z), transverse (y-perpendicular to the traffic flow) and longitudinal (x) directions and they also prevent its torsional rotation (θ_{xx}), whereas the rotation around the transverse axis (θ_{yy}) is released. The rotation around the vertical axis (θ_{zz}), in other words the transverse rotation of the deck, is also released. Allowing the transverse rotation of the deck at the abutments can increase the transverse seismic response of the pylon up to 40% in short cable-stayed bridges ($L_P = 200$ m), but it also reduces the seismic response of the deck at the abutments, which is important because the deck should behave elastically (Camara and Astiz 2011). In the side spans the intermediate piers constrain the vertical displacement and the torsional rotation of the deck. At the pylons the deck is restrained in the transverse (y) direction and it is released in all other directions assuming a floating type connection between the deck and the pylon. This type of deck-pylon connection is commonly adopted in the design of cable-stayed bridges in seismic prone regions.

The flexibility of the pylon foundations is simulated by means of translational springs in the x, y and z directions, rotational springs around x and y and dashpots in the respective directions whose properties account for the SSI. The stiffness of the springs and the dashpot coefficients are obtained by considering that the surrounding subsoil[1] is Type D according to Eurocode 8; Part 1 (2004) and by employing the impedance fuctions by Gazetas (1991), which will be discussed in detailed in Chapter 4.

[1]The surrounding subsoil is also taken as Type A in some cases, as will be discussed in Chapters 4 and 6, but for the main body of this thesis, soft soil conditions (Type D) are considered.

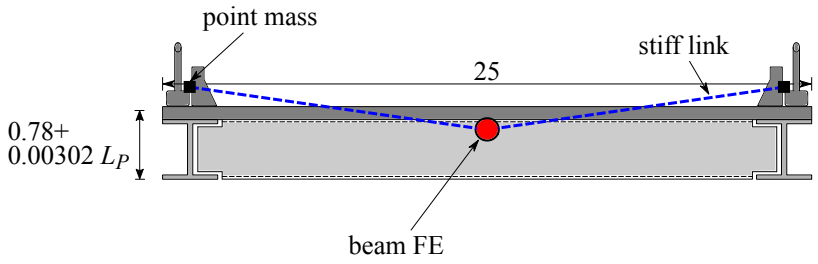

Figure 3.10: Finite element model of the deck section in bridges with two LCP's. Dimensions are in [m].

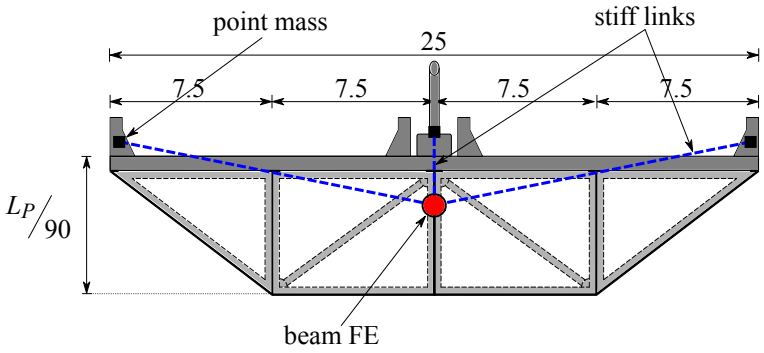

Figure 3.11: Finite element model of the deck section in bridges with one CCP. Dimensions are in [m].

3.3 Finite Element Models Description

The general Finite Element (FE) analysis software Abaqus (2018) has been employed to model the bridges and to conduct the complete sets of dynamic analyses both in the linear and nonlinear ranges. Different types of finite elements are used herein in an attempt to combine the maximum computation efficiency and the accuracy of the results. The rationale behind the definition of the parameters and the choice of the particular types of finite elements is presented in the following.

Deck

The cable-stayed bridges of this research have two different deck types, as discussed in Section 3.2.1. The shape of the deck section is influenced by the shape of the pylon and the pylon-cable system configuration.

The composite open deck section of the LCP and the closed box girder of the CCP bridges are modelled with linear interpolation, shear-flexible beam-type elements that pass through the centre of gravity of the sections and account for the structural (concrete slab, longitudinal and transverse steel girders and steel diaphragms) and nonstructural (deck asphalt) masses, as shown in Figs. 3.10 and 3.11.

A fictional density (ρ^*) for the composite section has been calculated in Eq. (3.11) in order to establish the mass that is attributed to the beam FE model of the deck:

$$\rho^* = \frac{\rho_c^* A_c + \rho_s A_s}{A_{tot}^*} \tag{3.11}$$

in which ρ_c^* and ρ_s are the densities of the concrete (increased to account for the mass of the asphalt: $\rho_a = 2300$ kg) and of the steel, respectively. The density of the concrete is increased in the numerical models as follows:

$$\rho_c^* = \frac{\rho_c A_c + \rho_a A_a}{A_c + A_a} \tag{3.12}$$

in which ρ_c is the density of the concrete, and A_c and A_a are the areas of the concrete and the asphalt sections, respectively. A_{tot}^* in Eq. (3.11) is the total cross section of the composite deck section homogenised to steel by means of the ratio of the Young's moduli E_c and E_s of the concrete and of the steel, respectively. A_s is the cross-sectional area of the steel parts of the deck section:

$$A_{tot}^* = \frac{A_c}{E_s/E_c} + A_s \tag{3.13}$$

The beam elements describing the deck have constant length regardless of the cable system configuration. This length is assumed as half the distance between two cable anchors. For the main span this length is equal to 5 m regardless of the main span length (L_P), whereas in the side spans this length is defined as $\Delta_{D,S} = L_S/N_T$, with L_S being the side span length and N_T the number of cables in one plane[1]

Pylon

The pylons are modelled with beam type elements through the centre of gravity of their sections. The 'fibre' model approach has been chosen which divides the section in discrete fibres that represent the concrete and each longitudinal reinforcement bar. This model integrates the stresses in the fibres across the section in each time step to obtain the force-displacement relation of the element, which allows to account for the nonlinear constitutive behaviours of the steel and the concrete. The representation of the FE model of the pylon is included in Fig. 3.12. The transverse reinforcement in the concrete section is not directly modelled in the fibre FE model of the pylons but the effect of the transverse reinforcement bars is inherent in the constitutive model of the concrete, which accounts

[1]In bridges with $L_P = 200$ m the number of cables in one plane is $N_T = 9$ and this increases to 19 and 29 for the 400- and 600-m bridges, respectively.

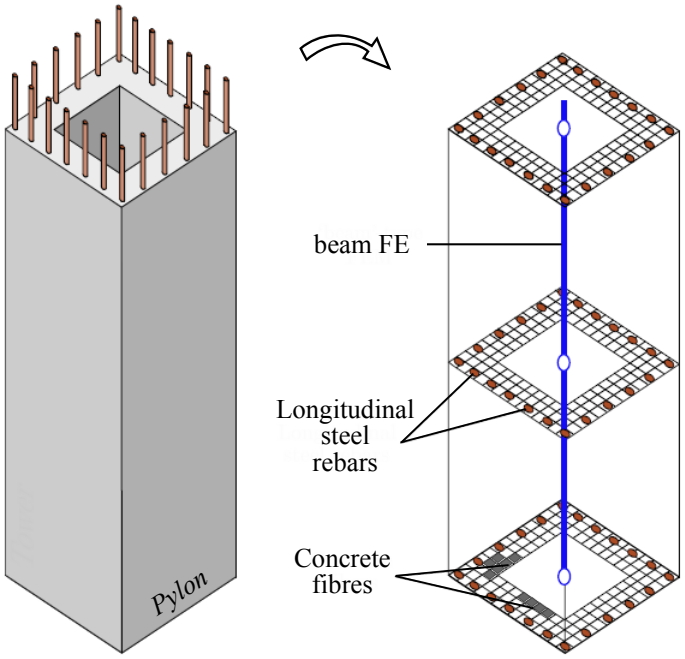

Figure 3.12: Finite element model of the pylon section having adopted the fibre section model (*taken from Camara (2011)*).

for the confinement of the cross-section, as it is described in Section 3.4.

The length of the beam elements in the pylon is associated with the length of the plastic hinge that can be developed in the concrete member during the earthquake and it is defined according to Paulay and Priestley (1992) as:

$$l_p = 0.08l + 0.022 d_b f_{sy} \tag{3.14}$$

in which l_p is he length of the plastic hinge in [m], l is the distance between the critical section of the plastic hinge and the point of contra-flexure in [m], d_b is the diameter of the longitudinal bars in [m] and f_{sy} is the yield stress of the reinforcing steel in [MPa]. Based on the results of the seismic analysis of the pylons that are presented in Fig. 3.13, the values for the parameters of Eq. (3.14) are taken as:

$$l = \begin{cases} 0.2\ H_{tot} & \text{for the lateral legs } (H_{tot} \text{ is the total height of the pylon [m]}) \\ 0.5\ B & \text{for the deck } (B \text{ is the width of the deck [m]}) \end{cases}$$

$$f_{sy} = 552 \text{ MPa} ; \quad d_b = 0.032 \text{ m}$$

Herein, the length of the beam element, L_{elem}, is defined as half the length of the plastic hinge: $L_{elem} = l_p/2$ according to the sensitivity analysis conducted by Camara (2011).The

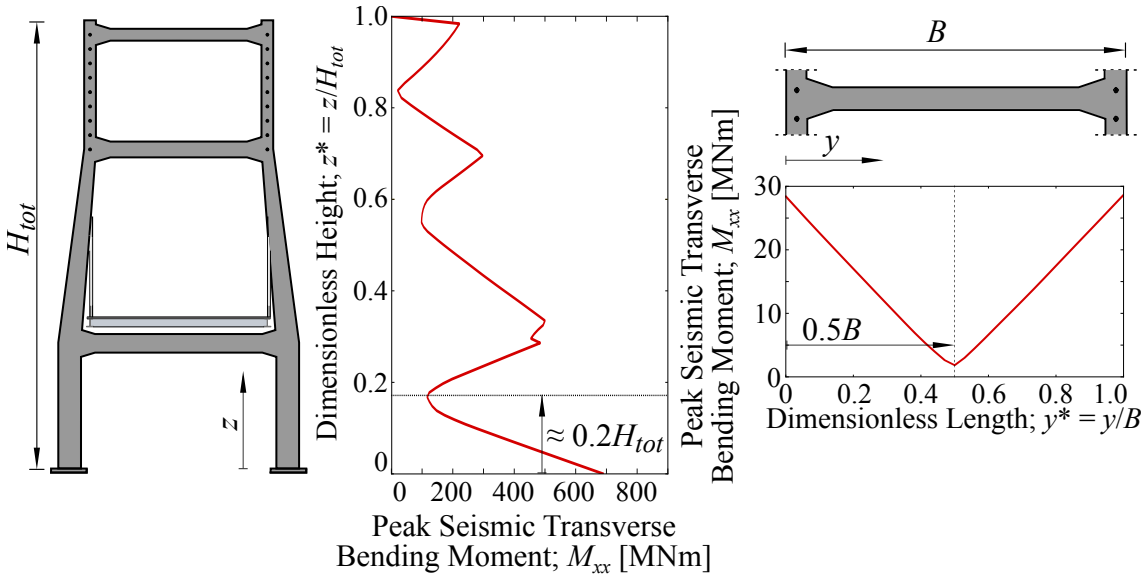

(a) (b)

Figure 3.13: Distance l between the critical section of the plastic hinge and the point of contra-flexure in the (a) pylons and (b) struts.

FE model of the pylon has been validated against experimental cyclic loading tests on solid and hollow reinforced concrete columns conduced by Takahashi and Iemura (2000), Orozco and Ashford (2002) and Sakai and Unjoh (2006).

Cable system

The cables of this study have been modelled with 3D trusses which use linear interpolation of the axial displacements. Each truss element represents one cable, ignoring the cable-structure interaction, and it is defined by two nodes located at the cable anchorages (i.e. at the pylon and deck ends of the cables). A preliminary comparison between the approaches of a single-element cable and of a cable defined by multiple truss elements showed that the seismic response of the pylons of a 400-m span cable-stayed bridge is more conservative when the cables are discretised with a single truss element (Efthymiou and Camara 2015). Additionally, it is noted that employing multiple elements for each cable would result in a significantly higher computational cost. Given the number of cable-stayed bridges considered this in research, the multi-element cable model was deemed unnecessary because the aim is to assess the seismic effects in different types of pylons and, therefore, the conclusions are not affected by the choice in the cable modelling.

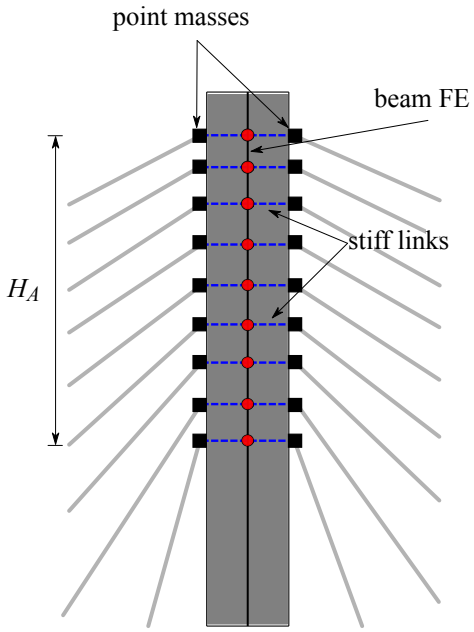

Figure 3.14: Modelling of the distance between the cable ends and the gravity centres of the pylon sections with rigid links.

Special-Purpose Elements

Nonstructural Masses

An important aspect of the FE model definition is the representation of the nonstructural masses that are applied to the deck and to the pylons of the bridges. Such masses include the asphalt layer on top of the concrete slab (which has been accounted for by increasing the density of the concrete in Eq. (3.12)), the masses of the cable anchors and the parapets along the decks of the LCP and the CCP models and the respective masses from the cable anchors on the pylons.

The consideration of the safety parapets and the cable anchors on the deck is considered by means of point masses at the centres of gravity of those elements, as shown in Figs. 3.10 and 3.11. The definition of the anchorage system in the pylons is completed by accounting for the dimensions of the sections of the pylons, as shown in Fig. 3.14. These figures also show that rigid links are employed to model the separation distance between the cable ends and the centre of gravity of the deck, and the separation distance between the other cable ends and the centre of gravity of the pylon.

Deck-Pylon Connection

The connection between the deck and the pylon is described in Section 3.2.2 and is shown in Fig. 3.5. Fig. 3.15 shows the concept of the floating type connection, which releases the longitudinal and the vertical displacements of the deck but constrains its lateral move-

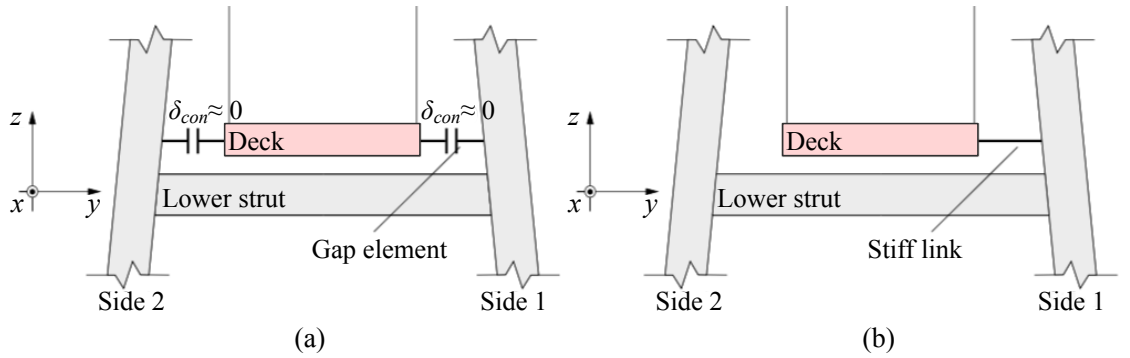

Figure 3.15: Different deck-pylon connection modelling approaches (a) Realistic connection with alternating contact of the deck to the pylons, (b) Simplified connection with the deck being rigidly connected to one pylon leg (*taken from Camara (2011)*).

ment. This configuration reduces the overall displacements of the deck during a seismic event but it might induce large moments and shear forces in the pylons due to the transverse force that is exerted alternately to the legs of the pylons (Gimsing and Georgakis 2012). In real projects this connection is usually accomplished through the use of bearings at the pylon legs leaving a small distance, δ_{con}, between these and the deck.

The accurate representation of the floating connection would involve the use of gap elements between the deck and the legs of the pylons to ensure the free longitudinal and vertical displacements of the deck. However this approach increases significantly the computational cost because of the rising nonlinearities (even in the elastic range) when the deck impacts the pylon legs during the earthquake. In this thesis a simplified transverse connection between the deck and the pylons is adopted by assuming that the deck is rigidly connected to one leg of the pylons and completely released from the other after Camara (2011), who concluded that the transverse seismic response of the pylon when the simplified connection is established is similar[1] to the response from the detailed connection.

Pylon Foundations

The properties of the foundations and of the surrounding soil have been modelled by means of linear springs and dashpots that connect fixed points representing the ground to the pylon base in the three orthogonal directions, as discussed in Section 3.2.2.

[1]Based on the findings of Camara (2011) the seismic transverse shear in the pylons of a cable-stayed bridge with $L_P = 400$ m is increased at the level of the deck by less than 7% when the simplified connection is considered compared to the results form the detailed deck-pylon connection with alternating contact through gap elements.

3.4 Materials

The materials (steel and concrete) that are used in the cable-stayed bridges are described through their constitutive models. In this research the characteristic properties of the materials have been adopted and no safety factors have been applied. The purpose of this work is to get an insight into the most realistic seismic response of cable-stayed bridges under the effect of differential support motion and hence the conservatism involved in the reduction of the material properties has been deemed unnecessary.

The material properties have been selected following the suggestions of international codes of practice. Specifically, the elastic and inelastic material behaviours have been defined based on Eurocode 2; Part 1.1 (2004), Eurocode 3; Part 1.1 (2005), Eurocode 3; Part 1.11 (2006) and Eurocode 8; Part 2 (2005).

The structural damping in the dynamic analysis is described by means of Rayleigh's damping theory and it is independent of the material (concrete or steel) in order to reduce the uncertainty that is involved in the prediction of the dissipation properties of the materials. The application of Rayleigh's damping to this work is discussed in Chapter 5.

Concrete

The concrete used in the pylons is confined by transverse reinforcement bars (hoops) as shown in Fig. 3.8. The confinement of the concrete is defined by the widely accepted model proposed by Mander *et al.* (1988), as shown in Fig. 3.16, which is also included in Eurocode 8; Part 2 (2005). C40 concrete with a characteristic strength of $f_{ck} = 40$ MPa has been used herein (Eurocode 2; Part 1.1 2004) and its main characteristics are presented in Table 3.6:

Young's modulus	E_c [GPa]	35
Poisson's ratio	ν_c	0.2
Density	ρ_c [kg/m^3]	2500
Mean elastic compressive strength	f_{cm} [MPa]	-48
Elastic compressive deformation	ε_{c1} [%]	-0.14
Ultimate compressive strength	$f_{cm,c}$ [MPa]	-64.28
Ultimate compressive deformation	$\varepsilon_{cu,c}$ [%]	-2.6
Maximum tensile strength	$f_{c,t}$ [MPa]	3
Cracking initiation	ε_{crack} [%]	0.0086
Maximum tensile deformation	$\varepsilon_{c,t}^{\max}$ [%]	0.035

Table 3.6: Material properties of the C40 confined concrete model employed in this research. The - sign denotes compression and the + sign denotes tension.

The nonlinear cyclic degradation of the confined concrete is defined through the smeared crack concrete model, which is available for fibre beam elements in Abaqus

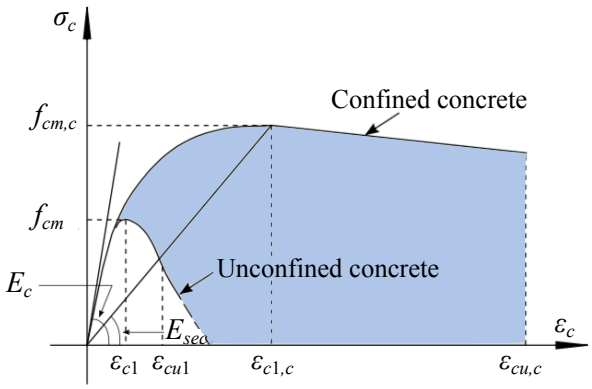

Figure 3.16: Stress-strain curve of the confined concrete considered herein proposed by Mander *et al.* (1988).

(2018). This model limits the damage prediction in the section in the sense that detailed failure mechanisms of the concrete such as cracking, spalling and pinching and buckling of the reinforcement bars, among others cannot be captured. The smeared crack model does not track the development of specific cracks but it treats them in an average (smeared) way along the element.

In this research the pylons are the only elements of the bridge that are allowed to have material nonlinearities. The concrete slab of the deck behaves elastically and its material properties are taken from the elastic part of Table 3.6.

Reinforcing and Structural Steel

In order to ensure adequate concrete confinement strong longitudinal and transverse reinforcement ratios[1] of 2.4% and 0.8%, respectively are assumed in the pylons. These ratios are defined to ensure adequate rotation capacity and they comply with the American (AASHTO 2011) and the Spanish (NCSP-07 2007) code provisions. For the reinforcing steel B500C grade is used whose main properties are included in Table 3.7. The yield stress of the steel is taken as 552 MPa and its stress-strain curve is included in Fig. 3.17. In the nonlinear analysis of Chapter 7, the reinforcing steel accounts for the effects associated with the cyclic plasticity by means of the kinematic hardening.

For the steel members forming the deck sections, such as the longitudinal and transverse girders in bridges with two LCP's and the steel open U-section in the bridges with one CCP, the same steel grade is used but only the elastic properties listed in Table 3.7 are considered because the deck responds in the elastic range.

[1]The reinforcement ratio is defined as the area of steel over the gross area of concrete in the section.

Young's modulus	E_s [GPa]	210
Poisson's ratio	ν_s	0.3
Density	ρ_s [kg/m^3]	7850
Yield stress	f_{sy} [MPa]	552
Elastic tensile deformation	ε_{sy} [%]	0.26
Ultimate tensile stress	$f_{s,t}$ [MPa]	665
Ultimate tensile deformation	ε_{su} [%]	11.4

Table 3.7: Material properties of the B500C steel used for the reinforcing and structural steel in this research.

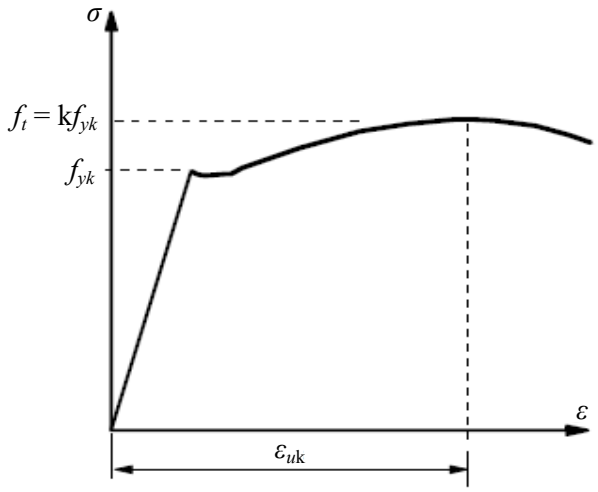

Figure 3.17: Stress-strain curve of the adopted B500C steel under monotonic loading (tension or compression) (*taken from Eurocode 2; Part 1.1 (2004)*).

Prestressing Steel

The material properties for the steel forming the cables is taken from Eurocode 3; Part 1.11 (2006).

Young's modulus	E_p [GPa]	195
Poisson's ratio	ν_s	0.3
Density	ρ_s [kg/m^3]	7850
Ultimate strength	f_{u} [MPa]	1770

Table 3.8: Material properties of the prestressing steel used in the cables.

3.5 Modal Analysis of the Cable-Stayed Bridges

The study of the vibration modes provides valuable information about the dynamic behaviour of a structure. This is an essential step prior to the seismic analysis and the necessity to perform a modal analysis in this case is reinforced by the fact that the seismic response of cable-stayed bridges that are subjected to multi-support excitation is significantly influenced by the contribution of higher modes to the seismic response that are mainly antisymmetric (Tzanetos *et al.* 2000, Sextos 2001) and that are not important when identical support motion is considered (Zerva 1990, Camara and Efthymiou 2016). This is observed and discussed in depth in Chapters 6 and 7.

The modal study conducted in this section is performed from the deformed configuration resulting from the dead loads (Abdel-Ghaffar and Nazmy 1991). Figs. 3.18 - 3.20 present the first vibration modes of the H-LCP models with $L_P = 200$, 400 and 600 m. The following discussion will focus on the effect of the increasing span length of the deck (and at the same time the increasing pylon height) on the vibration modes of the studied bridges.

In the 200-m main span bridge the first vibration mode involves the vertical flexure of the deck accompanied by the longitudinal flexure of the pylons with respect to the deck. The fundamental vibration frequency of this bridge is $f_1 = 0.50$ Hz ($T_1 = 2.0$ s). As the length of the bridge increases, the height of the pylons increases proportionally (Eqs. (3.5) - (3.7)), but the width of the deck remains constant at $B = 25$ m. This results in an increasingly flexible structure, especially in the transverse direction and it explains the fact that the fundamental mode in the longest bridge ($L_P = 600$ m) involves the transverse flexure of the deck.

It is observed that the first transverse mode is of lower order with increasing main span lengths. In the short-span bridge with $L_P = 200$ m the first transverse vibration mode is mode #4 and it combines the transverse movement of the deck, slightly coupled with

its transverse movement, and transverse flexure of the pylons. As the dimensions of the bridges increase the structure becomes more flexible and the order of the first transverse mode is reduced to mode #2 in the 400-m span bridge, and to mode #1 in the 600-m span bridge. It is important to note that in the intermediate and in the long-span bridges (with $L_P = 400$ and 600 m, respectively) the pylons are less influenced by the low-order transverse oscillation of the deck (Camara *et al.* 2014, Camara and Efthymiou 2016).

Finally, the dominant transverse vibration mode of the bridge is not directly linked with the dominant transverse vibration modes of the pylons, especially in the longer bridges, as it will be discussed in the following. It is noticed that in the bridge with $L_P = 200$ m the dominant mode in the transverse direction combines the transverse vibration of both the deck and the pylons, but in the longest bridge with $L_P = 600$ m the fundamental transverse mode is essentially a deck mode that does not excite the pylons because they are much stiffer than the deck in the transverse direction. The antisymmetric, higher-order mode #6 in Fig. 3.20 is the first one with a significant contribution to the transverse flexure of the pylons.

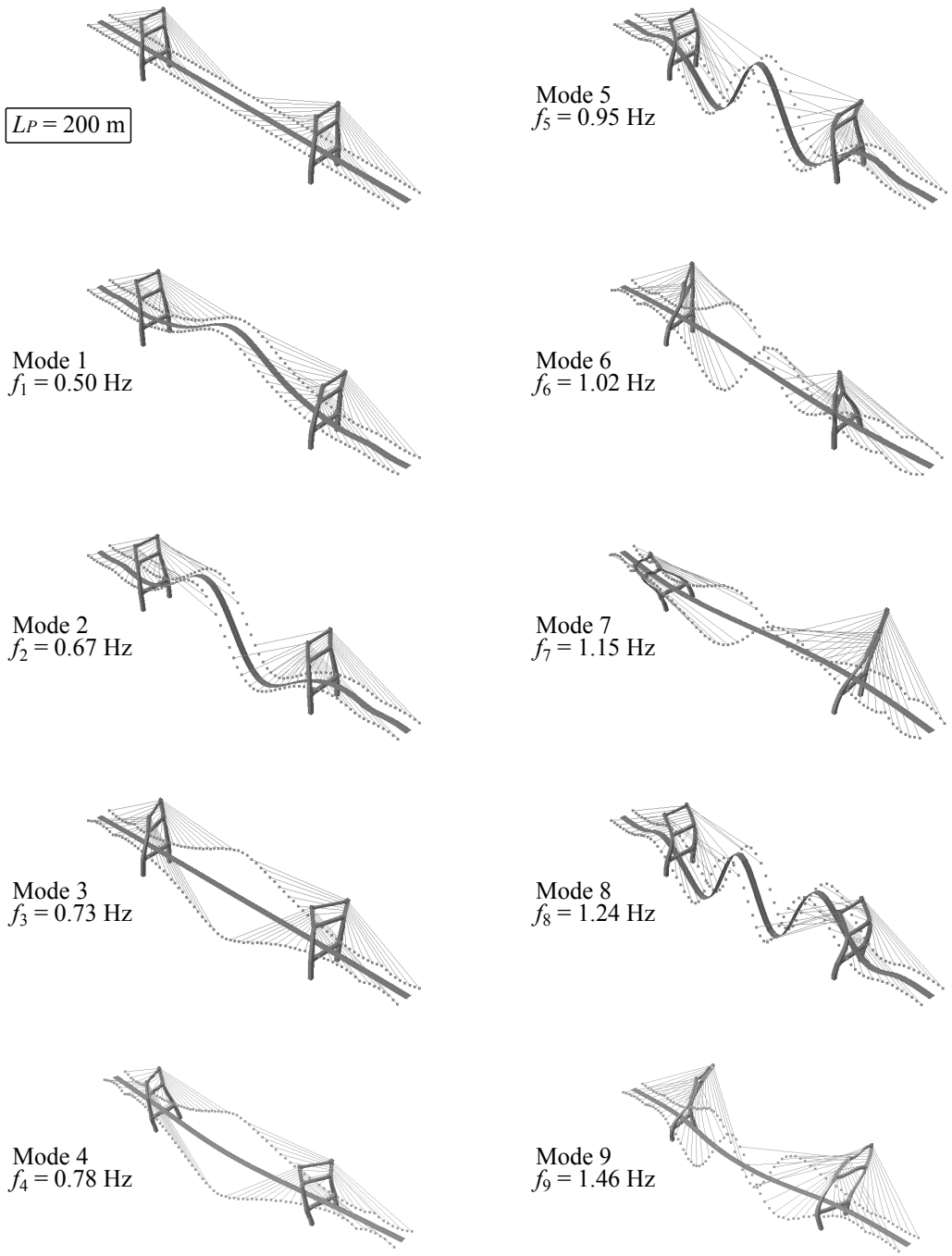

Figure 3.18: First vibration modes of the H-LCP model with $L_P = 200$ m.

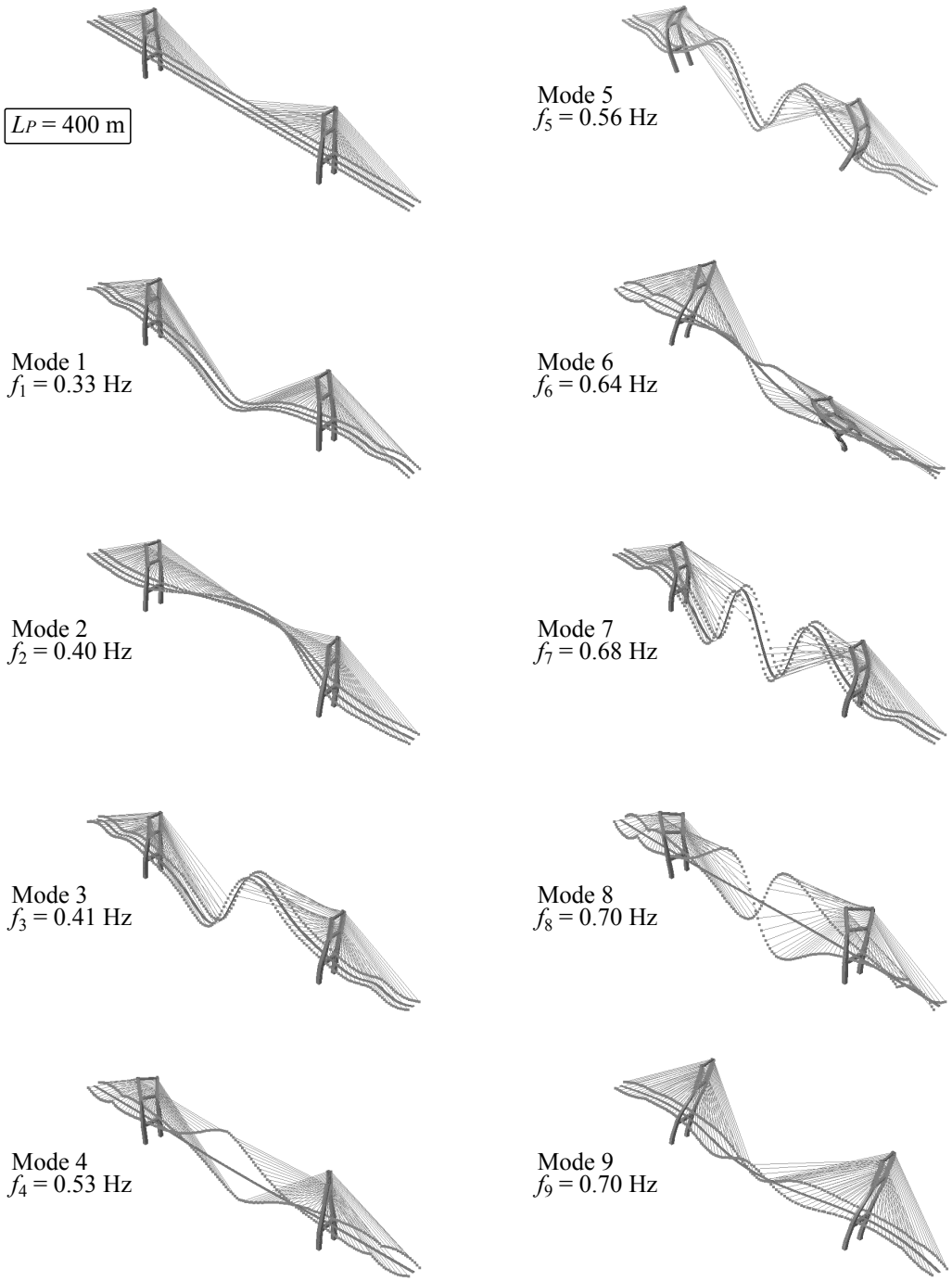

Figure 3.19: First vibration modes of the H-LCP model with $L_P = 400$ m.

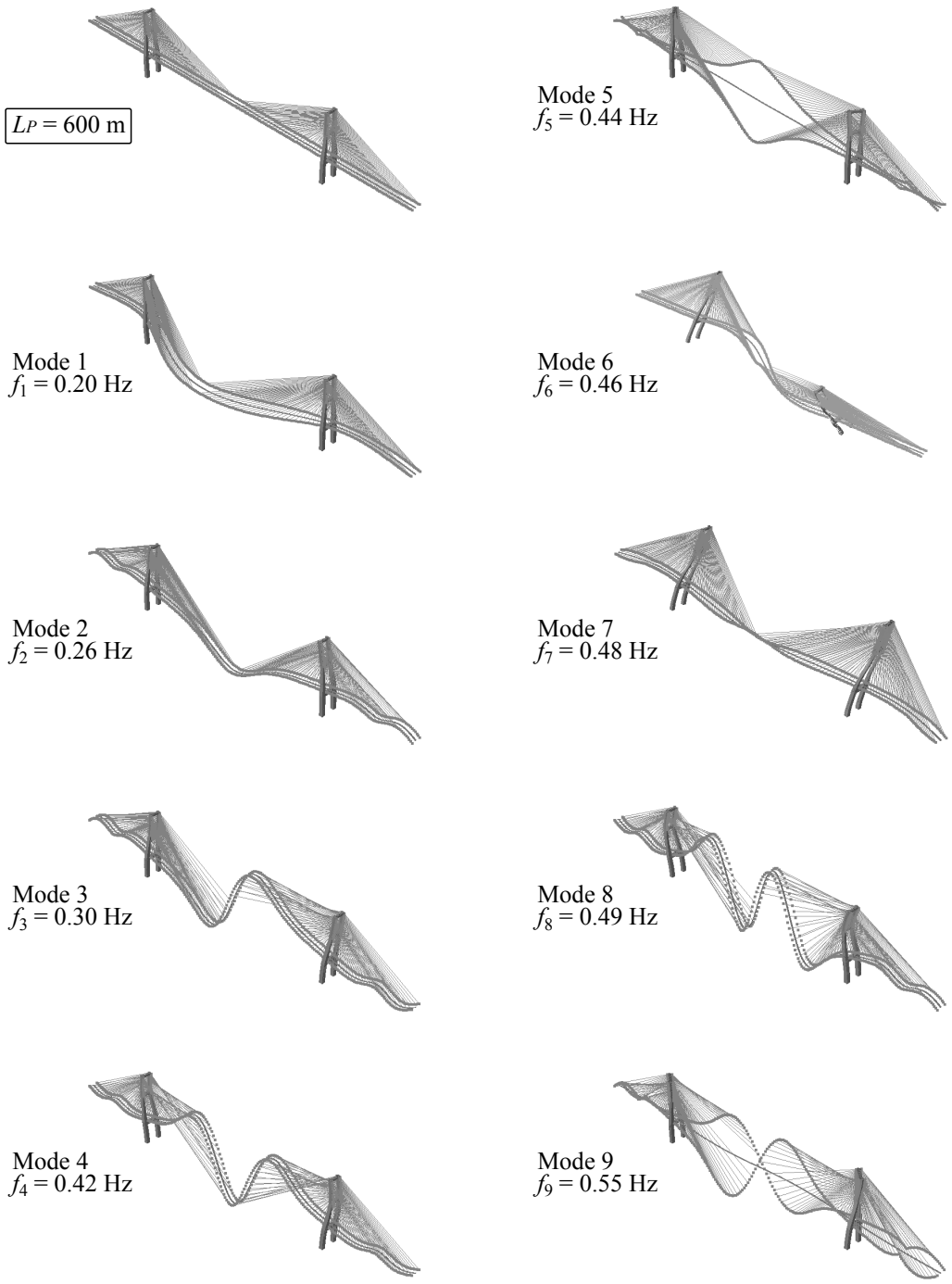

Figure 3.20: First vibration modes of the H-LCP model with $L_P = 600$ m.

Chapter 4

Seismic Action

Contents

4.1 Introduction

So far the nature of the SVGM and its effect on different types of bridges have been discussed in detail in Chapter 2 and the numerical models of the cable-stayed bridges that are studied herein have been presented in Chapter 3. There is considerable uncertainty when addressing the seismic action. There are different parameters of the seismic action that are involved in the decision making process and that require a detailed analysis of the site's hazard, including the return period, the magnitude and the duration of the earthquake, the frequency content, the source-to-site distance and the orientation of the structure with respect to the waves' propagation, among others. The complete identification of these parameters is not performed in this work because it would require considering a particular site and it could reduce the generality of the results obtained. Instead, code-based uniform hazard spectra and typical values of the seismological conditions are taken from the relevant literature.

This chapter presents an in-depth discussion of the seismic action that has been considered for this research. Only the horizontal components of the seismic actions have been considered because the vertical component of the earthquake reportedly does not affect the seismic response of cable-stayed bridges significantly (Camara and Astiz 2011, Gimsing and Georgakis 2012). In order to study the effect of the SVGM on the cable-stayed bridges and to examine the dynamic response of these structures RHA have been performed in the linear and nonlinear ranges (as it will be discussed further in Chapter 5). These types of analysis require different acceleration histories to be applied to the supports of the structures (corresponding to the end abutments and the pylons of the bridges). A description of the design seismic action introduces the discussion followed by a critical reference to the selection of natural or artificial seismic records which is concluded by justifying the selection of the latter for this research. In the present study the horizontal design spectrum of Eurocode 8; Part 1 (2004) has been adopted for the generation of artificial acceleration histories that are applied to the foundations of the horizontally constrained supports of the cable-stayed bridge models, corresponding to the abutments and the pylons[1]. Consequently, a detailed description of the adopted stochastic model to generate the signals is included along with the important components of the signal generation process. Finally, the obtained acceleration time-histories are presented along with the consideration of the angle of incidence in the seismic action and the implementation of the soil-structure interaction at the pylons of the cable-stayed bridges.

[1]Note that the intermediate piers at the side spans only constrain the vertical and the torsional movement of the deck (Chapter 3) and therefore no accelerograms are applied at these points.

4.2 Design Seismic Action: Target Response Spectra

Codes of practice (e.g. Eurocode 8; Part 1 (2004)), prescribe the use of a Uniform Hazard Spectrum (UHS), which is essentially a representation of the seismic hazard obtained from a probabilistic seismic hazard analysis in a range of different periods. UHS do not actually represent the effect of any particular earthquake, but instead they constitute a representation of the envelope of the effects of multiple seismic events with variable magnitudes and source-to-site distances. They are site-dependent, since they are based on the characteristics of the surrounding soil, and they are scaled appropriately to match the target spectral acceleration. Usually, the short period range of the spectrum is dominated by smaller magnitude earthquakes with short source-to-site distances, while the longer period range is obtained from the contribution of larger magnitude and more distant events.

4.2.1 Eurocode 8 Elastic Response Spectrum

The Type 1 elastic response spectrum prescribed by Eurocode 8; Part 1 (2004) has been adopted herein. This spectrum is recommended for regions that are mostly affected by earthquakes which are expected to have surface-wave magnitudes, M_S greater than 5.5 and it is more appropriate for the long period cable-stayed bridges of this study, as opposed to the Type 2 spectrum. Fig. 4.1(a) shows that the spectral acceleration (S_a) associated with the fundamental period of the shortest bridges[1] in the Type 2 spectrum is only 33% of that corresponding to the Type 1 spectrum.

In this thesis two significantly different soil categories have been considered. Specifically, the spectrum has been defined for soft soil conditions (ground type D) which has been deemed as the most unfavourable case when examining the seismic behaviour of cable-stayed bridges because these flexible structures are dominated by long vibration periods. However, the opposite case of firm soil conditions (ground type A) has been also examined in order to assess the difference that the variation in the underlying soil conditions may have on the structural response when asynchronous motion of the supports is considered. The response spectra are presented in Fig. 4.1(b).

4.3 Natural or Artificial Accelerations?

When it comes to the consideration of earthquake time-histories the choice between natural or artificial accelerograms needs to be carefully considered. Ideally, the study of the SVGM should be accomplished by selecting recorded seismic signals from strong motion

[1]The vibration periods of the proposed bridges are described in Chapter 6.

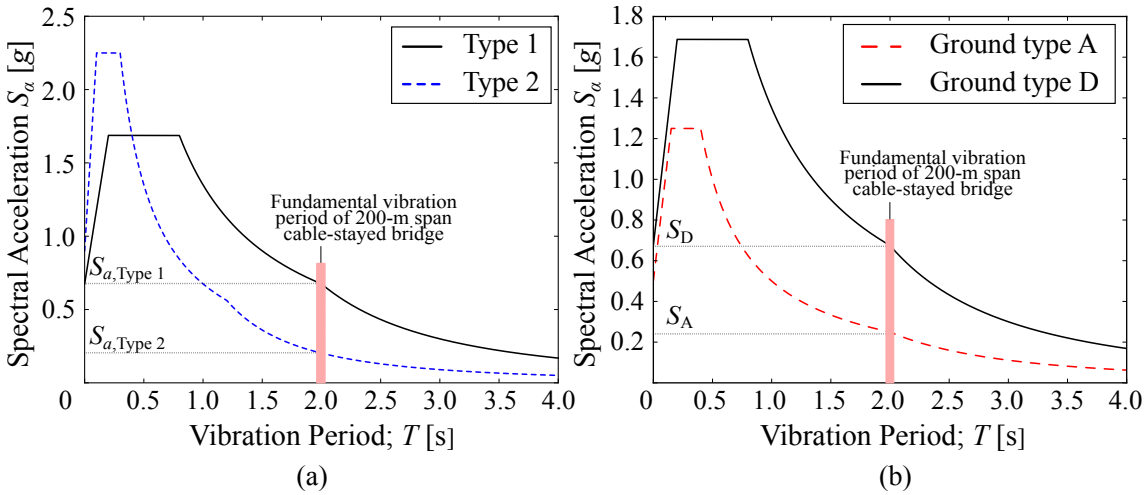

Figure 4.1: Eurocode 8; Part 1 (2004) elastic response spectra (a) Types 1 and 2 and (b) Type 1 for ground types A and D. $a_g = 0.5g$, ξ =5%.

arrays (e.g. the SMART-1 (Bolt *et al.* 1982) and the LSST (Abrahamson *et al.* 1991a, b) arrays, among others) provided that the distance between supports matches the distance between stations in the array and that the site characteristics of both regions are similar (Abdel-Ghaffar and Rubin 1983a, b). Another ideal option is to obtain the seismic signals from accelerometer arrays that are permanently installed on long and multiply supported structures (Sextos *et al.* 2014). However, both cases are not generally applicable to the study of a particular structure located at a different site or to the general study of this thesis. Previous works on the SVGM have considered natural ground motions that were modified to account for the multi-support excitation (e.g. Soyluk and Dumanoglu (2000)), or artificial signals generated as a combination of harmonics that respect the prescribed frequency content and correlations at different supports of the structure (e.g. Soyluk and Sicacik (2011)).

Both natural and artificial accelerograms have advantages and disadvantages. Natural records, can represent the actual parameters of the ground motion and they are realistically nonstationary both in the time and frequency domains. However, even though there exist databases (e.g. PEER-NGA (Ancheta *et al.* 2013)) that contain thousands of recordings from hundreds of earthquakes worldwide, natural accelerograms are not always compliant with the 'accepted' design seismic regulations. Current practice suggests the use of multiple[1] acceleration time-histories that match the prescribed design spectra for the site under consideration. It is not always possible to find records that are compatible with the design spectra in different directions (particularly from the same event), leading either to the scaling of the actual records or to the employment of records that have been recorded in regions with very different soil conditions, source-to-site distances or rupture mechanisms compared to those dictated by the seismic hazard in the site of the

[1]Eurocode 8; Part 1 (2004) prescribes the use of at least three acceleration time-histories when the maximum response is to be examined, or at least seven when the average response is to be considered.

structure under consideration. Scaling of natural records is often required so that their spectral amplitudes match those of the target spectrum. Moreover the initial frequency content of a natural record is often modified resulting in what can be considered eventually as an 'artificial' accelerogram.

On the other hand, there exist analytical models in order to generate acceleration time-histories. These are based on stochastic processes and they represent an adequate and widely accepted approach. It is acknowledged that artificial accelerograms may be unable to realistically capture the frequency content, nonstationary properties and input energy rate of natural records. To this end, several models have been developed to represent the nonstationarity, the strong motion window of the signal and its frequency content. An important advantage of artificial records is that any required level of accuracy in terms of the matching to a target spectrum, and any number of independent records with the same matching, can be obtained by simply increasing the computational time in the generation of these signals. Once the accelerograms are computed, they can be used in the structural analysis and the results are less affected by the record-to-record variability than the corresponding results from natural records, given their good fit to the target spectra in a given range of vibration periods of interest. Artificial signals also allow to represent the SVGM in the time and the frequency domains directly.

This work aims to obtain general conclusions on the effect of the SVGM in cable-stayed bridges. In order to avoid losing generality in the results the minimum prescriptions of the site characteristics and the seismic hazard were given in the previous section. This limits the applicability of natural records, which are strongly influenced by the site in which they were recorded and the magnitude of the event, among other seismological aspects. In addition, there are not sufficient unscaled natural records that can match the proposed design spectra in the range of important vibration periods for the short, intermediate and long-span bridges considered in this work. A more abstract definition of the seismic action is needed in order to focus on the effect of the SVGM and this can be provided by the artificial accelerograms which are adopted herein. Each set of records is comprised of ground motions along the two horizontal directions of motion, 'x' (direction of traffic) and 'y'. Moreover, due to the SVGM, each set is represented by a number of motions equal to the number of the supports that are affected by the earthquake.

To proceed with the generation of appropriate artificial accelerations, a spatial variability model must be considered in the form of a coherency function (as discussed in Section 2.3.4). There are two ways to generate spatially variable seismic motions and they are both accepted by the engineering community. One way is to apply a coherency model to a natural record that has been appropriately selected for the region under consideration. These simulations are often referred to as 'Conditional Simulations' (Zerva 2009) and have proved a powerful tool for the evaluation of the response of structures under differential support motions because they can capture the physical characteristics of natural

records (i.e. nonstationarity both in the frequency and time domains, distance between the source and the site and local soil conditions, among others). However, as the distance between the site under consideration and the site with the target motion increases, so does the variance of the generated signals at those sites. Moreover, as observed by Camara (2011) the unavoidable noise that is contained in the natural records tends to be filtered out along with important frequencies of the signals that fall below the cut-off frequency of 0.25 Hz, which can be important for the study of cable-stayed bridges. Another approach is to generate artificial signals based on a prescribed PSD or a Response Spectrum (RS) and modify them by a coherency function. It is acknowledged that artificial multi-support acceleration time-histories lack the ability to reflect the physical characteristics of their natural counterparts[1]. It has been proposed that a RS can be converted to a PSD spectrum and be used as the basis for the generation of spectrum compatible time-histories, but this approach may not yield accurate results. This is because, as observed by Zerva (2009), one frequency component of the time-history can affect other frequencies in the RS.

To summarise, for the present work artificial sets of acceleration time-histories have been generated based on a target spectrum (Eurocode 8; Part 1 2004) for two extremely different ground categories (ground types A and D) which were modified by an appropriate empirical loss of coherency model. The resulting acceleration histories have been used as input ground motions to the supports of the studied cable-stayed bridges.

4.4 Generation Scheme

The methodology proposed by Deodatis (1996) is employed in this work for the generation of spectrum compatible acceleration histories through an iterative scheme that is described below and was achieved by generating a computer program in Python (van Rossum 1995). Based on the assumption of Shinozuka (1972) that stochastic processes can be described as a sum of cosine functions with random phase angles, the representation of a homogeneous Gaussian random process $f(x)$ with zero mean and standard deviation $\sqrt{2S(\omega)\Delta\omega}$ can be described as:

$$f(t) = \sqrt{2}\sum_{i=1}^{K} C_k \cos(\omega_k t + \phi_k) \tag{4.1}$$

where C_k = $\sqrt{2S(\omega_k)\Delta\omega}$, S is the PSD, ω_k with $k = 1, 2, \ldots, K$ is the discrete circular frequency in [rad/s], $\Delta\omega$ is the frequency step and ϕ_k are independent random phase angles uniformly distributed over the range [0, 2π). The accelerograms are considered to be non-stationary processes, but the strong motion window of the time-histories can

[1]Herein, such properties are accounted for by implementing an empirical coherency model obtained from the SMART-1 array as will be discussed in Section 4.5.2.

be viewed as a stationary process (Harichandran and Vanmarcke 1986), hence for the generation of stationary acceleration time-histories the following methodology applies.

When considering multivariate, stationary stochastic processes with zero mean, the cross spectral density matrix is given as a function of the circular frequency ω in [rad]:

$$S(\omega) = \begin{bmatrix} S_{11}(\omega) & S_{12}(\omega) & \dots & S_{1m}(\omega) \\ S_{21}(\omega) & S_{22}(\omega) & \dots & S_{2m}(\omega) \\ \vdots & \vdots & \ddots & \vdots \\ S_{m1}(\omega) & S_{m2}(\omega) & \dots & S_{mm}(\omega) \end{bmatrix} \tag{4.2}$$

in which m is the number of stations, S_{jj} is the PSD (Eq. (2.1)) of the motion at station j with $j = 1, 2, \dots, m$, S_{jk} is the cross spectral density between stations j and k (with j and k = taking values of 1, 2,..., m, and $j \neq k$), $S_{jk}(\omega) = \sqrt{S_{jj}(\omega) S_{kk}(\omega)}\gamma_{jk}(\omega)$ and $\gamma_{jk}(\omega)$ is the complex coherency function between stations j and k as defined in Eq. (2.5).

Based on the theory of evolutionary spectra (Priestley 1965), one can consider a nonstationary process[1] of time and frequency by means of a modulating function, $I_{j,\,k}(\omega, t)$, as follows:

$$S_{jj}(\omega, t) = |I_j(\omega, t)|^2 S_{jj}(\omega) \tag{4.3a}$$

$$S_{jk}(\omega, t) = I_j(\omega, t) I_k(\omega, t) S_{jk}(\omega) \tag{4.3b}$$

For the resulting nonstationary process the cross spectral density matrix becomes a function of ω in [rad] and the time t in [s]:

$$S(\omega, t) = \begin{bmatrix} S_{11}(\omega, t) & S_{12}(\omega, t) & \dots & S_{1m}(\omega, t) \\ S_{21}(\omega, t) & S_{22}(\omega, t) & \dots & S_{2m}(\omega, t) \\ \vdots & \vdots & \ddots & \vdots \\ S_{m1}(\omega, t) & S_{m2}(\omega, t) & \dots & S_{mm}(\omega, t) \end{bmatrix} \tag{4.4}$$

The matrix is Hermitian and its elements have the following properties:

$$S_{jj}(\omega, t) = S_{jj}(-\omega, t), \quad j = 1, 2, \dots, m \tag{4.5a}$$

$$S_{jk}(\omega, t) = S^*_{jk}(-\omega, t), \quad j, k = 1, 2, \dots, m \text{ and } j \neq k \text{ for every } t \tag{4.5b}$$

$$S_{jk}(\omega, t) = S^*_{jk}(\omega, t), \quad j, k = 1, 2, \dots, m \text{ and } j \neq k \text{ for every } t \tag{4.5c}$$

[1] In contrast to a stationary process which only depends on the time lag τ, a nonstationary process depends on absolute time increments (t_1, t_2,...) and not just on time differences.

The symbol * denotes the complex conjugate of a number. The matrix of Eq. (4.4) can be decomposed at every time instant t into the following:

$$S(\omega, t) = H(\omega, t)H^{\mathrm{T}^*}(\omega, t) \tag{4.6}$$

The symbol $^{\mathrm{T}}$ denotes the transpose of a matrix. The decomposition can be performed by means of Cholesky's method in which case $H(\omega, t)$ is a lower triangular matrix, as follows:

$$H(\omega, t) = \begin{bmatrix} H_{11}(\omega, t) & 0 & \dots & 0 \\ H_{21}(\omega, t) & H_{22}(\omega, t) & \dots & 0 \\ \vdots & \vdots & \ddots & \vdots \\ H_{m1}(\omega, t) & H_{m2}(\omega, t) & \dots & H_{mm}(\omega, t) \end{bmatrix} \tag{4.7}$$

where $H_{jj}(\omega, t)$ are real non-negative values and $H_{jk}(\omega, t)$ with j, $k = 1, 2, \dots, m$ and $j \neq k$ are complex functions of the circular frequency ω [rad/s] and of time t [s]. H_{jk} can be re-written in polar form as follows:

$$H_{jk}(\omega, t) = |H_{jk}(\omega, t)| \exp\left[\mathrm{i}\, \theta_{jk}(\omega, t)\right] \tag{4.8}$$

$$\theta_{jk} = \tan^{-1} \frac{\mathrm{Im}\left[H_{jk}(\omega, t)\right]}{\mathrm{Re}\left[H_{jk}(\omega, t)\right]} \tag{4.9}$$

Finally, having decomposed the cross spectral density matrix $S_{jk}(\omega, t)$, the spectrum-compatible acceleration history at the j^{th} horizontal support of the bridge is extended from Eq. (4.1):

$$f^{(j)}(t) = 2 \sum_{m=1}^{4} \sum_{l=1}^{N} |H_{jm}(\omega_l, t)| \sqrt{\Delta\omega} \cos\left(\omega_l t - \theta_{jm}(\omega_l, t) + \Phi_{ml}\right), \quad j = 1, 2, 3, 4 \tag{4.10}$$

where j represents the support of interest and m the total number of supports between which the stochastic process is established[1], $\omega_l = l\Delta\omega$ (with l = 1, 2, ..., N) is the discrete frequency, $\Delta\omega = \omega_u/N$ is the frequency step, ω_u is the cut-off frequency beyond which the cross spectral density matrix has practically no effect on the simulations, Φ_{ml} are independent random phase angles uniformly distributed over the range [0, 2π).

[1] In the application to the proposed cable-stayed bridges it starts from the first abutment, where $m = 1$, and continues with the first pylon, $m = 2$, the second pylon, $m = 3$ and the second abutment, $m = 4$

The methodology to generate stationary spectrum compatible time-histories that account for the SVGM that is presented in the following was initially proposed by Deodatis (1996) following preceding work from Hao *et al.* (1989) and Abrahamson (1993). The approaches differ essentially in the manner that the target spectrum is considered. Deodatis (1996) proposed an iterative scheme. By initially introducing $S_{jj}(\omega)$ as constant noise for the whole frequency range, stationary histories are generated based on Eq. (4.10). The resulting stationary signals are consequently modulated by appropriately selected modulating functions to become non-stationary processes $\ddot{u}_g^{(j)}(t)$, $j = 1, 2, 3, 4$. For the seismic signals of the present study, uniformly modulated stochastic processes have been considered and hence the modulating function is reduced to a function of time only; $I(\omega, t) = I(t)$, which will be discussed in Section 4.5.5.

$$\ddot{u}_g^{(j)}(t) = I(t) f^{(j)}(t) \tag{4.11}$$

Then the RS obtained at the end of the i^{th} iteration from the generated acceleration history at support j, $\text{RS}_j^{(i)}$, is compared to the target $\text{RS}_j^{\text{target}}(\omega)$ and until acceptable convergence is reached the process is repeated with an updated S_{jj} as follows:

$$S_{jj}^{(i+1)}(\omega) = \left[\frac{\text{RS}_j^{\text{target}}(\omega)}{\text{RS}_j^{(i)}(\omega)} \right]^2 S_{jj}^{(i)}(\omega) \tag{4.12}$$

where: $S_{jj}^{(i+1)}$ is the resulting PSD at station j for the next iteration.

Later modifications/improvements on this approach have been proposed by several researchers and two of them are worth mentioning. Cacciola and Deodatis (2011) avoided the need for iterations by obtaining PSD spectra from the resulting RS after having scaled the latter to match the target RS at least at one point over the frequency range without exceeding the target values, and then by generating the final acceleration histories from the estimated PSD's. However, as mentioned in Section 4.1, there may be certain frequency components of the resulting time histories that can affect other frequencies of the RS and, hence, the accuracy of the matching may be compromised. Another approach was proposed by Shields (2014) who observed that as the iterations in Eq. (4.12) progress, the coherency is gradually lost and that the resulting signals deviate from the assumed Gaussian distribution. His proposal is summarised in the introduction of random perturbations after each iteration to ensure that the dependence of S_{jj} on the random angles (Φ) remains minimal and that there is no deviation from the Gaussian distribution. The main drawback of this methodology is that it requires thousands of iterations to converge, in comparison

to the original approach by Deodatis (1996) which usually converges after ten iterations[1]. The computational cost is deemed very high in the proposal given by Shields (2014) and for this reason, Deodatis' methodology is employed in the present study.

4.5 Components of the Signal Generation

4.5.1 Frequency Range

The cutoff frequency, ω_u, is considered equal to 220 rad/s ($f_u = 35$ Hz) because it is normally considered that beyond this limit the contribution of the vibration frequencies to the response of civil engineering structures is not significant (Chopra 2017). The lower limit of the frequency range, ω_{min}, is defined by the fundamental frequency of the structure. Eurocode 8; Part 1 (2004) defines the important range of periods to be in the range of [$0.2T_1$, $2T_1$], where T_1 is the fundamental vibration period of the structure. However, the upper bound of $2T_1$ is deemed too conservative, given that it is unlikely for a structure to elongate its fundamental period by a factor of two due to the damage induced by the earthquake (Sextos *et al.* 2011). Furthermore, the limit of $2T_1$ can be considered problematic in the case of long fundamental periods, especially in the cable-stayed bridges with the longest spans in this proposed study; for the 600-m span bridges the upper bound of the range of important periods would exceed 10 s, for which the definition of the target spectra is unclear. Eurocode 8; Part 2 (2005) has reduced the upper bound of the period range to $1.5T_1$ for bridges with medium to high ductility and previous studies on the seismic response of cable-stayed bridges (Camara 2011) have reduced it further to $1.2T_1$. The frequency step, $\Delta\omega$, is a function of ω_u and the number of discrete frequencies, M.

$$\omega_u = 220 \text{ rad/s } (f_u = 35 \text{ Hz});$$
$$\omega_{\text{min,200}} = 2.62 \text{ rad/s}; \quad \omega_{\text{min,400}} = 1.75 \text{ rad/s}; \quad \omega_{\text{min,600}} = 1.05 \text{ rad/s};$$
$$M = 440; \quad \Delta\omega = \frac{\omega_u}{M} = 0.5 \text{ rad/s}$$

Different values of M have been adopted by the author in order to reach an efficient value in terms of computational cost without losing any of the desired resolution. Initially a value of $M = 2200$ discrete frequencies was considered, leading to a frequency step $\Delta\omega = 0.01$ rad/s. This value was employed based on the assumption that a small frequency step would allow for a larger number of frequency components to be introduced to the signal generation process for every time increment (Eq. (4.10)), and hence it would result in a more detailed and realistic signal. Moreover, the matching between the target RS and the obtained RS from the acceleration time-histories at the end of each iteration

[1] Using a relatively powerful computer (installed RAM memory of 8 GB) to generate accelerograms with a duration of 20 s, a single iteration takes about 2 minutes to complete. By considering ten iterations, 20 minutes are required to obtain one acceleration time-history, which is deemed acceptable.

would be performed at more frequency points. Unfortunately, this process was too expensive in terms of computational cost. When operating on uniformly modulated[1] stochastic processes, the frequency step needs not be as small as $\Delta\omega = 0.01$ rad/s. Deodatis (1996), proposed a frequency step equal to $\Delta\omega = 1.0$ rad/s. Finally, $M = 440$ frequency components ($\Delta\omega = 0.5$ rad/s) have been employed for the generation of uniformly modulated, nonstationary signals herein.

4.5.2 Coherency

A thorough discussion on the coherency function and on the different empirical and semi-empirical models that are available to describe the loss of coherency with frequency and distance has been included in Section 2.3.4. Coherency models that allow for high correlation between signals in the frequency range that is close to the structure's natural frequencies[2] result in the dynamic component of the response being more pronounced than the pseuso-static component (Zerva 2009).

A sensitivity analysis has been performed by examining three of the most commonly used coherency models. The model proposed by Harichandran and Vanmarcke (1986) is compared to the model of Luco and Wong (1986) as defined in Eqs. (2.9) and (2.10), respectively. For the first model, two different earthquake scenarios have been considered, namely 'H&V' and 'H&W' cases which correspond to Event 20 (recorded at the SMART-1 array) as originally proposed by Harichandran and Vanmarcke (1986), and to Event 24 as proposed by Harichandran and Wang (1990), respectively. For the model of Luco and Wong (1986), 'L&W', a moderate coherency drop (i.e. $a_{\mathrm{LW}} = 2{\cdot}10^{-4}$ s/m) has been considered. Fig. 4.2 compares different lagged coherency models by means of the peak seismic transverse shear force along the height of the pylon in the bridge with 400 m main span. It is observed that the 'H&V' model results in shear forces that lie between the respective values of the two other limiting lagged coherency models and for this reason this model is eventually adopted for the accelerograms. The 'H&W' model presents higher loss of coherency than 'H&V' in the low frequency range and this might overestimate the effect of the SVGM on the response of the bridges. This is because a lower rate of coherency between signals results in larger differential displacements between the corresponding supports. On the other hand, the 'L&W' model seems to underestimate the effect of the SVGM because it assumes completely coherent motions in the low frequency range which is important in cable-stayed bridges. To this end, the model of Harichandran and Vanmarcke (1986) (H&V) has been adopted to model the coherency loss in this thesis.

[1] A uniformly modulated process is defined as one whose frequency content remains constant, and only its amplitude changes as a function of time.

[2] In this work low frequencies are of interest because of their characteristic importance for the seismic response of cable-stayed bridges.

$L_P = 200$ m				$L_P = 400$ m				$L_P = 600$ m			
t_{A1}	t_{P1}	t_{P2}	t_{A2}	t_{A1}	t_{P1}	t_{P2}	t_{A2}	t_{A1}	t_{P1}	t_{P2}	t_{A2}
0	0.08	0.28	0.36	0	0.16	0.56	0.72	0	0.24	0.84	1.08

Table 4.1: Time instances t_i with i = A1, P1, P2, A2 of the arrival of the seismic waves at different supports of the cable-stayed bridges depending on the main span length of the bridges. $\theta = 0°$, t_i in [s].

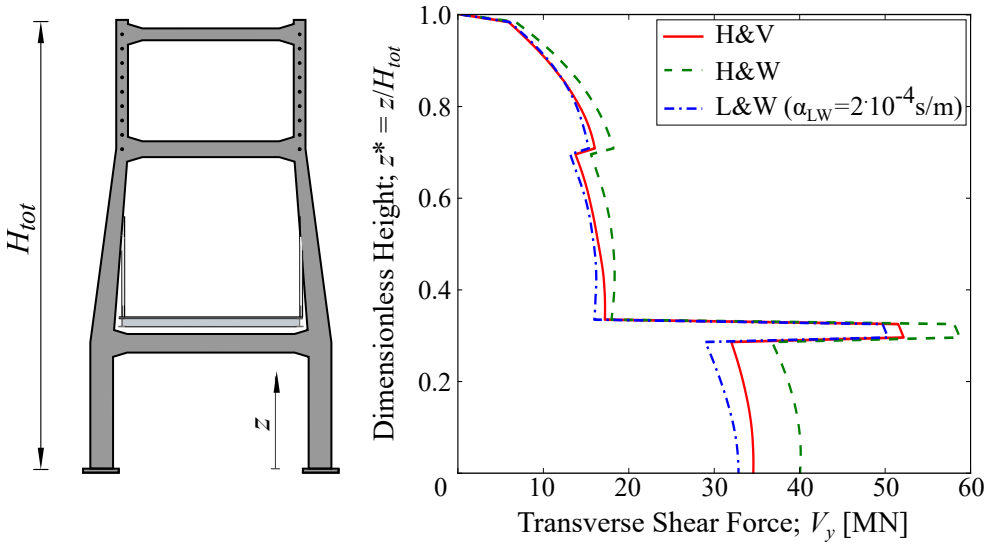

Figure 4.2: Peak transverse, V_y, shear force along the pylon of the bridge with $L_P = 400$ m for different coherency models. $c = 1000$ m/s, Ground type D.

4.5.3 Temporal Variability

In the case of long structures the time delay can reach several seconds (Soyluk and Dumanoglu 2000). Apart from the loss of coherency, the present research accounts for the temporal variability of the ground motion by means of the time delay between subsequent supports. The wave passage effect is described by Eqs. (2.15) and (2.16). The reference support is the first abutment (A1) which is considered to be affected by the earthquake at time instance $t_{A1} = 0$ s. Table 4.1 includes the time instances when the earthquake reaches each support calculated on the basis of the different span lengths when the earthquake propagates parallel to the deck ($\theta = 0°$) and the time delay is maximised, as it will be explained in Section 4.7.

In order to get a more comprehensive idea of the effect of the SVGM on the seismic response of cable-stayed bridges it is common to compare the response quantity of interest from the spatial variability scenarios to the respective quantity from identical support motion (Shinozuka *et al.* 2000, Sextos *et al.* 2003). To this end, infinite velocity of the seismic waves has been also considered in this research representing the synchronous motion scenario (SYNC). In this case the reference action at the abutment A1 is applied

Ground Type	ω_j [rad/s] (Soyluk and Dumanoglu 2004)	ξ_j (Der Kiureghian and Neuenhofer 1992)
A (Firm Ground)	15	0.6
D (Soft Soil)	5	0.2

Table 4.2: Soil parameters for the frequency-response function of Eq. (4.13).

to the four supports of the cable-stayed bridges simultaneously.

4.5.4 Local Soil Conditions

The soil conditions may vary significantly among the supports of long structures (Der Kiureghian 1996). The site response effect is accounted for by means of Eq. (2.17) and (2.18). For the frequency-response functions $H_j(\omega)$ at each support j of Eq. (2.18), the following model is adopted which idealises the soil layer as a SDoF oscillator with frequency ω_j and damping ξ_j (Der Kiureghian 1996):

$$H_j(\omega) = \frac{\omega_j^2 + 2\,\mathrm{i}\,\xi_j\omega_j\omega}{\omega_j^2 - \omega^2 + 2\,\mathrm{i}\,\xi_j\omega_j\omega} \tag{4.13}$$

The values for ω_j and ξ_j are adopted from Soyluk and Dumanoglu (2004) and Der Kiureghian and Neuenhofer (1992), respectively for the different ground types that are assumed herein. These values are presented in Table 4.2. To explore the effect of the local soil conditions at the supports two extremely different ground categories are examined between the abutments and the pylons, corresponding to ground type A (as defined in Eurocode 8; Part 1 (2004)) at the abutments and type D at the pylons.

4.5.5 Modulating Function

The stationary signal obtained from Eq. (4.10) is modulated in time to be assigned a finite total duration and a strong motion window. In this research the modulating function introduced by Amin and Ang (1966) and included in Fig. 4.3 has been adopted following the suggestions from Jennings *et al.* (1968):

$$I(t) = \begin{cases} (t/t_1)^2 & \text{if } 0 \le t < t_1 \\ 1 & \text{if } t_1 \le t < t_2 \\ \exp\left[-c(t-t_1)\right] & \text{if } t \ge t_2 \end{cases}$$

It should be noted that the strong motion window of this intensity modulating function preserves the target PGA of the stationary signal ($I(t) = 1$) if $t_1 \leq t \leq t_2$: The values for the modulating function are taken as follows:

$$t_1 = 1.5 \text{ s}; \quad t_2 = 9 \text{ s}; \quad c = 0.4 \text{ s}^{-1}$$

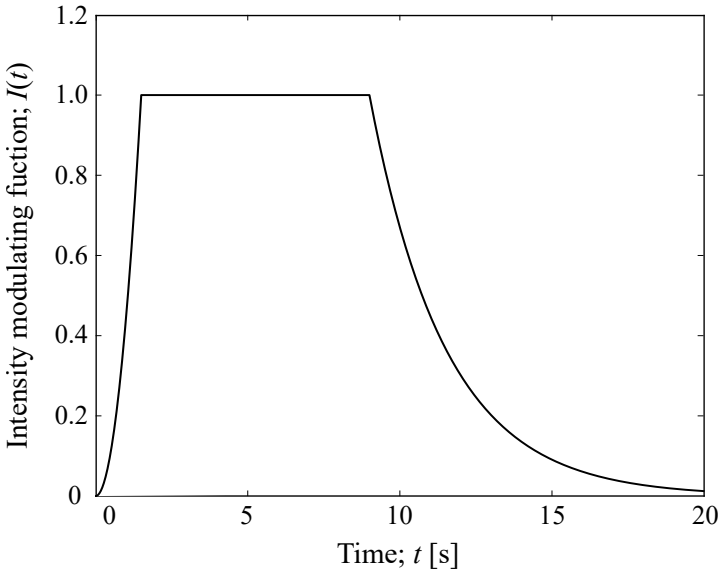

Figure 4.3: Intensity modulating function for the generated seismic signals. Proposed by Amin and Ang (1966).

4.6 Proposed Accelerogram Sets

For the purpose of the present study, spectrum-compatible acceleration histories have been generated parallel to the two horizontal components of the seismic action, namely 'Fault Parallel' (FP) and 'Fault Normal' (FN), the latter coinciding with the direction of wave propagation. For the generation of the accelerograms corresponding to the FP component of the motion a reduced target spectrum was adopted by 70% (Lopez *et al.* 2006) to account for the principal components of the earthquake motion. The coherency has been assumed independent of the direction of propagation, allowing for the same loss of coherency model to be used for the generation of signals corresponding to the FN and FP components (Sextos *et al.* 2003).

The resulting accelerograms are considered acceptable when the obtained RS of each signal falls within the range 90%-110% of the target spectrum (herein the Eurocode 8; Part 1 (2004) elastic design spectrum as defined in Section 4.2.1, see Fig. 4.1(b)) in the range of important periods of the structures: [$0.2T_1$, $1.2T_1$], T_1 being the fundamental vibration period of the structure in each case. Considering the seven different structural typologies, T_1 is obtained as 2.0, 2.87 and 5.09 s on average for the different pylon shapes and cable arrangements in the bridges with 200, 400 and 600 m main spans, respectively.

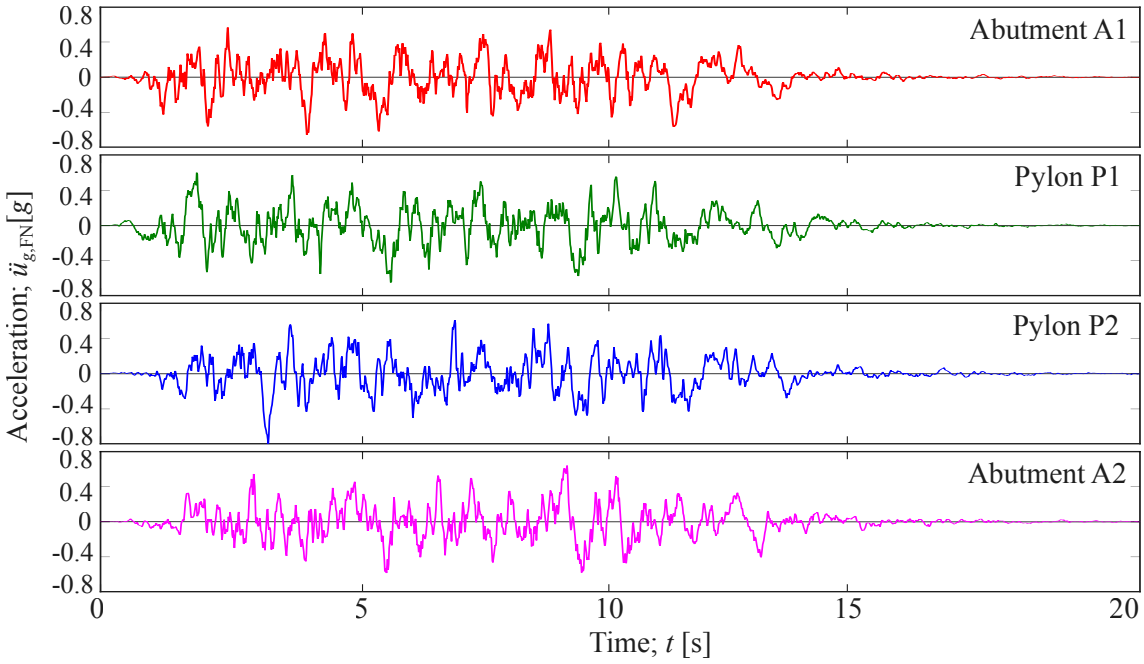

Figure 4.4: Sample set of acceleration histories in the x direction (coinciding with the deck axis). $L_P = 400$ m, c =1000 m/s.

An indicative set of accelerograms generated for the supports of the 400-m main span bridge is included in Fig. 4.4, where the time delay and the loss of coherency between supports can be appreciated. The generated sets of accelerograms have been baseline corrected to remove the baseline drift at the end of the displacement time-histories. For the baseline correction of the accelerograms the software Seismosignal has been used (SeismoSoft 2018). The baseline correction in the software is performed by determining, through regression analysis, the 3rd degree polynomial curve that best fits the time-acceleration pairs of values and then by subtracting from the actual acceleration values their corresponding counterparts as obtained with the regression-derived equation. Fig. 4.5 shows a good match between the FN and FP target spectra and those of the resulting signals.

4.6.1 Coherency of the Generated Accelerograms

The coherency of the generated signals has been obtained and compared to the target coherency from the model of Harichandran and Vanmarcke (1986). The approach of Abrahamson *et al.* (1991b) and Zerva and Zervas (2002) is employed to obtain the resulting coherency based on the assumption that the cross and power spectra at two supports j and k are the Discrete Fourier Transforms (DFT), $A_j(\omega_n)$ and $A_k(\omega_n)$, of the acceleration series, $\ddot{u}_{g,j}$ and $\ddot{u}_{g,k}$ at j and k, respectively:

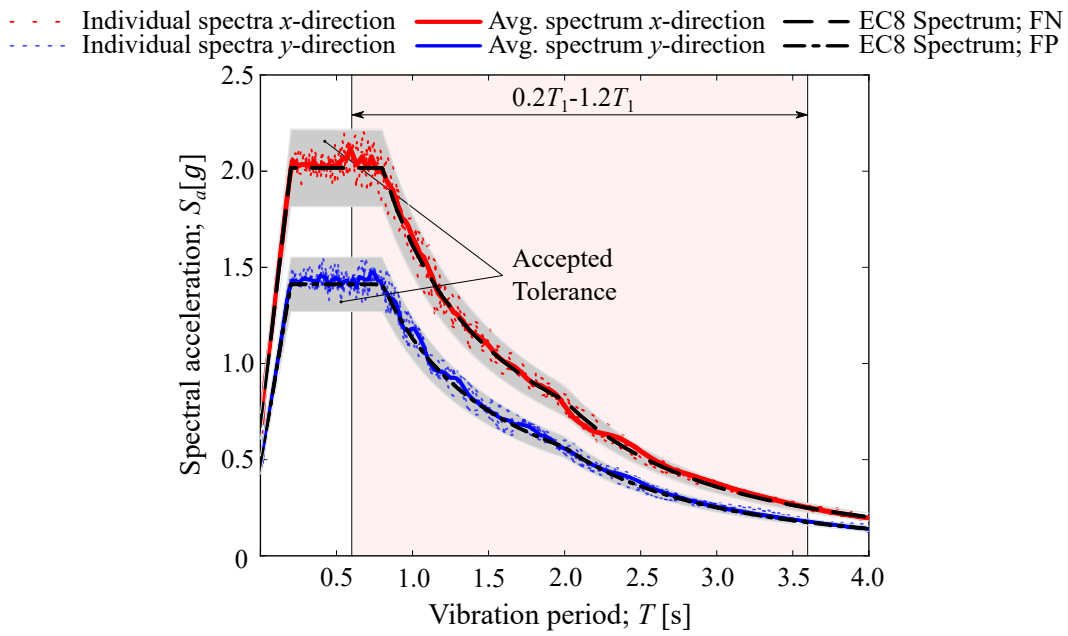

Figure 4.5: Average (Avg.) of the acceleration spectra at the four supports of the 400-m span bridge when $\theta = 0°$, i.e. deck in the FN direction. The target spectra are also included.

$$A_{j,k}(\omega) = \sqrt{\frac{\Delta t}{2\pi N}} \sum_{l=0}^{N-1} \ddot{\mathrm{u}}_{g,j,k}(l\Delta t) \exp\left[-\mathrm{i}\,\omega l \Delta t\right] \tag{4.14}$$

Then the smoothed cross spectrum becomes:

$$S_{jk}(\omega) = \sum_{m=-M}^{M} W(m\Delta\omega) A_j^*(\omega_n + m\Delta\omega) A_k(\omega_n + m\Delta\omega) \tag{4.15}$$

where the spectral window, $W(\omega)$, is the Fourier transform of the lag window $\omega(\tau)$, $\Delta\omega$ is the frequency step and M is the parameter that defines the smoothing window. Finally the resulting smoothed coherency between the ground motions at supports j and k is calculated from Eq. (2.5):

$$\gamma_{jk}^{M}(\omega) = \frac{S_{jk}^{M}(\omega)}{\sqrt{S_{jj}^{M}(\omega) S_{kk}^{M}(\omega)}} \tag{4.16}$$

The choice of the smoothing window is important. The higher the value of the smoothing window, the lower the observed bias, but the resolution is also affected (Harichandran and Vanmarcke 1986). A 15-point ($M = 7$) Hamming smoothing window is applied to reduce the variance. Another reason why smoothing is necessary is that in lack of it, the coherency would equal unity in the frequency range considered (Abrahamson *et al.* 1991b, Zerva 2009).

Fig. 4.6 presents the obtained lagged coherency between the acceleration time histories at the first (in the direction of the eartquake propagation) abutment (A1) and at the first pylon (P1). It can be seen that there is a good agreement between the obtained coherency and the target coherency of Harichandran and Vanmarcke (1986), which validates the induced spatial variability between the signals in terms of the coherency loss and highlights the efficiency of the adopted iterative algorithm of Deodatis (1996). The observed spurious peaks, especially at the higher frequencies, are due to the lower values of the resulting power spectra (Zerva 2009) and possibly due to the increased weight of the random phase angles (Φ) at higher frequencies, where the influence of the PSD is lower than the influence of Φ. Zerva (2009) suggested that in the estimation of the resulting coherency only the stationary part of the signal may be considered. This is because the generation of signals involves the modulation of stationary random processes (Harichandran and Vanmarcke 1986) by time-dependent envelope functions $I(t)$ which may affect the phase of the resulting signals.

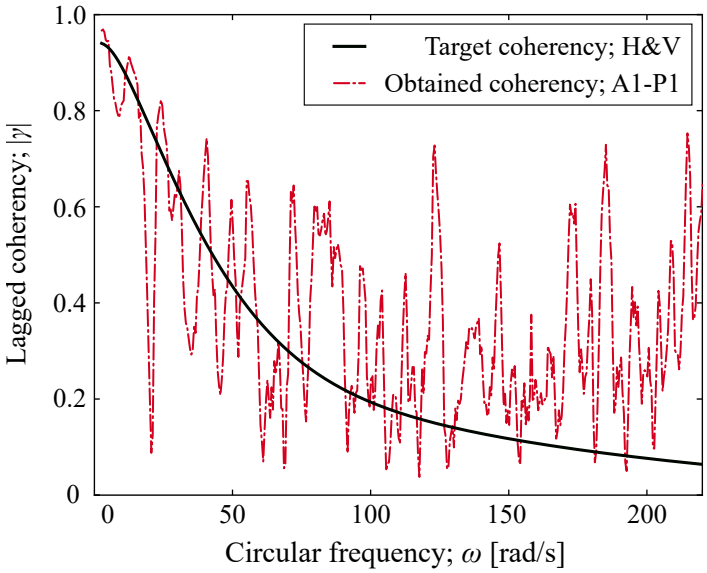

Figure 4.6: Estimated lagged coherency, between the ground motions at the first abutment (A1) and at the first pylon (P1); $L_P = 200$ m.

4.7 Angle of Incidence

Following the discussion of the effect of the angle of incidence in Section 2.3.7 it is important to consider this parameter when the seismic response of the cable-stayed bridges under the effect of the SVGM is assessed. According to Mackie *et al.* (2011) there are two interpretations with regard to the incidence angle of the seismic waves. The first one assumes that the structure remains the same but the motions are rotated so that the angle they form with the axis of the structure varies. The second interpretation assumes that the earthquake remains unaltered with respect to the structure's degrees of freedom (dof)

and the complete structure is rotated so that an angle θ is formed with the axis x_{L}. Both approaches are illustrated in Fig. 4.7. In this research the second method is followed by rotating the bridge in the range of [0°, 180°] with increments of 30° and taking advantage of the symmetry of the structure. This approach allows to consider the loss of coherency and the time delay in terms of the incidence angle of the seismic action. Following the prescriptions of Allam and Datta (2004) and of Khan (2012) the coherency is considered orientation-dependent. In the lagged coherency model of Eq. (2.9), the separation distance l_{mn} between supports m and n is modified to $l_{mn}\cos\theta$ to account for the angle of incidence, θ. In the same manner, the time delay depends on the orientation of the bridge with respect to the propagation of the earthquake.

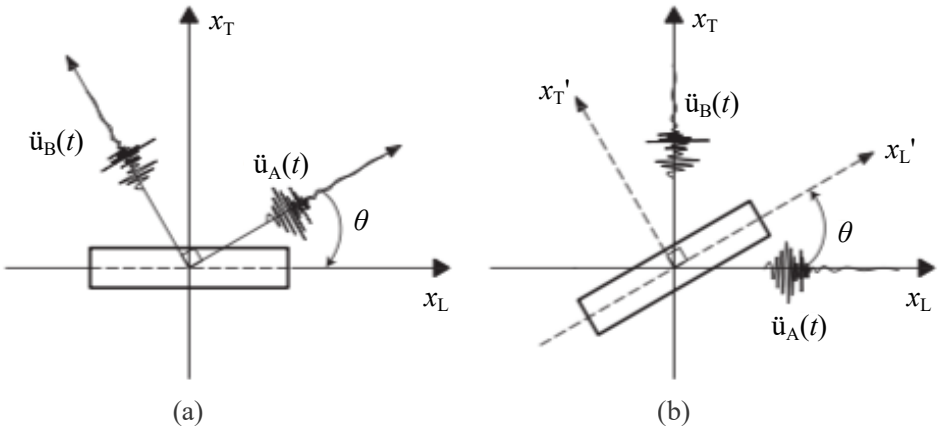

Figure 4.7: Different interpretations of the incidence angle of ground motion with respect to the structure. (a) The ground motion is rotated and (b) the structure is rotated (*taken from Mackie et al. (2011)*).

The generated accelerograms correspond to the FN and FP components of the ground motion. Fig. 4.8 shows that the axis of the bridge forms an angle θ with the FN component of the earthquake. When $\theta = 0°$ the FN earthquake component coincides with the bridge axis and when $\theta = 90°$ the bridge is rotated clockwise so that the FP component of the earthquake is parallel to the bridge axis. The different orientations of the bridge considered in this work are shown in Fig. 4.9. In the intermediate angles of incidence, the accelerograms are projected to the local x (bridge axis) and y axes of the bridge by means of the rotation matrix of Eq. (4.17):

$$\begin{pmatrix} \ddot{u}_{g,x} \\ \ddot{u}_{g,y} \end{pmatrix} = \begin{pmatrix} \cos\theta & \sin\theta \\ \sin\theta & -\cos\theta \end{pmatrix} \begin{pmatrix} \ddot{u}_{g,\mathrm{FN}} \\ \ddot{u}_{g,\mathrm{FP}} \end{pmatrix} \tag{4.17}$$

where $\ddot{u}_{g,x}$ and $\ddot{u}_{g,y}$ are the accelerations corresponding to the x and y axes of the bridge and $\ddot{u}_{g,\mathrm{FN}}$ and $\ddot{u}_{g,\mathrm{FP}}$ are the accelerations corresponding to the FN and FP components of the earthquake, respectively. The rotation of the incoherent and delayed ground motions

is presented in Fig. 4.8.

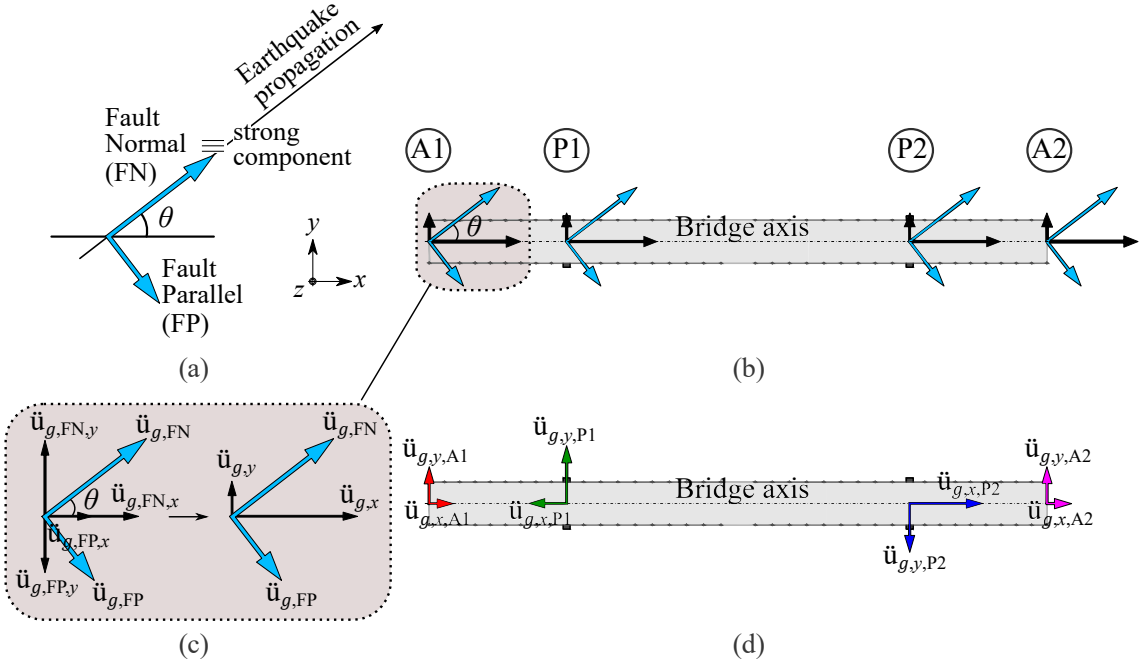

Figure 4.8: Incidence angle of the seismic waves with respect to the axis of the bridge; (a) principal components of the earthquake, (b) incidence angle θ of the seismic waves and corresponding projected earthquake components (black lines) in the case of synchronous motion of the supports and (c) detailed projection of the principal earthquake components to the local x and y axes of the bridge (*following from (b)*), (d) projected earthquakes $\ddot{u}_{g,\,i,\,j}$, with $i = x,\ y$ and $j =$ A1, P1, P2, A2 at time instance t from the start of the earthquake and for a given coherency γ.

4.8 Soil-Structure Interaction

The SVGM is closely linked with the effect of the interaction of the foundation with the surrounding soil and the structure (SSI), as discussed in Section 2.3.6, especially when the latter is founded on soft soil. Moreover, the SSI has been found to affect the stiffness and damping characteristics of a bridge (Zheng and Takeda 1995, Spyrakos and Loannidis 2003, Khan *et al.* 2004a) and to this end it is accounted for in the present research.

The foundations of the pylons are assumed to be of surface type (spread footings) laying down in a deep soil considered as a homogeneous half-space. These foundations are considered massless and rigid and their dimensions have resulted from a specific study on cable-stayed bridges (Camara 2011). These are 2.1·a × 2.1·b, with a, b the dimensions of the pylon sections at their base and a ≥ b in [m], as listed in Table 3.4. The soil around the foundation of the pylons is replaced by a system of springs and dashpots whose stiffness and damping properties are obtained from Gazetas (1991) to simulate, in a simplified manner, the SSI.

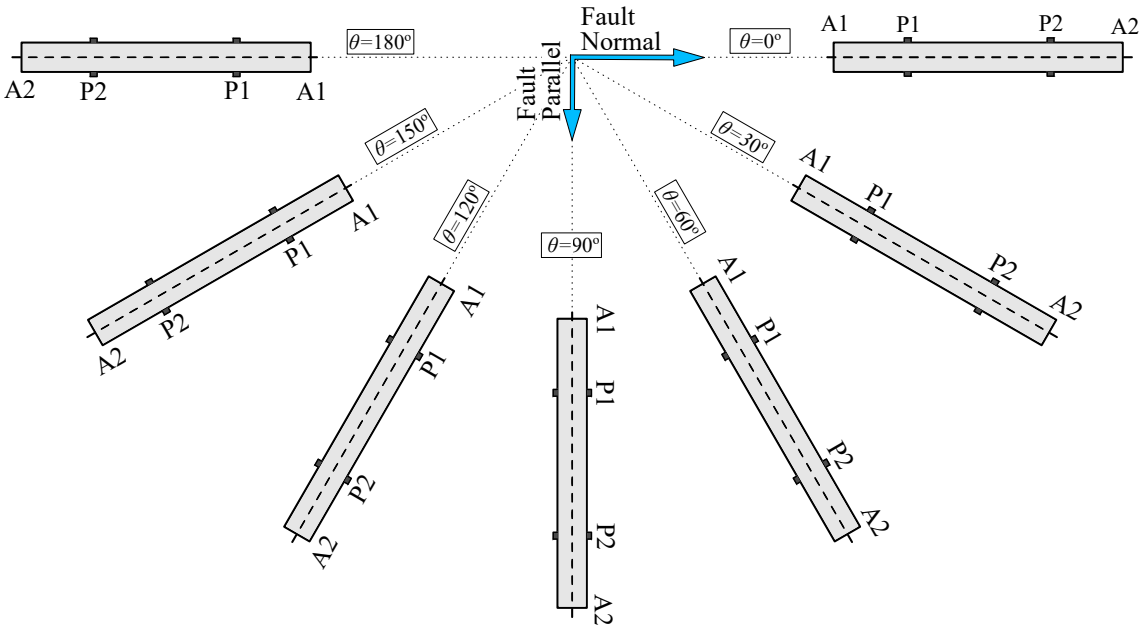

Figure 4.9: Rotation of the bridge to examine the effect of the angle of incidence of the seismic waves in range [0°, 180°] at 30° increment.

The spring-dashpot system has constant properties which are calibrated to the mean frequency of the earthquake, f_m. This measure has been adopted as an appropriate indicator of the frequency content of the ground motion (Málaga-Chuquitaype and Elghazouli 2012, Stefanidou *et al.* 2017, Demirci *et al.* 2018) and is calculated as (Rathje *et al.* 1998):

$$f_m = \frac{\sum_i C_i^2}{\sum_i C_i^2 \, (1/f_i)} \tag{4.18}$$

where C_i is the Fourier amplitude coefficient at the i^{th} discrete frequency component f_i, with 0.25 Hz $\leq f_i \leq$ 20 Hz and with $\Delta f \leq$ 0.05 Hz being the frequency interval used in the Fast Fourier Amplitude. A representative value of the mean frequency of the earthquakes considered herein is $f_m = 1.40$ Hz which has been obtained by using an *ad-hoc* code and has been verified against the resulting value from SeismoSoft (2018).

For a harmonic excitation the dynamic impedance of the soil-foundation system is defined as the ratio between the force (or moment) and the resulting steady-state displacement (or rotation) at the centroid of the base of the massless foundation (Gazetas 1991):

$$\mathrm{S}_i = \frac{\mathrm{R}_i(t)}{\mathrm{U}_i(t)} \tag{4.19}$$

where $\mathrm{R}_i(t) = R_z \exp(\mathrm{i}\,\omega t)$ is a harmonic force (or moment) and $\mathrm{U}_i(t)$ is the resulting from $\mathrm{R}_i(t)$ steady-state displacement (or rotation) along the direction i of the excitation. Impedances S_i are computed herein for the longitudinal motion in the direction parallel

to the traffic (S_x, longitudinal swaying), for the transverse motion perpendicular to the traffic (S_y, lateral swaying), for the vertical motion (S_z), for the rotational motion of the foundation about the longitudinal axis (S_{rx}, rocking) and for the rotational motion along the transverse axis (S_{ry}, rocking). For each direction the impedance is:

$$S = \overline{K} + i\,\omega C \tag{4.20}$$

in which $\overline{K}$ and C are functions of the circular frequency ω. The real component $\overline{K}$ of the complex Eq. (4.20) is the dynamic stiffness reflecting the stiffness and inertia of the surrounding soil. The imaginary component ωC is the product of the circular frequency ω multiplied by a dashpot coefficient C which reflects the material damping and the radiation of energy in the soil-foundation system.

The dynamic stiffness is estimated as the product of the static stiffness, K, times the frequency-dependent dynamic stiffness coefficient, k:

$$\overline{K}_i(\omega) = K_i \cdot k_i(\omega) \quad \text{with } i = z, y, x, rx, ry \tag{4.21}$$

The static stiffness is computed as follows (Gazetas 1991):

$$K_z = [2GL/(1-\nu)](0.73 + 1.54\chi^{0.75}) \quad \text{with } \chi = A_b/4L^2 \tag{4.22a}$$

$$K_y = [2GL/(2-\nu)](2 + 2.50\chi^{0.85}) \tag{4.22b}$$

$$K_x = K_y - [0.2/(0.75-\nu)]GL[1-(B/L)] \tag{4.22c}$$

$$K_{rx} = [G/(1-\nu)]I_{bx}^{0.75}(L/B)^{0.25}[2.4 + 0.5(B/L)] \tag{4.22d}$$

$$K_{ry} = [3G/(1-\nu)]I_{by}^{0.75}(L/B)^{0.15} \tag{4.22e}$$

where: B, L are the half-width and the half-length of the foundation, respectively, G and ν are the shear modulus and the Poisson's ratio of the soil under the foundation, respectively, A_b is the area of the surface foundation and I_{bx} and I_{by} are the area moments of inertia about the x and y axes of the soil-foundation contact surface. The dynamic stiffness coefficient for each direction is defined by means of the ratio L/B and of the dimensionless frequency factor $\alpha_0 = \omega B/V_s$, in which ω is the frequency of the excitation in [rad/s] and V_s is the shear wave velocity of the soil.

Similarly, the dashpot coefficients are obtained as follows:

$$C_z = (\rho V_{La} A_b) \cdot \overline{c}_z \tag{4.23a}$$

$$C_y = (\rho V_s A_b) \cdot \overline{c}_y \tag{4.23b}$$

$$C_x = \rho V_s A_b \tag{4.23c}$$

$$C_{rx} = (\rho V_{La} I_{bx}) \cdot \overline{c}_{rx} \tag{4.23d}$$

$$C_{ry} = (\rho V_{La} I_{by}) \cdot \overline{c}_{ry} \tag{4.23e}$$

in which $\rho = 1400$ kg/m^3 is the density of the soil under the foundation, $V_s = 250$ m/s (Soyluk and Sicacik 2011), V_{La} is Lysmer's analog wave velocity and $\overline{c}_i$ with $i = z, y, x, rx, ry$ depend on α_0 and L/B (Gazetas 1991).

$$V_{La} = \frac{3.4}{\pi(1-\nu_{\text{TD}})} V_s = 416 \text{ m/s} \tag{4.24}$$

The foundation dimensions are defined as functions of the height of the pylon above the deck, H (which is, in turn, a function of the main span length L_P, as discussed in Section 3.2). The soil characteristics are taken as $E_{\text{TD}} = 0.5$ GPa, $\nu_{\text{TD}} = 0.35$ and $G_{\text{TD}} = E_{\text{TD}}/\left[2(1+\nu_{\text{TD}})\right] = 0.185$ GPa.

4.9 Number of Earthquake Sets

Bommer and Ruggeri (2002) reviewed international codes of practice to find out that the minimum number of accelerations to be used in the seismic analysis is three or four in order to obtain the maximum response, or at least seven in order to assess the average structural response. In this section different numbers of accelerogram sets are applied to the supports of the bridge with 'H'-shaped pylons and $L_P = 400$ m and the average seismic response is obtained from ground motion sets with five, seven, ten, twelve and fifteen records in order to explore the effect of the record-to-record variability on the seismic behaviour of the pylons. Fig. 4.10 presents the average longitudinal and transverse elastic seismic response along the pylon. It is seen that the seismic response is not modified significantly with the maximum differences reaching 8% and 9.5% in the longitudinal and transverse shear forces, respectively. In this research seven sets of acceleration time-histories have been employed. This number of seismic signals is considered a good balance between the accuracy of the results and the efficiency of the analysis.

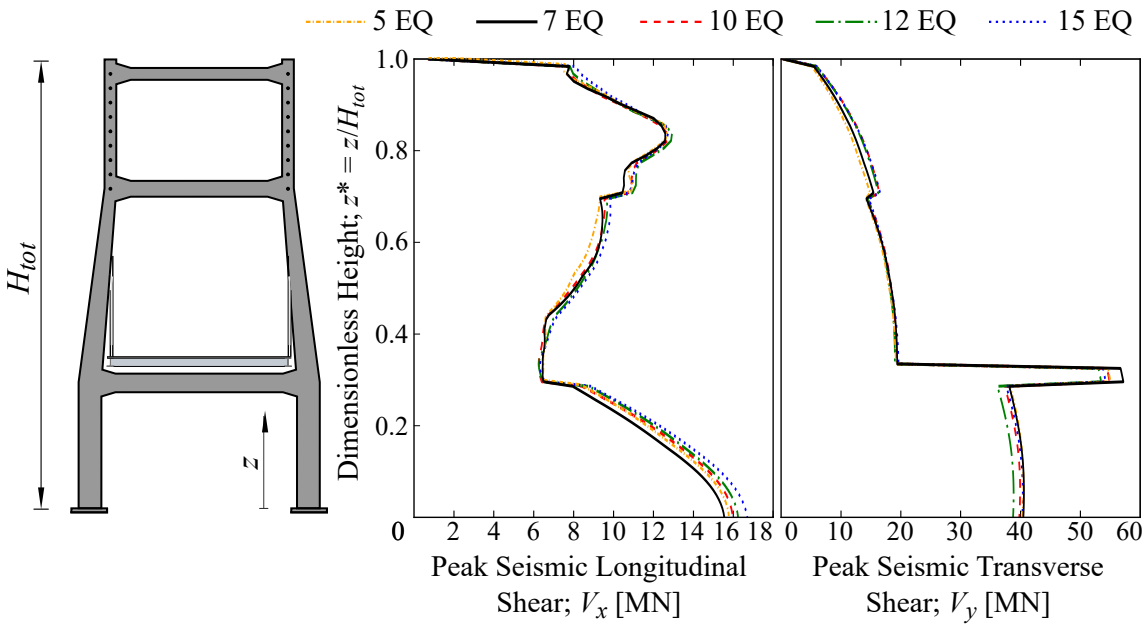

Figure 4.10: Average longitudinal, V_x, and transverse, V_y, shear forces along the pylon of the bridge with $L_P = 400$ m for different numbers of asynchronous excitations (EQ). Elastic analysis.

4.10 Conclusions

1. A computer program has been developed in Python (van Rossum 1995) to generate spatially variable ground motions that account for the loss of coherency and for the time delay following the iterative methodology of Deodatis (1996). Sets of accelerograms have been generated for ground types A and D (Eurocode 8; Part 1 2004).

2. The coherency loss has been considered by means of the empirical model proposed by Harichandran and Vanmarcke (1986). This coherency model assumes partially correlated motions at the low frequency range (<1 Hz) which is important for the seismic response of cable-stayed bridges. The choice of the coherency model influences the effect of the SVGM and hence it should be made by considering the site conditions, the distance between supports and the desired coherency drop.

3. Where the local soil conditions (site response component of the SVGM) have been considered, ground type A at the abutments is combined with ground type D at the pylons.

4. The velocity of wave propagation has been considered equal to $c = 1000$ m/s.

5. The angle of incidence (θ) has been accounted for in the generation of the accelerogram sets by considering different angles in the range [0°, 180°] at increments of 30°.

6. The loss of coherency and time delay of the ground motions between supports have been combined with the orientation of the bridge. When the earthquake propagates parallel to the bridge ($\theta = 0°$) both the aforementioned components are maximised, but when the bridge is rotated by 90° the ground motions are assumed to reach all supports simultaneously, hence having no loss of coherency or time delay.

7. The SSI has been implemented in the modelling of the faoundations at the pylons by means of simplified spring-dashpot systems following the formulas and charts proposed by Gazetas (1991). The dynamic impedances have been computed for the movement in the three principal directions of the bridge (x-traffic, y and z) and for the rotation around the x and y axes.

Chapter 5

Seismic Analysis

Contents

5.1 Introduction

The previous chapters of this thesis presented the description of the cable-stayed bridge models that have been analysed considering the SVGM (Chapter 3) and the seismic action that has been applied to the foundations of bridges (Chapter 4). This chapter comes as the logical sequence presenting the seismic analysis methodology that has been followed by the author in order to obtain the effect of the multi-support excitation on the seismic response of cable-stayed bridges.

A complete reference to the available methodologies to perform seismic analysis of long structures accounting for the effect of the SVGM has been presented in Section 2.3.8. These approaches can be static or dynamic and they can also be deterministic or stochastic. Deterministic approaches, in terms of the SVGM, usually incorporate only the time delay between supports, whereas the stochastic approaches may also account for the coherency loss and the local site conditions near the supports.

The aim of this chapter is to present the methodology adopted to perform seismic analysis of the cable-stayed bridges in this work. The discussion starts with the description of the general analysis procedure, followed by the specific parameters that allowed for the complete sets of analyses to be completed both in the elastic and the inelastic ranges.

5.2 The System of Dynamics

The system of dynamics for a linear MDoF system that is subjected to an earthquake excitation is repeated here for the reader's convenience and is written as (Clough and Penzien 2015):

$$[\mathbf{M}]\{\ddot{\mathbf{u}}\} + [\mathbf{C}]\{\dot{\mathbf{u}}\} + [\mathbf{K}]\{\mathbf{u}\} = -[\mathbf{M}]\{\boldsymbol{\iota}\}\{\ddot{\mathbf{u}}_{\mathrm{g}}\} \tag{5.1}$$

where $[\mathbf{M}]$, $[\mathbf{C}]$, $[\mathbf{K}]$ are the mass, damping and stiffness matrices, respectively, $\{\ddot{\mathbf{u}}\}$, $\{\dot{\mathbf{u}}\}$, $\{\mathbf{u}\}$ are the acceleration, velocity and displacement vectors, respectively, $[\mathbf{M}]\{\boldsymbol{\iota}\}\{\ddot{\mathbf{u}}_{\mathrm{g},i}\}$ is the support excitation and $\{\boldsymbol{\iota}\}$ is the influence vector which links the dof's of the structure and the ones which the earthquake is applied.

In order to include the SVGM to the system of dynamics, Eq. (5.1) is extended to:

$$\begin{bmatrix}\mathbf{M}_{ff} & \mathbf{M}_{fs}\\ \mathbf{M}_{sf} & \mathbf{M}_{ss}\end{bmatrix}\begin{Bmatrix}\ddot{\mathbf{u}}_f\\ \ddot{\mathbf{u}}_s\end{Bmatrix} + \begin{bmatrix}\mathbf{C}_{ff} & \mathbf{C}_{fs}\\ \mathbf{C}_{sf} & \mathbf{C}_{ss}\end{bmatrix}\begin{Bmatrix}\dot{\mathbf{u}}_f\\ \dot{\mathbf{u}}_s\end{Bmatrix} + \begin{bmatrix}\mathbf{K}_{ff} & \mathbf{K}_{fs}\\ \mathbf{K}_{sf} & \mathbf{K}_{ss}\end{bmatrix}\begin{Bmatrix}\mathbf{u}_f\\ \mathbf{u}_s\end{Bmatrix} = \begin{Bmatrix}\mathbf{0}\\ \mathbf{F}_s\end{Bmatrix} \tag{5.2}$$

in which $\mathbf{u}_f = \left[\mathbf{u}_{f,1}, \ldots, \mathbf{u}_{f,n}\right]^{\mathrm{T}}$ is the N-vector of total displacements at the unconstrained ('f') dof's, $\mathbf{u}_s = \left[\mathbf{u}_{s,1}, \ldots, \mathbf{u}_{s,r}\right]^{\mathrm{T}}$ is the R-vector of the prescribed support displacements ('s' dof's), $\mathbf{M}_{ff}$, $\mathbf{C}_{ff}$ and $\mathbf{K}_{ff}$ are the $N \times N$ mass, damping and stiffness matrices, respectively, associated with the unconstrained dof's, $\mathbf{M}_{ss}$, $\mathbf{C}_{ss}$ and $\mathbf{K}_{ss}$ are the $R \times R$ matrices associated with the supports, $\mathbf{M}_{fs}$, $\mathbf{C}_{fs}$ and $\mathbf{K}_{fs}$ are the $N \times R$ coupling matrices associated with both sets of dof's (with $\mathbf{M}_{sf}$, $\mathbf{C}_{sf}$ and $\mathbf{K}_{sf}$ being the transpose of $\mathbf{M}_{fs}$, $\mathbf{C}_{fs}$ and $\mathbf{K}_{fs}$, respectively) and $\mathbf{F}_s$ is the R-vector of the reaction forces at the support dof's.

5.3 Elastic Analysis

The elastic analysis of the bridges assumes that the constituent materials behave in a linear and elastic manner during the seismic excitation.

The geometric nonlinearities arising from the large deformations, which is a feature of cable-stayed bridges (Abdel-Ghaffar and Nazmy 1991), has been accounted for in the elastic analysis of the bridges. This is an essential consideration, especially due to the effect of the SVGM because it may induce relative movements between the pylons in the longitudinal and in the transverse directions, which may result in increased structural response in the pylons (Apaydin *et al.* 2016).

The possible impact of the deck on the pylon legs during the earthquake in the transverse direction is linearised in all cases following the simplified deck-pylon connection described in Section 3.3. This allows to suppress the nonlinearity resulting from the deck-pylon connection.

The elastic seismic analysis of the bridges can be perfomed efficiently by means of modal superposition, however, the Direct Response History Analysis (DRHA) has been adopted in this work to facilitate the comparison with the subsequent nonlinear dynamic analysis, in which modal dynamics cannot be applied. The DRHA is based on the direct step-by-step integration of the system of dynamics of Eq. (5.2) with a linearised stiffness matrix in each step (this matrix is equal to the elastic stiffness with geometric nonlinearities in the linear elastic analysis). This methodology is accompanied by a high computational cost[1], given that the coupled system of dynamics is integrated step-by-step[2]. In this research the time step has been taken as $\Delta t = 0.01$ s after a preliminary study with different values of this parameter. Fig. 5.1 shows the results of this analysis in terms of the peak transverse shear force (V_y) along the pylon leg that is connected rigidly to the

[1]Using a '*powerful*' computer (installed RAM memory of 8GB) each individual elastic analysis takes from 10 minutes in the 200-m main span bridges to 15 mins in the 600-m main span bridges.

[2]The duration of the signals is $t_{total} = 20$ s and the time step is $\Delta t = 0.01$ s, resulting in 2000 steps.

deck[1] considering time steps of 0.005, 0.01 and 0.02 s. It is noticed that for the different time steps considered, the shear force remains almost unaffected and for this reason, the intermediate value of 0.01 s is adopted, which also coincides with the time step of the acceleration histories generated in Chapter 4. However, it is acknowledged that this observation is limited by the fact that the analysis is performed in the elastic range (smaller time steps are allowed in the nonlinear analysis to account for the material degradation).

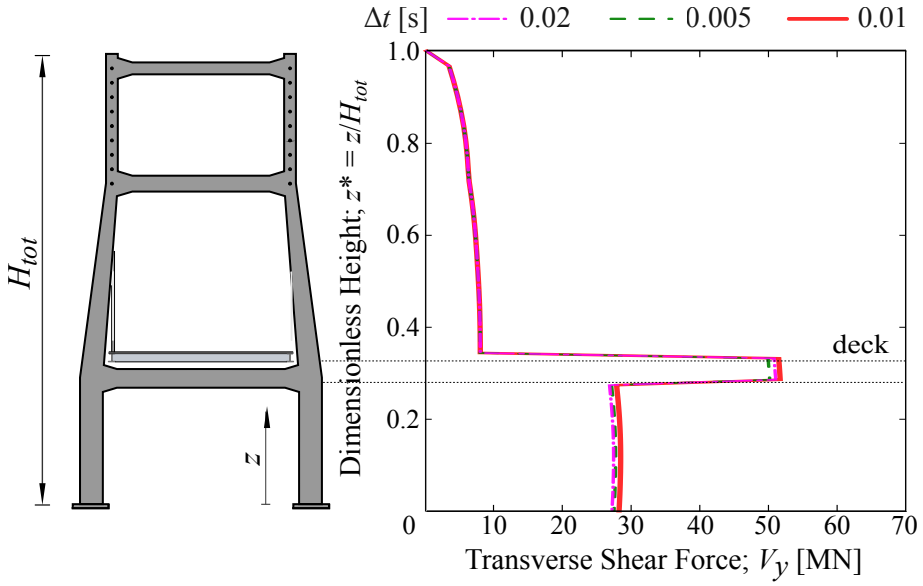

Figure 5.1: Seismic transverse shear force, V_y along the pylon leg for various integration time steps. $L_P = 200$ m, $c = 250$ m/s, $\theta = 0°$, elastic analysis.

To solve the system of differential Eqs. (5.1) and (5.2), the direct implicit HHT algorithm (Hilber *et al.* 1977) has been employed. Originally, a family of time step methods was developed, based on the following equations (Newmark 1959):

$$\dot{\mathrm{u}}_{i+1} = \dot{\mathrm{u}}_i + [(1-\gamma)\,\mathrm{d}t]\,\ddot{\mathrm{u}}_i + (\gamma \mathrm{d}t)\,\ddot{\mathrm{u}}_{i+1} \tag{5.3a}$$

$$\mathrm{u}_{i+1} = \mathrm{u}_i + (\mathrm{d}t)\dot{\mathrm{u}}_i + [(0.5-\beta)(\mathrm{d}t)^2]\ddot{\mathrm{u}}_i + [\beta(\mathrm{d}t)^2]\ddot{\mathrm{u}}_{i+1} \tag{5.3b}$$

Parameters 'β' and 'γ' define the change of the acceleration within a time step and ensure the validity of the method. A typical value for γ is $\frac{1}{2}$, while β must take values within the range $\left[\frac{1}{6}, \frac{1}{4}\right]$. Later, Hilber *et al.* (1977) developed a new, one-step implicit method, based on the existing family of Eqs. (5.3) proposed by Newmark (1959). Essentially, the new algorithm, most commonly known as the 'HHT' algorithm or the 'α method', replaces the general equation of motion (Eq. (2.30)) with a balance of d'Alembert forces at the end of the time step, t_{i+1}, and a weighted average of the static forces at the beginning, $t = t_i$, and at the end of the time step as follows:

[1]The results are obtained by means of estimating the seismic response quantities in the leg that is rigidly connected to the deck because the opposite 'free' leg does not receive a representative seismic response.

$$[\mathbf{M}]\{\ddot{\mathbf{u}}_{i+1}\} + (1+\alpha)\left([\mathbf{C}]\{\dot{\mathbf{u}}_{i+1}\} + [\mathbf{K}]\{\mathbf{u}_{i+1}\}\right) - \\ - \alpha\left([\mathbf{C}]\{\dot{\mathbf{u}}_{i}\} + [\mathbf{K}]\{\mathbf{u}_{i}\}\right) = \{\mathbf{F}_{t_{in}}\} \quad (5.4)$$

in which $\{\mathbf{F}\}$ is the force vector, α is the parameter introduced by Hilber *et al.* (1977) to control the numerical damping and $t_{in} = t_i + (1+\alpha)\,\mathrm{d}t$ is a time instance between the beginning and the end of the time step, depending on the value of α. The proposed values for parameters α, β and γ are $-\frac{1}{3} \leq \alpha \leq 0$, $\beta = \frac{1}{4}(1-\alpha)$ and $\gamma = \frac{1}{2} - \alpha$, respectively. Obviously, when $\alpha = 0$, the HHT method reduces to the trapezoidal rule established by Newmark (1959).

The structural damping is defined by means of Rayleigh's distribution which is frequency dependent. This type of damping distribution is widely used in the DRHA. The maximum damping ratio is taken equal to 2% accounting for the low structural dissipation that characterises the elastic response of cable-stayed bridges (Kawashima and Unjoh 1991). The range of important frequencies for the structural response of the bridges, and consequently the range of modes which are assigned a lower damping than 2%, is defined at the lower bound by the fundamental frequency (f_1) of the bridges. f_1 is equal to 0.50, 0.35 and 0.20 Hz for the 200, 400 and 600-m span bridges, respectively, and it is almost insensitive to the pylon shape and to the type of cable system. The upper bound of the important frequency range is set as 20 Hz in all cases (Camara 2011).

According to Rayleigh the variable damping ratio, ξ, associates, for each mode i, the damping matrix ($[\mathbf{c}]$) with the mass ($[\mathbf{m}]$) and stiffness ($[\mathbf{k}]$) matrices:

$$\xi_i = \frac{a_R}{2\omega_i} + \frac{\beta_R \omega_i}{2} \quad (5.5)$$

in which $\omega_i = 2\pi f$ is the circular frequency of the i^{th} mode in [rad/s] and a_R and β_R are the factors that define the proportionality of $[\mathbf{c}]$ with $[\mathbf{m}]$ and $[\mathbf{k}]$, respectively.

Eq. 5.5 implies that the mass proportional factor a_R is responsible for damping the lower frequencies and the stiffness proportional factor β_R damps the higher frequencies. The two factors are defined by associating the constant damping $\xi = 2\%$ with the minimum and maximum frequencies of interest: ω_{min} and ω_{max}, respectively:

$$a_R = \xi \frac{2\omega_{\text{min}}\omega_{\text{max}}}{\omega_{\text{min}} + \omega_{\text{max}}} \quad \text{and} \quad \beta_R = \xi \frac{2}{\omega_{\text{min}} + \omega_{\text{max}}} \quad (5.6)$$

Fig. 5.2 presents the variable Rayleigh's damping adopted in this study including the lower and higher frequencies of interest for the bridges with $L_P = 200$ m. It is seen

that the target structural damping $\xi = 2\%$ is the maximum damping that is applied to the vibration modes included in the range of frequencies of interest.

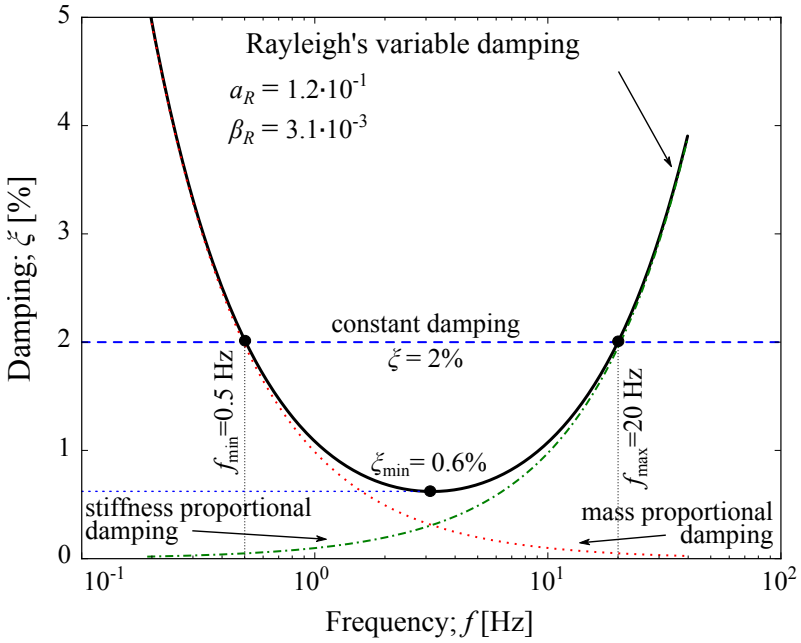

Figure 5.2: Rayleigh's variable damping introduced to the dynamic analysis of the bridges with $L_P = 200$ m.

5.4 Inelastic Analysis

When a structure is subjected to large magnitude seismic excitations it is possible that it will exceed the elastic range suggesting the need to predict their nonlinear response. In this research the NonLinear Reasponse History Analysis (NL-RHA) is employed as a means to predict the post-elastic behaviour of the cable-stayed bridges when material and geometric nonlinearities due to large deformations are accounted for. In this case the system of dynamics of Eqs. 5.2 and 5.1 is integrated step-by-step by considering the tangent stiffness in each step to linearise the problem. It is essentially the DRHA methodology examined in Section 5.3 extended to consider material nonlinearities in addition to the geometric ones (already considered in elastic analysis).

The HHT algorithm is used in the nonlinear analysis of the bridges. Abaqus (2018) suggests that a small numerical damping can reduce the high frequency noise that is introduced to the integration with every time step, prescribing that $\alpha = -0.05$. This value of α results in the remaining parameters that describe the implicit HHT algorithm (Hilber *et al.* 1977) of Eq. (5.4) to be $\beta = 0.2756$ and $\gamma = 0.55$.

The time step for the integration is equal to $\Delta t = 0.01$ s, as in the DRHA but it can be reduced down to $\Delta t = 0.00001$ s so that numerical convergence is reached. However, when this is not possible due to high nonlinearities arising, the analysis stops and in those

cases the results are not taken into consideration. The exception is made when 88% (or more) of the analysis is completed, in which case the results are then acceptable. This is the case because after the 88% of the analysis is completed (i.e. after 17.5 s from the start of the 20-s earthquakes) the strong motion windows of the applied earthquakes are exceeded even at the last support to receive the ground motion[1] and at least 95% of the cumulative Arias Intensity (I_a) is reached. The Arias Intensity is a means to measure the strength of the ground motion by measuring the acceleration of transient seismic waves as:

$$I_a = \frac{\pi}{2g} \int_0^{t_{\mathrm{EQ}}} \ddot{u}_{\mathrm{g}}^2 (t) \quad dx \tag{5.7}$$

where $\ddot{u}_{\mathrm{g}}$ is the ground acceleration in [m/s^2] and t_{EQ} in [s] is the total duration of the earthquake.

[1]The time delay is calculated as a function of the distance from the first abutment (A1), which is considered the reference support, and of the velocity of wave propagation c. Table 4.1 showed that in the 600-m span bridge the seismic waves might take up to 1.08 s to reach the second abutment (A2) when $c = 1000$ m/s.

Chapter 6

Elastic Seismic Behaviour

Contents

6.1 Introduction

Up to this point the numerical models of the cable-stayed bridges examined herein have been presented in detail, the modelling assumptions and considerations that have been made along the way have been discussed and the definition of the seismic action has been detailed step-by-step. Specifically, the modelling process has been discussed in Chapter 3 in terms of the geometric considerations in the models and of the properties of the materials in the composing parts of the bridges. The seismic action applied to the models has been presented in Chapter 4 with all relevant assumptions on the definition of the SVGM from the seismological point of view and the methodology to analyse the bridges has been presented in Chapter 5.

This chapter is the first step towards the interpretation of the seismic response of cable-stayed bridges that are subjected to asynchronous motion of their supports. In this chapter the seismic behaviour of the bridge models is addressed with the materials considered linear and elastic.

To this end, the elastic seismic behaviour of the pylons in cable-stayed bridges with 'H', inverted 'Y' and 'A' shapes with two lateral cable planes and one single central plane of cables in the case of the inverted 'Y'-shaped pylons (Y-LCP and Y-CCP models, respectively), and with and without lower diamond configurations in the inverted 'Y'- and 'A' shaped pylons (i.e. 'D' notation in the models reference keywords) is presented in this chapter. The elastic seismic response is examined in bridges with main spans (L_P) of 200, 400 and 600 m in order to explore the effect of the SVGM on a relatively short, an intermediate- and a long-span cable-stayed bridge. This is performed in the context of the current code provisions and guidelines (Eurocode 8; Part 2 2005, JRA 2002, AASHTO 1996, ATC32 1996) which associate the SVGM with the length of the bridge and with the underlying soils conditions.

6.2 Methodology

The aim of the present chapter is to interpret the effect of the differential motion of the pylons, combined with the effect of the incidence angle of the seismic waves with respect to the deck. The chapter starts by exploring the elastic dynamic behaviour of the pylons, in terms of the maximum forces that are developed along their height and the examination of the effect of the SVGM on the seismic forces compared to the synchronous (SYNC) motion. The discussion follows by addressing the influence of the pylon shape and the pylon-cable system configuration. Finally, the effect of the earthquake's incidence angle combined with the out-of-phase motion of the pylons is explored with the aim to discover critical orientations of the bridge in which the seismic response and the effect of the SVGM

per se are maximised. Additionally, the effect of the SVGM is examined in terms of the wave propagation velocity (c), as discussed in Chapter 4, which equals 1000 m/s. The dynamic analysis of the bridge finite element models is performed by means of the Direct Response History Analysis (DRHA), as discussed in Chapter 5.

The results of the elastic seismic analysis are presented in terms of the peak seismic axial load (N), the longitudinal shear force (V_x) and the transverse shear force (V_y) along the pylon legs. The influence of the incidence angle of the seismic waves with respect to the bridge (θ) is explored by examining the response of the pylons under different values of θ. This is achieved by means of polar plots of the seismic forces in the most critical regions of the pylons. The assessment of the results in all cases is targeted to the leg of each pylon that is connected rigidly to the deck, as discussed in Section 3.3. Fig. 6.1 shows the methodology to obtain the peak seismic response in the pylons. The results are initially obtained in the form of time-histories of the response in different sections of the leg along its height. Subsequently, for each earthquake the peak (maximum absolute) value of the seismic response quantity under consideration is identified in the time-history for the different sections along the pylon. Fig. 6.1 illustrates the methodology for the peak seismic transverse shear and the peak longitudinal bending moment. The effect of the self-weight is subtracted from the time-histories recorded, so that the only the seismic response is examined. Finally, the arithmetic mean (μ) response is calculated from the individual seismic responses R_i (with $i = 1 \rightarrow 7$ denoting the sets of earthquakes applied) to obtain the mean peak seismic response of the pylons, as shown in Eq. (6.1a). In the seismic design of structures, in addition to the mean seismic response, it is important to account for the dispersion of the individual seismic responses (from the individual earthquakes). In this research the dispersion is considered in terms of the standard deviation (SD) from the arithmetic mean, as shown in Eq. (6.1b).

$$\mu = \frac{1}{7}\sum_{i=1}^{7} R_i \tag{6.1a}$$

$$\text{SD} = \sqrt{\frac{1}{7}\sum_{i=1}^{7}\left(R_i - \mu\right)^2} \tag{6.1b}$$

6.3 Effect of the Foundation Soil

The effect of the foundation soil is an important consideration in the design of every structure because it dictates many important aspects including the definition of the seismic action. Cable-stayed bridges are long structures and it is possible that the type of soil changes at different supports. This possibility, and in a broader sense the 'site response

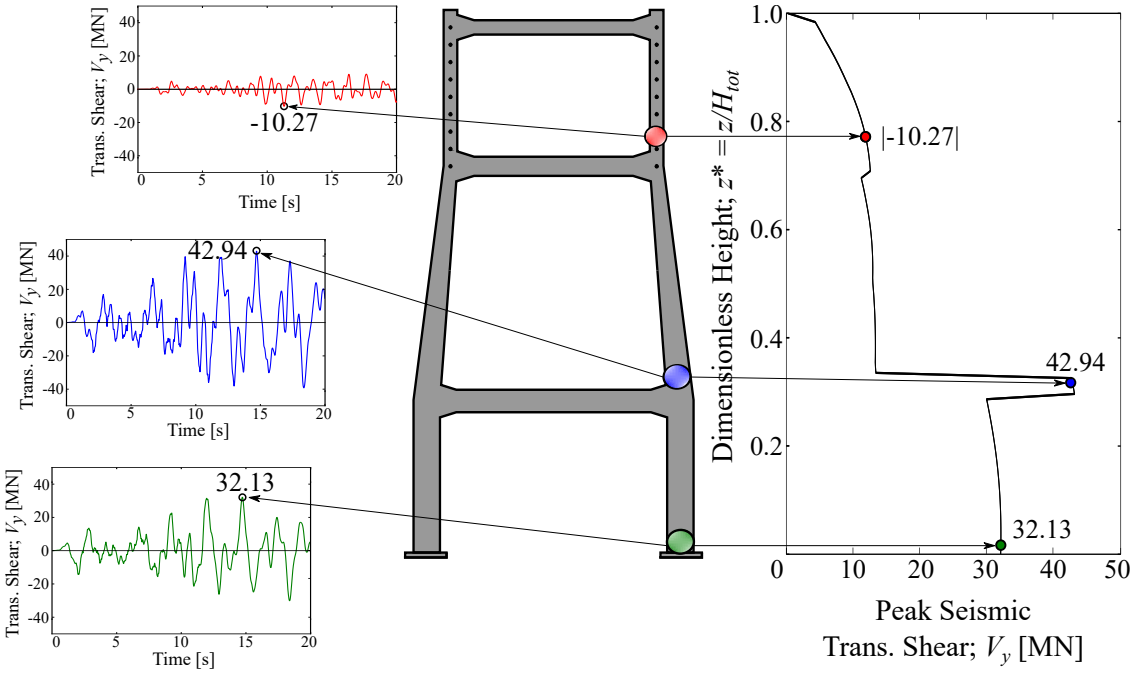

(a)

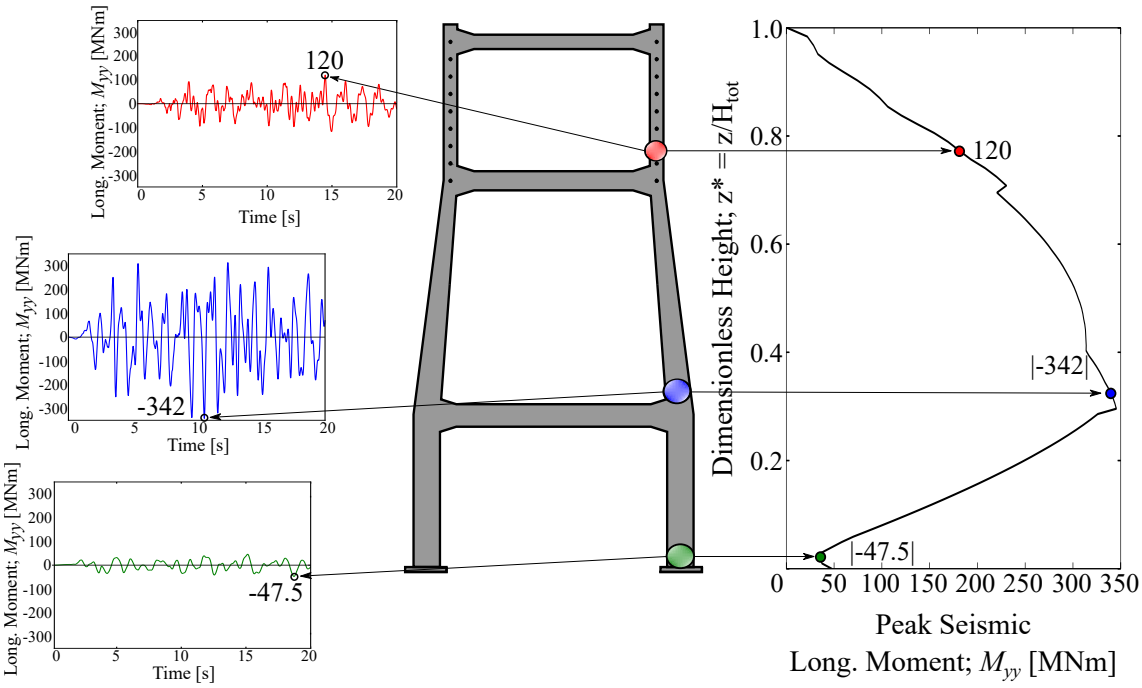

(b)

Figure 6.1: Description of the procedures to obtain the peak seismic (a) transverse shear, V_y, and (b) longitudinal bending moment, M_{yy}, along the height of the pylon when the SVGM ($c = 1000$ m/s) is considered. H-LCP model; $L_P = 400$ m; $\theta = 0°$; Seismic record #1.

effect' of the SVGM, is an aspect that should be taken into consideration when examining the multi-support excitation in cable-stayed bridges. This section explores the influence of the foundation soil on the seismic response and also the lack of uniformity among the foundation soils at the abutments and the pylons. Specifically, three different foundation scenarios are examined in the H-LCP model with $L_P = 400$ m when the strong component of the earthquake (FN) is applied parallel to the deck ($\theta = 0^\circ$) and when $c = 1000$ m/s. The case of uniform soil conditions at the four supports is considered for rocky ground corresponding to ground category A (AAAA) of Eurocode 8; Part 1 (2004), and for soft soil corresponding to ground category D (DDDD) of the same code. The site response effect is examined by considering a case of nonuniform foundation soils at the supports which corresponds to ground type A under the two abutments of the cable-stayed bridge and ground type D under the two pylons (ADDA). To account for the site response component of the SVGM sets of accelerograms have been generated to match the elastic response spectra for ground types A and D of Eurocode 8; Part 1 (2004) at the abutments and the pylons, respectively. Furthermore, the frequency-response function $H_j(\omega)$ at each support j of Eq. (2.18) has been updated for the different ground categories, as discussed in 4.5.4. Finally, for the site response effect two different scenarios are examined. In the first scenario the nonuniform foundation sites are examined alone, without the loss of coherency and the wave passage components of the SVGM in order to isolate the effect of the foundation soil on the seismic response, whereas in the second scenario the effects of the three components are combined. When soft soil is considered at the pylons (i.e. in the cases DDDD and ADDA) the SSI is accounted for by means of springs and dashpots, as detailed in Section 4.8.

Fig. 6.2 presents the peak seismic response along the height of the pylon in the axial, longitudinal and transverse directions of the bridge by means of the seismic forces developed in the pylon legs (N, V_x and V_y, respectively). The results show that the two cases of uniform soil conditions are generally associated with the lowest (AAAA) and the highest (DDDD) seismic responses in the part of the pylon above the deck level. The maximum response is obtained at the base of the pylon, where the axial load and the longitudinal shear force are examined (Fig. 6.2(a),(b), respectively), and at the level of the deck in the transverse direction of the response (Fig. 6.2(c)). When the ground scenario DDDD is considered there is an increase of 135%, a reduction of 14% and an increase of 104% in the peak values of N_{base}, $V_{x,\text{base}}$ and $V_{y,\text{deck}}$, respectively, compared to the peak values responses obtained from ground scenario AAAA. The increments in N and V_y are due to the higher spectral acceleration that is associated with dominant vibration modes of the structures when ground type D is considered compared to the respective accelerations of the ground type A spectrum. Fig. 6.3 shows that the fundamental vibration mode of the 400-m main span bridge, which involves the vertical flexure of the deck combined with the longitudinal flexure of the pylons in opposite directions, and the first transverse mode of

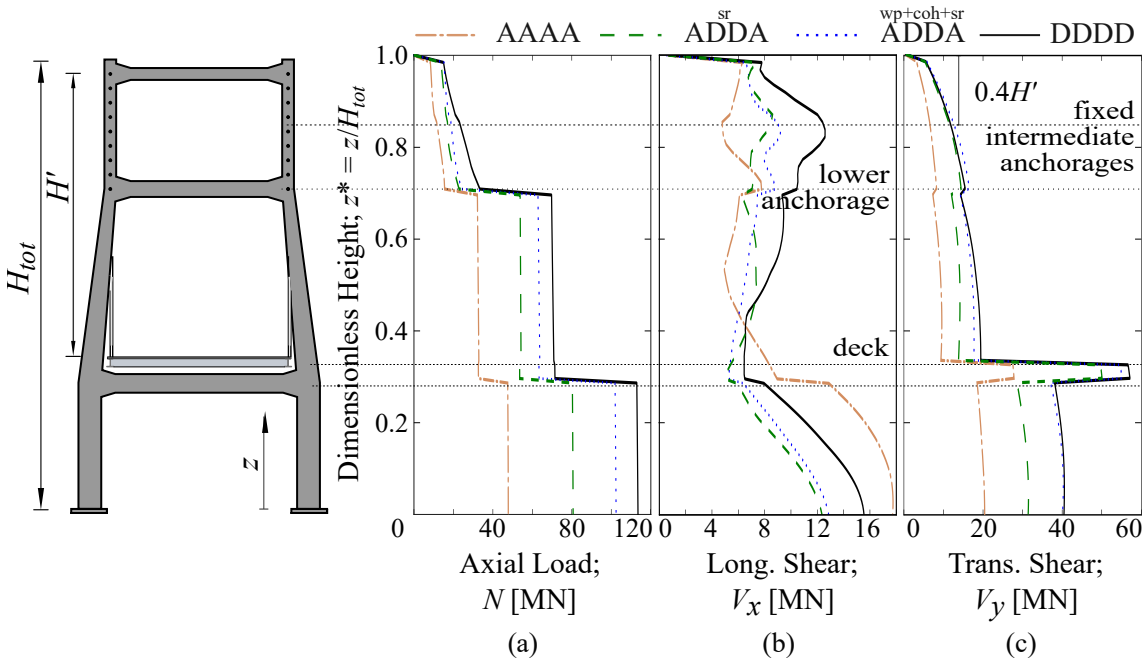

Figure 6.2: Influence of the foundation soil under the different supports of the cable-stayed bridge on (a) the peak seismic axial force N, (b) the longitudinal shear force V_x and (c) the transverse shear force V_y. H-LCP model; $L_P = 400$ m; $\theta = 0°$, $c = 1000$ m/s. 'A' and 'D' denote the respective ground categories of Eurocode 8; Part 1 (2004) at the foundations of the supports, 'wp' stands for wave passage, 'coh' for incoherence and 'sr' stands for the site response components of the SVGM.

the bridge, which involves the transverse flexure of the deck and the pylons, are associated with higher spectral accelerations ($S_{a,\mathrm{D}}^{T_x}$ and $S_{a,\mathrm{D}}^{T_y}$, respectively) than the respective ones for ground type A ($S_{a,\mathrm{A}}^{T_x}$ and and $S_{a,\mathrm{A}}^{T_y}$, respectively). However, the similar longitudinal response at the base of the pylons in the two cases with uniform grounds is associated with the SSI when ground type D is considered. It is consistently noticed in Fig.6.2(b) that when the SSI is included (in ADDA and DDDD cases) V_x is reduced compared to the respective shear force when the pylons are founded on rock and their base is assumed fixed. The flexibility of the foundation in the former ground scenarios compensates for the increased seismic forces resulting from the higher spectral acceleration when soil type D is considered compared to ground type A.

The effect of the soft soil conditions is also noticed at the anchorage area of the pylon in the longitudinal response in which there is an increase of 150% in V_x compared to the response when ground type A is considered at the foundation of the four supports. This is attributed to the longitudinal restraint introduced by the cables anchored to the abutments and to the and to the vertical piers, which gains importance due to the increment of $S_{a,\mathrm{D}}^{T_x}$.

When nonuniform soil conditions are considered (ADDA) the seismic response generally falls within the limits defined by AAAA and DDDD. Lower values of V_x are obtained below the deck level down to the base of the pylon legs in which the peak longitu-

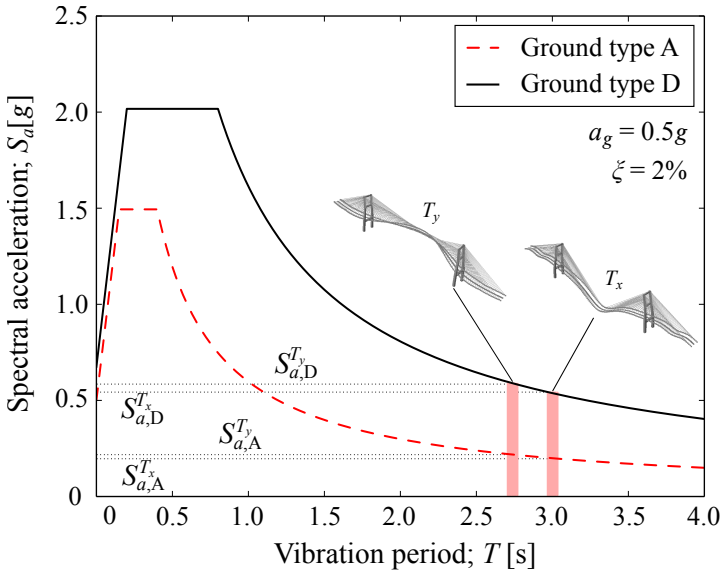

Figure 6.3: Eurocode 8; Part 1 (2004) Type 1 elastic response spectra for ground types A. $a_g = 0.5g$, ξ =2%.

dinal shear force is 23% smaller than the longitudinal response from the DDDD ground scenario. Moreover, when the three components of the SVGM are combined (i.e. $\overset{\text{wp+coh+sr}}{\text{ADDA}}$) the axial, longitudinal and transverse response of the pylons, in almost all their height, is larger than the response when only the site response effect is considered alone (i.e. $\overset{\text{sr}}{\text{ADDA}}$).

The aim of this research is to obtain general and practical assumptions on the effect of the SVGM on the seismic behaviour of the pylons. Moreover, the large number of bridge models and the even larger number of analysis cases dictate that the worst case of ground conditions is considered throughout, both from the points of view of the maximum seismic response and of the induced structural damage that is discussed in Chapter 7. Therefore, from this point onwards the site response effect of the SVGM will not be accounted for and uniform soft soil conditions will be considered at the four supports of the bridges (i.e. DDDD). In the next sections only the wave passage and the incoherence effects are considered.

6.4 Multi-Angle Response

6.4.1 Asymmetry of the Response

The apparent symmetry of the structures described in Chapter 3 is somewhat lost in the seismic response for different incidence angles (θ) due to: (1) the lack of symmetry of the support conditions at the abutments A1 and A2 with respect to the centreline of the deck (axis x), as shown in Fig. 3.5; (2) the longitudinal movement of the deck during the

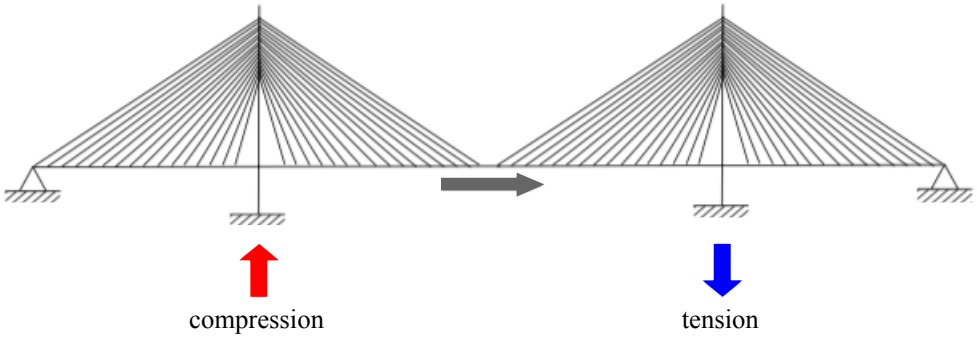

Figure 6.4: Schematic representation of the asymmetry in the response of the pylons due to the longitudinal seismic action (*taken from Camara (2011)*).

earthquake, which introduces axial compression in one pylon and tension in the opposite due to the effect of the cable system, as shown in Fig. 6.4; and (3) the difference in the ground motion at different supports due to the loss of coherency and the time lag of the SVGM (Fig. 4.8(d)). The objective of this section is to explore the effect of the asymmetry on the seismic response.

Fig. 6.5 shows the arithmetic mean of the peak longitudinal and the transverse seismic forces along the legs of the two pylons under the SVGM and the SYNC motion when the strong earthquake component (FN) is considered parallel to the deck of the bridge but with different signs: $\theta = 0°$ and $\theta = 180°$. The effect of the asymmetry of the response is reflected in this figure by comparing the seismic shear forces in pylon P1 when $\theta = 0°$ with the response of P2 when $\theta = 0°$. It is observed that the asymmetry of the response is relevant in the longitudinal direction and under the SVGM in the anchorage system, as shown in Fig. 6.5(a). This is attributed to the effect of the cable system transferring the longitudinal shear forces from the asynchronous motion (SVGM) of the supports from one pylon to the opposite. This effect increases with the restraint of the cable system to the relative (out-of-phase) longitudinal movement between the pylons, and it is maximised at the sections around the cable anchorages that connect the pylons with the vertically restrained points of the deck at the vertical piers in the side spans. At these points the error in the maximum seismic forces introduced by considering that the response is symmetric between the two pylons when $\theta = 0°$ is up to 18%. Fig. 6.5(b) indicates that in the transverse direction the effect of the asymmetry is maximised at the deck level in the pylon, where the difference in V_y between pylons P1 and P2 is 14% when $\theta = 0°$. On the other hand, the maximum difference between the transverse seismic forces in the two pylons when the bridge is subjected to SYNC motions is negligible.

Fig. 6.5 also allows to compare the seismic response of pylon P1 when $\theta = 0°$ to that of the same pylon when $\theta = 180°$. Both the longitudinal and the transverse response (i.e. V_x and V_y, respectively) are almost identical throughout the pylon's height. The

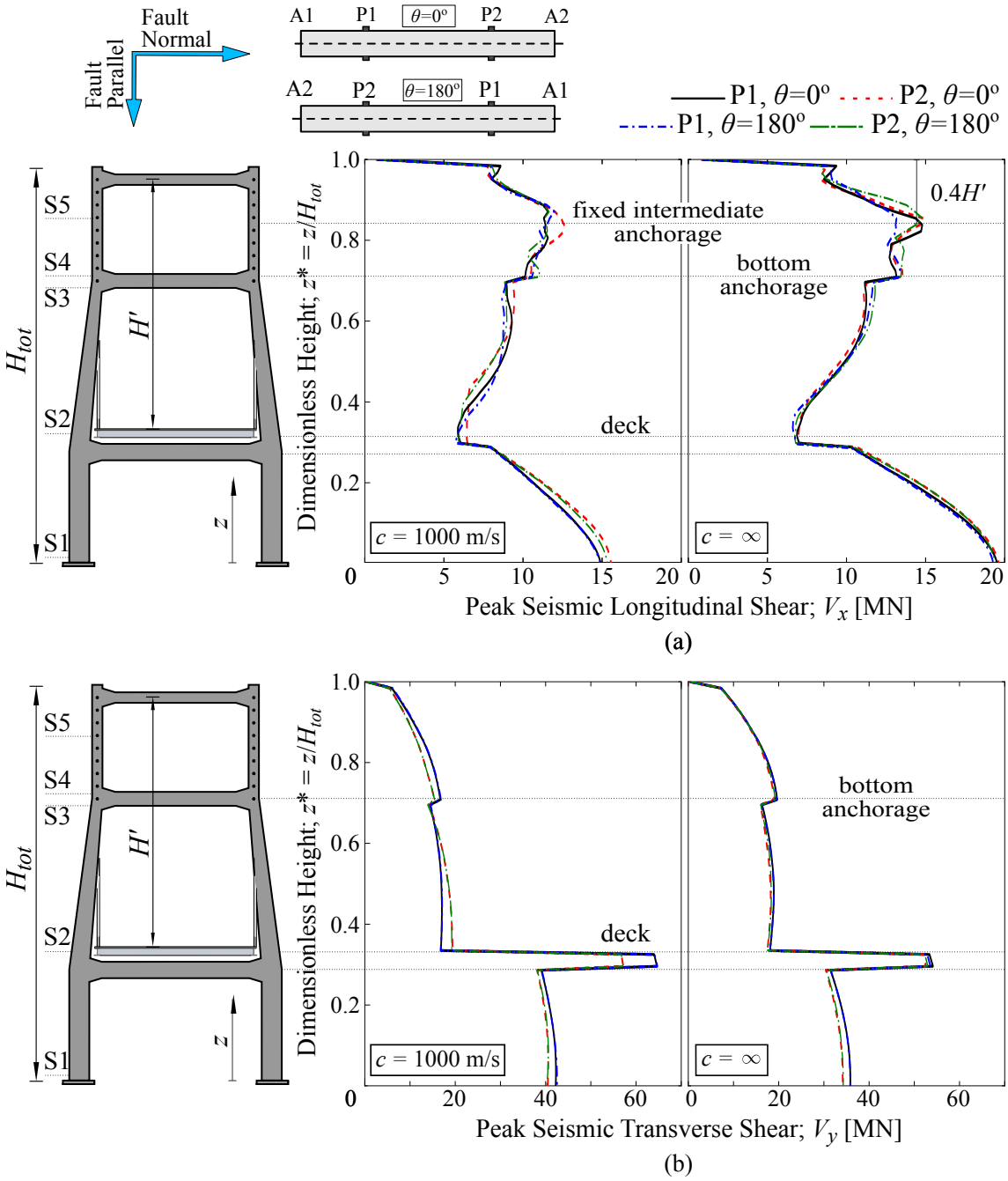

Figure 6.5: Mean peak seismic (a) longitudinal (V_x) and, (b) transverse (V_y) shear forces along the height of pylons P1 and P2. H-LCP bridge; $L_P = 400$ m.

maximum difference of 15% is observed at the middle of the anchorage system in the longitudinal direction of the response and it is attributed to the asymmetry of the boundary conditions at the supports (Fig. 3.5) and to the longitudinal movement of the deck that causes alternating tension and compression between the two pylons (Fig. 6.4).

In light of the results, it can be possible to consider symmetric conditions in the study of the pylons. For this reason the range of angles in which the seismic response is examined in this thesis is defined from $\theta = 0^\circ$ to 180° hereinafter. Furthermore, because the seismic response of the second pylon to receive the ground motion (i.e. P2 when $\theta = 0^\circ$ and P1 when $\theta = 180^\circ$) is the largest when the SVGM is examined, the results of the following sections are targeted to this one.

6.4.2 Critical Bridge Orientations

This section discusses the influence of the bridge orientation with respect to the earthquake propagation by studying the peak seismic forces in the second pylon to receive the ground motion of the models under different incidence angles (θ) of the seismic waves. These angles are considered in the range of $\theta = 0^\circ$ to 180° with increments of 30°. In Fig. 6.6 the results are presented in the form of polar plots for the bridge with 'H'-shaped pylons and $L_P = 400$ m. These are created for the peak axial seismic force (N), the peak seismic longitudinal shear force (V_x) and the peak seismic transverse shear force (V_y) at the most critical regions of the pylon. These start from the base (referred to as position S1 in Fig. 6.5) and move upwards to the level of the deck (position S2), to the region below the bottom cable anchorage (position S3) and to the section immediately above this (position S4). The coloured line in each plot represents the arithmetic mean of the response obtained from the seven records of the set that account of the SVGM, whilst the width of the shaded band indicates two standard deviations ($\pm$SD) centred in the mean SYNC result (which is taken as the reference). Fig. 6.6 shows that the seismic response strongly depends on the value of θ. This is mainly due to the larger spectral acceleration in the direction normal to the fault (FN), as it was described in Chapter 4. The longitudinal shear force in the pylon (middle column in Fig. 6.6) is maximised when the strong component of the earthquake is parallel ($\theta = 0^\circ$ or 180°) to the direction of the deck. Accordingly, the transverse shear force in the pylon (right column in Fig. 6.6) is maximised when the strong component of the earthquake is perpendicular ($\theta = 90^\circ$) to the direction of the deck. The minimum seismic response is usually obtained by rotating the earthquake by 90° from the angle in which the response is maximised, so that the minor horizontal earthquake component, i.e. the fault parallel (FP) direction, is aligned with the direction of the response under consideration. The ratio between the minimum and the maximum response for different bridge orientations is approximately 0.7, which coincides with the ratio between the spectral accelerations of FP and the FN target spectra that is considered

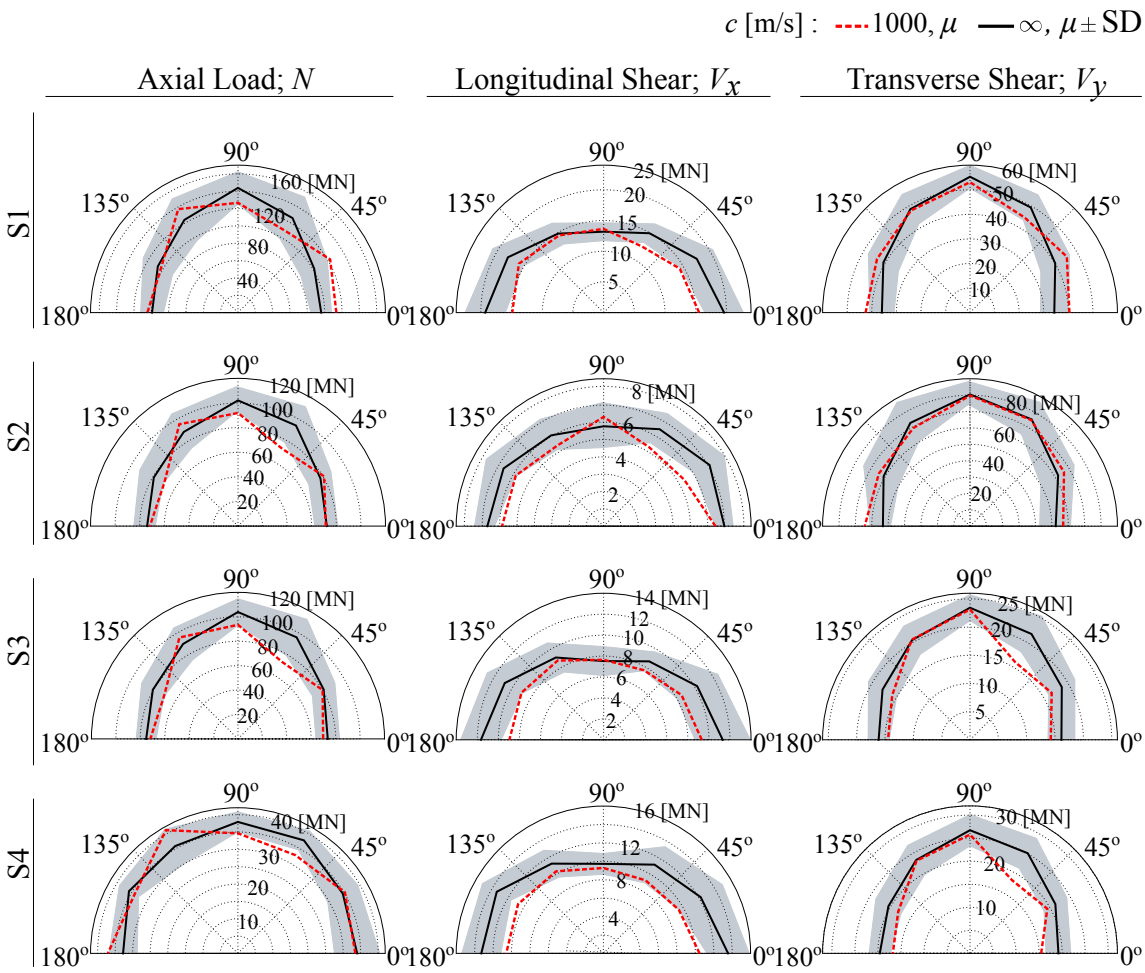

Figure 6.6: Peak seismic response at critical sections of pylon (P2) for different incidence angles (θ). H-LCP model, $L_P = 400$ m $c = 1000$ m/s.

in this work, as it was presented in Chapter 4.

The SVGM has a more pronounced effect on the longitudinal response at the base of the pylon than on the transverse response which generally falls within the limits of the dispersion of the results obtained from the SYNC motion. In the majority of the incidence angles the SVGM reduces the longitudinal shear force compared to the SYNC motion and it increases the transverse shear force at the pylon base. This is due to the connection between the deck and the pylon, which releases the longitudinal movement of the deck and restrains its transverse movement, introducing out-of-phase transverse force from the deck to the two pylons.

The difference in the values of N and V_y when $\theta = 30°$ and $\theta = 120°$ that is observed in the response from the SVGM is due to the time-lag and the fact that depending on the angle of incidence that is examined, the pylon under consideration receives first or second the ground motion. For example when $\theta = 30°$ pylon P2 is the second one to be reached by the seismic waves, and when $\theta = 120°$ P2 receives the earthquake first, as detailed in Fig. 4.9. When the ground motion at the two pylons is not identical (i.e.

when the SVGM is considered) it can lead to differences in the response of the pylon for different values of θ.

6.4.3 Magnitude of the SVGM

In order to quantify the effect of the asynchronous excitation on the seismic behaviour of the bridges, the response ratio ρ_j is calculated as;

$$\rho_j = \frac{R_{\text{SVGM},j}}{R_{\text{SYNC},j}} \tag{6.2}$$

in which $R_{i,j}$ with i = SVGM, SYNC is the arithmetic mean (from the seven sets of accelerograms) of the peak response quantity under consideration: $j = N$,V_x,V_y. Fig. 6.7 presents this ratio in polar form obtained from the longitudinal and the transverse shear forces at the base of the pylon P2. This represents a critical region of the pylon in terms of the peak longitudinal seismic response and of the maximum effect of the SVGM in the transverse response. The ratio is presented for the H-LCP model with $L_P = 400$ m.

The results show that the transverse response ratio (ρ_{V_y}) is larger than the longitudinal ratio (ρ_{V_x}) confirming that the effect of the SVGM at the base is more important in the transverse direction of the response. It is seen that V_x is reduced at the base of the pylon (i.e. $\rho_{V_x} < 1$) when the bridge is subjected to asynchronous motion of its supports for all incidence angles except for $\theta = 90°$, wherein $\rho_{V_x} \simeq 1$. Therefore, it can be argued that the SVGM is beneficial for the seismic response at this region of the pylon from the point of view of the longitudinal seismic forces. On the other hand, the base of the pylon seems to be more vulnerable against the SVGM with ρ_{V_y} taking values of up to 1.2 when the strong earthquake component is parallel to the bridge ($\theta = 0°$ and 180°). It is interesting to note the shape of the polar plots of Fig. 6.7 compared to the respective polar plots for the longitudinal and transverse seismic shear forces of Fig. 6.6. It is seen that the effect of the SVGM is minimised (in the case of ρ_{V_x}) and maximised (in the case of ρ_{V_y}) in the direction perpendicular to the one wherein the response, in terms of V_x and V_y, is maximised. This finding proves that the critical orientations of the bridge when the maximum seismic response (V_x or V_y) is examined do not coincide with its critical orientations when the maximum effect of the SVGM is examined. However, it is also found that in the case of the intermediate-span bridge ($L_P = 400$ m) the principal orientations[1] of the bridge, i.e. $\theta = 0°$, 90° and 180°, are the most significant ones.

[1]The principal orientations of the bridge are defined as the ones wherein the strong (FN) or the weak (FP) components, in other words, the principal components of the earthquake are aligned with the deck.

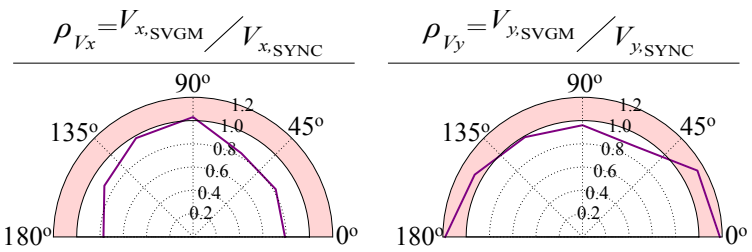

Figure 6.7: Polar ratio ρ of the (a) longitudinal shear force (V_x) and (b) transverse shear force (V_y) at the base of the pylon (position S1) for different incidence angles (θ). Pylon P2, $c = 1000$ m/s.

6.5 Influence of the Main Span Length

The discussion will focus now on the comparison between the peak seismic response along the height of the pylons in bridges with different spans under the SVGM and the SYNC ground motion when the strong component of the earthquake (FN) is aligned with the deck: $\theta = 0°$. Fig. 6.8 presents the longitudinal (top row) and the transverse (bottom row) shear forces in the lateral legs of the second pylon that receives the ground motion (P2) in the H-LCP bridge models with $L_P = 200$, 400 and 600 m (which corresponds to pylon heights, H_{tot}, of 62.5, 125 and 187.5 m, respectively). The results show that the SVGM can have either a favourable or an unfavourable effect on the seismic response, in terms of reducing or increasing the peak SYNC response, depending on the part of the pylon under consideration, on the length of the bridge and on the direction of the response.

Fig. 6.8 distinguishes three regions of the pylons on which the effect of the SVGM is significant. These correspond to the top part of the pylons which holds the anchorage system, the inclined part of the legs between the intermediate and the lower transverse struts and the region below the transverse strut down to the base. It is significant that in the middle part of the inclined legs of the pylons in the 200-m main span bridge the peak seismic longitudinal response is reduced by approximately 20% when the SVGM is considered (Fig. 6.8(a)), but the transverse response in the same region is increased by 30%. Considering the transverse response, the effect of the SVGM varies depending on the region of the pylon in which it is examined. Fig. 6.8(b) shows that the SVGM reduces V_y by 25% at the level of the bottom anchorage compared to the SYNC motion, but increases it by 18% at the base of the pylon. The effect of the asynchronous oscillation of the pylon will be discussed in detail in the following sections, but it is important at this point to highlight the variable effect of the SVGM on the structures, which depends on the region of the pylon and the direction of the response under examination. A typical example is the lowest part of the legs of the pylon.

In the longitudinal direction the effect of the SVGM generally reduces the seismic response of the pylon compared to the SYNC motion, as shown in Fig. 6.8(a), regardless of

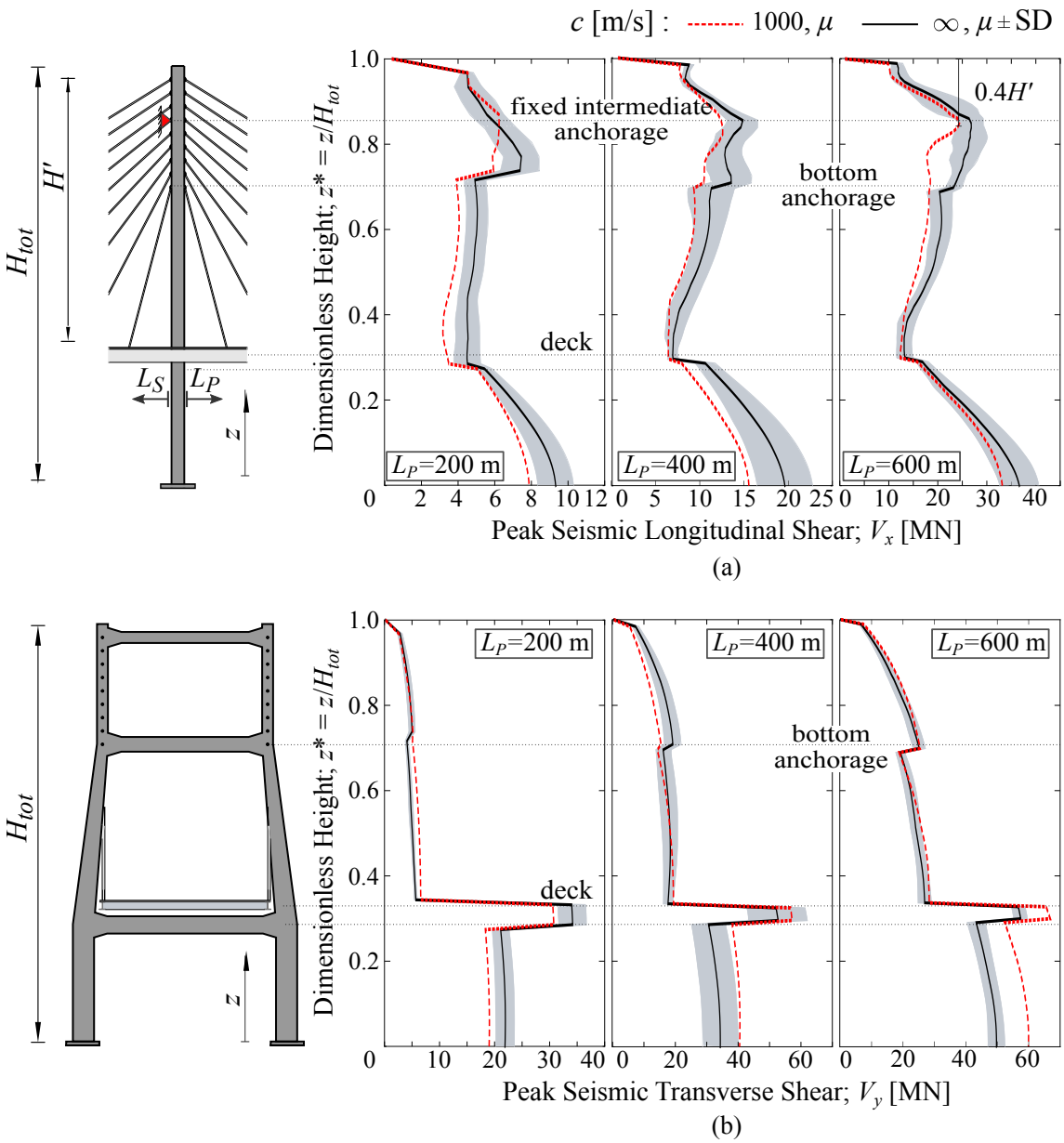

Figure 6.8: Effect of the SVGM for different main span lengths (L_P) on the peak seismic response of pylon P2: (a) longitudinal shear force V_x, (b) transverse shear force V_y. H-LCP model; $\theta = 0°$.

L_P. The influence of the SVGM is not significant in the transverse response of the pylons above the deck level (Fig. 6.8(b)) because the cable system hardly restrains the lateral movement of the pylons. This is especially clear above the deck, where the pylons can oscillate asynchronously without the development of significant forces under the SVGM excitation, leading to a response that is similar to the SYNC motion in terms of seismic forces. However, the effect of the SVGM in the transverse direction can be relevant at the connection between the deck and the pylons down to the base where the increment of the transverse shear is observed. This is due to the constraint between the deck and the pylons through the rigid transverse correction between them, and it is also due to the larger sections of the legs at the base compared to the intermediate and top segments of the legs (Table 3.4). Due to the lateral restraint of the pylon movement provided by the deck, the deck-pylon reaction increases up to 20% in the 600-m span H-LCP bridge subjected to the SVGM and this is responsible for larger seismic forces below the bottom transverse strut of the 'H'-shaped pylon. This increment is also noticeable in the transverse response of the short- and intermediate-span bridges with $L_P = 200$ and 400 m, respectively when the SVGM is considered and it can be attributed to the increased influence of the vibration modes that involve the transverse flexure of the pylons and the deck, which are of increasing order as the main span increases, as already discussed in Section 3.5.

The increase in the pylons' height that results from the increase in the main span length is not directly associated with the effect of the SVGM, as the current codes of practice imply (Eurocode 8; Part 1 2004). Specifically, the transverse shear from the SVGM at the level of the bottom anchorage is 25% increased and 25% reduced from the shear force from the SYNC motion in the bridges with $L_P = 200$ and 400 m, and V_y is similar for both ground motion scenarios in the 600-m span bridge. On the other hand, the effect of the SVGM is larger at the base of the longest bridge compared to its intermediate-span and shortest counterparts at the base and this is due to the largest sections of the pylons with increasing height making them more stiff and, hence, more vulnerable to the multi-support excitation.

6.6 Influence of the Pylon Shape

The objective of this section is to explore how the geometry of the pylons affects the response of cable-stayed bridges that are subjected to multiple excitations of their supports. An intuitive approach to assess the influence of the pylon shape on the seismic response is to examine the transverse response of the pylon by means of the transverse shear force (V_y), given that the differences between pylon geometries are mostly relevant in the direction perpendicular to the deck. Furthermore, the effect of the SVGM is more pronounced in this direction, as it has been already discussed and as it can be also seen in Fig. 6.7, in which the maximum value of ρ reaches 1.2 in the transverse direction as opposed to

the respective value of 1.0 in the longitudinal direction (ρ_{V_x}). Fig. 6.8(a) enhances the observation that the effect of the SVGM is more pronounced in the transverse direction of the response in the sense that $\rho_{V_x} < 1$ along the height of the pylon, regardless of L_P. As a result, the transverse magnitude of the SVGM (ρ_{V_y}) will be considered as the basis for the discussion in this section.

Fig. 6.9 presents the transverse response ratio along the height of the pylons with different shapes. In general the effect of the SVGM on the seismic response varies with the pylon shape and with the region of the pylon that is examined. However, the SVGM is detrimental for the transverse response of the pylons below the deck level down to the base of the pylon regardless of the pylon shape, with ρ_{V_y} ranging from 1.1 to 1.5 due to the transverse reaction of the deck to the pylons. The exception to this is the lower part of the Y-LCP model in which the SVGM and the SYNC motion result in the same transverse shear force ($\rho_{V_y} \simeq 1$). The difference between the minimum value of ρ_{V_y} in the Y-LCP model and the maximum value of ρ_{V_y} in the YD-LCP model is attributed to the change in the inclination of the individual legs in the inverted 'Y'-shaped pylon when they are connected to the common member/diamond (Fig. 3.3(d), (e)).

At the intermediate part of the legs between the deck level and the anchorage of the bottom cable only the pylons with lower diamonds present increased V_y from the SVGM compared to the respective shear force from the SYNC motion of the supports. These pylons are of 'A' and inverted 'Y' shapes and they have in common the high inclination of their intermediate legs, which is reversed below the deck until they are connected to the common vertical member at the bottom (Fig. 3.3). On the other hand, the intermediate part of the Y-CCP, Y-LCP and A-LCP models, whose individual legs have constant inclination along their length, is not vulnerable to the SVGM (i.e. $\rho_{V_x} < 1$ between the bottom anchorage and the deck).

Generally, the pylons with two individual legs throughout their height are better candidates to resist the SVGM compared to the ones with lower diamonds. The SVGM has been found to increase the transverse displacement at the top of the YD-LCP pylon by 45% compared to the SYNC motion, whereas in the Y-LCP model the transverse displacement from the SVGM is 5% smaller than the one from the SYNC motion. Similarly, in the 'A'-shaped pylons with and without lower diamonds there is an increase of 37% and 6%, respectively in the transverse displacement at the top when the pylons oscillate out-of phase compared to the SYNC motion.

Fig. 6.10 presents the increase in the required reinforcement ratios from the SVGM compared to the SYNC motion at the base of the different pylons. It is observed that the large transverse displacements in the pylons under the SVGM are also reflected in the required reinforcement ratios at the base sections of the inverted 'Y'- and 'A'- shaped pylons with two cable planes and lower diamonds, when subjected to multi-support excitations,

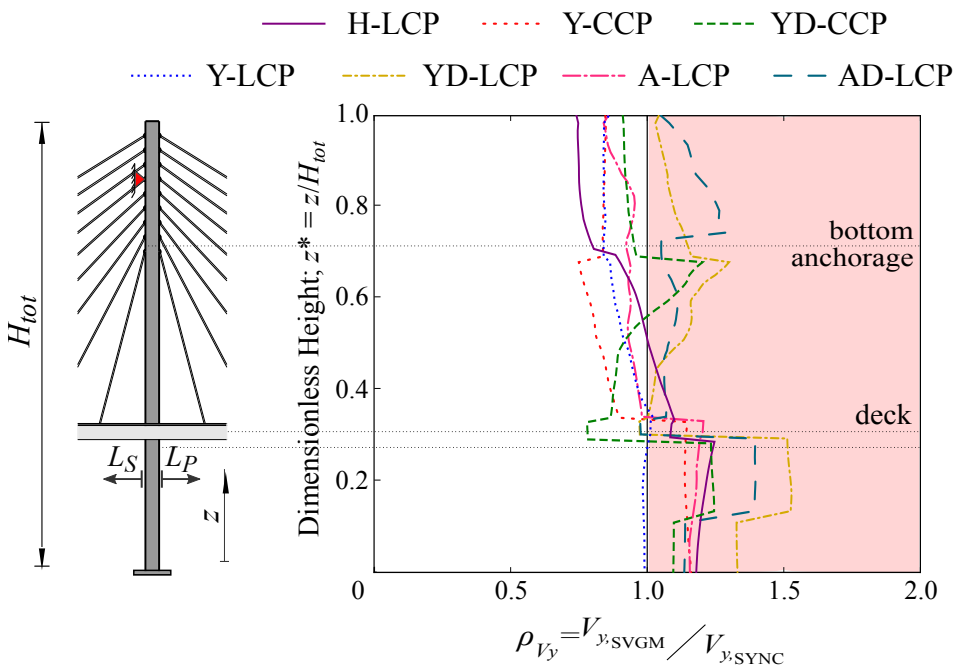

Figure 6.9: Transverse response ratio ρ_{V_y} along the height of pylon P2. $L_P = 400$ m, $\theta = 0°$, $c = 1000$ m/s. The red band denotes $\rho_{V_y} > 1.0$ for which the SVGM increases the seismic response

which are increased by 69% and 46%, respectively from the required reinforcement when SYNC motion of the supports is considered, as shown in Fig. 6.10. On the other hand, a smaller increase is observed at the base of the respective pylons without lower diamonds where the required reinforcement resulting from the SVGM is 6% less and 32% more in the Y-LCP and A-LCP models, respectively compared to the SYNC motion. However, in all pylon configurations, with the exception of the Y-LCP pylon, the base section is significantly affected by the SVGM resulting greater reinforcement ratios than the SYNC motion, that cannot be accommodated by the material safety factors ($\gamma_s = 1.15$) as defined in Eurocode 2; Part 1.1 (2004).

Fig. 6.11 shows in polar form the normalised axial response (N) in critical sections of the pylon with respect to the maximum response. It is observed that the critical orientations of the bridge in terms of the axial load depend on the shape of the pylon and the section in which the force is examined. This is also observed in Fig. 6.6 for the seismic axial force at the base of the 'H'-shaped pylons, which is maximised at the same angles as the transverse shear and it suggests that at this position and for this pylon shape the axial response is dominated by the transverse flexure of the bridge. In order to facilitate the comparison of the results at different pylon sections, the axial load in Fig. 6.11 is normalised with respect to the one obtained in the orientation for which it is maximum. At positions in which the pylon has two legs resisting the lateral movement, which induces tension in one of them and compression in the other, the polar plots reveal that the axial

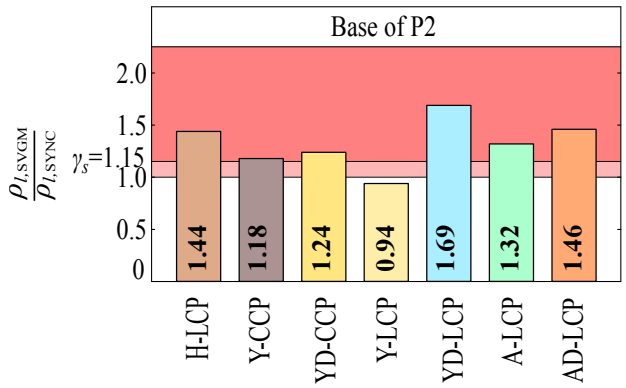

Figure 6.10: Increase in the required reinforcement from the SVGM compared to the SYNC motion at the base of the seven pylon configurations. The light and dark red bands denote slight and large increase in the reinforcement from the SVGM compared to the SYNC motion, respectively.

load is dominated by the transverse flexure of the bridge, and therefore maximised for $\theta = 90°$, as it is illustrated in Fig. 6.12. This is the case for the 'H'- and 'A'-shaped pylons without lower diamonds, as well as the inverted 'Y'-shaped pylons below the anchorage area. Fig. 6.11 shows that in those cases the axial load is maximum when the considered value of θ maximises the transverse component of the ground motion (i.e. the FN direction for which $\theta = 90°$). However, the polar plots of the peak axial load in Fig. 6.11 are rotated by 90° at the positions in which the two lateral legs are connected to a single vertical member. This is what happens at the cable anchorage area in inverted 'Y'-shaped pylons, and also at the vertical pier below the deck in the pylons with lower diamond configurations, as shown in Fig. 6.12. The explanation can be found in the axial load path induced by the lateral deformation of the pylons that is included in this figure. When the lateral legs are connected to a single vertical member the tension coming from one of the inclined legs reduces the compression introduced from the opposite leg. Due to the transverse symmetry of the pylon at any instant during the earthquake both forces have the same magnitude and the axial load in the vertical member introduced by the transverse flexure of the bridge is cancelled. Consequently, the only source of seismic axial load in these members comes from the longitudinal flexure of the pylons[1], which is maximised when $\theta = 0°$. This explains why the axial load at the section above the lowest cable anchorage (S4) in the inverted 'Y'-shaped pylon is dominated by the longitudinal seismic action in Fig. 6.11, whilst the section that is just below this cable (S3) is dominated by the response of the bridge in the transverse direction. The importance of the pylon shape combined with the critical value of the seismic incidence angle is deemed to be relevant in the design of cable-stayed bridges in seismic prone regions.

[1]Note that the vertical component of the earthquake is not considered in this study

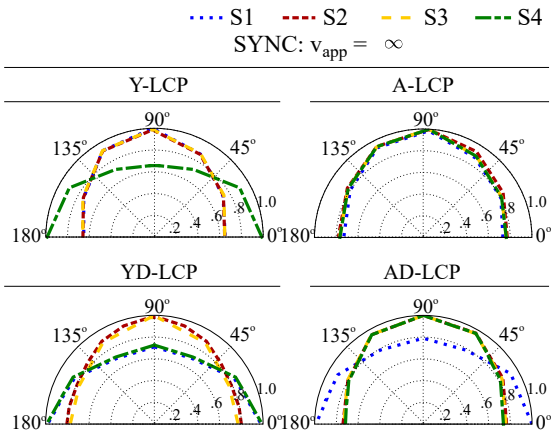

Figure 6.11: Normalised peak seismic axial load in different sections of pylon P2 under the SYNC motion of the support ($c = \infty$); $L_P = 600$ m.

6.7 Effect of the Cable System and its Configuration

Apart from the pylon shape, another aspect in which the designer can chose among different solutions is the arrangement of the cables. The peak seismic response of the intermediate-span bridge with inverted 'Y'-shaped pylons is compared in Fig. 6.13 for central and lateral cable systems (CCP and LCP, respectively). Before comparing the results, it should be noted that due to the influence of the cable arrangement to the cross-section of the deck the latter is 1.25 - 1.3% stiffer and 10 - 15% heavier in bridges with CCP systems and 200 - 600 m span, in comparison to the homologue LCP structures. Fig. 3.6 illustrates the differences between the decks of CCP and LCP bridges. However, Fig. 6.9 shows that the changes in the stiffness and the mass of the deck cannot explain by themselves the increased effect of the SVGM in the lower part of pylon of the CCP model, which reaches 17% in terms of the transverse response ratio. On the other hand, the effect of the cable system on this response quantity is minimised at the anchorage area of the pylon, where the ρ_{V_y} is identical between the two models. Fig. 6.14 shows that the Y-CCP with $L_P = 400$ m bridge maximises the transverse deck-pylon reaction which is 10% larger than the one in the Y-LCP bridge when SYNC motion is considered. This difference is increased to 24% when the pylons move asynchronously in the transverse direction under the SVGM.

The influence of the cable-system is less significant in the longitudinal direction (ρ_{V_x}) in which the SVGM reduces the seismic response along the pylon when $\theta = 0°$ and the longitudinal component of the earthquake is maximised (i.e. FN // deck). The exception is the top part of the cable system in the CCP and LCP models above the intermediate anchorage, as can be seen in Fig. 6.13, where the SVGM slightly increases the longitudinal shear compared to the response from the SYNC motion by (ρ_{V_x}) 1.1 times, concluding that the effect of the cable system is more obvious is the transverse direction of the response,

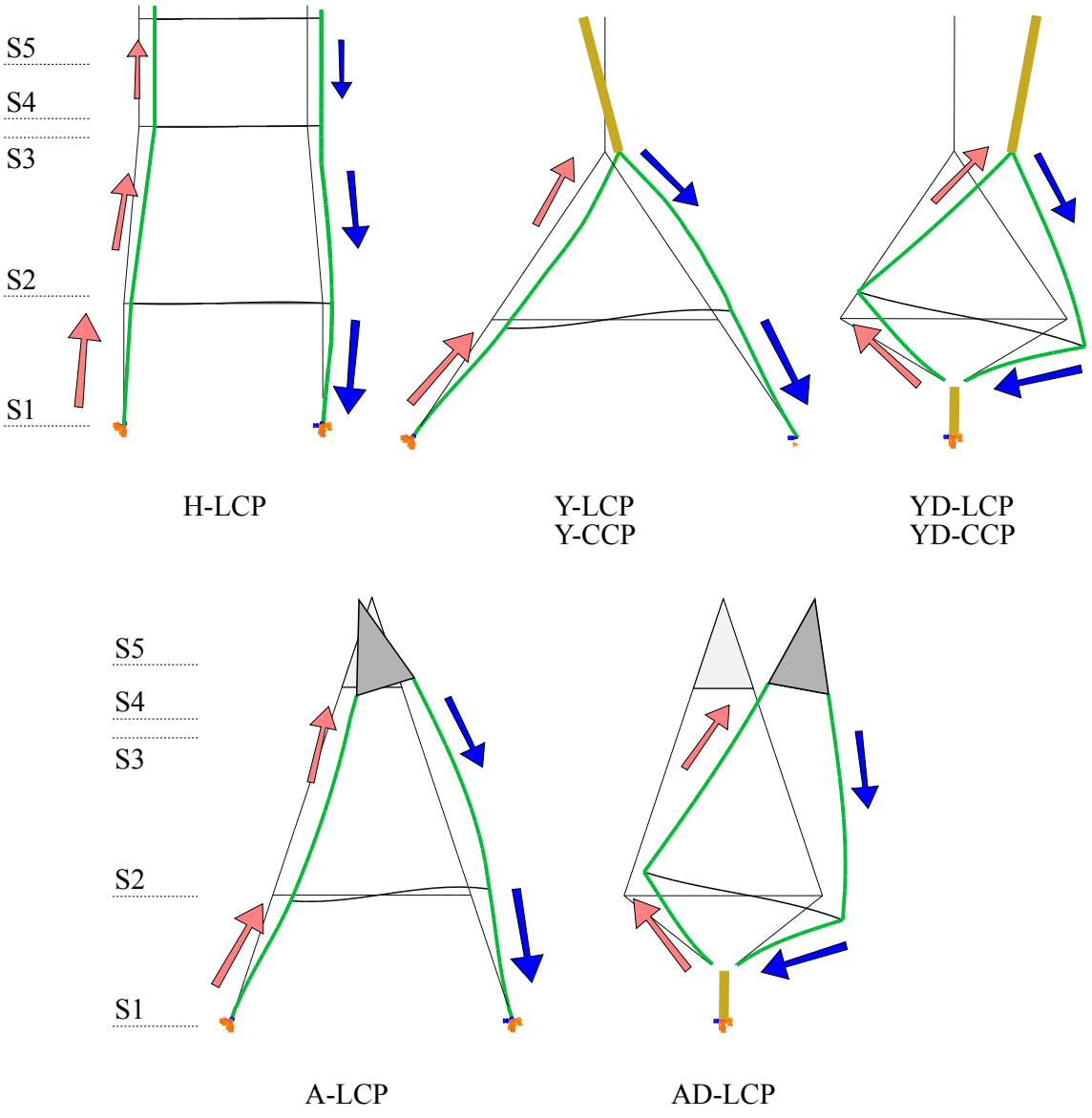

Figure 6.12: Schematic representation of the lateral load path along the lateral legs of the different pylons.

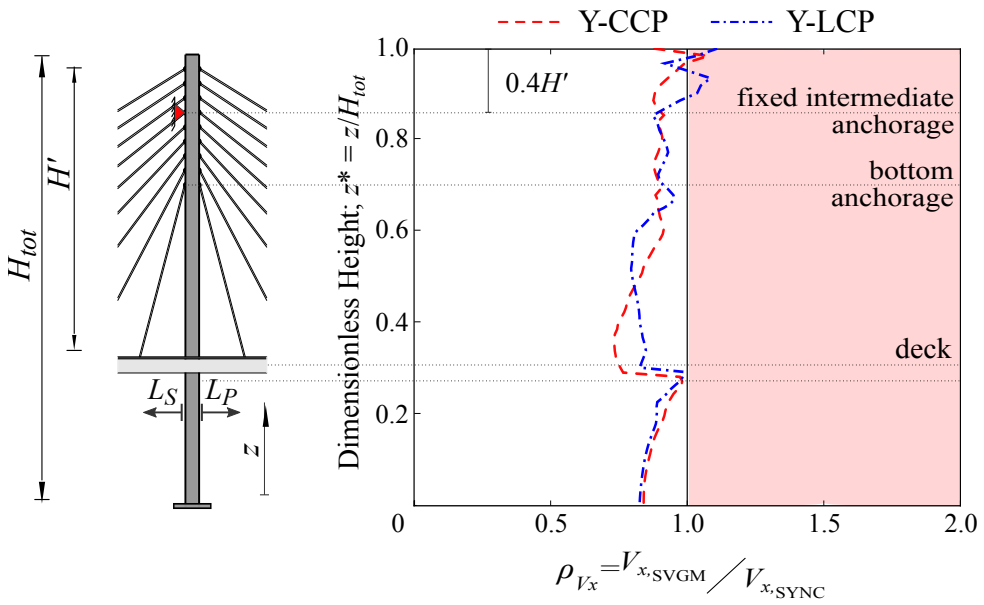

Figure 6.13: Longitudinal response ratio ρ_{V_x} in pylon P2 of the Y-CCP and Y-LCP models. $L_P = 400$ m, $\theta = 0°$. The red band denotes $\rho_{V_x} > 1.0$ for which the SVGM increases the seismic response.

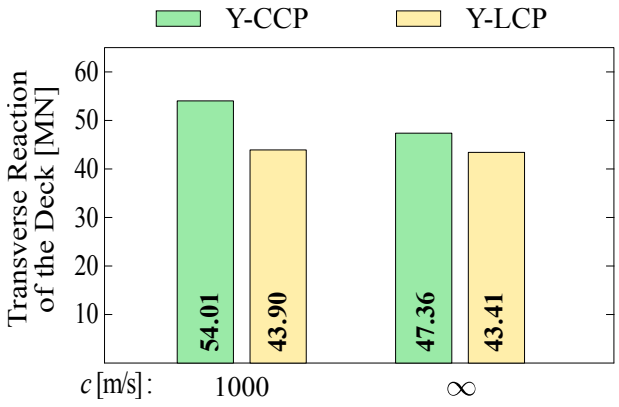

Figure 6.14: Transverse seismic reaction of the deck to the pylons legs in the Y-CCP and Y-LCP models. $L_P = 400$ m, $\theta = 0°$.

i.e. $\rho_{V_y} > \rho_{V_x}$. This is explained by the different configuration of the cable anchorages along the deck in CCP and LCP bridges. When the bridge has a single CCP the cables are perpendicular to the deck and the transverse seismic loads coming from the girder are concentrated to the deck-pylon connection. However, in LCP bridges the two cable planes are anchored at the edges of the deck and an additional path is eventually provided to transmit the transverse deck loads through the inclined cable-system to the pylons.

6.8 Modal Contribution to the Seismic Response

This section connects the effect of the multi-support excitation on the seismic response of the pylons with the frequency content of their response. In order to examine the contribution of different modes to the seismic response, the time-histories of the axial load and of the longitudinal and the transverse shear forces at the base of the pylons during the earthquakes (removing the effects of the permanent loads) have been studied. Fig. 6.15 compares the response time-histories of the axial force at the base of pylon P2 (position S1) from the SVGM and from the SYNC motion in the bridges with a central cable system with or without the lower diamond configuration. The difference in the response of different pylons under the SVGM can be explained by the changes in the contribution of certain vibration modes.

The close spacing between consecutive peaks in the response time-history of the axial load from the SVGM at the pylon base in Fig. 6.15(b) indicates that the response is dominated by a high-order vibration mode. According to previous studies on the seismic response of cable-stayed bridges under SYNC motion, the mode that governs the axial load in the pylon involves the vertical deformation of the lateral legs, which are especially stiff in the lower diamond pylons due to the dimensions of the vertical pier below the deck (Camara 2011). However, when the ground motion is asynchronous the axial response in the pylons with lower diamonds is dominated by a low-order vibration mode, as shown in Fig. 6.15(b). This is observed for all the records but only in bridges with lower diamonds. The effect is further explored in the DFT presented in Fig. 6.16, which represents the frequency content of the response time-history included in Fig. 6.15 for seismic record #1. The DFT shows that in the bridge with lower diamond pylons under the SVGM the contribution to the axial response of the fundamental mode (f_1), which involves the transverse flexure of the deck, increases significantly and becomes dominant: $f_{1,N} = f_1 =$ 0.35 Hz in Fig. 6.16(b) (where $f_{1,j}$ represents the dominant mode in the response j, with $j = N$,V_x,V_y). This mode is responsible for the low-frequency oscillation observed in the time-history illustrated in Fig. 6.15(b). However, the frequency content of the axial response of the bridge with inverted 'Y'-shaped pylons without lower diamonds from the asynchronous motion is dominated by the higher transverse mode #11 of the pylons, as shown in Fig. 6.16(a). This occurs because inverted 'Y'-shaped pylons without lower

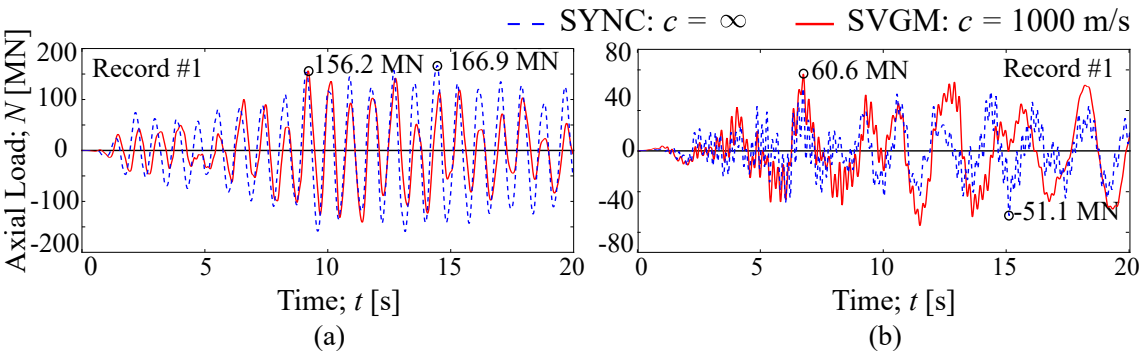

Figure 6.15: Time-history response of the seismic axial force (N) at the base of pylon P1 in the models: (a) Y-CCP, (b) YD-CCP. Results for record #1, $\theta = 0°$, $L_P = 400$ m. The peak responses are annotated.

diamonds are very stiff in the transverse direction due to the constraint provided by the connection of the two lateral legs above the deck (Camara and Efthymiou 2016). The main difference with the YD-CCP model is that the pylons with lower diamonds have a certain rotation capacity and this helps to accommodate the differential pylon movements in the transverse direction, which ultimately reduces (by 60%) the peak axial load in the lower diamond in comparison to the Y-CCP bridge under the same record #1 when the SVGM is considered.

By exploring the mode shapes of important modes included in Fig. 6.16 it is observed that the axial response of both bridges under SYNC motion is significantly affected by longitudinal and transverse modes in which the movement of the pylons occurs in the same direction (longitudinal or transverse). This is the case of Modes #11 and #27 in the Y-CCP bridge and of modes #1, #4 and #10 in the YD-CCP model. However, under the SVGM modes with opposite movement of the pylons, and usually lower frequencies, gain importance. This is the case of mode #1 (fundamental vertical mode with opposite longitudinal movement of the pylons) in the Y-CCP and bridge. This result confirms that the SYNC ground motion excites symmetric modes in symmetric cable-stayed bridges, whereas the SVGM also excites antisymmetric modes, which was first pointed out by Zerva (1990) in multi-span beams.

It has been discussed that the axial force in the pylons is affected by the longitudinal flexure of the deck and the cable system, as well as by the transverse response of the pylons. The discussion will now focus on the longitudinal and the transverse shear forces at the base of the pylon in order to isolate the response of the bridge in each of the two principal directions. Fig. 6.17 shows the evolution of the longitudinal and the transverse shear forces at the base of pylon P2 during earthquake #1 in the two CCP models. The response time-history suggests that the longitudinal shear force is governed by vibration modes with higher frequencies than the transverse response, which is confirmed in the

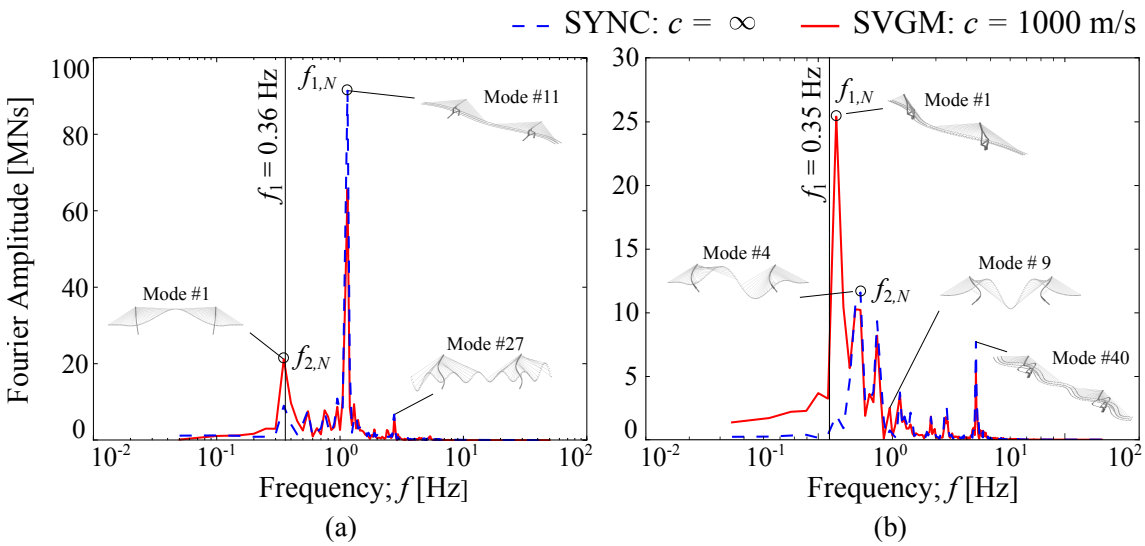

Figure 6.16: Frequency content of the seismic axial load (N) at the base of pylon P2 in models: (a) Y-CCP, (b) YD-CCP. Record #1, $\theta = 0°$, $L_P = 400$ m.

corresponding DFT presented in Fig. 6.18. It is also observed that the shear forces (and the corresponding bending moments) induced by the SVGM in the pylons are dominated by the same frequencies as the ones observed under the SYNC motion: $f_{1,V_x} = 0.78$ Hz being the dominant vibration frequency in the longitudinal direction (Fig. 6.18(a)), and $f_{1,V_y} = 1.14$ Hz for the transverse one (Fig. 6.18(b)). Nevertheless, the contribution of these frequencies to the total response changes under the SVGM. Fig. 6.18(b) shows that the asynchronous motion of the pylons reduces the presence of the dominant vibration mode in the transverse response of the pylon (f_{1,V_y}). This figure also highlights that the antisymmetric mode #7 ($f_7 = 0.81$ Hz) has a significant contribution to the transverse response of the bridge under the SVGM, as opposed to the SYNC motion in which it is de-amplified. This is explained by the opposite movement of the pylons in mode #7. On the other hand, in the longitudinal response of the pylon the contribution of the dominant vibration modes #6 ($f_6 = 0.78$ Hz) and #27 ($f_{27} = 2.72$ Hz) is reduced when the SVGM is considered, which is attributed to the larger longitudinal shear force in the pylon when the SYNC motion is considered compared to the SVGM.

6.9 Conclusions

This chapter has focused on the effect of the SVGM on the elastic seismic response of the pylons of cable-stayed bridges. In order to obtain a general view of the problem, seven different pylon-cable system configurations and three main span lengths (L_P) of 200, 400 and 600 m have been considered. A number of increments of the seismic incidence angle with respect to the bridge axis have been examined, combined with the effect of the SVGM introduced by means of a semi-empirical loss of coherency model (Harichandran

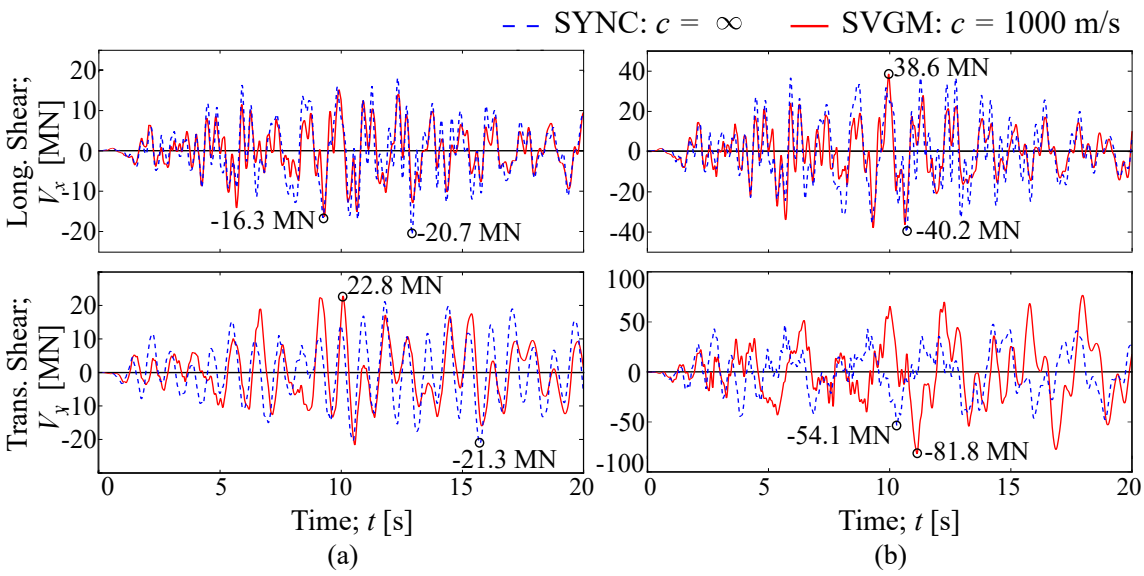

Figure 6.17: Time-history response of the longitudinal (V_x) and the transverse (V_y) shear forces at the base of pylon P2 in the models: (a) Y-CCP, (b) YD-CCP. Record #1, $\theta = 0°$, $L_P = 400$ m. The peak responses are annotated.

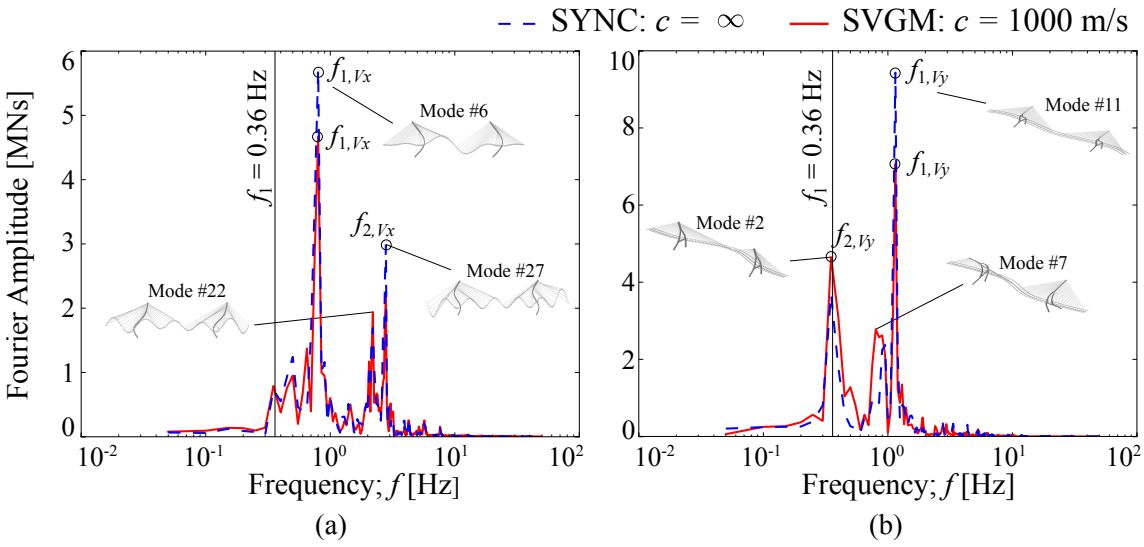

Figure 6.18: Frequency content of: (a) longitudinal shear force (V_x), (b) transverse shear force (V_y). Results at the base of pylon P2 in the Y-CCP model. Record #1, $\theta = 0°$, $L_P = 400$ m.

and Vanmarcke 1986) and by the time-lag of the arrival of the earthquake at different supports ($c = 1000$ m/s). The main conclusions of this chapter are summarised in the following:

1. The foundation soil affects the seismic response of the pylons. Generally, uniform sites at the supports of the bridge, corresponding to ground types A and D (Eurocode 8; Part 1 2004), are associated with the lowest and the highest seismic responses in the pylon, respectively. The increments in the response are due to the higher spectral acceleration that is associated with dominant vibration modes of the structures when ground type D is considered compared to the respective accelerations of the ground type A spectrum. When nonuniform soil conditions are considered the seismic response generally falls within the limits defined by the uniform site conditions defined by ground types A and D. Moreover, when the three components of the SVGM are combined the axial, longitudinal and transverse response of the pylons, in almost all their height, is larger than the response when only the site response effect is considered alone.

2. The effect of the SVGM varies depending on the response quantity of interest and the region of the pylons in which it is considered. The asynchronous motion generally reduces the longitudinal (parallel to the deck axis) seismic response of the pylon with the exception of the anchorage system in the pylon where increments of the longitudinal force from the SVGM are observed, which are explained by the restraint provided by the cables to the out-of-phase oscillation of the pylons. In the transverse direction the out-of-phase oscillation of the pylons above the deck level is relatively unconstrained by the cables and the girder. However, the reaction of the deck to the pylons when the latter oscillate asynchronously can increase considerably the seismic response of the pylons below the deck in the transverse direction.

3. The angle of incidence of the ground motion with respect to the axis of the bridge, θ, is an important factor in the assessment of the seismic response of the pylons. The longitudinal shear forces in the pylon are maximised when the deck is parallel to the strong component of the ground motion (which usually corresponds to the Fault Normal orientation), whereas the transverse shear forces are maximised if the deck is perpendicular to this component (i.e. Fault Parallel). The axial response is generally dominated by the transverse response, however, in the vertical members of the pylons that connect two lateral legs the leading action is the longitudinal component of the earthquake. The maximum effect of the SVGM on the seismic response is usually observed in the Fault Normal or Fault Parallel cases but it does not coincide with the directions of the maximum response. It can be concluded that the full assessment of the seismic response of a cable-stayed bridge requires several orientations of the deck with respect to the earthquake propagation and these should include at least the principal orientations ($\theta = 0^\circ$ and 90°), in which one of the two

earthquake components are aligned with the deck, or the range of orientations from 0° to 180° for a more complete assessment.

4. The overall dimensions of the bridge influence the effect of the SVGM on the pylon. The SVGM typically increases the seismic response in the stiffer regions of the pylons which are, in turn, affected by their overall dimensions and the dimensions of their sections. In longer bridges (400 and 600 m spans) the effect of the SVGM tends to be more pronounced at the bottom part of the pylon from the deck down to the base. The increasing dimensions of this part of the pylons with increasing height, makes it more vulnerable against the pseudo-static forces introduced by the differential movement of the supports.

5. The pylon-cable system configuration is an important factor in the assessment of the SVGM. Bridges with a central cable plane tend to maximise the effect of the asynchronous excitation at the lower part of the pylon in the transverse direction, where the pylon shape also plays an important role in the response. It is observed that pylons which feature lower diamonds are more vulnerable against the multi-support excitation, mainly because of the large stiffness of the common member at their base and due to the rotation capacity of the connection between the vertical pier and the inclined legs of the pylon below the deck, which maximises the transverse displacement of the pylon. The pylons with lower diamonds require larger amounts of reinforcement at their base when subjected to multi-support excitations than the case of the SYNC motion of the supports. On the other hand, the individual legs of the H-LCP model and the central cable system of the Y-CCP and YD-CCP models are better candidates to accommodate the out-of-phase motion of the supports above the deck because they constitute more 'flexible' configurations than the other pylon-cable system configurations studied.

6. There is a close link between the effect of the asynchronous motion on the seismic response and the vibration modes of the structure. Higher-order antisymmetric vibration modes are excited by the SVGM and are de-amplified by the SYNC motion.

Chapter 7

Inelastic Seismic Behaviour

Contents

7.1 Introduction

So far the elastic seismic response under synchronous and asynchronous ground motions at the supports of cable-stayed bridges have been studied. The work included variable span lengths, with lateral and central cable configurations, open-section and closed-box deck sections and 'H'-, inverted 'Y'- and 'A'-shaped pylons, the last two cases with and without lower diamonds. In all the previous results the materials were considered linear. However, it is of paramount importance to examine the seismic behaviour of cable-stayed bridges under the impact of very strong earthquakes[1] when their constituent materials enter the inelastic range. In this chapter realistic nonlinear models of the concrete in the pylons and the reinforcing steel are considered.

The aim of this chapter is to examine the effect of the SVGM and of the seismic incidence angle on the damage initiation and propagation in the two pylons. Several observations are obtained through the comparison between the elastic and the inelastic seismic behaviours of the bridge models of this work. The importance of the pylon shape as a means to resist the SVGM is also highlighted. To this end, Sections 7.3 and 7.4 discuss the different seismic forces developed in models with different pylon shapes and variable main span lengths. Section 7.5 presents the inelastic deformation demand along the height of the pylons in the same models, Section 7.6 discusses the damage induced in the pylons through a damage factor, defined as the cumulative dissipated energy in the pylon through plasticity over the respective input energy from the earthquake. Finally, Section 7.7 discusses the influence of the earthquake intensity on the seismic behaviour of the bridge, in terms of the curvature ductility at the base of the pylons, of the drift ratio at their top and of the cable stresses. The selected demand parameters are compared with adopted capacity models and the probability of failure is computed for these components of the cable-stayed bridge with 'H'-shaped pylons.

The nonlinear dynamic analysis of the bridges is performed by means of the Non-Linear Response-History Analysis (NL-RHA). The study of the inelastic seismic behaviour of the cable-stayed bridges is focused on models with 'H'- and inverted 'Y'-shaped pylons, the latter with two lateral cable planes and main span lengths of L_P = 200, 400 and 600 m. The same seismic records are applied to the foundations of the bridges which present loss of coherency (Harichandran and Vanmarcke 1986) and time delay (c = 1000 m/s). The results of the analyses are compared with the results from the SYNC motion of the supports ($c = \infty$). In an attempt to control the high computational cost associated with the analysis, only two different values of θ are considered in this chapter; $\theta = 0^\circ$ and 90° i.e. the strong earthquake component (FN) is parallel and perpendicular to the deck, respectively, as can be seen in Fig. 7.1.

[1]The structural integrity of bridges must be ensured under strong earthquakes with a return period of 475 years following the no-collapse requirement of the ultimate limit state (ULS) in EN1998-1:2004 (Eurocode 8; Part 1 2004)

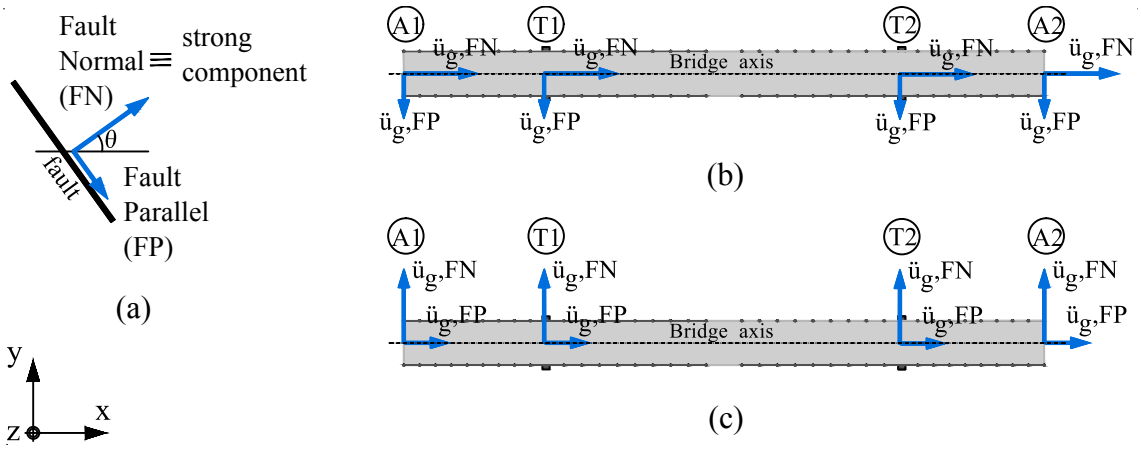

Figure 7.1: Proposed angles of incidence (θ) of the seismic waves with respect to the axes of the bridge models in the inelastic dynamic analysis. (a) Principal components of the earthquake; (b) $\theta = 0°$ and (c) $\theta = 90°$.

7.2 Methodology

The results of the nonlinear dynamic seismic analysis are presented in terms of the peak seismic axial load (N), the longitudinal (V_x) and the transverse (V_y) shear forces along the pylon legs. Furthermore, the deformations of the concrete and the steel reinforcement (ε_{tot}) in the pylons are examined, and the energy dissipation in the pylons and the individual segments that form the pylons (i.e. lateral legs, transverse struts) is also discussed. The assessment of the results in all cases is targeted to the leg of each pylon that is connected rigidly to the deck. Finally, the stresses (σ) during the earthquakes are obtained in selected cables that correspond to the ones that connect the pylons to the deck at the abutments and at the vertical piers in the side spans, and also to the shortest and longest cables of the cable system.

As in the elastic analysis, the results are initially obtained in the form of time-histories of the forces and the deformations that are developed in the pylon leg. Subsequently, for each earthquake the peak value of the seismic response quantity under consideration, excluding the effect of the self-weight, is obtained for the different regions of the leg. The maximum seismic response along the pylon is obtained for the individual earthquakes and it is followed by the calculation of the average values (μ) and the standard deviation (SD). In the case of the deformations of the concrete and the steel reinforcement, the post-processing procedure also takes account of the initial strain induced by the self-weight. The deformations are examined in the corner of the concrete sections of the pylons, where the maximum strains are recorded, and in the reinforcement bars located at the corners, as can be seen in Fig. 7.2. In addition time-histories of the the external work introduced by the earthquake and of the energy dissipated by the structure are obtained, of the curvature ductility at the base of the pylons and of the cable stresses.

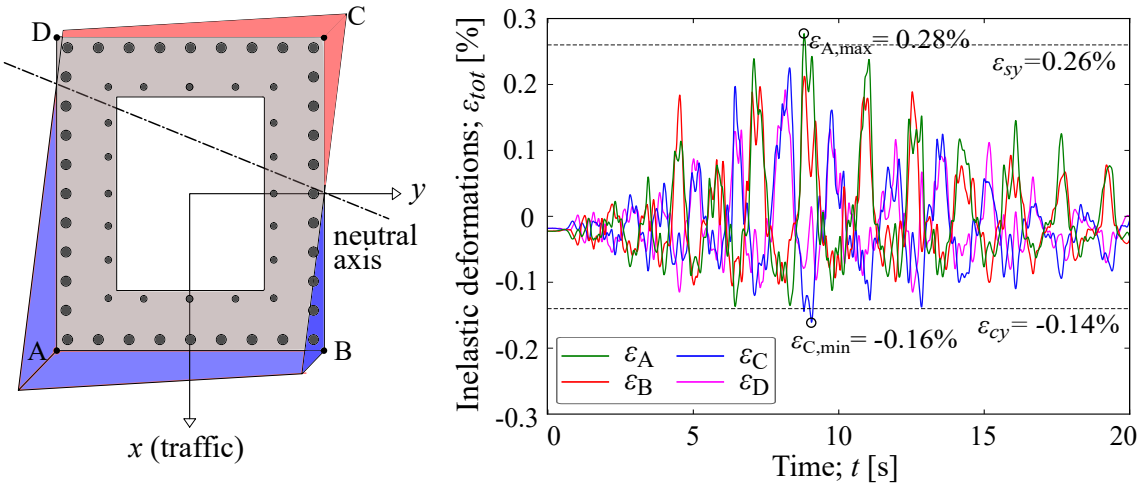

Figure 7.2: (a) Schematic representation of the strain distribution in a typical section of the pylon and (b) Time-histories of the deformation at the corners of the section; H-LCP model; $L_P = 200$ m; $\theta = 0°$; seismic record #7; SYNC motion.

7.3 Seismic Forces

This section discusses the effect of the SVGM on the peak seismic response along pylon P2, the second one to receive the ground motion, in bridges with 'H'- and inverted 'Y'-shaped pylons and main span lengths of $L_P = 200$, 400 and 600 m. Figs. 7.3 - 7.5 include the axial force (N), the longitudinal (V_x) and the transverse (V_y) shear forces. The reference synchronous (SYNC) motion case is also included in the figures. As in the elastic analysis discussed in the previous chapter, in the plots the black solid line represents the mean peak seismic response (μ) from the SYNC motion of the supports and the total width of the shaded band centred in this represents two standard deviations ($\pm$SD) from the mean response. The red line refers to the peak mean seismic response from the SVGM, namely; $c = 1000$ m/s.

7.3.1 Effect of the Material Nonlinearity

The intermediate-span bridge, with a main span of 400 m, will be examined first. Fig. 7.3 shows that when the nonlinear properties of the materials are considered the seismic axial force (Fig. 7.3(a)), the longitudinal (Fig. 7.3(b)) and the transverse shear forces (Fig. 7.3(c)) are reduced, compared to the respective elastic forces. This effect is clearer in the SYNC motion. Reductions of approximately 35%, 10% and 24% are observed in the axial load (N) at the base of the pylon, in the longitudinal shear force (V_x) at the same point, and in the transverse shear force (V_y) at the area between the deck and the lower strut, respectively. The higher 'rate of reduction' in N and V_y is associated mainly with the transverse flexure of the pylon, which introduces compression in one leg and tension in the second leg (Fig. 6.12), and with the transverse reaction that the deck exerts to the

pylon, respectively. The transverse deck-pylon reaction is dominated by the fundamental transverse vibration mode of this bridge ($L_P = 400$ m) (Camara and Efthymiou 2016). These conditions result, as it will be discussed in detail in Section 7.6, in increased damage due to the axial and the transverse responses of the pylon compared to the longitudinal one. The larger reduction in the transverse seismic forces due to the material nonlinearity is because of two reasons; (1) the plastic dissipation of the input energy provides an additional damping mechanism in the pylons, and (2) important vibration periods for the structure are elongated due to damage and these are associated with lower spectral accelerations.

In Fig. 7.3(a) it is observed that the elastic and the inelastic axial responses of the pylon from the SVGM are increased at the region of the intermediate anchorage and, more importantly, at the base compared to the SYNC motion. The increments in the elastic axial load due to the SVGM (e.g. $N_{\text{EL,SVGM}}$) can be quantified by the ratio of the mean peak seismic response from the SVGM over the respective mean peak response quantity from the SYNC motion (e.g. $N_{\text{EL,SYNC}}$), i.e. by the ratio ρ as defined in Eq. (6.2). In the middle of the anchorage area $\rho_{N,\text{EL},anc}$ reaches 1.12, when $c = 1000$ m/s, whereas the same ratio at the base of the pylon is increased to $\rho_{N,\text{EL},base} = 1.17$. In the former case the seismic axial load obtained from the SVGM is kept within the limits of SD from the mean SYNC response, as opposed to the latter case wherein $N_{\text{EL,SVGM}}$ exceeds the SD from the SYNC motion. The inelastic axial response from the SVGM is significant at the same sections as the elastic results but in this case $\rho_{N,\text{IN},anc} = 1.25$ and is considered a large increase from the SYNC motion because it exceeds the range defined by the SD. Furthermore, it can be observed that the axial load from the SVGM, $N_{\text{IN,SVGM}}$, at the base of the pylon is reduced by 39% compared to the elastic $N_{\text{EL,SVGM}}$. The corresponding reduction of the inelastic SYNC response, $N_{\text{IN,SYNC}}$, equals 35% compared to $N_{\text{EL,SYNC}}$, which suggests that there is greater damage at the base of the pylon when the SVGM is considered and this results in the effect of the out-of-phase motion of the supports being less pronounced in the peak seismic forces obtained in the inelastic analysis of the bridges.

In Fig. 7.3(b) it is shown that the SVGM consistently reduces the longitudinal seismic shear force along the pylon compared to the SYNC motion implying that in the longitudinal direction of the response the multi-support excitation favours the seismic behaviour of the bridge. Furthermore, it is seen that $V_{x\,\text{IN,SYNC}}$ is reduced by 13% from the respective elastic response at the base, whereas the longitudinal shear from the SVGM ($V_{x\,\text{IN,SVGM}}$) is not reduced when the material nonlinearities are considered, suggesting that the pylon is not damaged when subjected to out-of-phase motion among the bridge's supports.

Fig. 7.3(c) shows that when material nonlinearities arise the transverse response from the SVGM is generally very similar to the respective seismic SYNC response in the inelastic range at the part of the pylon above the deck level. This is because the out-of-

phase oscillation of the two pylons is not significantly restrained the cable-system. On the other hand, the SVGM reduces the seismic shear force at the deck level of the pylon in the inelastic results compared to the SYNC motion, as opposed to the elastic results in which the SVGM increases the response. At this region of the pylon $V_{y\,\text{IN,SVGM}}$ is reduced by 47% in the inelastic analysis compared to the elastic behaviour ($V_{y\,\text{EL,SVGM}}$) of the pylon, but the respective response from the SYNC motion, $V_{y\,\text{IN,SYNC}}$, is reduced by 25% from $V_{y\,\text{EL,SYNC}}$ suggesting that the damage from the multi-support excitation is larger at the deck level of the pylon. The results from Figs. 7.3(a) and (c) prove that the SVGM is more important in the transverse direction of the pylon wherein the damage is also greater than that from the SYNC motion.

Fig. 7.4 includes the peak seismic forces in the pylon when the strong component of the earthquake is perpendicular to the bridge axis ($\theta = 90°$). The inelastic response of the pylon is modified from the respective response when $\theta = 0°$ (right column of Fig. 7.3). The inelastic SYNC longitudinal shear ($V_{x\,\text{IN,SYNC}}$) at the base of pylon P2 is reduced by approximately 25% compared to the $V_{x\,\text{IN,SYNC}}$ when $\theta = 0°$, whereas the transverse shear ($V_{y\,\text{IN,SYNC}}$) at the level of the deck-pylon connection is increased by 15%. This is expected, as it is also seen in the elastic analysis presented in Chapter 6, because the seismic response in each direction is maximised when the strong earthquake component is applied parallel to this direction. The axial load at the base of the pylon is not modified with the change of the orientation of the bridge when identical support motion is considered. Fig. 7.4 also shows that when $\theta = 90°$, the effect of the SVGM on the three directions of the seismic response is negligible because of the increased damage from the SVGM in this orientation of the bridge, as it will be detailed in the following sections.

7.3.2 Influence of the Pylon Shape

Fig. 7.5 gives an insight into the effect of the SVGM on the peak inelastic seismic response of cable-stayed bridges with inverted 'Y'-shaped pylons and two lateral cable planes (LCP) in the intermediate-span cable-stayed bridge ($L_P = 400$ m) when $\theta = 0°$. Fig. 7.5(a) presents the peak seismic axial force and Figs. 7.5(b), (c) include the longitudinal and transverse seismic shear forces, respectively. The vertical common member of the pylon in the Y-LCP bridge differentiates the effect of the multi-support excitation from that obtained in the individual legs of the 'H'-shaped pylon (Fig. 7.3). In Fig. 7.5(a) it is observed that the SVGM increases by a maximum of 40%, compared to the SYNC motion, the peak axial load at the anchorage area of the pylon with inverted 'Y' shape. The values of the inelastic response ratio in the anchorage area of the pylon increase in the Y-LCP bridge: $\rho_{N,\text{Y-LCP}}$ takes values of 1.41 compared to the values of $\rho_{N,\text{H-LCP}}$ which average 1.0. The increment can be explained by the increased stiffness of the top part of

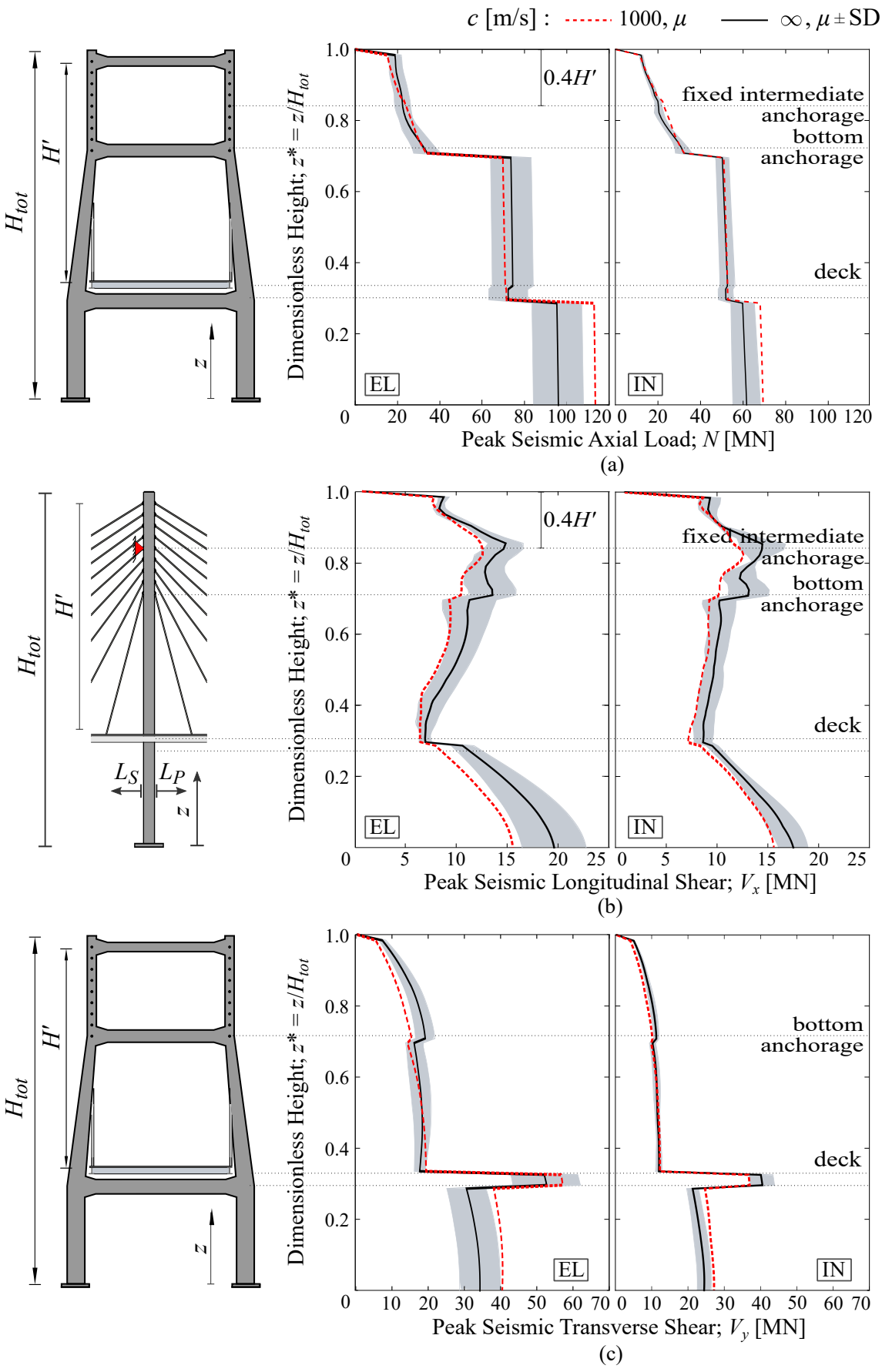

Figure 7.3: Peak elastic (left column) and inelastic (right column) seismic response in pylon P2. H-LCP bridge; $L_P = 400$ m; $\theta = 0°$ (i.e. FN // bridge axis).

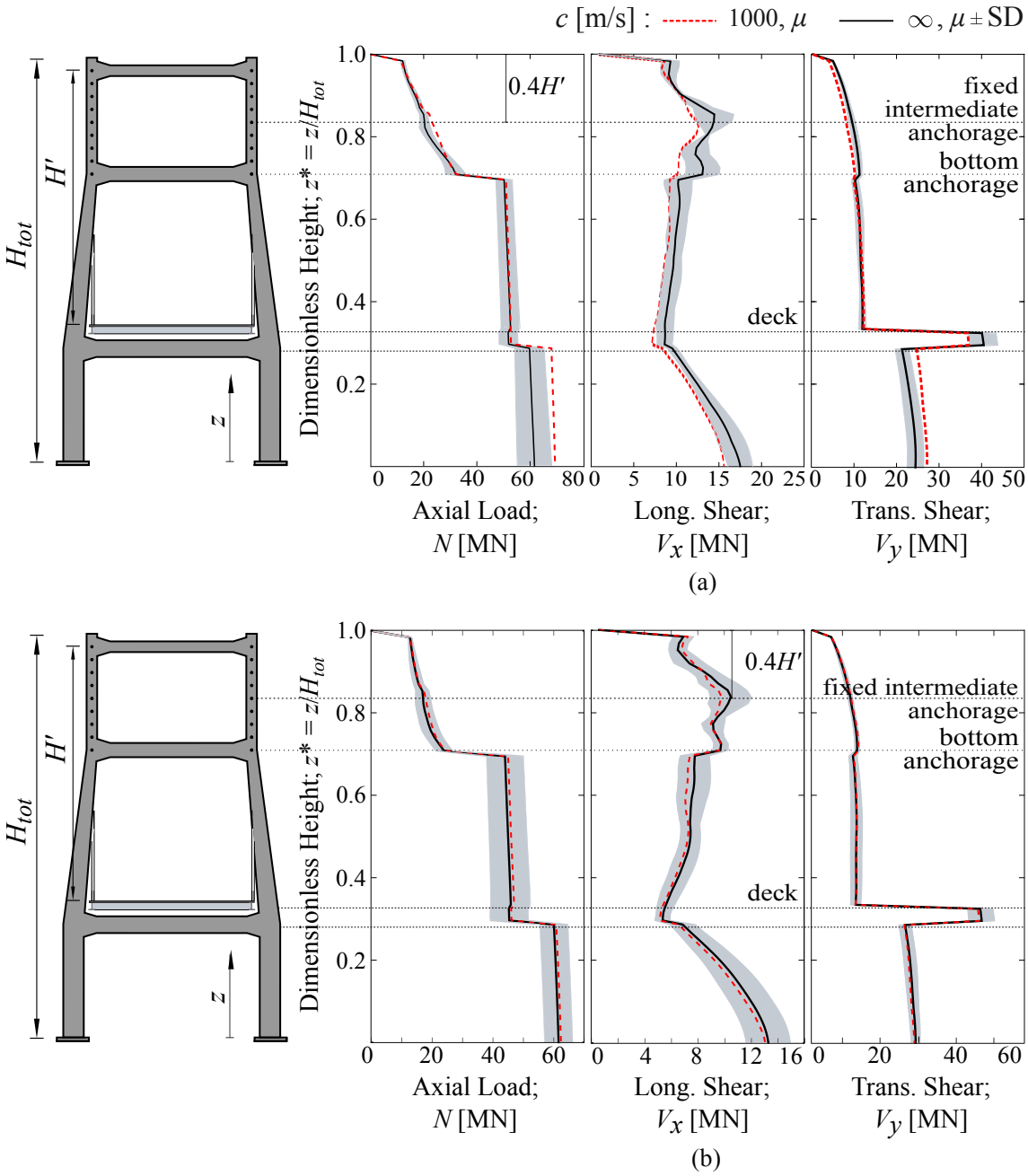

Figure 7.4: Mean peak inelastic seismic axial load (N), longitudinal (V_x) and transverse (V_y) shear forces along the height of pylon P2 when (a) $\theta = 0°$ and (b) $\theta = 90°$. H-LCP bridge; $L_P = 400$ m (i.e. FN $\perp$ bridge axis).

the Y-LCP model compared to the H-LCP model.

Despite the different geometry between the inverted 'Y'- and the 'H'-shaped pylons the part of the legs at the level of the deck in both configurations is the most affected by the SVGM. In the Y-LCP model the response ratio takes the value of $\rho_{V_y,\text{Y-LCP}} = 1.09$ whereas for the 'H'-shaped pylon $\rho_{V_y,\text{H-LCP}} = 0.92$ at the deck-pylon connection. The comparison suggests that the stiffer configuration of the inverted 'Y'-shaped pylon makes it less capable to accommodate effectively the multi-support excitation than the more flexible 'H'-shaped pylon. In the longitudinal direction the SVGM reduces the seismic response of both pylons along their height compared to the SYNC excitation.

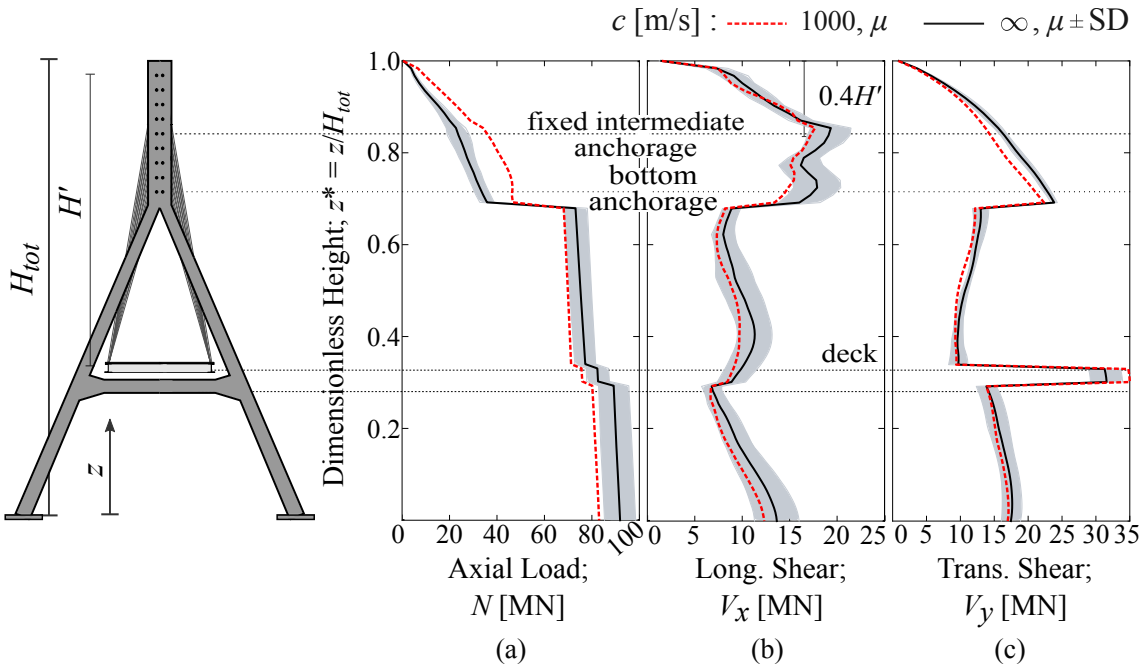

Figure 7.5: Mean peak inelastic seismic (a) axial load (N), (b) longitudinal (V_x) and (c) transverse (V_y) shear forces along the height of pylon P2. Y-LCP model; $L_P = 400$ m; $\theta = 0°$ (i.e. FN // bridge axis).

7.3.3 Influence of the Main Span Length

Fig. 7.6 shows the peak seismic response in terms of N, V_x and V_y in the 'H'-shaped pylons of the bridges with 200, 400 and 600 m main spans and heights of 62.5, 125 and 187.5 m, respectively. It is observed that by increasing the main span length (L_P) the pylons are less vulnerable to the asynchronous motion in terms of the vertical (axial) direction of the response. The SVGM in this direction results in higher peak axial forces (N) along the height of the pylon of the 200-m span bridge, but it leads to similar values of N under the SYNC motion in the intermediate- and long-span bridges with $L_P = 400$ and 600 m, respectively. The effect of the multi-support excitation varies with the value of L_P. For example, the SVGM increases by $\rho_N = 1.11$ the SYNC axial response at the base

of the pylon in the 400-m span bridge and at the intermediate part of the legs (inclined part between the deck and the anchorage system) in the pylon of the 600-m bridge. This indicates that the overall dimensions of the structure combined with the plasticity in the pylon affects the influence of the SVGM on the seismic response.

In the longitudinal direction of the response the SVGM generally reduces the seismic response of the pylon, regardless of the main span length, with response ratios ρ_N ranging from 0.89 in the 200- and the 400-m span bridges to 0.86 in the 600-m span bridge. On the other hand, the increase in L_P has a considerable effect on the transverse shear from the SVGM at the lower part of the pylon which takes values that are different from the respective ones from the SYNC motion of the supports. It is observed that V_y is increased when the out-of-phase motion in the pylons of the 200- and the 600-m span bridges and is reduced in the intermediate-span bridge ($L_P = 400$ m). The increase in the shortest bridge can be explained by the stiffer configuration of the shortest pylon compared to its long counterpart, given that stiff structures are vulnerable against the pseudo-static forces that are induced by the asynchronous motion of the supports (Nazmy and Abdel-Ghaffar 1992, Sextos and Kappos 2008). On the other hand, the increase in the longest bridge is due to the relative motion of the lateral legs of the pylon which becomes more pronounced as their height increases. Finally, it can be concluded that the out-of-phase oscillation of the pylons is more onerous for the response of the bridge in the transverse direction of the response.

7.3.4 Modal Contribution to the Inelastic Response of the Pylons

It has been observed so far that the effect of the SVGM on the seismic response may vary among bridges with different dimensions, among various orientations with respect to the earthquake's propagation, and even between the elastic and inelastic analyses of the bridges. A characteristic example is the transverse shear force at the level of the deck (i.e. the region of the pylon with the maximum transverse response) which is reduced in the elastic analysis when the SVGM is considered with the response ratio $\rho_{V_y,\mathrm{EL}} = 0.86$, as can be seen in Fig. 6.8, but it is increased in the inelastic analysis at the same region by ($\rho_{V_y,\mathrm{IN}}$) 1.14 (Fig. 6.8(c)).

In order to explore the effect of the SVGM on the seismic response, Fig. 7.7 shows the DFT of the time-histories of the elastic and the inelastic transverse shear forces at the level of the deck in pylon P2 of the 200-m main span bridge when $\theta = 0°$. Fig. 7.7(a) reveals that the first transverse vibration mode of the bridge (Mode #4, as shown in Fig. 3.18), which involves the transverse flexure of the pylons combined with the transverse movement of the deck and has a frequency of $f_4 = 0.78$ Hz, is excited both by the SVGM and the SYNC motion. However, the amplitude of the DFT is larger for the

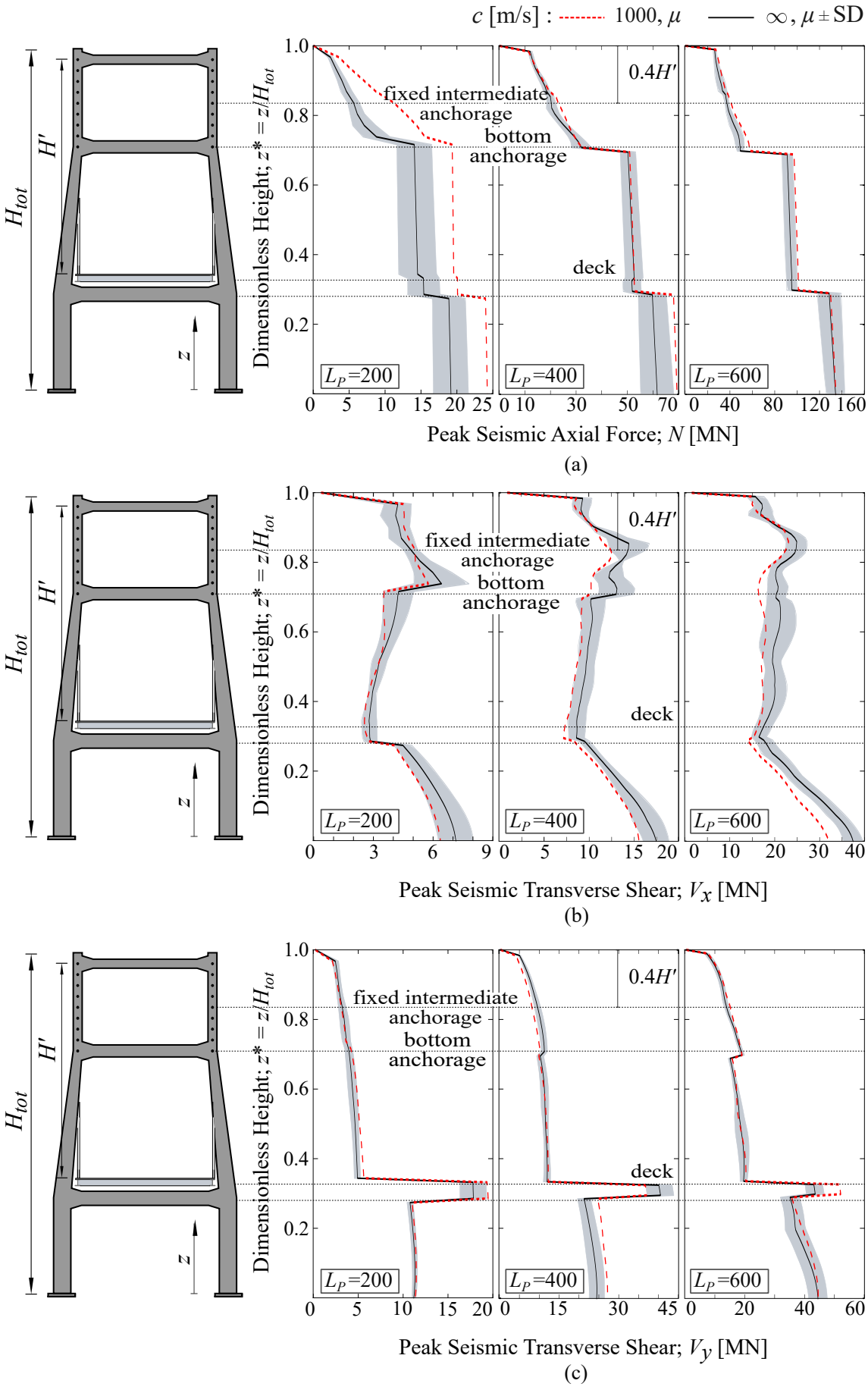

Figure 7.6: Mean peak inelastic seismic (a) axial load (N), (b) longitudinal (V_x) and (c) transverse (V_y) shear forces along the height of pylon P2. H-LCP models; $\theta = 0°$ (i.e. FN // bridge axis).

SYNC motion in the elastic results, which may explain the larger response obtained from the SVGM compared to the respective transverse shear at deck-pylon connection when identical supports motion is considered. On the other hand, the transverse response is increased from the SVGM in the inelastic analysis and it exceeds the value of V_y obtained from the SYNC motion, which can be attributed to the increased amplitude of the same vibration mode when the time-history of the transverse shear in the pylon is examined. In the nonlinear response the frequency of mode #4 is shifted from point A to A′, at $f_4 =$ 0.6 Hz, due to the period elongation that is caused by the induced damage in the pylons of the bridge, as will be discussed in detail in the next sections.

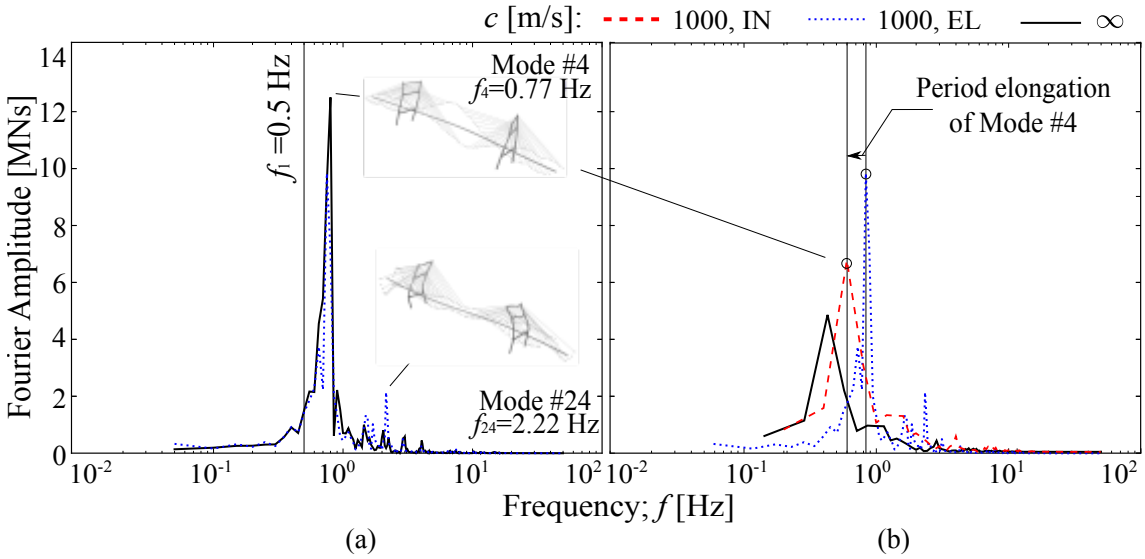

Figure 7.7: DFT of the time-histories of the (a) elastic and (b) inelastic V_y at the deck level of pylon P2. $L_P = 200$ m; H-LCP model; $\theta = 0°$; the period elongation of Mode #4 in the inelastic analysis is noted.

7.4 Magnitude of the SVGM in the Inelastic Range

In the elastic analysis of the cable-stayed bridge models the dimensionless response ratio ρ (Eq. (6.2)) was employed as a means to quantify the effect of the SVGM on the pylons. The values of ρ_j, with $j = N, V_x, V_y$, are obtained from the arithmetic mean (from the applied sets of accelerograms) of the peak response quantity under consideration from the SVGM over the SYNC motion.

The effect of the SVGM differs when the material nonlinearities are considered. A full comparison between the same quantity ratios ρ_{EL} and ρ_{IN} from the elastic and the inelastic results, respectively is presented in Fig. 7.8 for the H-LCP models with $L_P = 200$, 400 and 600 m for the three directions of the seismic response (N, V_x, V_y) in the regions of the pylons where the peak structural response is recorded when $\theta = 0°$.

Specifically, ρ_N and ρ_{V_x} are obtained at the base of pylon P2 and ρ_{V_y} is obtained at the level of the deck of the same pylon. The ratios are also examined for the two proposed orientations of the intermediate-span bridge with $L_P = 400$ m ($\theta = 0^\circ$ and 90° in Fig. 7.9).

The effect of the SVGM on the axial load at the base of the pylon is increased in the nonlinear analysis of the short-span bridge ($L_P = 200$ m) from $\rho_{N,\text{EL}} = 1.16$ to $\rho_{N,\text{IN}} = 1.27$ when $\theta = 0^\circ$. The effect of the SVGM is significant in this case because it exceeds the standard deviation from the mean seismic response from the SYNC motion ($\mu+$ SD). For the same value of θ, the effect of the multi-support excitation also increases the seismic response in the inelastic range ($\rho_{N,\text{IN}} > \mu+$SD) for the intermediate-span bridge and it is only in the long-span bridge that the effect of the SVGM is reduced compared to elastic results with the response ratio being reduced from 1.04 (which is not significant because $\rho_{N,\text{IN}} < \mu+$SD) in the elastic range to 1.0 in the inelastic range. The reduction is not significant but only mentioned because in this case the SVGM is not 'detrimental' to the response of the pylon in the inelastic range. However, from a quantitative point of view, the effect of the SVGM is not modified in the inelastic range in the pylons of the 200- and 400-m span bridges in the sense that $\rho_{N,\text{IN}} > \mu+$SD in both cases.

The ratios obtained for the longitudinal shear force, V_x, show that the SVGM reduces the seismic response of the pylons regardless of the main span length and of the material nonlinearities when $\theta = 0^\circ$. Fig. 7.9 shows that in the rotated orientation of the bridge, wherein the strong earthquake component is perpendicular to the deck the SVGM reduces the shear force in the inelastic range when $\theta = 90^\circ$ but the difference between $\rho_{V_x,\text{EL}}$ and $\rho_{V_x,\text{IN}}$ is insignificant.

Finally, in the transverse direction of the response the SVGM is critical in the shortest bridge with $L_P = 200$ m because of the increased stiffness of the pylons compared to their taller counterparts of the 400- and 600-m bridges. However, in the flexible pylon of longest bridge ($L_P = 600$ m, $H_{tot} = 187.5$ m) the pronounced relative motion of its lateral legs of the pylon increase the effect of the SVGM. The pylon of the intermediate-span bridge falls between the stiff pylon of the 200-m span bridge and the flexible pylon of the 600-m bridge for which, however, the loss of coherency and the time lag are more pronounced. It can be argued at this point that the SVGM is more detrimental for the pylon of the short-span bridge because $\rho_{V_y,\text{IN}} > \mu+$SD in the inelastic range ($\rho_{V_y,\text{EL}} = 1.1$), as opposed to the respective elastic response ratio which equals $\rho_{V_y,\text{EL}} = 0.9$. This can be attributed to the period elongation that is caused by the induced damage in the structure which modifies the participation of certain important vibration modes to the response, such as the dominant Mode #4 whose magnitude is increased in the inelastic range under the SVGM, as observed in Fig. 7.7.

When the earthquake is rotated by 90° and the strong earthquake component is per-

pendicular to the bridge, as shown in Fig. 7.9, the effect of the SVGM is not significantly affected by the material nonlinearity. Comparing the elastic and the inelastic analyses for $\theta = 90°$, the SVGM results in a slightly increased longitudinal seismic response (V_x) from the SYNC motion, and in a slightly reduced transverse response (V_y). However, these effects seem to be negligible and kept within the limits of SD, as shown in Fig. 7.4.

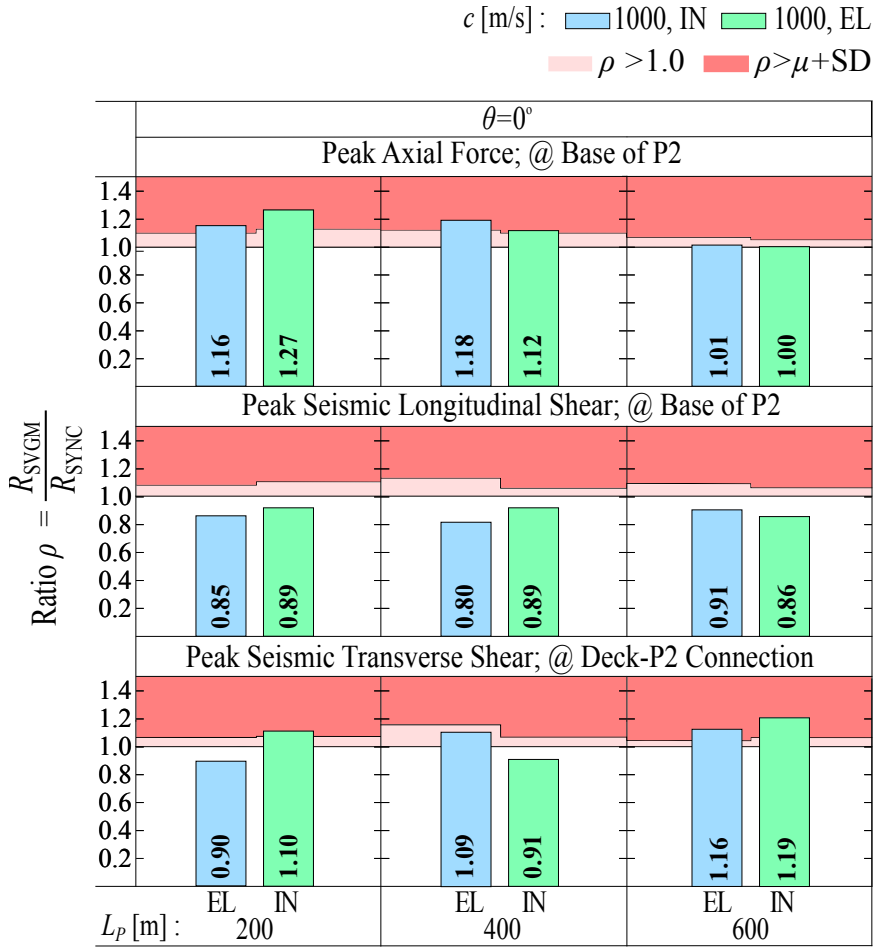

Figure 7.8: Response ratio ρ obtained from the mean peak N and V_x at the base and the mean peak V_y at deck level of pylon P2; 'EL' and 'IN' stand for elastic and inelastic analysis, respectively, $\theta = 0°$, the light and dark red bands denote $\rho > 1$ and $\rho > \mu$+SD, respectively. H-LCP model.

7.5 Inelastic Demand for Deformations in the Pylons

In this section the peak seismic demand for inelastic deformations at the sections is presented for the pylons with 'H' and inverted 'Y' shapes, the latter with two lateral planes of cables. Bridges with $L_P = 200$, 400 and 600 m are examined in the two different values of the seismic incidence angle ($\theta = 0°$ and 90°). These results are discussed in order to identify the areas of the pylons with the highest seismic demand and to address the influence of the orientation of the structures combined with the SVGM. In the following

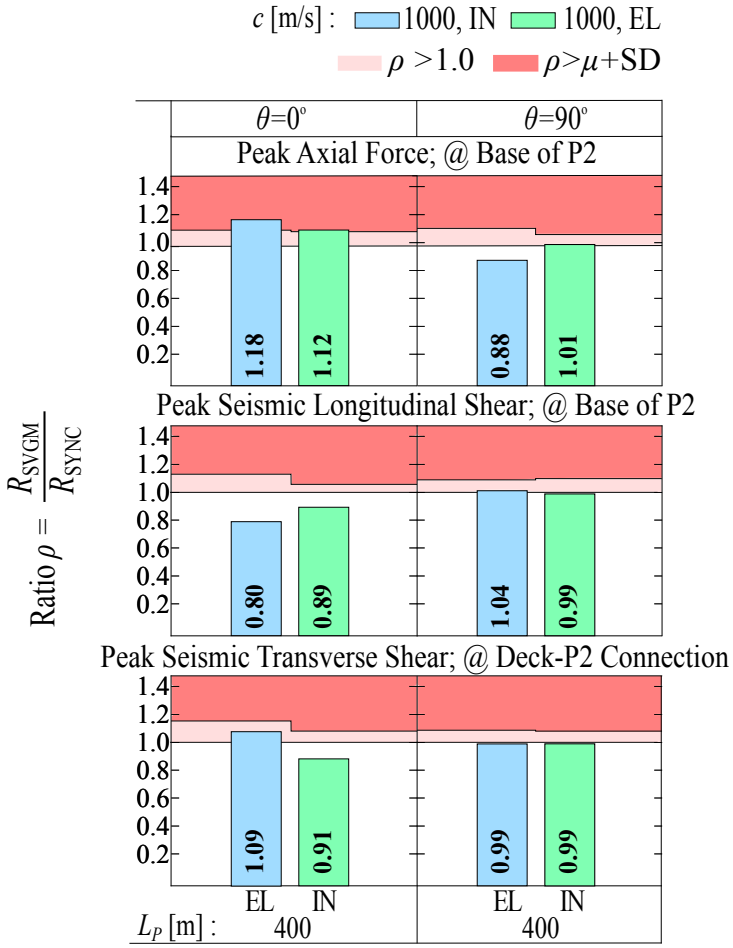

Figure 7.9: Response ratio ρ obtained from the mean peak N and V_x at the base and the mean peak V_y at deck level of pylon P2; 'EL' and 'IN' stand for elastic and inelastic analysis, respectively, $\theta = 90°$, the light and dark red bands denote $\rho > 1$ and $\rho > \mu$+SD, respectively. $L_P = 400$ m, H-LCP model.

results the peak seismic deformations are examined at the corner of the concrete section and at the corner reinforcement bar (Fig. 7.2). The positive values of the deformations (ε^{+}) denote tension and the negative values (ε^{-}) denote compression. The cracking in the concrete sections is considered inadmissible under the design earthquake ($a_g = 0.5g$) when the steel reinforcement yields in tension (i.e. when $\varepsilon_{sy} \geq 0.26\%$), whereas the compressive deformation demand in the concrete is considered large when the compressive elastic limit $\varepsilon_{cy} =^{1} 0.14\%$ is exceeded. These deformation demands can be characterised as slight structural damage (HAZUS 1997). The areas of the pylons with longitudinal reinforcement bars yielding in tension are highlighted with red colour in the following figures.

The inelastic analysis of the bridges reveals the regions of the pylons whose sections are subjected to larger deformations. Fig. 7.10 highlights these areas on the H-LCP bridge with $L_P = 400$ m when the strong component of the earthquake is considered parallel ($\theta = 0°$) and perpendicular ($\theta = 90°$) to the axis of the bridge under the SYNC motion. In order to distinguish between the effects of the SVGM and the SYNC motion, the plastic strains when $\theta = 0°$ are noted on the left half of the pylon and, accordingly, the strains from the analyses when $\theta = 90°$ are included on the right half. The demand for inelastic deformations along the pylon is compared to the respective elastic demand. The increase of the plastic strains compared to the elastic demand of the steel reinforcement suggests that the connection of the lateral legs with the upper and the intermediate struts, and also with the foundation of the pylon legs, are the most sensitive regions of the pylon against the ground motion. In these areas the steel exceeds the yielding deformation (ε_{sy}), which is associated with slight to moderate concrete cracking, and the concrete softens in compression ($\varepsilon > \varepsilon_{cy}$). The peak tensile deformations (of the steel reinforcement) are larger than the respective compressive peak deformations (of the concrete). This is because when cracking is initiated in the concrete ($\varepsilon_{c,crack} = 0.0086\%$) the neutral axis of the section is shifted towards the compression part of the section, resulting in higher increments in the tensile deformation. It is seen that the SVGM has a qualitatively similar effect on the concrete (compression) as it has on the steel reinforcement (tension). The incidence angle of the ground motion influences the amount of cracking, which is larger when the strong earthquake component is perpendicular to the bridge axis ($\theta = 90°$), as shown in Fig. 7.10(b). When $\theta = 90°$ the earthquake is applied parallel to the axis of the struts and the relative motion of the lateral legs of the pylon is more pronounced, which explains the increase of 50% in the inelastic deformation at the region of the connection of the lateral legs with the upper transverse struts compared to the respective value for $\theta = 0°$ in Fig. 7.10(a). Similarly, the plastic deformation is increased by 17% at level of the connection between the lateral legs with the intermediate transverse struts and by 150% at the base of the pylon when the bridge is rotated by 90° with respect to the propagation

[1]The compressive elastic limit of the concrete is calculated based on the mean elastic compressive stress (f_{cm} = -48 MPa) that was defined in Table 3.6 as $\varepsilon_{cy} = f_{cm}/E_c$ = -0.14%.

of the earthquake.

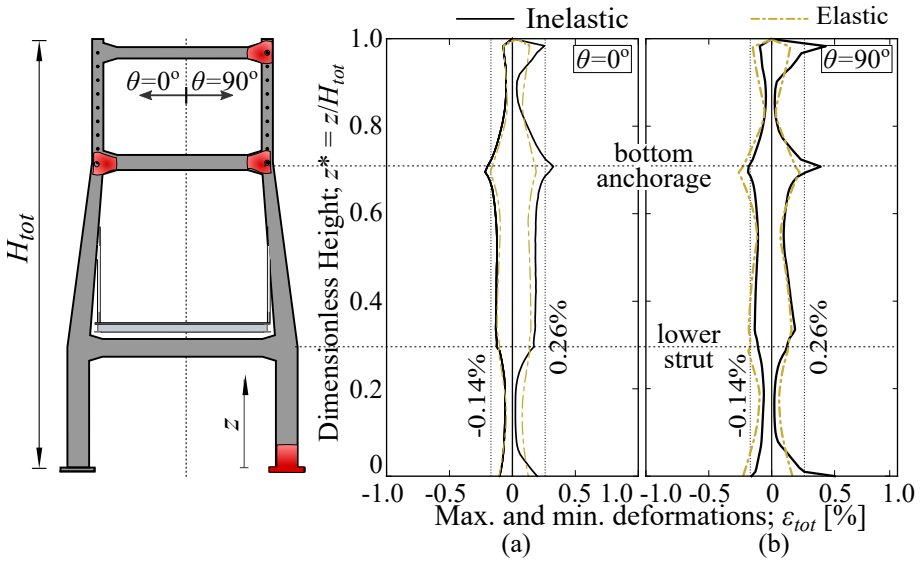

Figure 7.10: Peak elastic and inelastic deformations of the concrete (compression) and the steel reinforcement (tension) in pylon P2 when (a) $\theta = 0°$ and (b) $\theta = 90°$. H-LCP, $L_P = 400$ m, SYNC ground motion, the coloured areas denote damage in the pylon.

Fig. 7.11 presents the deformation demands in the two pylons of the 200-m span bridge. It is seen that for the SVGM and for the SYNC motion (with $\theta = 0°$) there is large cracking at the base of the two pylons with the reinforcement bars yielding in tension. The effect of the SVGM on the inelastic deformations at the base of pylon P1 is appreciable with $\varepsilon_{\text{SVGM}} = 0.48\%$ and $\varepsilon_{\text{SYNC}} = 0.85\%$, as opposed to the deformations obtained at the base of P2 from the SVGM and the SYNC motion which are similar. This finding implies that the SYNC motion results in larger damage at the base of the pylons. On the contrary, the connection of the intermediate struts to the lateral legs of the 'H'-shaped pylon represents a region which is more sensitive to the asynchronous excitation of the supports than it is to the SYNC motion. This is reflected in the significantly larger value of ε when the bridge is subjected to multi-support excitations. Specifically, when the SVGM is considered the inelastic deformation reaches $\varepsilon_{\text{SVGM}} = 1.28\%$ in pylon P2, and it is twice as high as the respective deformation in the section from the SYNC motion. In the first pylon (P1), the effect of the SVGM is negligible and it can be concluded that the second pylon to receive the earthquake is more vulnerable against the multi-support excitation. This is because of the incoherence and the wave passage effects combined with the presence of the cable system which transfers forces from the first pylon to the second in the direction of the bridge, and with the relative movement of the legs of the pylon in the transverse direction of the bridge.

Fig. 7.12 presents the peak deformations in pylon P2 in the bridges with 200, 400 and 600 m main spans and 'H'-shaped pylons. As the span length increases, the height

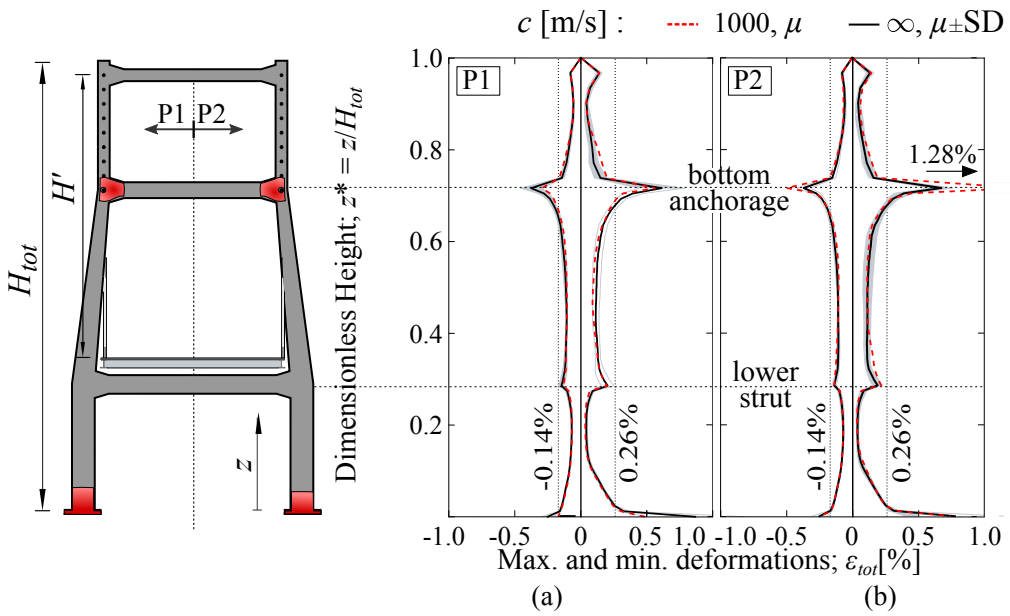

Figure 7.11: Peak deformations of the concrete and steel reinforcement in pylon (a) P1 and (b) P2. $L_P = 200$ m; $\theta = 0°$.

of the pylon increases proportionally[1] and it is observed that the peak deformations also increase in the connection between the upper strut with the lateral legs. However, in the region of the connection between the legs and the intermediate struts it is the short-span bridge ($L_P = 200$ m) the one in which the inelastic deformation is the largest, with the 400-m span bridge barely exceeding its yielding point of the reinforcement in tension. The stiff configuration of the short pylon of the 200-m span bridge proves to be sensitive to the ground motion, especially under the multi-support excitation, in which case the deformation ratio, defined as $\rho_\varepsilon = \varepsilon_{\text{SVGM}}/\varepsilon_{\text{SYNC}}$, is 2. At the other end, the flexible 'H'-shaped pylon of the 600-m bridge is also susceptible to damage at the intermediate strut-leg connection, but this is due to the relative oscillation between the legs that is received by the struts and their connection with the legs. Furthermore, as the height of the pylon increases, the number of the cables per cable plane in the half-span (N_T) increases from 9 in the 200-m main span bridge, to 19 and 29 cables in the bridges with $L_P = 400$ and 600 m, respectively. The increased mass due to the larger number of anchors with increasing spans, combined with the increased length of the upper part of the pylon to accommodate the anchorage system results in more pronounced oscillations of the upper part of the pylons for the longer spans.

Fig. 7.13 compares the peak demand for inelastic deformations in the H-LCP and Y-LCP models with $L_P = 400$ m when $\theta = 0°$. In the inverted 'Y'-shaped pylon the most critical region is the connection between the individual inclined legs and the top

[1]The total height of the pylon (H_{tot}) is defined parametrically as a function of the main span length (L_P) of the bridge: $H_{tot} = 1.5L_P/4.8$. With increasing main span length, the height of the pylon increases proportionally.

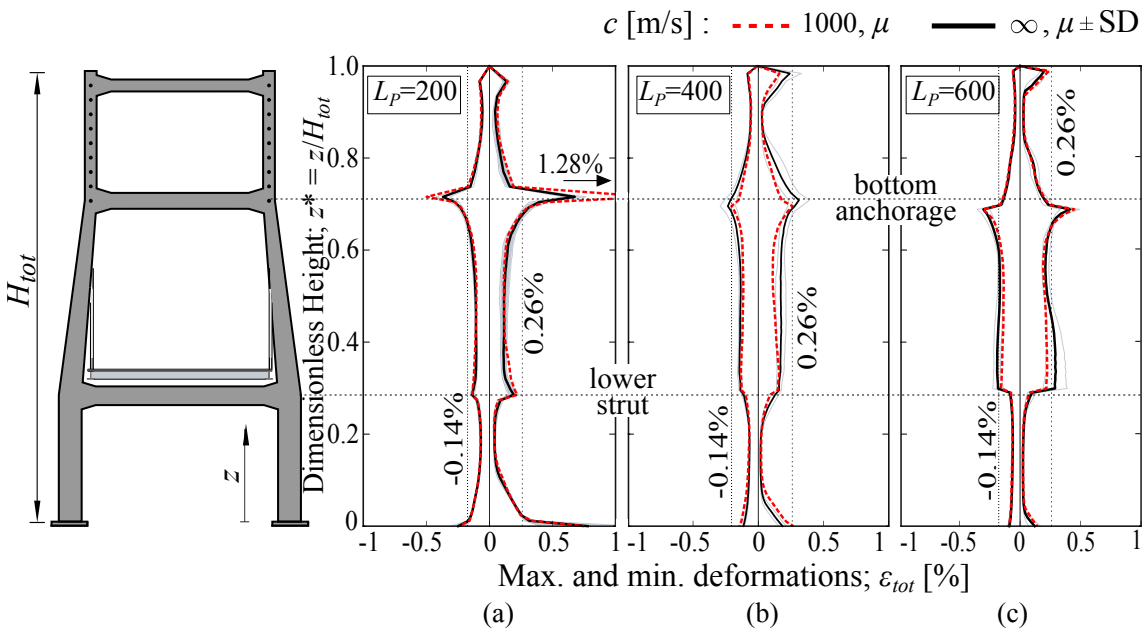

Figure 7.12: Peak inelastic deformations of the concrete and the steel reinforcement in pylon P2 in the bridges with (a) $L_P = 200$ m, (b) $L_P = 400$ m and (c) $L_P = 600$ m. $\theta = 0°$. H-LCP models.

vertical member, where the largest plastic strains reach 1.02% and 1.10% for the SVGM and the SYNC motions, respectively. This is due to the connection of the inclined legs at this point which strongly constrains the pylon in the transverse direction, as detailed in Fig. 6.12. The connection between the legs and the transverse strut, and the base of the pylon also exceed the elastic range of deformations with the reinforcement yielding in tension and the concrete softening in compression. However, the SVGM is not detrimental to the inverted 'Y'-shaped pylon since the peak plastic strains when $c = 1000$ m/s are kept below the respective strains when $c = \infty$ by (ρ_ϵ) 0.57.

The stiff configuration of the inverted 'Y'-shaped pylon results in larger deformations at the critical sections compared to the 'H'-shaped pylon, as shown in Fig. 7.13, suggesting that the 'H'-shaped pylon is a better candidate to accommodate the seismic action in the range of intermediate spans; $L_P \approx 400$ m. This is in agreement with the elastic seismic analysis of cable-stayed bridges under synchronous motion conducted by Camara and Efthymiou (2016) who observed that bridges with 'H'-shaped pylons are less sensitive to the transverse seismic reaction of the deck compared to the Y-LCP models. The SVGM is, however, beneficial to the response of both pylon shapes when $\theta = 0°$.

7.6 Damage Propagation in the Pylons

This section addresses the distribution of damage in the pylons in order to discuss the influence of the SVGM and the SYNC motions in the damage initiation and propagation.

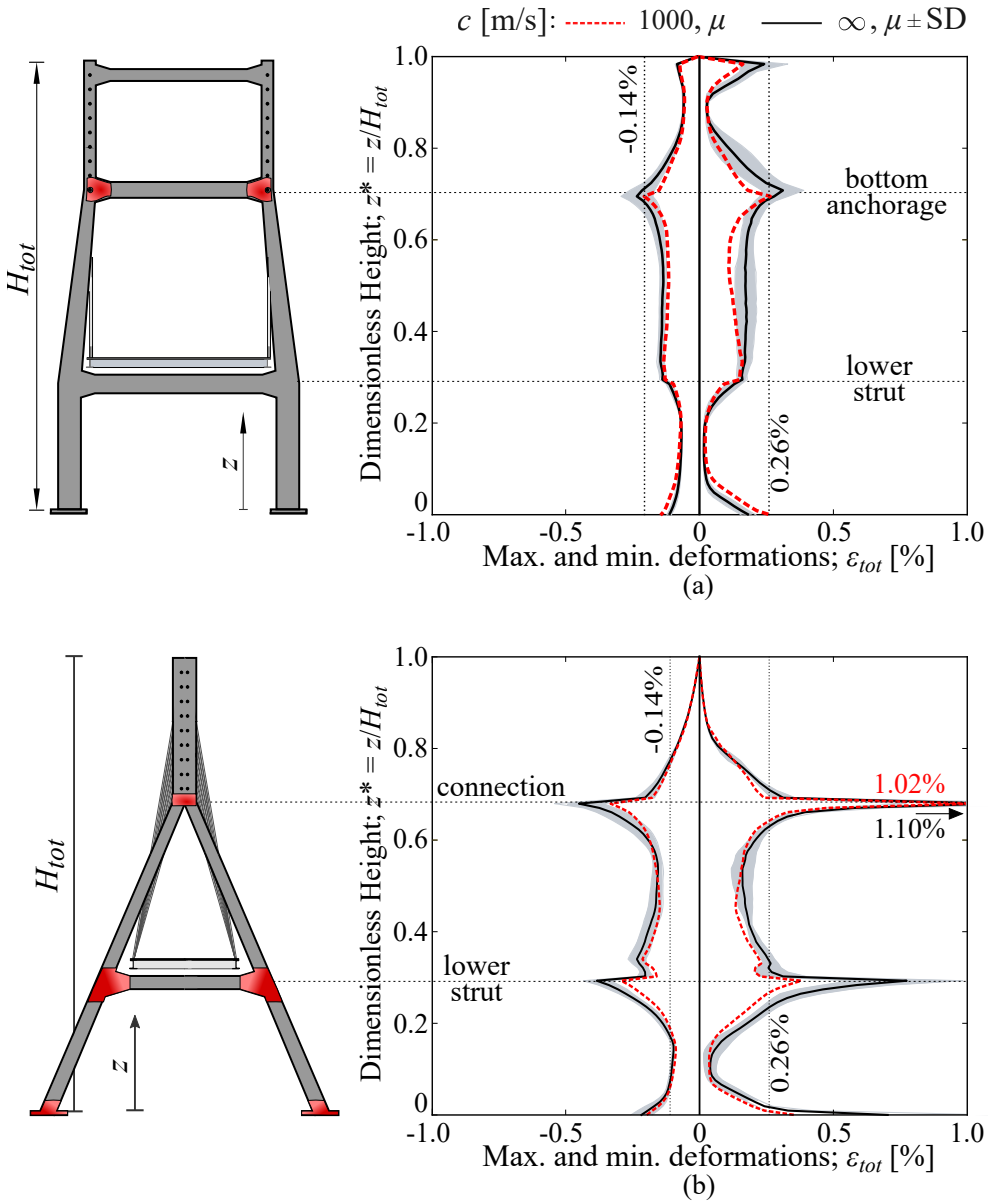

Figure 7.13: Peak inelastic deformations of the concrete and the steel reinforcement in pylon P2 in the (a) H-LCP and (b) Y-LCP models. $L_P = 400$ m, $\theta = 0°$.

This is achieved by means of a damage factor Ω (Camara *et al.* 2013, Camara and Astiz 2014), defined as the percentage of the total work dissipated in the structure through plasticity (E_{Sp}) over the total work (E_W) input to the structure by the seismic forces:

$$\Omega = \frac{E_{Sp}}{E_W} \cdot 100(\%) \tag{7.1}$$

E_W is the time-integral of the work introduced to the structure by the seismic forces and E_{Sp} is the time-integral of the energy dissipated by material plasticity in the part of the structure under consideration.

$$\Omega\left(t\right) = \frac{E_{Sp}\left(t\right)}{E_W\left(t\right)} \cdot 100 = \frac{\displaystyle\int_0^t \left(\int_V \boldsymbol{\sigma}^c : \dot{\boldsymbol{\varepsilon}}^{pl} \ \mathrm{d}V \right) \ \mathrm{d}\tau}{\displaystyle\int_0^t \left(\int_{V_{tot}} \left(-\mathbf{m}\boldsymbol{\iota}\ddot{\mathbf{u}}_g\right) \mathbf{v} \ \mathrm{d}V \right) \ \mathrm{d}\tau} \cdot 100 \tag{7.2}$$

In Eq. (7.2) $\displaystyle\int_V (\cdot)\,\mathrm{d}V$ is the integral over the volume V of the part of the structure under consideration. In this case the volume of the complete cable-stayed bridge is considered (i.e. V_{tot}), however the pylons are the only members of the structure that can present material nonlinear behaviour; $\boldsymbol{\sigma}^c$ is the stress derived from the constitutive equation, ignoring any viscous dissipation effects, $\dot{\boldsymbol{\varepsilon}}^{pl}$ is the plastic strain rate, $\mathbf{m}$ and $\boldsymbol{\iota}$ are the mass and influence matrices, respectively, $\ddot{\mathbf{u}}_g$ represents the vector of accelererograms applied to the structure (in this case $\ddot{u}_g^x$ and $\ddot{u}_g^y$, with x and y the directions parallel and perpendicular to the bridge, respectively), $\mathbf{v}$ is the velocity field vector, t is the time duration in which $\Omega\left(t\right)$ is calculated, τ is the time instance during the duration of the earthquake that E_{Sp} and E_W are evaluated, and ':' denotes the scalar product of matrices $\boldsymbol{\sigma}^c$ and $\dot{\boldsymbol{\varepsilon}}^{pl}$.

Fig. 7.14 shows the individual time-histories of the damage progression in pylons P1 and P2 of the H-LCP model with 400 m main span when $\theta = 0°$ for the SVGM and the SYNC motion. In each subplot the time instances that signify the damage initiation, t_d, are noted for the two pylons. The figure shows that when the SYNC motion is considered the majority of analyses result in identical damage between the two pylons. Exceptions are the difference in the damage between P1 and P2 from earthquakes #4 and #6 in Fig. 7.14, which is connected to the longitudinal oscillation of the deck coupled with its vertical flexure. This is more pronounced when the strong earthquake component is parallel to the bridge ($\theta = 0°$). The longitudinal oscillation triggered by the earthquake induces alternating tension in one pylon and compression in the other, resulting in a slightly different damage between P1 and P2 in some of the SYNC analysis cases. However this effect is considered negligible compared to the difference in the damage between the two pylons under the SVGM and hence the variation in the damage factor 'Ω' between the two pylons is examined only when the SVGM is considered.

When the multi-support excitation is included, one of the two pylons receives a greater amount of damage than the other at the end of the excitation and usually it is the second pylon in the direction of the excitation that is more damaged. This difference can be attributed to excitation of antisymmetric modes under the SVGM that are not contributing to the response when identical support motion is considered. This is the case of Mode #6 in the 200-m span bridge which involves the anti-symmetric transverse motion of the pylons and is not excited when the SYNC excitation is considered (Fig. 7.7).

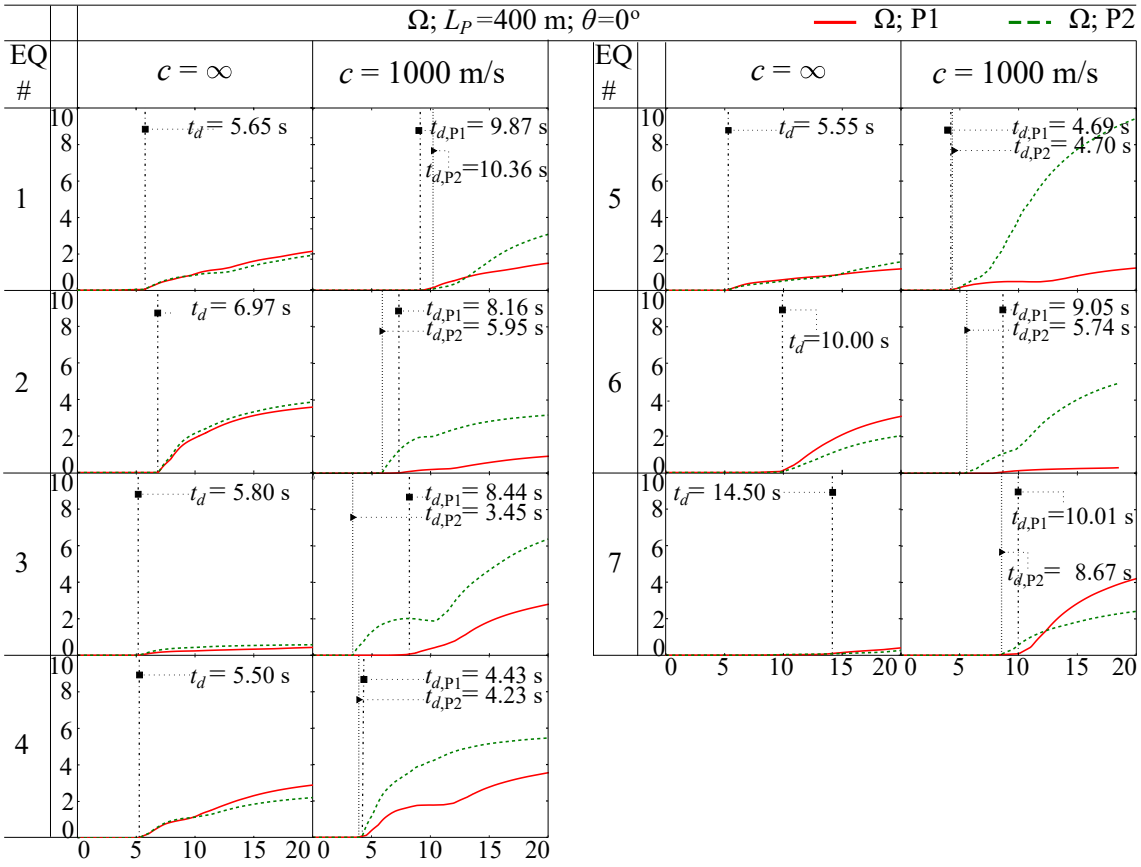

Figure 7.14: Time-histories of Ω (%) in pylons P1 and P2 of the H-LCP model with L_P = 400 m, when $\theta = 0°$ and $c = 1000$ and ∞ m/s; $t_{d,i}$ with i = P1, P2 is the time instance of damage initiation. The horizontal and vertical axes in each subplot denote the time in [s] and the damage factor Ω (%), respectively.

Compared to the SYNC motion, the SVGM in all cases increases the proportion of the seismic energy that is dissipated by plasticity in the pylons of the H-LCP model with $L_P = 400$ m, which indicates that the multi-support excitation is onerous for the seismic behaviour of the bridge and it should not be neglected.

The distribution of damage in the different components of the two pylons under the effect of SVGM also varies from pylon to pylon and from record to record. In Fig. 7.15 the time-history of the damage propagation is isolated for one of the earthquakes (#4), for the SVGM and for both orientations of the intermediate-span ($L_P = 400$ m) H-LCP bridge. The damage in the different components of the pylons is computed from Eq.

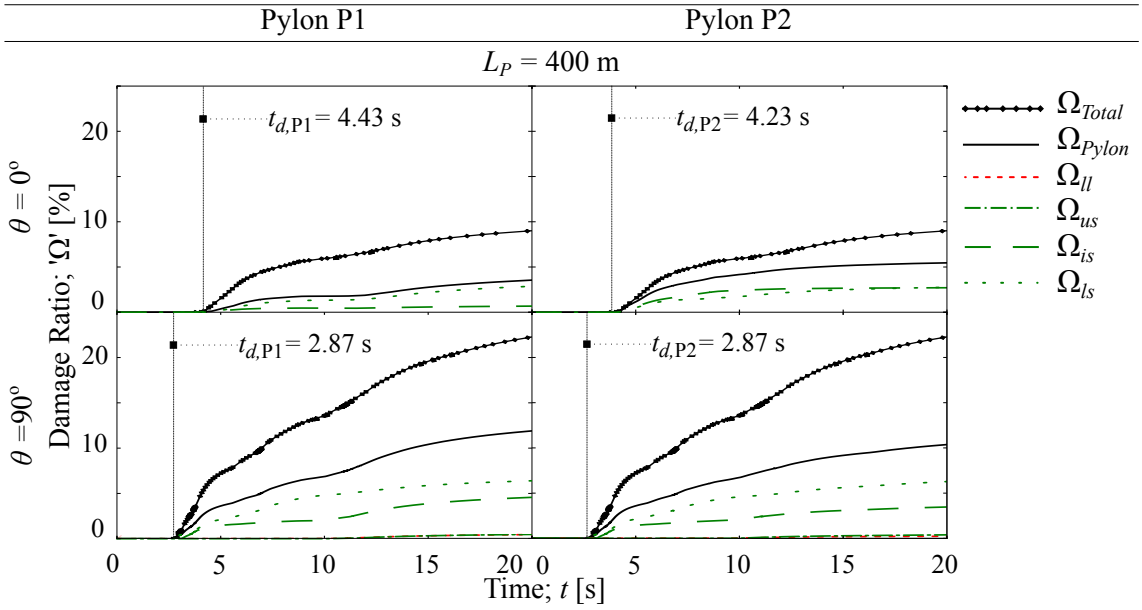

Figure 7.15: Time-histories of the damage factor Ω (%) in pylons P1 and P2 of the H-LCP bridge model with $L_P = 400$ m, when $\theta = 0°$ and 90° and $c = 1000$ m/s; the 'll', 'us', 'is' and 'ls' denote the lateral legs, upper, intermediate and lower strut of each pylon, respectively. Record #4.

(7.2) by assuming $E_{Sp,i}$ individually for each component i. In the left column the damage propagation with time is plotted for pylon P1 and in the right column for P2. The damage is significantly larger, by almost 4 and 2 times in P1 and P2, respectively, and it propagates earlier when $\theta = 90°$ in both pylons compared to $\theta = 0°$. This confirms that the bridge is more vulnerable in the transverse direction from the point of view of the induced damage in the structure. Between the two pylons, P2 receives larger damage than P1 (by 57%) when $\theta = 0°$ and similar amount of damage when $\theta = 90°$. The cable system contributes to the second pylon being more critical when the strong earthquake component is aligned with the bridge.

The components of the pylons that are most vulnerable to receive damage are the lower struts, noted as 'ls' in Fig. 7.15, due to the asynchronous transverse reaction of the deck to the pylons and because of their increased dimensions compared to the intermediate and upper struts (Chapter 3) making the former stiffer and more prone to damage.

So far, the time-histories of the damage propagation have been examined through the damage factor $\Omega(t)$. At this point the time dependent factor $\Omega(t)$ is reduced to Ω, which has been calculated at the end of the earthquake by considering $t = t_{\text{EQ}}$ in Eq. (7.2), t_{EQ} being the total duration of the earthquake. In Figs. 7.16 and 7.17 the maximum Ω ratios at the end of the earthquake, averaged from the total number of earthquakes applied to the structures, are presented for the different components that form the two pylons, for the SVGM and the SYNC motion in the 200-, 400- and 600-m span bridges in the former case and for the 400-m bridge when the strong earthquake component is

assumed parallel ($\theta = 0°$) and perpendicular ($\theta = 90°$) to the bridge in the latter case. The numerical results are also included in Table 7.1, where the standard deviation (SD) from the mean (μ) peak response from the SYNC motion is also included in brackets. The difference in the damage between the two pylons of the H-LCP model that is reflected in Fig. 7.16 for the SVGM which, also shown in the time-histories of Ω (Figs.7.14 and 7.15), can be attributed to the differential movement of the pylons. The slight difference in the maximum damage between P1 and P2 when the SYNC motion is considered, is due to the effect of the cable system in the longitudinal oscillation of the bridge, which was also noticed in Fig. 7.14. When $\theta = 0°$ the most critical members of the bridges are the lower struts in the 200- and 400-m span bridges in which the larger difference between Ω from the SVGM and the SYNC motion are obtained.

The second pylon in the propagation of the earthquake is more damaged in the short- and intermediate-span bridges by 1.9 and 2.4 times, respectively compared to the first pylon. This results from the asynchronous deck reaction to the pylons, especially in the 200-m span bridge in which the increase in the damage is concentrated to the lower struts and the lateral legs. In the 400-m bridge, pylon P2 is affected significantly by the SVGM at the intermediate and lower strut connections with the legs and it sustains larger damage than the one from the SYNC motion of the supports.

However, the damage distribution is modified significantly when the bridge is rotated to $\theta = 90°$, in which case the intermediate and the upper struts become the most vulnerable members due to the transverse flexure of the pylons above the deck. Finally, the large dispersion from the mean damage factor in the 'H'-shaped pylons and their individual components that is included in Table 7.1 highlights the strong record-to-record variability. This is also illustrated in the damage propagation with time included in Fig. 7.14.

7.7 Probability of Failure in the Bridge

So far the different effect of the SVGM on the seismic response of the bridges and on the damage propagation in the pylons has been examined for a certain earthquake intensity and compared to the respective values from the SYNC motion in order to identify whether the SVGM is important for the design of cable-stayed bridges. In this section the cable-stayed bridge with $L_P = 400$ m and 'H'-shaped pylons is subjected to higher intensity earthquakes by means of the Incremental Dynamic Analysis (IDA) in order to identify the vulnerability of the structure to more severe ground motions (Vamvatsikos and Cornell 2002).

When subjected to ground motions, the different components that constitute a cable-

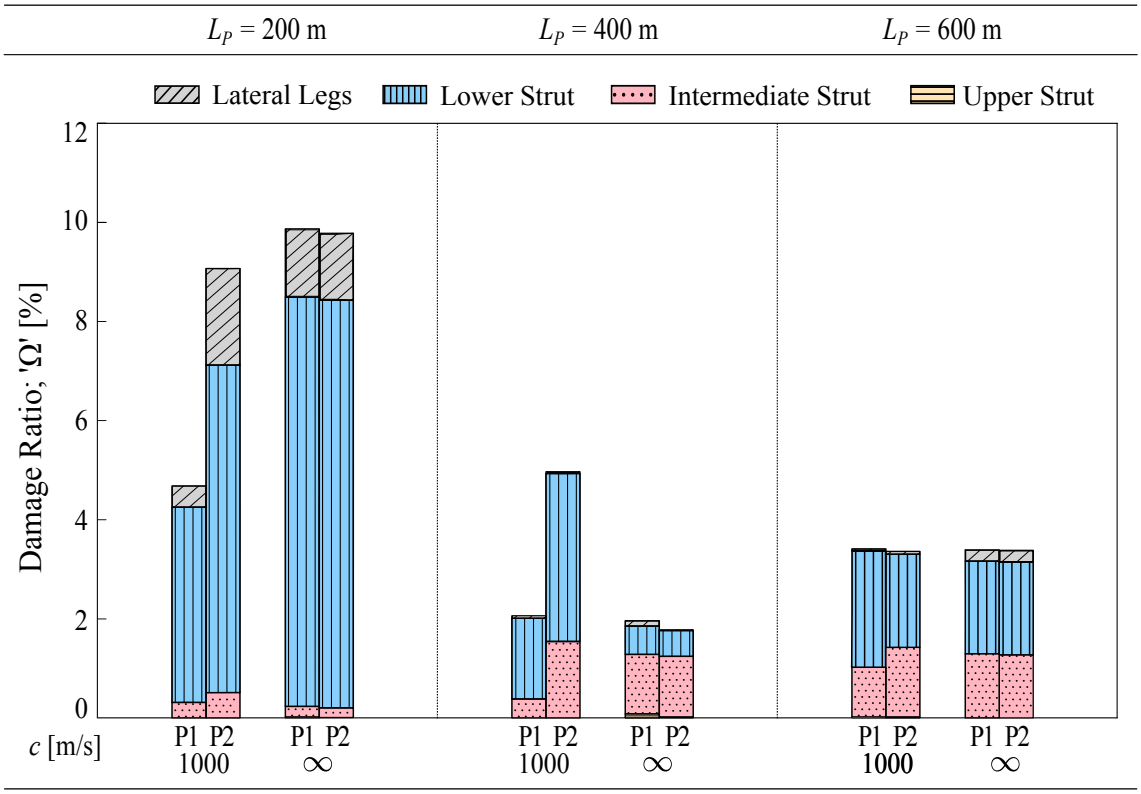

Figure 7.16: Average values for the damage factor Ω (%) at the end of the records in the individual components of pylons P1 and P2 when $c = 1000$ and ∞ m/s. H-LCP model; $L_P = 200$, 400 and 600 m, respectively. $\theta = 0°$.

	$L_P = 200$ m		$L_P = 400$ m		$L_P = 600$ m	
	1000	∞	1000	∞	1000	∞
	[c in m/s]		[c in m/s]		[c in m/s]	
$\Omega_{ll,\text{P1}}$	0.43	1.38(± 0.95)	0.05	0.11(± 0.15)	0.04	0.23(± 0.29)
$\Omega_{ll,\text{P2}}$	1.94	1.35(± 0.94)	**0.04**	0.02(± 0.02)	0.06	0.24(± 0.31)
$\Omega_{ls,\text{P1}}$	**3.94**	0.83(± 2.0)	**1.63**	0.57(± 0.47)	2.35	1.87(± 0.85)
$\Omega_{ls,\text{P2}}$	**6.61**	0.82(± 0.21)	**3.39**	0.52(± 0.43)	1.88	1.87(± 0.83)
$\Omega_{is,\text{P1}}$	0.31	0.21(± 0.31)	0.38	1.20(± 0.80)	1.00	1.29(± 1.06)
$\Omega_{is,\text{P2}}$	**0.51**	0.17(± 0.21)	1.54	1.22(± 0.80)	1.40	1.27(± 1.10)
$\Omega_{us,\text{P1}}$	0	0	0	0.08	**0.02**	0
$\Omega_{us,\text{P2}}$	0	0	0	0.02	**0.02**	0

Table 7.1: Damage factors Ω (%) at the end of the seismic records for the different components of pylons P1 and P2 in the H-LCP bridges with $L_P = 200$, 400 and 600 m for the SVGM and the SYNC motion when $\theta = 0°$. The mean value, μ, is presented in the table followed by the standard deviation, SD, in brackets. 'll', 'ls', 'is' and 'us' denote the lateral legs, lower, intermediate and upper struts of each pylon, respectively. The **bold** font denotes damage from the SVGM for which $\Omega \geq \mu$+SD from the SYNC motion.

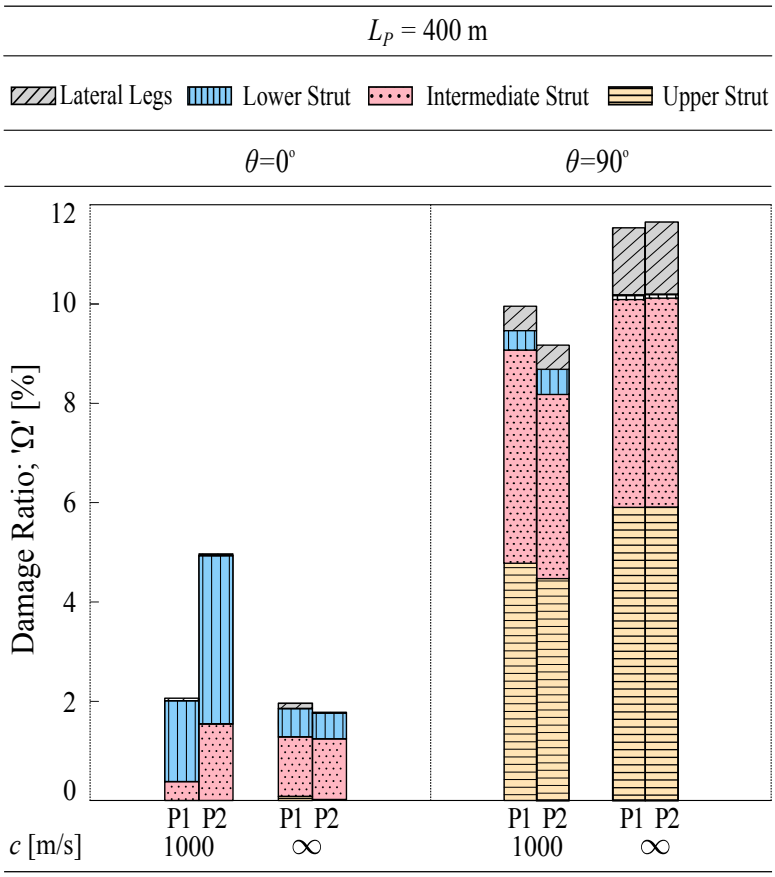

Figure 7.17: Average values for the damage factor Ω (%) at the end of the records in the individual components of pylons P1 and P2 when $c = 1000$ and ∞ m/s and $\theta = 0°$ and $\theta = 90°$. H-LCP model; $L_P = 400$ m.

stayed bridge may receive different amounts of damage, as it has been discussed in Section 7.6. In order to predict the sensitivity of those components to the SVGM and the SYNC motion several demand parameters (S_d) have been identified and monitored under a defined intensity measure (IM). In this study the widely used peak ground acceleration (PGA) has been chosen as the IM to assess the vulnerability of the bridge to lower probability ground motions (Padgett and DesRoches 2008, Ramanathan 2012, Stefanidou and Kappos 2017) with earthquakes that are scaled[1] in the range of 0.05g - 1.5g. The scaling of the accelerograms does not affect their frequency content or the components that define the SVGM in Section 4.5.

For the demand parameters, during the dynamic analyses of the 400-m H-LCP model different response quantities have been monitored at various regions of the bridge resulting in demand-IM pairs which are used to estimate the probability of failure at different components of the bridge. In this thesis the longitudinal and transverse curvature ductilities of the pylons (μ_ϕ), pylon drift ratios (r) and cable forces (f) have been obtained for the various earthquake intensities. The time-histories of the longitudinal and transverse curvature ductilities have been monitored at the base of the pylons and at the connection between the intermediate struts and the legs for the SVGM and the SYNC motion, with the peak value being considered. The drift ratio has been computed in the transverse direction as the ratio of the maximum seismic transverse displacement at the top of the pylon normalised by its total height as; $r = u_{y,\max}/H_{tot}$. The cable forces have been obtained in critical cables including the ones that connect the pylon to the deck at the abutments and the vertical piers in the side spans, the longest cables that connect the top of the pylons to the middle of the main span and the cables that are adjacent to the pylons. The maximum responses that have been obtained from the analyses are compared with predefined capacity parameters (S_c) and eventually, the probability of failure is computed. The probability of failure is defined as the probability that the demand on the structure exceeds the structural capacity and it can be obtained as:

$$p_f = P\left[\frac{S_d}{S_c} \geq 1\right] \tag{7.3}$$

where S_d and S_c are demand and capacity parameters, respectively. The probability of failure is estimated as the ratio of the number of accelerograms for which the S_d exceeds a certain S_c divided by the total number of accelerograms. The capacity parameters can be obtained based on engineering judgement, experimental data or from numerical results (Li *et al.* 2018). In this thesis, those parameters are determined from capacity based limit state (LS) models, that follow the description of the damage states included in HAZUS (1997), as shown in Table 7.2. For the slight, moderate and extensive damage and for the collapse LS that have been adopted herein, the limiting values of the different demand

[1]The design earthquake intensity has been taken as 0.5g in this thesis.

Damage states	Description
No damage (N)	No damage to a bridge
Slight/minor damage (S)	Minor cracking and spalling to the abutment, cracks in shear keys at abutments, minor spalling and cracks at hinges, minor spalling at the column (damage requires no more than cosmetic repair) or minor cracking to the deck
Moderate damage (M)	Any column experiencing moderate cracking and spalling (column structurally still sound), any connection having cracked shear keys or bent bolts, or moderate settlement of the approach
Extensive damage (E)	Any column degrading without collapse (column structurally unsafe), any connection losing some bearing support, or major settlement of the approach
Complete damage (C)	Any column collapsing and connection losing all bearing support, which may lead to imminent deck collapse

Table 7.2: Description of bridge damage states (*taken from HAZUS (1997)*).

Damage Parameter	Slight	Moderate	Extensive	Collapse
μ_ϕ pylon's base	≥ 1	≥ 2	≥ 4	≥ 7
r pylon's top	≥ 0.007	≥ 0.015	≥ 0.025	≥ 0.05
f cables	$\geq 0.4 f_u$	$\geq 0.6 f_u$	$\geq 0.85 f_u$	$\geq f_u$

Table 7.3: Limit states of the different components of the cable-stayed bridge. f_u is the ultimate strength of the cables.

parameters are adopted from previous studies (Choi *et al.* 2004, Yi *et al.* 2007, Li *et al.* 2018) and are included Table 7.3.

Fig. 7.18 presents the results of the IDA in terms of the transverse curvature ductility at the base of the pylons when the SVGM and the SYNC motion are considered. It can be seen that the pylons receive great amounts of damage that reach the level of collapse in the case of P2 when PGA = $1.5g$. When the bridge is subjected to multi-support excitations the two pylons receive different levels of damage; the second pylon in the direction of the earthquake's propagation (P2) reaches the level of slight structural damage when the design earthquake is considered (PGA = $0.5g$), however the pylon P1 reaches the same LS at PGA = $0.75g$. At higher LS the difference between the ground motion intensities for which the pylons receive the respective amounts of damage increases. Specifically, P2 reaches the level of extensive damage at PGA $\approx 0.8g$, whereas pylon P1 receives the same amount of damage when PGA $\approx 1.3g$. Furthermore, at the same earthquake intensity ($1.3g$) pylon P2 is expected to reach the collapse limit state. This finding highlights the fact that the SVGM is more detrimental for the second pylon than it is for P1.

When the SYNC motion of the support is considered the damage in the pylons generally falls within the range defined by the damage in P1 and P2 from the SVGM . Up to the level of PGA $\approx 0.75g$ and the state of slight damage, the same damage propagation is observed between P1 when the SVGM is considered and the pylons under the SYNC motion. The out-of-phase transverse reaction of the deck to the pylons combined with the pronounced oscillation of the pylons above the deck, which is received by the transverse struts, are responsible for the difference in the damage evolution between the two pylons under the SVGM.

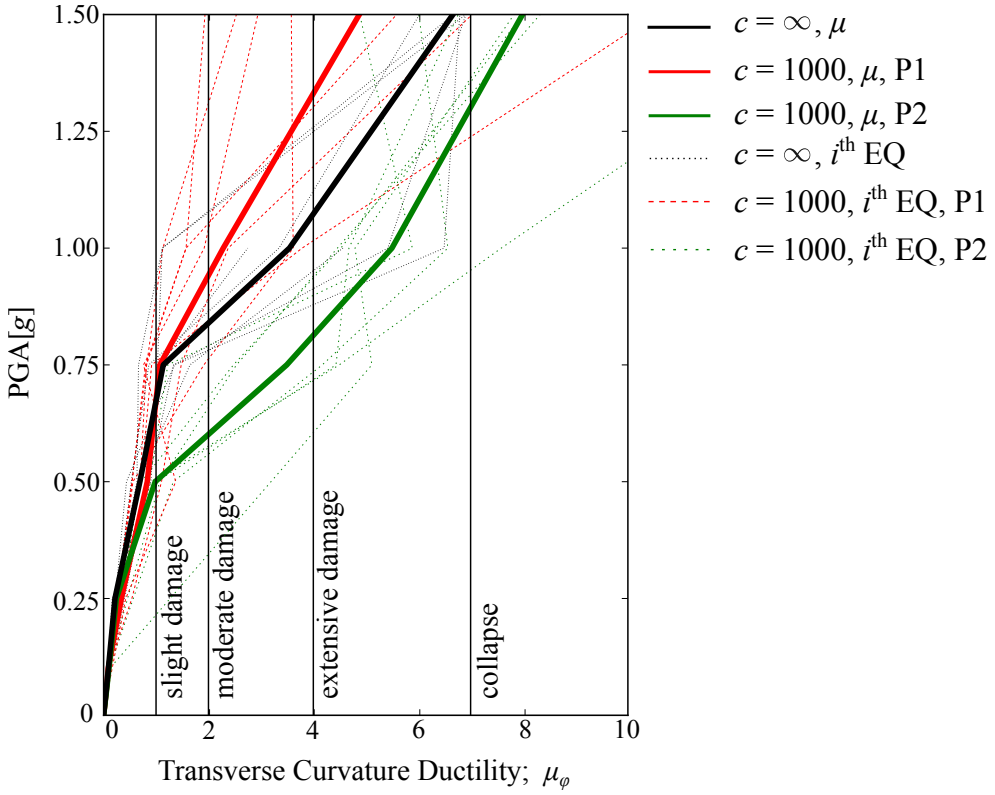

Figure 7.18: Evolution of damage in terms of the transverse curvature ductility, μ_ϕ, at the base of the pylons versus earthquake intensities. c in [m/s], $\theta = 0°$, H-LCP model, $L_P =$ 400 m.

Figs. 7.19 and 7.20 show the probability of damage for the different limit states with increasing earthquake intensities at the base of the pylons of the 400-m bridge in terms of the curvature ductilities, μ_ϕ, in the transverse and longitudinal directions of the bridge. The figures compare the failure probabilities for the two pylons of the cable-stayed bridge when the SVGM is considered and for one of the pylons when the SYNC motion is considered. The probability of failure is increased, as expected, with increasing earthquake intensities. The pylons present a 30-40% probability to receive slight damage for the design earthquake when the SVGM is considered, and 15% to receive the same level of damage under the SYNC motion for the same earthquake intensity.

In all cases the second pylon in the direction of the earthquake propagation (P2) has a larger probability of failure than P1 and than the two pylons when the SYNC motion is

considered. The difference in the probabilities of failure between P2 when the SVGM is considered and the SYNC motion increases with increasing PGA. Both pylons present 15% and 25% probabilities of collapse, respectively under the highest magnitude earthquake (PGA = $1.5g$), as opposed to the SYNC motion case wherein the pylon is not prone to collapse (i.e. $p_f = 0$).

On the other hand, the probability of failure at the base is significantly reduced in the longitudinal direction of the pylon as shown in Fig. 7.20 in which, under the strongest earthquakes (PGA = $1.5g$), only pylon P2 presents 50% and 20% probabilities of receiving slight and moderate damage, respectively. This observation highlights the fact that the pylons are more vulnerable in the transverse direction for all damage states than in the longitudinal direction, which is in agreement with previous findings on cable-stayed bridges subjected to multi-support excitations (Zhong *et al.* 2017).

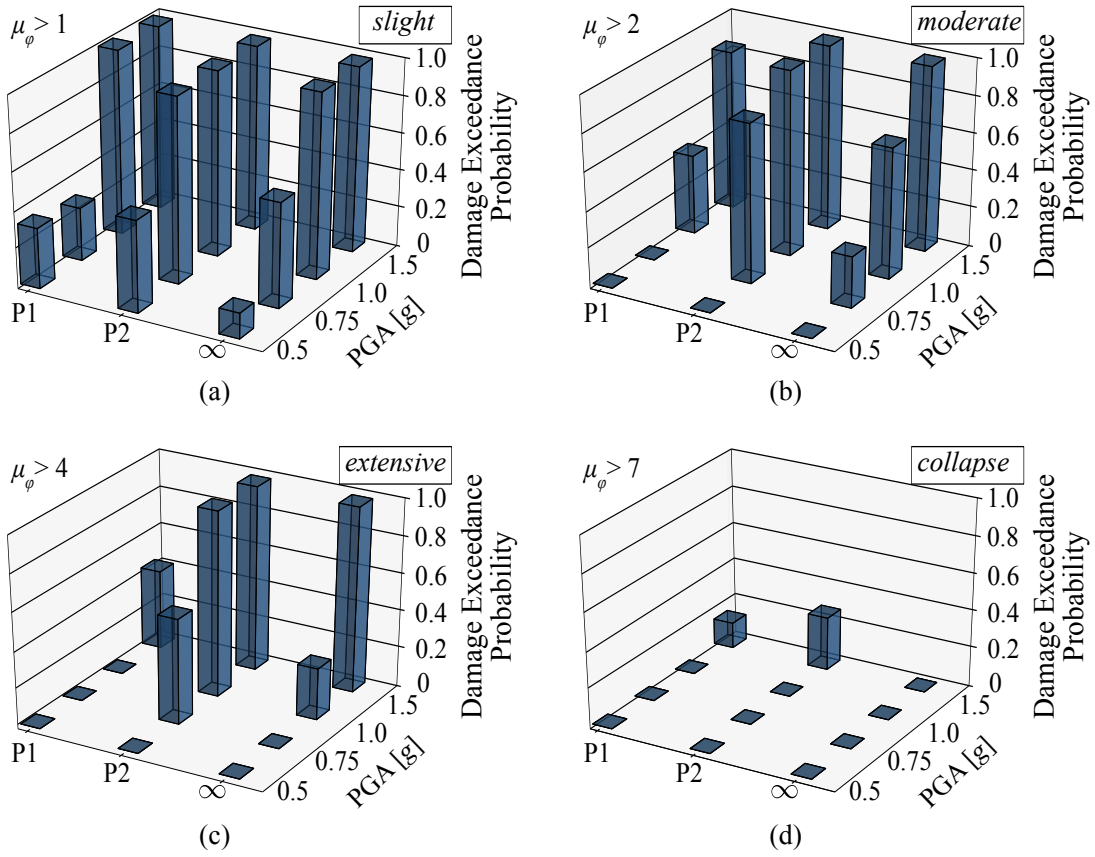

Figure 7.19: Probability of exceedance of the damage limit states at the base of the pylon in terms of the transverse curvature ductility. P1 and P2 denote the first and second pylons in the direction of the earthquake, respectively and ∞ denotes the case of the SYNC motion of the supports.

The probability of failure is also examined at the level of the connection between the individual legs and the intermediate transverse strut which, has proven a vulnerable region in the pylons in Sections 7.5 and 7.6. Fig. 7.21 verifies that this connection is more critical than the base of the pylons (Fig. 7.19). The strut-leg connection is prone to reach the collapse LS when subjected to the highest intensity earthquakes (PGA = $1.5g$), with

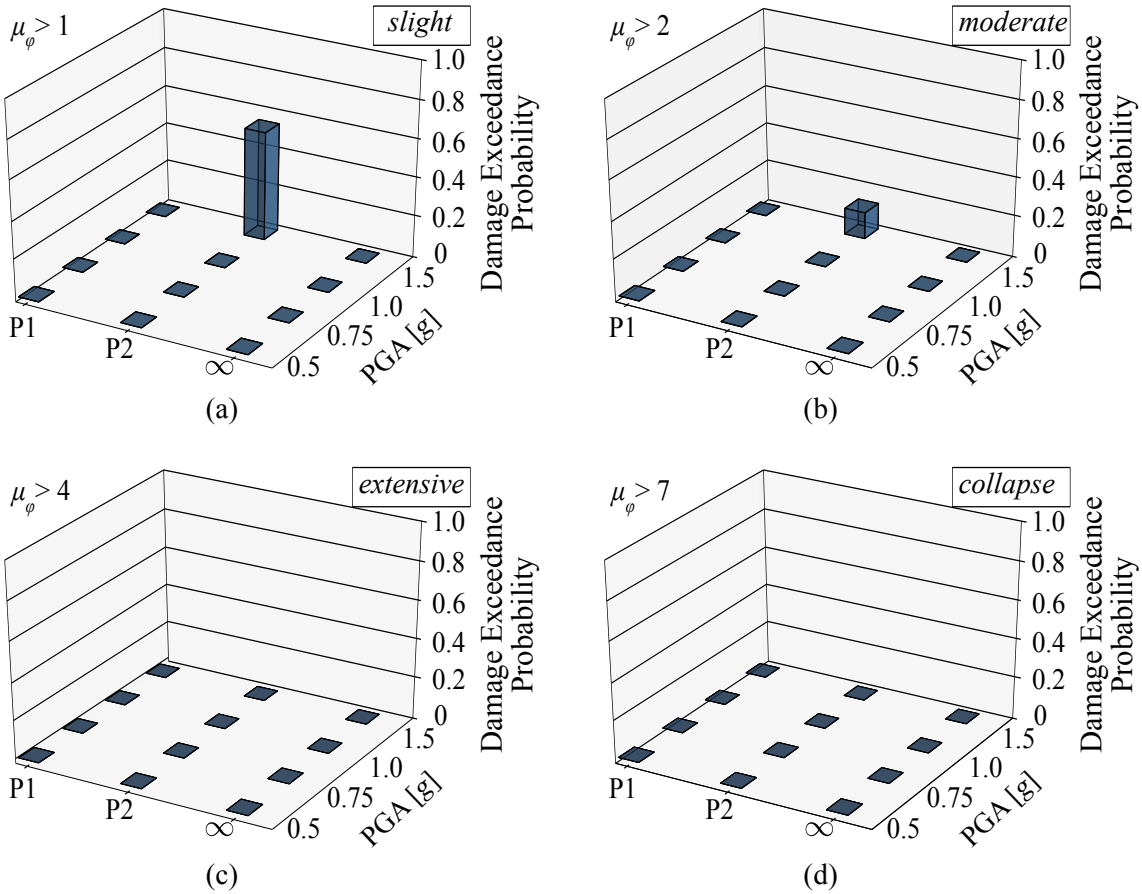

Figure 7.20: Probability of exceedance of the damage limit states at the base of the pylon in terms of the longitudinal curvature ductility. P1 and P2 denote the first and second pylons in the direction of the earthquake, respectively and ∞ denotes the case of the SYNC motion of the supports.

a probability of almost 60% when the SYNC motion is considered, contrary to the 40% failure probability under the effect of the SVGM. At this part of the pylon the effect of the SVGM varies with increasing earthquake intensities. For instance, P2 has a higher probability to receive extensive damage than P1 and the pylons under the SYNC motion when PGA = $1.0g$, but the SYNC motion exceeds the probability of failure of pylons P1 and P2 when PGA = $1.5g$. This can be explained by the increase in the induced damage in the pylons at earlier parts of the response time-histories with increasing earthquake intensities, combined with the period elongation of important vibration modes for the response that can be excited at one intensity level but suppressed at a different one (Vamvatsikos and Cornell 2002). In general, however, the probability of failure is higher when the SVGM is considered.

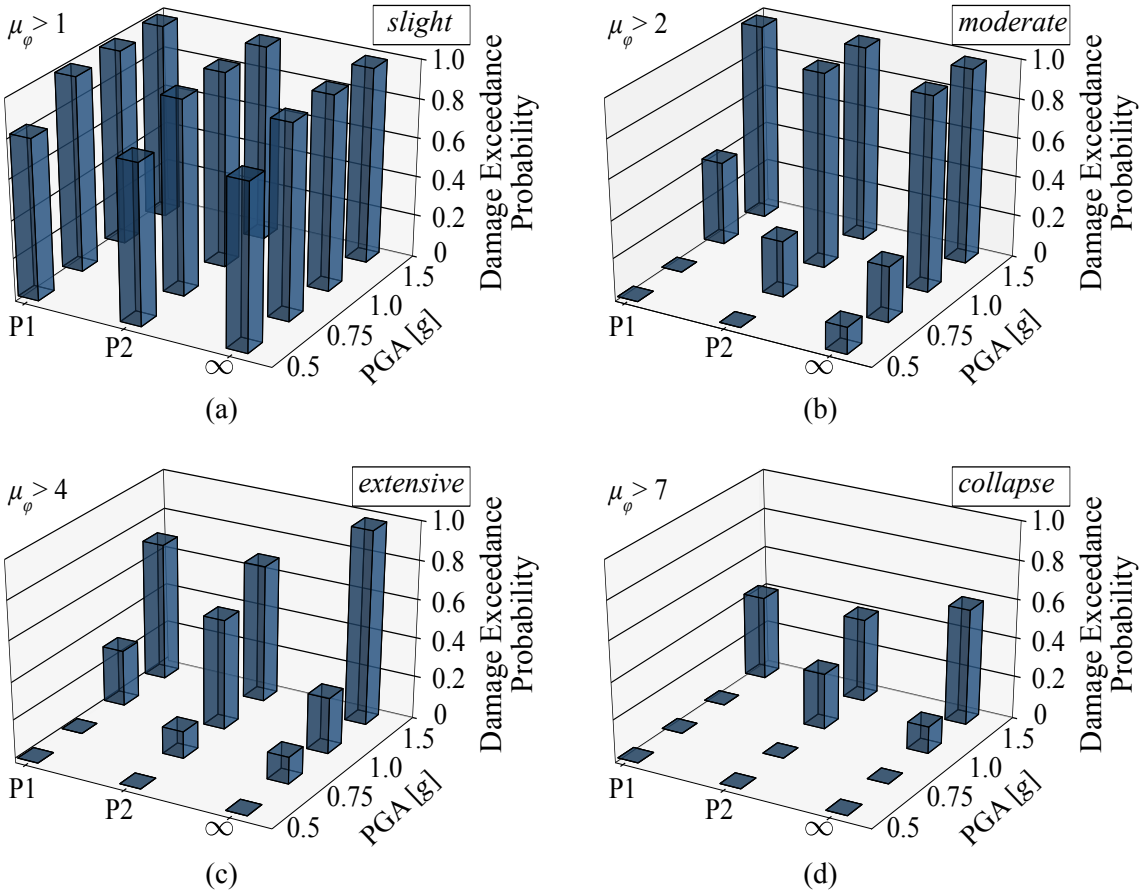

Figure 7.21: Probability of exceedance of the damage limit states at the level of the connection between the legs and the intermediate transverse struts in the pylon in terms of the transverse curvature ductility. P1 and P2 denote the first and second pylons in the direction of the earthquake, respectively and ∞ denotes the case of the SYNC motion of the supports.

The probability of failure has been examined in the transverse direction of pylon P2 in terms of the drift ratio r for the SVGM and the SYNC motion, as shown in Fig. 7.22. The SVGM consistently results in higher probabilities that the transverse displacement of the bridge will cause slight or moderate damage in the pylon than the SYNC motion, and the difference between the two probabilities is increased with increasing intensities.

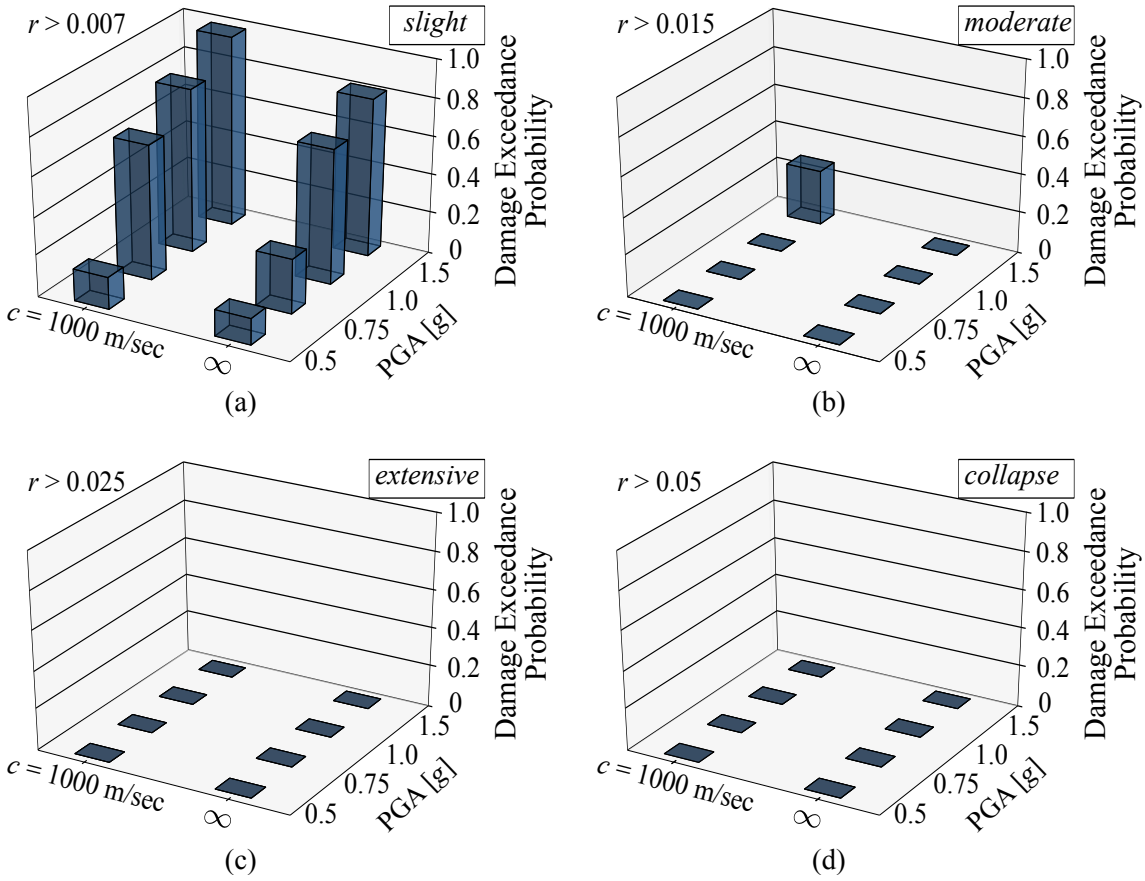

Figure 7.22: Probability of exceedance of the damage limit states in terms of the transverse drift ratio of pylon P2 when $c = 1000$ m/s and ∞.

Finally, the probability of failure has been computed in the most critical cables of the bridge corresponding to the adjacent cables to the pylon. Fig. 7.23 shows that these cables are prone to receive moderate damage, even at the level of the design earthquake, under the SVGM which exceeds the respective probability of failure when the SYNC motion is considered. The SYNC motion only increases the probability of slight damage in the cables at the lower earthquake intensities compared to the SYNC motion, but as the PGA increases the latter becomes more onerous, suggesting that the SVGM is detrimental for these bridge components.

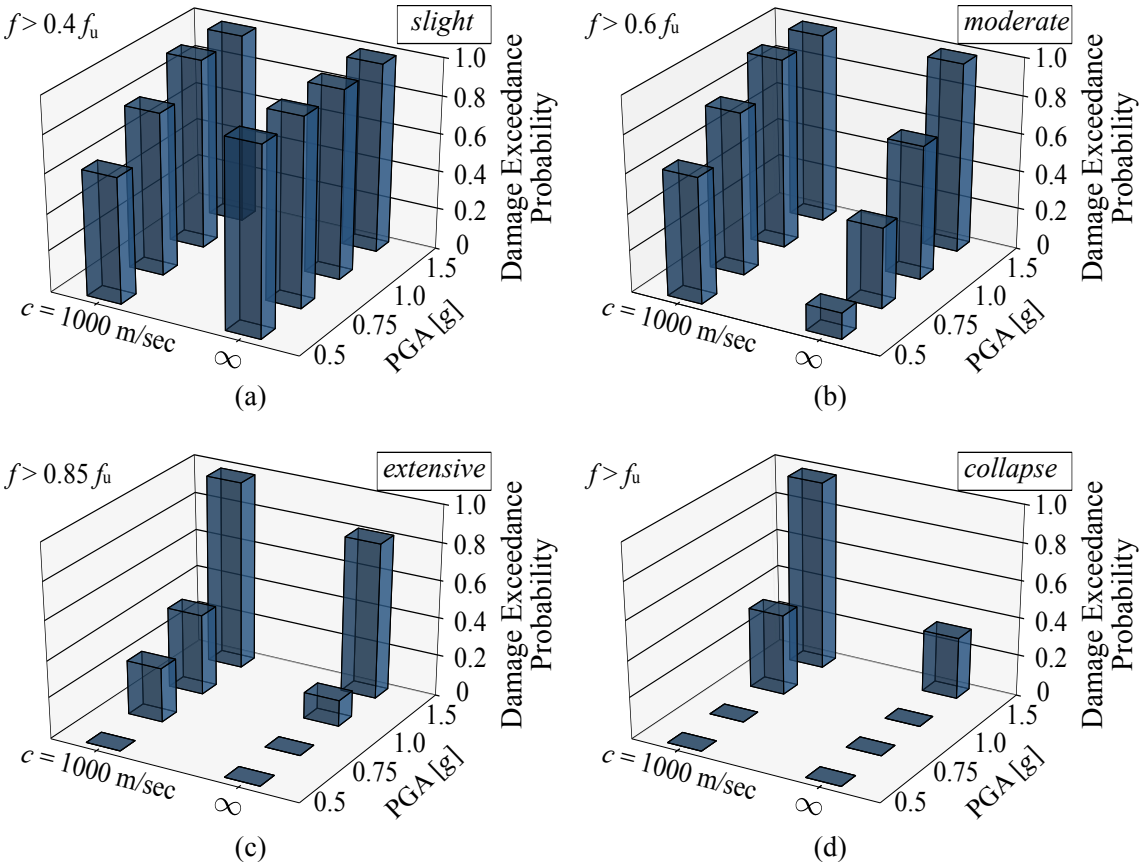

Figure 7.23: Probability of exceedance of the damage limit states in the cables.

The findings of this section suggest that, among the examined demand parameters, the most critical components of the bridge are the connection of the intermediate strut to the legs in the pylons and the cables that are adjacent to the pylons. Those have the highest probabilities of failure even at the level of the design earthquake and may reach the collapse LS at the higher intensities (i.e. PGA = $1.0g$ and $1.5g$). The SVGM generally results in higher probabilities of failure in the LS examined herein. The second pylon in the propagation of the earthquake consistently receives more damage than the first one and generally more damage than it does when SYNC motion of the supports is considered. The results indicate that the multi-support excitation should not be ignored.

7.8 Conclusions

The purpose of this chapter has been to examine the inelastic seismic response of cable-stayed bridges with 'H'- and inverted 'Y'-shaped pylons and main span lengths of 200, 400 and 600 m. The seismic response of these bridges has been discussed herein in terms of seismic forces (N, V_x and V_x), deformation demands of the structural materials (ε_{tot}), the magnitude of the SVGM (ρ) and the damage propagation ($\Omega\,(t)$). The chapter is concluded by subjecting the cable-stayed bridge with 'H'-shaped pylons to higher intensity earthquakes in order to predict its structural response and the probability of failure of important components of the bridge. The main conclusions drawn from the nonlinear dynamic analysis of the bridges are the following:

1. The shortest bridge ($L_P = 200$ m) is more sensitive to the effect of the SVGM than the intermediate- and long-span bridges with $L_P = 400$ and 600 m, respectively. It is observed that when the nonlinear behaviour of the concrete and the steel in the pylons is considered the effect of the SVGM alone is more pronounced in the short-span bridge and this is reflected in the forces, inelastic deformations and the damage propagation in the pylons. In the 400- and 600-m main span bridges the SVGM generally results in response quantity values that match closely the ones from the SYNC motion. The damage propagation in the pylons also suggests that the most sensitive are the ones of the 200-m main span bridge, because of their increased stiffness compared to the taller pylons of the 400-m and 600-m span bridges, which is more important than the time delay of the earthquake or the loss of coherency. Furthermore, the pylons of the intermediate-span bridge ($L_P = 400$ m) generally behave differently than their shorter and taller counterparts. This bridge falls between the stiff configuration of the 200-m span bridge and the flexible configuration of the 600-m span bridge in which the effect of the components of the SVGM (wave passage and incoherence) are more significant because they are both functions of the separation distance between supports. These findings emphasise the need for code-based provisions in which the importance of the SVGM for the design and assessment of bridges is established not only in terms of the total length but also in terms of the vibration properties of the structure.

2. Generally, the most critical regions of the pylons are the connections between the legs and the transverse struts. This is explained by the lateral flexure of the pylons which is resisted by the struts. The rate of damage that is induced to the different components of the bridge depends on the height of the pylon; the lateral legs and the lower struts are more damaged in the short-span bridge, whereas the intermediate struts tend to receive more damage with increasing heights because of the more pronounced transverse oscillation of the part of the pylons above the deck as the height increases. This is due to the increasing flexibility in the pylons with

increasing heights.

3. The effect of the earthquake's incidence angle with respect to the bridge (θ) on the seismic response is closely linked to the response quantity under consideration. The peak longitudinal shear force, V_x, along the pylons is larger when the strong component of the earthquake is applied parallel to the axis of the bridge (i.e. when $\theta = 0^\circ$), as in the elastic case. Accordingly, the peak V_y is maximised when $\theta = 90^\circ$ and the strong earthquake component is perpendicular to the bridge axis. The effect of the SVGM is also modified with the value of θ and it results in increased structural response values when $\theta = 90^\circ$. (i.e. the strong earthquake component is parallel to the axis of the struts), in which case the peak deformation of the steel is increased in the 400-m main span bridge. This is attributed to the more pronounced transverse oscillation of the pylon when $\theta = 90^\circ$ compared to the case when the strong earthquake component is aligned with the deck ($\theta = 0^\circ$). In terms of the maximum damage in the pylons, the maximum values of the damage factor Ω are obtained when the strong earthquake component is considered perpendicular to the bridge axis ($\theta = 90^\circ$) regardless of the main span length or of the SVGM being considered.

4. In most cases the effect of the SVGM is the same between the elastic and the inelastic analyses. In other words, when the seismic response due to the SVGM is greater than that from the SYNC motion in the elastic range (in which case the response ratio $\rho_{\text{EL}} > 1$), the same observation is made in the inelastic range ($\rho_{\text{NL}} > 1$). The maximum differences between the results from the two types of analysis are obtained in the transverse direction of the response, for which symmetric and antisymmetric vibration modes contribute more to the SVGM.

5. The shape of the pylon influences the sensitivity to the asynchronous motion when material nonlinearities are considered. It is observed that the stiffer configuration of the inverted 'Y'-shaped pylon is more vulnerable to the SVGM, as opposed to the more flexible 'H'-shaped pylon. Moreover, the effect of the SVGM is more detrimental in the transverse direction of the response because the pylons are stiffer in this direction. At the other end, the multi-support excitation reduces the seismic response in the longitudinal direction regardless of the main span length or the shape of the pylon.

6. When the bridge is subjected to higher intensity earthquakes (up to $1.5g$) certain components are expected to receive large amounts of damage and, in the case of the pylon and certain cables, they are expected to reach the ultimate limit state of collapse. The SVGM has a detrimental effect to the seismic behaviour of the bridge by increasing the probability of the failure in the pylons and the cables compared to the SYNC motion. Between the two pylons of the bridge, the second one to

receive the ground motion is more affected by the multi-support excitation. This is reflected in the probability of failure that is consistently higher than the one of the first pylon, and in the damage propagation in this pylon even at the level of the design earthquake.

Chapter 8

Conclusions & Future Work

Contents

The purpose of this thesis has been to examine the effect of the Spatial Variability of the Ground Motion (SVGM) on the seismic response of cable-stayed bridges with variable span lengths and different pylon-cable system configurations in order to obtain general conclusions and make practical observations. This research work is differentiated from previous works on this topic because the focus is mainly placed on the seismic response of the pylons, which constitute significant components of the structure that are responsible for the overall integrity of a cable-stayed bridge and because it combines the effects of the SVGM and of the seismic incidence angle. Furthermore, the vulnerability of the complete bridge to the SVGM is predicted by estimating the failure probability of various significant components of the bridge.

The thesis presents a comprehensive study on the effect of the SVGM on the seismic response of cable-stayed bridges by examining design decisions that define the overall configuration of such structures. The rigorous and extensive analysis that has been presented herein allows for design recommendations to be made in the context of examining when the SVGM is detrimental for the bridge. To this end, the cable-stayed bridge models have been analysed in the time and frequency domains and they have also been subjected to higher intensity earthquakes than the design level ground motion ($0.5g$).

In terms of the SVGM the phenomenon has been defined by means of the time delay of the arrival of the earthquakes at different supports and by means of the loss of coherency between signals at different supports. The former is accounted for by assuming a finite value for the velocity of the wave propagation; $c = 1000$ m/s, and the latter is considered by means of the empirical model proposed by Harichandran and Vanmarcke (1986). This coherency model assumes partially correlated motions at the low frequency range (<1 Hz) which is important for the seismic response of cable-stayed bridges.

The final parameter that has been examined in this research is the effect of the angle of incidence, θ, of the seismic waves by considering different angles in the range [0°-180°] at increments of 30°. The combined effect of the seismic incidence angle with the SVGM has gained some attention by the research community but, to the author's best knowledge, there is general lack of work on this topic.

Finally, the SSI has been implemented in the pylons by means of simplified spring-dashpot systems following the formulas and charts proposed by Gazetas (1991). The dynamic impedances have been computed for the movement in the three principal directions of the bridge (x-traffic, y and z) and for the rotation around the x and y axes.

8.1 Conclusions

On the State of the Art

1. The SVGM reportedly modifies the response of long structures and it cannot be neglected, because doing so might underestimate the structural response. However, its complex nature and unpredictable effect on the structural response only has allowed to identify various trends without being able to establish a general and robust framework to deal with this phenomenon. This uncertainty justifies to a certain extent the observed discrepancy among different approaches and the obtained results (Shinozuka *et al.* 2000).

2. The effect of the SVGM depends on the span length, the soil conditions at the supports and at the surrounding soils, the rigidity of the structure and the degree of redundancy (Nazmy and Abdel-Ghaffar 1992). This has also been observed in the present study.

On the Elastic Seismic Response

1. The foundation soil affects the seismic response of the pylons. Generally, uniform sites at the supports of the bridge, corresponding to ground types A and D (Eurocode 8; Part 1 2004), are associated with the lowest and the highest seismic responses in the pylon, respectively. The increments in the response are due to the higher spectral acceleration that is associated with dominant vibration modes of the structures when ground type D is considered compared to the respective accelerations of the ground type A spectrum. On the other hand, when nonuniform soil conditions are considered at the foundations the seismic response generally falls within the limits defined by the uniform site conditions defined by ground types A and D. Finally, when the site response effect is combined with the incoherence and wave passage effects of the SVGM the seismic response of the pylons is generally larger than the one when only the site response effect is considered alone.

2. The effect of the SVGM varies depending on the response quantity of interest and the region of the pylons in which it is examined. The asynchronous motion generally reduces the longitudinal (parallel to the deck axis) seismic response of the pylon with the exception of the anchorage system in the pylon where increments of the longitudinal force from the SVGM are observed. These result from the restraint provided by the cables to the longitudinal out-of-phase oscillation of the pylons. On the other hand, the transverse asynchronous oscillation of the pylons above the deck level is relatively unconstrained by the cables and the deck. It is the

asynchronous reaction of the deck to the pylons that can increase considerably the seismic response of the latter below the deck in the transverse direction.

3. The angle of incidence of the ground motion with respect to the axis of the bridge, θ, is an important factor in the assessment of the seismic response of the pylons. The longitudinal shear forces in the pylon are maximised when the deck is parallel to the strong component of the ground motion, whereas the transverse shear forces are maximised when the deck is perpendicular to this component. The axial response is generally dominated by the transverse response, however, in the vertical members of the pylons that connect two lateral legs the leading action is the longitudinal component of the earthquake. The maximum effect of the SVGM on the seismic response is usually observed in the Fault Normal or Fault Parallel cases but it does not coincide with the orientations of the maximum response. Hence, it can be concluded that the full assessment of the seismic response of a symmetric cable-stayed bridge requires several orientations of the deck with respect to the earthquake propagation and these should include at least the principal orientations ($\theta = 0^\circ$ and 90°), in which one of the two earthquake components are aligned with the deck, or the range of orientations from 0° to 180° for a more complete assessment.

4. The dimensions of the bridge influence the effect of the SVGM on the seismic response. The SVGM typically increases the seismic response in the stiffer regions of the pylons which are, in turn, affected by their overall dimensions and their sections' dimensions. The pylons of the 400- and 600-m span bridges are generally more affected by the SVGM at their bottom parts; from the deck down to the base. The increasing section dimensions of this region of the pylons with increasing height, makes them more vulnerable against the pseudo-static forces introduced by the differential movement of the supports.

5. The pylon-cable system configuration is an important factor in the assessment of the SVGM. Bridges with a central cable plane tend to maximise the effect of the asynchronous excitation at the lower part of the pylon in the transverse direction, wherein the pylon shape also plays an important role. Pylons with lower diamonds are more vulnerable against the multi-support excitation, mainly because of the large stiffness of the common member at their base and due to the rotation capacity of the connection between the vertical pier and the inclined legs of the pylon below the deck, which maximises the transverse displacement of the pylon. These pylons require larger amounts of reinforcement at their base when subjected to multi-support excitations than the case of the SYNC motion of the supports. On the other hand, the individual legs of the H-LCP model and the central cable system of the Y-CCP and YD-CCP models are better candidates to accommodate the out-of-phase motion of the supports above the deck because they constitute more 'flexible' configurations than the other pylon-cable system configurations studied.

6. There is a close link between the effect of the asynchronous motion on the seismic response and the vibration modes of the structure. Higher-order antisymmetric vibration modes are excited by the SVGM and are de-amplified by the SYNC motion.

On the Inelastic Seismic Response

1. The bridge with $L_P = 200$ m is more sensitive to the effect of the SVGM than the 400- and 600-m main span bridges. When the nonlinear behaviour of the concrete and the steel in the pylons is considered the effect of the SVGM alone is more pronounced in the 200-m span bridge and this is reflected in the seismic forces, inelastic deformations and the damage propagation in the pylons. In the intermediate- and long-span bridges the SVGM generally results in similar response quantity values to the SYNC motion. The damage propagation in the pylons also suggests that the most sensitive are the ones of the 200-m main span bridge, because of their increased stiffness compared to the taller pylons of the 400-m and 600-m span bridges, which is more important than the time delay of the earthquake or the loss of coherency. Furthermore, the pylons of the bridge with $L_P = 400$ m generally behave differently than their shorter and taller counterparts. This bridge falls between the stiff configuration of the 200-m span bridge and the flexible configuration of the 600-m span bridge in which the effect of the components of the SVGM (wave passage and incoherence) are more significant because they are both functions of the separation distance between supports. These findings emphasise the need for code-based provisions in which the importance of the SVGM for the design and assessment of bridges is established not only in terms of the total length but also in terms of the vibration properties of the structure.

2. Generally, the most critical regions of the pylons are the connections between the legs and the transverse struts. This results from the lateral flexure of the pylons which is resisted by the struts. The rate of damage that is induced to the different components of the bridge depends on the height of the pylon; the lateral legs and the lower struts are more damaged in the short-span bridge, whereas the intermediate struts tend to receive more damage with increasing heights because of the more pronounced transverse oscillation of the part of the pylons above the deck as the height increases. This is due to the increasing flexibility in the pylons with increasing heights.

3. The effect of the earthquake's incidence angle with respect to the bridge (θ) on the seismic response is closely linked to the response quantity under consideration. The peak longitudinal shear force, V_x, in the pylons is larger when the strong component of the earthquake is applied parallel to the axis of the bridge and the peak V_y is maximised when the same earthquake component is perpendicular to the bridge

axis, similarly to the results from the elastic analysis. The effect of the SVGM is also modified with the value of θ and it results in increased structural response values when $\theta = 90^\circ$ (i.e. the strong earthquake component is parallel to the axis of the struts), in which case the peak deformation of the steel is increased in the 400-m main span bridge. This is attributed to the more pronounced transverse oscillation of the pylon when $\theta = 90^\circ$ compared to the case when the strong earthquake component is aligned with the deck ($\theta = 0^\circ$). In terms of the induced damage in the pylons, the maximum values of the damage factor Ω are obtained when the strong earthquake component is considered perpendicular to the bridge axis ($\theta = 90^\circ$) regardless of the main span length or of the SVGM being considered.

4. In most cases the effect of the SVGM is the same between the elastic and the inelastic analyses. When the seismic response due to the SVGM is greater than that from the SYNC motion in the elastic range (in which case the response ratio $\rho_{\text{EL}} > 1$), the same observation is made in the inelastic range ($\rho_{\text{NL}} > 1$). The maximum differences between the results from the two types of analysis are obtained in the transverse direction of the response, for which symmetric and antisymmetric vibration modes contribute more to the SVGM.

5. The shape of the pylon influences the sensitivity to the asynchronous motion when material nonlinearities are considered. It is observed that the stiffer configuration of the inverted 'Y'-shaped pylon is more vulnerable to the SVGM, as opposed to the more flexible 'H'-shaped pylon. Moreover, the effect of the SVGM is more detrimental in the transverse direction of the response because the pylons are stiffer in this direction. At the other end, the multi-support excitation reduces the longitudinal seismic response regardless of the main span length or the shape of the pylon.

6. When the bridge is subjected to lower probability earthquakes certain components are expected to receive large amounts of damage and, in the case of the pylons and certain cables, they are expected to reach the ultimate limit state of collapse. The SVGM has a detrimental effect on the seismic behaviour of the bridge by increasing the probability of the failure in the pylons and the cables compared to the SYNC motion. Furthermore, between the two pylons, the second one to receive the ground motion is more affected by the multi-support excitation. This is reflected in the probability of failure that is consistently higher than the one of the first pylon, and in the damage propagation in this pylon even at the level of the design earthquake.

8.2 Future Work

The effect of the SVGM on the seismic response of cable-stayed bridges is a reportedly complex and multi-parametric problem with various interpretations depending on

the manner in which the phenomenon is perceived (i.e. which components of the SVGM are considered), on the analysis tools and on the response quantity of interest, among others. The unpredictable nature of the multi-support excitation has been acknowledged by the research community and hence, suggestions for future work in the direction of simplifying and understanding this complex phenomenon are suggested:

- The vertical earthquake component should be included in the seismic analysis of the bridges by accounting for the spatial and temporal variability of the multi-support excitation. Cable-stayed bridges are good candidates to resist the vertical component of the earthquakes since they are designed to withstand very large dead loads, but the earthquake-induced axial load can accelerate cracking in the concrete and the effect of the multi-support vertical excitation should be included in the assessment of the effect of the SVGM on the response.

- The site response effect of the SVGM can be important for the seismic response of cable-stayed bridges. To this end, more extensive research should be performed in this direction by assuming different combinations of foundation soils among the supports of cable-stayed bridges with various main spans and different pylon-cable system configurations.

- The control of cable-stayed bridges subjected to multiple excitations is an open topic. The design of control strategies should take account of the higher-order (and antisymmetric even in the case of symmetric bridges) modes that are important to the seismic response when the SVGM is considered and that are not excited under the assumption of synchronous motion.

- A more computationally efficient approach to the problem of assessing the effect of the SVGM than the time-consuming dynamic analysis is necessary, especially in the first stages of the design when detailed analyses are not justified. A new pushover methodology that can account for the components of the SVGM would consist a powerful tool.

- The height of the lower part of the pylon (i.e. below the deck level; H_i in this thesis) is an important factor for the seismic response of the structure. In this study it has been considered as half the height of the pylon above the deck because this is a relatively conventional case. It would be interesting to examine the influence of this parameter when the SVGM is considered, by considering different values of H_i.

Appendix A

Stochastic Process

Contents

A.1 Introduction

In order for the SVGM to be fully comprehended along with its basic parameters and components, an introduction needs to be made on the basic definitions of random variables and stochastic processes. There is a number of important books on the field of statistics, random processes and stochastic processes. For the present research, only the fundamental definitions of the aforementioned processes are presented, but the interested reader is referred to Ang and Tang (1975), Vanmarcke (1983), Papoulis (1984), Pham (2006), among others.

A.2 Random Variables

A random variable is defined as a function which assigns real numbers to the results/observations of a phenomenon (Pham 2006). Random variables can be categorised into 'discrete' and 'continuous' variables. A discrete random variable may only be assigned a finite number of distinct values, whereas a continuous random variable is defined over an interval of values.

Assuming X to be a continuous random variable, the Cumulative Distribution Function (CDF) of X is $F_X(x)$ and is defined as:

$$F_X(x) = P\left(X \leq x\right) \text{ for all } x \tag{A.1}$$

in which x denotes the value of the random variable X, and $P\left(\cdot\right)$ is the probability that X will take on values less or equal than x. The Probability Density Function (PDF), $f_X(x)$, of (the continuous) X is defined as the probability that X will take on the value x in a given interval and is calculated as the derivative of the CDF

$$f_X(x) = \frac{\mathrm{d}F_X(x)}{\mathrm{d}x} \tag{A.2}$$

if the derivative $\mathrm{d}F_X(x)/\mathrm{d}x$ exists. The mean value, μ_X, and the variance $\mathrm{var}\left(X\right)$, are defined by the expectation $E\left(X\right)$ and the standard deviation, σ, respectively as following:

$$\mu_X = E\left(X\right) = \int_{-\infty}^{\infty} x f_X(x)\ \mathrm{d}x \tag{A.3}$$

$$\mathrm{var}\left(X\right) = \sigma^2 = \int_{-\infty}^{\infty} (x - \mu_X)^2 f(x)\ \mathrm{d}x \tag{A.4}$$

When two random variables X and Y are considered, the joint CDF and PDF are defined by Eqs. (A.5) and (A.6), respectively:

$$F_{X,Y}(x,y) = P\left(X \leq x, Y \leq y\right) \text{ for all } x, y \tag{A.5}$$

$$f_{X,Y}(x,y) = \frac{\mathrm{d}^2 F_{X,Y}(x,y)}{\mathrm{d}x\mathrm{d}y} \tag{A.6}$$

given that the derivatives $\mathrm{d}F_X(x)/\mathrm{d}x$ and $\mathrm{d}F_Y(y)/\mathrm{d}y$ exist. Finally, the covariance of the two random variables X and Y is estimated as:

$$\begin{aligned} \mathrm{cov}\left(X,Y\right) &= E\left[\left(X-\mu_X\right)\left(Y-\mu_Y\right)\right] \\ &= E\left(XY\right) - \mu_X\mu_Y \end{aligned} \tag{A.7}$$

in which μ_Y is the mean value of Y and $E\left(XY\right)$ is the joint second moment of X and Y:

$$E\left(XY\right) = \int_{-\infty}^{\infty}\int_{-\infty}^{\infty} xy f_{X,Y}(x,y)\ \ \mathrm{d}x\mathrm{d}y \tag{A.8}$$

A.3 Stochastic Process

A stochastic process is merely a statistical process that involves an infinite number of random variables which depend on a variable parameter (usually time). In other words we assume random variables X_1, X_2,..., X_n that depend on time instances t_1, t_2,..., t_n, respectively. The statistical process $x(t)$ is described by the n^{th} order joint CDF, as an extension to the 2^{nd} order joint CDF of X and Y in Eq. (A.5).

$$F_{X_1,....,X_n}(x_1,....,x_n;t_1,....,t_n) = P\left[x(t_1) \leq x_1,....,x(t_n) \leq x_n\right] \tag{A.9}$$

The mean value, $\mu_x(t)$, of such the stochastic process $x(t)$ is defined as:

$$\mu_x(t) = E\left[x(t)\right] = \int_{-\infty}^{\infty} x f_X(x,t)\ \ \mathrm{d}x \tag{A.10}$$

in which $f_X(x,t)$ is the PDF of X as defined in Eq. (A.2) and its autocovariance function can be written as an extension to Eq. (A.7) in the following form:

$$\begin{aligned} R_{xx}(t_1, t_2) &= E\left\{[x(t_1) - \mu_x(t_1)]\,[x(t_2) - \mu_x(t_2)]\right\} \\ &= E\left[x(t_1)x(t_2)\right] - \mu_x(t_1)\mu_x(t_2) \end{aligned} \tag{A.11}$$

in which $E\left[x(t_1)x(t_2)\right]$ can be re-written based on Eq. (A.8) as:

$$E\left[x(t_1), x(t_2)\right] = \int_{-\infty}^{\infty}\int_{-\infty}^{\infty} x_1 x_2 f_{X_1,X_2}(x_1, x_2; t_1 t_2)\ \mathrm{d}x_1 \mathrm{d}x_2 \tag{A.12}$$

Seismic signals can be treated as stochastic processes of time. The acceleration at each time instance is the realisation of a random variable, which in this case is a random phase angle (ϕ) as described in detail in Chapter 4. For the prediction of the characteristics of any random field from recorded data, the assumption of Gaussianity[1] applies. Gaussian processes are described through their PDF with known mean value μ_x and standard deviation σ as follows:

$$f_X(x) = \frac{1}{\sigma\sqrt{2\pi}} \exp\left[-\frac{1}{2}\left(\frac{x - \mu_X}{\sigma_X}\right)^2\right] \quad -\infty < x < \infty \tag{A.13}$$

A.4 Power Spectral Density

The Power Spectral Density (PSD), $S_{xx}(\omega)$, of the stochastic process $x(t)$ is the Fourier Transform of its autocovariance function $R_{xx}(\omega)$ (Vanmarcke 1983).

$$S_{xx}(\omega) = \frac{1}{2\pi}\int_{-\infty}^{\infty} R_{xx}(\tau) \exp\left(-\mathrm{i}\,\omega\tau\right)\ \mathrm{d}\tau \tag{A.14}$$

in which ω is the circular frequency in [rad/s], τ represents the difference in [s] between two time instances: $\tau = t_2 - t_1$ and $\mathrm{i} = \sqrt{-1}$ is the imaginary unit.

Here applies the assumption of stationarity of a random process $x(t)$ which is summarised in that the mean value (μ_x) and autocovariance function (R_{xx}) of $x(t)$ are not functions of specific time instances ($t_1, ..., t_n$), but depend only on the time lag τ. Based on this assumption the autocovariance function in Eq. (A.11) reduces to:

$$R_{xx}(t_1, t_2) = R_{xx}(t_1, t_1 + \tau) = R_{xx}(\tau) \tag{A.15}$$

[1] A Gaussian distribution is usually employed to predict the unknown distribution of multiple random variables (Ryan 2007).

Following from Eqs. (A.15) and (A.7), the cross-covariance function for two seismic records $a(m, t_1)$ and $a(n, t_2)$ at two discrete stations m and n on the ground surface and at two discrete time instances t_1 and t_2 can be written as:

$$R_{mn}(t_1, t_2) = R_{mn}(t_1, t_1 + \tau) = R_{mn}(\tau) \tag{A.16}$$

which can be transformed (based on Eq. (A.14)) to the PSD between the same seismic records:

$$S_{mm}(\omega) = \frac{1}{2\pi} \int_{-\infty}^{\infty} R_{mn}(\tau) \exp\left(-\mathrm{i}\,\omega\tau\right) \quad d\tau \tag{A.17}$$

in which ω is the circular frequency in [rad/s] and τ represents the difference in [s] between two time instances: $\tau = t_2 - t_1$.

Bibliography

AASHTO (1996). *Standard specifications for highway bridges*. Cited on pages 38, 43, 46, and 110.

AASHTO (2011). *Guide Specifications for LRFD Seismic Bridge Design - 2nd Edition*. Cited on page 70.

Abaqus (2018). *ABAQUS 2018. Finite elements analysis program; Providence, RI, Dassault Systèmes Simulia*. Cited on pages 63, 69, and 106.

Abdel-Ghaffar, A. (1991). Cable - stayed bridges under seismic action. In *Cable - stayed Bridges; Recent Developments and their Future*, pages 171–192, Yokohama (Japan). Elsevier Science Ltd. Cited on pages 2, 13, 14, and 15.

Abdel-Ghaffar, A. and Khalifa, M. (1991). Importance of cable vibration in dynamics of cable-stayed bridges. *Journal of Engineering Mechanics*, 117:2571–2589. Cited on pages 2 and 13.

Abdel-Ghaffar, A. and Nazmy, A. (1991). 3D nonlinear seismic behavior of cable-stayed bridges. *Journal of Structural Engineering*, 117:3456–3476. Cited on pages vii, 7, 12, 13, 14, 15, 26, 27, 29, 30, 72, and 103.

Abdel-Ghaffar, A. and Rubin, L. (1983a). Lateral earthquake response of suspension bridges. *Journal of Structural Engineering*, 109:664–675. Cited on pages 14, 25, 29, 31, and 80.

Abdel-Ghaffar, A. and Rubin, L. (1983b). Vertical seismic behaviour of suspension bridges. *Earthquake Engineering & Structural Dynamics*, 11(1):1–19. Cited on pages 14 and 80.

Abdel Raheem, S. and Hayashikawa, T. (2003). *Tower nonlinear dynamic response of cable-stayed bridges under great earthquake ground motion*. PhD thesis, Hokkaido University, Sapporo. Cited on page 35.

Abdel Raheem, S., Hayashikawa, T., and Dorka, U. (2011). Ground motion spatial variability effects on seismic response control of cable-stayed bridges. *Earthquake Engineering and Engineering Vibration*, 10:37–49. Cited on page 33.

Abrahamson, N. (1993). Spatial variation of multiple support inputs. In *1st U.S. Seminar on Seismic Evaluation and Retrofit of Steel Bridges*, University of California at Berkeley (San Fransisco). Cited on page 85.

Abrahamson, N., Bolt, B., Darragh, R., Penzien, J., and Tsai, Y. (1987). The SMART-1 accelerograph array (1980-1987): A review. *Earthquake Spectra*, 3:263–287. Cited on page 16.

Abrahamson, N., Schneider, J., and Stepp, J. (1991a). Empirical spatial coherency functions for applications to soil-structure interaction analyses. *Earthquake Spectra*, 7:1–27. Cited on pages 15, 22, and 80.

Abrahamson, N., Schneider, J., and Stepp, J. (1991b). Spatial coherency of shear waves from the Lotung Taiwan Large-Scale Seismic Test. *Structural Safety*, 10:145–162. Cited on pages vii, 15, 17, 20, 22, 80, 91, and 92.

Adanur, S., Altunısık, A., Soyluk, K., and Dumanoglu, A. (2017). Stationary and transient responses of suspension bridges to spatially varying ground motions including site response effect. *Advanced Steel Construction*, 13:378–398. Cited on page 28.

Allam, S. and Datta, T. (2000). Analysis of cable-stayed bridges under multi-component random ground motion by response spectrum method. *Engineering Structures*, 22:1367–1377. Cited on page 42.

Allam, S. and Datta, T. (2004). Seismic response of a cable-stayed bridge deck under multi-component non-stationary random ground motion. *Earthquake Engineering & Structural Dynamics*, 33:375–393. Cited on pages vii, 14, 26, 36, 37, 39, and 94.

Amin, M. and Ang, A.-S. (1966). A nonstationary stochastic model for strong-motion earthquakes. Technical report, Structural Research Series No. 306, University of Illinois, Department oF Civil Engineering. Cited on pages viii, 89, and 90.

Ancheta, T., Darragh, R., Stewart, J., Seyhan, E., Silva, W., Chiou, B., Wooddell, K., Graves, R., Kottke, A., Boore, D., Kishida, T., and Donahue, J. (2013). PEER NGA-West 2 database. Technical report, Pacific Earthquake Engineering Research Center. Report PEER 2013/03. Cited on page 80.

Ang, A.-S. and Tang, W. (1975). *Probability concepts in engineering planning and design. Volume I - Basic principles*. John Wiley & Sons Inc., New York. Cited on page 184.

Apaydin, N., Bas, S., and Harmandar, E. (2016). Response of the Fatih Sultan Mehmet Suspension Bridge under spatially varying multi-point earthquake excitations. *Soil Dynamics and Earthquake Engineering*, 86:44–54. Cited on pages 30 and 103.

Astiz, M. (2001). Specific wind problems affecting composite bridges. In *III Meetings on composite bridges*, Madrid (Spain). Cited on page 56.

ATC32 (1996). *Improved Seismic Design Criteria for California Bridges*. Cited on pages 38, 43, 46, and 110.

ATC49/MCEER (2003). *Recommended LRFD guidelines for the seismic design of highway bridges, California*. Cited on pages 43 and 44.

Ates, S., Bayraktar, A., and Dumanoglu, A. (2006). The effect of spatially varying earthquake ground motions on the stochastic response of bridges isolated with friction pendulum systems. *Soil Dynamics and Earthquake Engineering*, 26:31–44. Cited on page 29.

Bi, K., Hao, H., and Ren, W. (2010). Response of a frame structure on a canyon site to spatially varying ground motions. *Structural Engineering and Mechanics*, 36:111–127. Cited on pages 25, 27, 29, and 34.

Bolt, B., Loh, C., Penzien, J., Tsai, Y., and Yeh, Y. (1982). Preliminary report on the SMART-1 strong motion array in Taiwan. Technical report, Earthquake Engineering Research Center Report No. UCB/EERC-82/13, University of California, Berkeley CA. Cited on pages vii, 15, 17, and 80.

Bommer, J. and Ruggeri, C. (2002). The specification of acceleration time-histories in seismic design codes. *European earthquake engineering*, 16:3–17. Cited on page 98.

BS 5896:2012 (2012). *High tensile steel wire and strand for the prestressing of concrete – Specification*. BS 5896:2012. No cited.

Burdette, N., Elnashai, A., Lupoi, A., and Sextos, A. (2006). The effect of asynchronous earthquake motion on complex bridges. Technical report, Mid-America earthquake center, Department of civil engineering, University of Illinois at Urbana-Champaign. Cited on pages 15 and 34.

Bycroft, G. (1982). El Centro differential ground motion array. Technical report, U.S Geological Survey. Cited on page 16.

Cacciola, P. and Deodatis, G. (2011). A method for generating fully non-stationary and spectrum-compatible ground motion vector processes. *Soil dynamics and earthquake engineering*, 31:351–360. Cited on page 85.

Camara, A. (2011). *Seismic behaviour of cable-stayed bridges: Design, analysis and seismic devices*. PhD thesis, Universidad Politécnica de Madrid, Spain. Cited on pages viii, ix, 46, 50, 56, 61, 62, 65, 68, 82, 86, 95, 105, 116, and 130.

Camara, A. (2018). Seismic behaviour of cable-stayed bridges: A review. *Medcrave Online Journal of Civil Engineering*, 4:161–169. Cited on pages 12 and 13.

Camara, A. and Astiz, M. (2011). Typological study of the elastic seismic behaviour of cable-stayed bridges. In *Proceedings of the 8th European Conference on Structural Dynamics (2011)*, Leuven (Belgium). Cited on pages 9, 62, and 78.

Camara, A. and Astiz, M. (2012). Pushover analysis for the seismic response prediction of cable-stayed bridges under multi-directional excitation. *Engineering Structures*, 41:444–455. Cited on pages 14 and 59.

Camara, A. and Astiz, M. (2014). Analysis and control of cable-stayed bridges subject to seismic action. *Structural Engineering International: Journal of the International Association for Bridge and Structural Engineering (IABSE)*, 24:27–36. Cited on pages 14 and 157.

Camara, A., Astiz, M., and Ye, A. (2014). Fundamental mode estimation for modern cable-stayed bridges considering the tower flexibility. *Journal of Bridge Engineering*, 19. Cited on pages 13, 50, 54, 57, 59, and 73.

Camara, A. and Efthymiou, E. (2016). Deck-tower interaction in the transverse seismic response of cable-stayed bridges and optimum configurations. *Engineering Structures*, 124:494–506. Cited on pages 9, 13, 14, 32, 72, 73, 131, 141, and 155.

Camara, A., Ruiz-Teran, A., and Stafford, P. (2013). Structural behaviour and design criteria of under-deck cable-stayed bridges subjected to seismic action. *Earthquake Engineering & Structural Dynamics*, 42:891–912. Cited on page 157.

Chen, M.-T. and Harichandran, R. (2001). Response of an earth dam to spatially varying earthquake ground motion. *Journal of Engineering Mechanics*, 127:932–939. Cited on page 26.

Chen, W. and Duan, L. (2014). *Bridge engineering handbook. Second edition: Seismic design*. CRC Press. Cited on pages 13 and 41.

Choi, E., DesRoches, R., and Nielson, B. (2004). Seismic fragility of typical bridges in moderate seismic zones. *Engineering Structures*, 26:187–199. Cited on page 164.

Chopra, A. (2017). *Dynamics of structures, theory and applications to earthquake engineering. Fifth edition*. Prentice Hall, University of California, Berkeley. Cited on page 86.

Clough, R. and Penzien, J. (2015). *Dynamics of structures. Second edition*. McGraw-Hill, New York. Cited on pages vii, xiii, xxvi, xxvii, xxxii, 18, 19, 26, 35, 41, and 102.

Demirci, C., Málaga-Chuquitaype, C., and Macorini, L. (2018). Seismic drift demands in multi-storey cross-laminated timber buildings. *Earthquake Engineering & Structural Dynamics*, 47:1014–1031. Cited on page 96.

Deodatis, G. (1996). Non-stationary stochastic vector processes: seismic ground motion applications. *Probabilistic Engineering Mechanics*, 11:149–168. Cited on pages 82, 85, 86, 87, 93, and 99.

Deodatis, G., Saxena, V., and Shinozuka, M. (2000). Effect of spatial variability of ground motion on bridge fragility curves. In *Proceedings of the 8th ASCE Specialty Conference on Probabilistic Mechanics and Structural Reliability*, University of Notre Dame. Cited on page 31.

Der Kiureghian, A. (1996). A coherency model for spatially varying ground motions. *Earthquake Engineering & Structural Dynamics*, 25:99–111. Cited on pages 14, 15, 20, 22, 23, 24, 28, 29, 44, and 89.

Der Kiureghian, A. and Neuenhofer, A. (1992). Response spectrum method for multi support seismic excitations. *Earthquake Engineering & Structural Dynamics*, 21:713–740. Cited on pages vii, xiii, 14, 15, 19, 39, 42, 44, and 89.

Dyke, S., Caceido, J., Turan, G., Bergman, L., and Hague, S. (2003). Phase I benchmark control problem for seismic response of cable-stayed bridges. *Journal of Structural Engineering*, 129:857–872. Cited on pages 14 and 33.

Efthymiou, E. and Camara, A. (2015). Spatial variability effects of the seismic action in cable-stayed bridges and modelling techniques. In *IABSE Conference – Structural Engineering: Providing Solutions to Global Challenges*, Geneva (Switzerland). Cited on pages 50 and 66.

Eurocode 2; Part 1.1 (2004). *Eurocode 2: Design of concrete structures. Part 1.1: General rules and rules for buildings*. EN 1992-1-1:2004. Cited on pages viii, 69, 71, and 125.

Eurocode 3; Part 1.1 (2005). *Eurocode 3: Design of steel structures. Part 1.1: General rules and rules for buildings*. EN 1993-1-1:2005. Cited on page 69.

Eurocode 3; Part 1.11 (2006). *Eurocode 3: Design of steel structures. Part 1.11: Design of structures with tension components*. EN 1993-1-11:2006. Cited on pages 69 and 72.

Eurocode 8; Part 1 (2004). *Eurocode 8: Design of structures for earthquake resistance. Part 1: General rules, seismic actions and rules for buildings*. EN 1998-1:2004. Cited on pages viii, ix, 4, 38, 45, 62, 78, 79, 80, 82, 86, 89, 90, 99, 113, 114, 115, 123, 134, 138, and 177.

Eurocode 8; Part 2 (2005). *Eurocode 8: Design of structures for earthquake resistance. Part 2: Bridges*. EN 1998-2:2005. Cited on pages vii, xiii, 2, 14, 38, 44, 45, 46, 69, 86, and 110.

Falamarz-Sheikhabadi, M. and Zerva, A. (2017). Simplified displacement loading patterns for incorporation of spatially variable ground motions in bridge seismic design codes. *Journal of Bridge Engineering*, 22. Cited on page 47.

Fleming, J. (1979). Nonlinear static analysis of cable-stayed bridge structures. *Computers & Structures*, 10:621–635. Cited on page 12.

Gazetas, G. (1991). Formulas and charts for impedances of surface and embedded foundations. *Journal of Geotechnical Engineering*, 117(9):1363–1381. Cited on pages 62, 95, 96, 97, 98, 100, and 176.

Gazetas, G. and Mylonakis, G. (1998). Seismic soil-structure interaction: new evidence and emerging issues. *Geotechnical Special Publication*, 2(75):1119–1174. Cited on page 35.

Gimsing, N. and Georgakis, C. (2012). *Cable-supported bridges concept and design. Third edition*. John Wiley & Sons, Ltd. Cited on pages 2, 6, 7, 9, 11, 14, 68, and 78.

Hao, H. (1997). Pipeline response to random ground motion. *Stability of simple beam subjected to multiple seismic excitations*, 123:739–742. Cited on page 25.

Hao, H., Oliveira, C., and Penzien, J. (1989). Multiple-station ground motion processing and simulation based om SMART-1 array data. *Nuclear Engineering and Design*, 111:293–310. Cited on pages 2, 14, 26, and 85.

Harichandran, R. and Vanmarcke, E. (1986). Stochastic variation of earthquake ground motion in space and time. *Journal of Engineering Mechanics*, 112:154–174. Cited on pages vii, xxviii, xxx, xxxi, 20, 21, 25, 83, 87, 91, 92, 93, 99, 132, 138, and 176.

Harichandran, R. and Wang, W. (1990). Effect of spatially varying seismic excitation of surface lifelines. In *Proccedings of the 4th U.S. National Conference on Earthquake Engineering*, Palm Springs, CA. Cited on pages vii, 21, 25, and 87.

HAZUS (1997). *HAZUS. Earthquake loss estimation methodology. Technical Manual*. HAZUS. Cited on pages xiii, 152, 163, and 164.

Hilber, H., Hughes, T., and Taylor, R. (1977). Improved numerical dissipation for time integration algorithms in structural dymanics. *Earthquake Engineering and Sructural Dynamics*, 5:283–292. Cited on pages 42, 104, 105, and 106.

Hindy, A. and Novak, M. (1980). Pipeline response to random ground motion. *Journal of the Engineering Mechanics Division*, 106:339–360. Cited on page 25.

Jennings, P., Housner, G., and Tsai, N. (1968). Simulated earthquake motions. Technical report, Technical Report, Earthquake Engineering Research Laboratory, California Institute of Technology. Cited on page 89.

JRA (2002). *Design specifications of highway bridges, Part V. Seismic Design, Tokyo*. Cited on pages 38, 43, 44, 46, and 110.

Kanai, K. (1957). Semi-empirical formula for the seismic characteristics of the ground. *Bulletin of the Earthquake Research Institute*, 35:309–325. Cited on pages vii, xxvi, xxvii, xxxii, 18, 19, and 23.

Kawano, K. and Furukawa, K. (1988). Random seismic response analysis of soil-cable-stayed bridge interaction. In *Proceedings of the 9th of the World Conference on Earthquake Engineering*, page 495 – 500, Tokyo-Kyoto (Japan). Cited on page 35.

Kawashima, K. and Unjoh, S. (1991). Seismic behaviour of cable stayed bridges. In *Cable - stayed Bridges; Recent Developments and their Future*, pages 193–212, Yokohama (Japan). Elsevier Science Ltd. Cited on pages 2, 13, and 105.

Kennedy, R., Cornell, C., Campbell, R., Kaplan, S., and Perla, H. (1980). Probabilistic seismic safety study of an existing nuclear power plant. *Nuclear Engineering and Design*, 59:315–338. Cited on page 31.

Khan, R. (2012). *Earthquake-Resistant Structures – Design, Assessment and Rehabilitation*, chapter Seismic reliability analysis of cable-stayed bridges against first passage failure. INTECH Open Access Publisher. Cited on pages 36 and 94.

Khan, R., Ahmad, S., and Datta, T. (2004a). Effect of soil-structure interaction on seismic risk of fan type cable stayed bridges. *JSEE*, 6:47–56. Cited on page 95.

Khan, R. A., Datta, T., and Ahmad, S. (2004b). Seismic risk analysis of cable-stayed bridges with support flexibility. In *Proceedings of the 13th World Conference on Earthquake Engineering*, Vancouver, B.C. (Canada). Cited on page 35.

Kim, S. and Feng, M. (2003). Fragility analysis of bridges under ground motion with spatial variation. *International Journal of Non-Linear Mechanics*, 38:705–721. Cited on page 31.

Krawinkler, H. and Seneviratna, G. (1998). Pros and cons of a pushover analysis of seismic performance evaluation. *Engineering Structures*, 20:452–464. Cited on page 42.

Lee, M. and Penzien, J. (1983). Stochastic analysis of structures and piping systems subjected to stationary support excitations. *Earthquake Engineering & Structural Dynamics*, 11:91–110. Cited on page 25.

Leonhardt, F. and Zellner, W. (1980). Cable-stayed bridges. In *IABSE surveys*. S-13/80. Cited on pages vii, 6, 7, 8, and 11.

Li, C., Li, H., Hao, H., Bi, K., and Chen, B. (2018). Seismic fragility analyses of sea-crossing cable-stayed bridges subjected to multi-support ground motions on offshore sites. *Engineering Structures*, 165:441–456. Cited on pages 163 and 164.

Lopez, O., Hernandez, J., Bonilla, R., and Fernandez, A. (2006). Response spectra for multicomponent structural analysis. *Earthquake Spectra*, 22:85–113. Cited on page 90.

Lou, L. and Zerva, A. (2004). Effects of spatially variable ground motions on the seismic response of a skewed, multi-span, RC highway bridge. *Soil Dynamics and Earthquake Engineering*, 25:729–740. Cited on page 34.

Luco, J. and Wong, H. (1986). Response of a rigid foundation to a spatially random ground motion. *Earthquake Engineering & Structural Dynamics*, 14:891–908. Cited on pages vii, xxv, 21, 25, 26, 44, and 87.

Lupoi, A., Franchin, P., Pinto, P., and Monti, G. (2005). Seismic design of bridges accounting for spatial variability of ground motion. *Earthquake Engineering & Structural Dynamics*, 34:327–348. Cited on page 31.

Mackie, K., Cronin, K., and Nielson, B. (2011). Response sensitivity of highway bridges to randomly oriented multi-component earthquake excitation. *Journal of Earthquake Engineering*, 15:850–876. Cited on pages ix, 37, 93, and 94.

Málaga-Chuquitaype, C. and Elghazouli, A. (2012). Inelastic displacement demands in steel structures and their relationship with earthquake frequency content parameters. *Earthquake Engineering & Structural Dynamics*, 41:831–852. Cited on page 96.

Mander, J. B., Priestley, M. J. N., and Park, R. (1988). Theoretical stress-strain model for confined concrete. *Journal of Structural Engineering*, 114(8):1804–1826. Cited on pages viii, 69, and 70.

Mezouer, N., Silhadi, K., and Afra, H. (2010). Importance of spatial variability of seismic ground motion effects on long beams response. *Journal of Civil Engineering and Construction Technology*, 1:1–13. Cited on pages 27 and 28.

Moschonas, I. and Kappos, A. J. (2012). Assessment of concrete bridges subjected to ground motion with an arbitrary angle of incidence: Static and dynamic approach. *Bulletin of Earthquake Engineering*, 11:581–605. Cited on page 37.

Nazmy, A. and Abdel-Ghaffar, A. (1992). Effects of ground motion spatial variability on the response of cable-stayed bridges. *Earthquake Engineering & Structural Dynamics*, 21:1–20. Cited on pages 14, 29, 30, 47, 146, and 177.

NCSP-07 (2007). *Norma de Construcción Sismorresistente: Puentes (in spanish)*. Cited on page 70.

Newmark, N. (1959). A method of computation for structural dynamics. *Journal of the Endineering Mechanics Division. Proceedings of the American Society of Civil Engineering*, pages 67–94. Cited on pages 42, 104, and 105.

Novak, M., Lazarević, D., and Atalić, J. (2015). Influence of spatial variability of ground motion on seismic response of bridges. *GRAĐEVINAR, Journal of the Croatian Association of Civil Engineers*, 67(10):943–957. Cited on page 43.

Nuti, C. and Vanzi, I. (2005). Influence of earthquake spatial variability on differential soil displacements and SDF system response. *Earthquake Engineering & Structural Dynamics*, 34(11):1353–1374. Cited on page 46.

Orozco, G. and Ashford, S. (2002). Effects of large velocity pulses on reinforced concrete bridge columns. Technical report, Pacific Earthquake Engineering Research Center (PEER). Cited on page 66.

Padgett, J. E. and DesRoches, R. (2008). Methodology for the development of analytical fragility curves for retrofitted bridges. *Earthquake Engineering & Structural Dynamics*, 37:1157–1174. Cited on page 163.

Papadopoulos, S., Lekidis, V., Sextos, A., and Karakostas, C. (2013). Assessment of EC8 procedures for the asynchronous excitation of bridges based on numerical analyses and recorded data. In *CompDyn 2013, 4th ECCOMAS*, Kos Island (Greece). Cited on page 46.

Papadopoulos, S. and Sextos, A. (2018). Anti-symmetric mode excitation and seismic response of base-isolated bridges under asynchronous input motion. *Soil Dynamics and Earthquake Engineering*. Cited on pages 32, 34, and 46.

Papadopoulos, S., Sextos, A., Kwon, O., Gerasimidis, S., and Deodatis, G. (2017). Impact of spatial variability of earthquake ground motion on seismic demand to natural gas transmission pipelines. In *Proccedings of the 16th World Conference on Earthquake, 16WCEE 2017*, Santiago, Chile. Cited on page 25.

Papoulis, A. (1984). *Probability, random variables and stochastic processes*. McGraw-Hill, New York. Cited on page 184.

Parke, G. and Hewson, N. (2008). *ICE Manual of bridge engineering: Second edition*. ICE Publishing, Thomas Telford Ltd. Cited on pages vii, 6, 9, 10, 11, and 51.

Paulay, T. and Priestley, M. (1992). *Seismic Design of Reinforced Concrete and Masonry Buildings*. John Wiley & Sons Inc. Cited on page 65.

Pender, M. (1993). Aseismic pile foundation design analysis. *Bulletin of the New Zealand National Society on Earthquake Engineering*, 26(1):49–161. Cited on page 35.

Pham, H. (2006). *Handbook of engineering statistics*. Springer. Cited on page 184.

Pipinato, A. (2016). *Chapter 25 - Case study: the Russky Bridge*. Butterworth-Heinemann, Boston. Cited on page 7.

Priestley, M., Seible, F., and Calvi, G. (1996). *Seismic design and retrofit of bridges*. John Wiley & Sons Ltd. Cited on pages vii, 26, 27, 29, 39, 40, 42, and 44.

Priestley, M. B. (1965). Evolutionary spectra and non-stationary processes. *J. Royal Statistical Society*, 27(2):204–237. Cited on page 83.

Quan, W., Li, H., and Liu, X. (2008). Seismic response of large-span cable-stayed bridge under multi-component multi-support earthquake excitation. In *Proceedings of the 14th World Conference on Earthquake Engineering*, Beijing, China. Cited on page 30.

Ramanathan, K. N. (2012). *Next generation seismic fragility curves for California bridges incorporating the evolution in seismic design philosophy*. PhD thesis, Georgia Institute of Technology, Atlanta. Cited on page 163.

Rathje, E., Abrahamson, N., and Bray, J. (1998). Simplified frequency content estimates of earthquake ground motions. *Journal of Geotechnical and Geoenvironmental Engineering*, 124:150–159. Cited on page 96.

Ryan, T. (2007). *Modern engineering statistics*. John Wiley & Sons Inc., New York, NY. Cited on page 186.

Sakai, J. and Unjoh, S. (2006). Shake table experiment on circular reinforced concrete bridge column under multidirectional seismic excitation. *Earthquake Engineering and Engineering Vibration*, 5(1):103–110. Cited on page 66.

Saxena, V. (2000). *Spatial variation of earthquake ground motion and development of bridge fragility curves*. PhD thesis, Department of Civil & Environmental Engineering, Princeton University. Cited on page 31.

Saxena, V., Deodatis, G., Shinozuka, M., and Feng, M. (2000). Development of fragility curves for multi-span reinforced concrete bridges. In *Proceedings of the International Conference on Monte Carlo Simulation*, Principality of Monaco. Balkema Publishers. Cited on page 31.

SeismoSoft (2018). *Seismosoft 2018 – "SeismoSignal - A computer program for signal processing of time-histories" available from http://www.seismosoft.com*. Cited on pages 91 and 96.

Sextos, A. (2001). *Effect of spatial variability of seismic motion, local site conditions and soil-structure interaction dynamic analysis of RC bridges*. PhD thesis, Aristotle University Thessaloniki, Greece. Cited on pages 15, 32, and 72.

Sextos, A. (2013). *Handbook of seismic risk analysis and management of civil infrastructure systems*, chapter Effect of soil–structure interaction and spatial variability of ground motion on seismic risk assessment of bridges. Woodhead Publishing in Materials. Elsevier Science & Technology, Woodhead Publishing Ltd. Cited on page 43.

Sextos, A. and Kappos, A. (2008). Asynchronous seismic excitation practice (*in greek*). In *3rd Panhellenic Conference on Earthquake Engineering and Engineering Seismology*, Athens (Greece). Cited on pages 30, 32, and 146.

Sextos, A. and Kappos, A. (2009). Evaluation of seismic response of bridges under asynchronous excitation and comparisons with Eurocode 8-2 provisions. *Bulletin of Earthquake Engineering*, 7:519–545. Cited on pages 25, 43, and 46.

Sextos, A., Kappos, A., and Mergos, P. (2004). Effect of soil-structure interaction and spatial variability of ground motions on irregular bridges: The case of the Krystallopigi Bridge. In *13th World Conference on Earthquake Engineering*, Vancouver (B.C. Canada). Cited on pages 15, 25, 34, 35, and 36.

Sextos, A., Karakostas, C., Lekidis, V., and Papadopoulos, S. (2014). Multiple support seismic excitation of the Evripos Bridge based on free-field and on-structure recordings. *Structure and Infrastructure Engineering*, 11:1510–1523. Cited on pages 26, 32, and 80.

Sextos, A., Katsanos, E., and Manolis, G. (2011). EC8-based earthquake record selection procedure evaluation: Validation study based on observed damage of an irregular R/C building. *Soil Dynamics and Earthquake Engineering*, 31:583–597. Cited on page 86.

Sextos, A., Pitilakis, K., and Kappos, A. (2003). Inelastic dynamic analysis of RC bridges accounting for spatial variability of ground motion, site effects and soil–structure interaction phenomena. Part 1: Methodology and analytical tools. *Earthquake Engineering & Structural Dynamics*, 32(4):607–627. Cited on pages 88 and 90.

Shields, M. (2014). Simulation of spatially correlated nonstationary response spectrum–compatible ground motion time histories. *J. Eng. Mech.*, 141. Cited on pages 85 and 86.

Shinozuka, M. (1972). Monte Carlo solution of structural dynamics. *Computers & Structures*, 2:855–874. Cited on page 82.

Shinozuka, M., Saxena, V., and Deodatis, G. (2000). Effect of spatial variation of ground on highway structures. Technical report, MCEER ISN 1520-295X. Cited on pages 15, 25, 28, 31, 38, 47, 88, and 177.

Soyluk, K. and Dumanoglu, A. (2000). Comparison of asynchronous and stochastic dynamic responses of a cable-stayed bridge. *Engineering Structures*, 22:435–445. Cited on pages 14, 15, 26, 27, 29, 30, 80, and 88.

Soyluk, K. and Dumanoglu, A. (2004). Spatial variability effects of ground motions on cable-stayed bridges. *Soil Dynamics and Earthquake Engineering*, 24:241–250. Cited on pages 14, 26, 27, 30, and 89.

Soyluk, K., Dumanoglu, A., and Tuna, M. (2004). Random vibration and deterministic analyses of cable-stayed bridges to asynchronous ground motion. *Structural engineering and mechanics*, 18:231–246. Cited on page 42.

Soyluk, K. and Sicacik, E. (2011). Soil-structure interaction analysis of cable-stayed bridges for multiple-support excitations. In *Proceedings of the 8th International Conference on Structural Dynamics, EURODYN*, page 495 – 500, Leuven (Belgium). Cited on pages 35, 80, and 98.

Spudich, P. and Cranswick, E. (1984). Direct observation of rupture propagation during the 1979 Imperial Valley earthquake using a short baseline accelerometer array. *Bulletin of the Seismological Society of America*, 74:2083–2114. Cited on pages vii, 15, and 17.

Spyrakos, C. (1992). Seismic behaviour of bridge piers including soil-structure interaction. *Computer & Structures*, 43(2):373 – 384. Cited on page 35.

Spyrakos, C. and Loannidis, G. (2003). Seismic behavior of a post-tensioned integral bridge including soil–structure interaction (ssi). *Soil Dynamics and Earthquake Engineering*, 23:53–63. Cited on page 95.

Stefanidou, P. P. and Kappos, A. J. (2017). Methodology for the development of bridge-specific fragility curves. *Earthquake Engineering & Structural Dynamics*, 46:73–93. Cited on page 163.

Stefanidou, S., Sextos, A., Kotsoglou, A., Lesgidis, N., and Kappos, A. (2017). Soil-structure interaction effects in analysis of seismic fragility of bridges using an intensity-based ground motion selection procedure. *Engineering Structures*, 151:366–380. Cited on page 96.

Tajimi, H. (1960). A statistical method for determining the maximum response of a building structure during an earthquake. In *Proceedings of the 2nd World Conference on Earthquake Engineering*, Tokyo and Kyoto (Japan). Cited on pages vii, xxvi, xxvii, xxxii, 18, and 19.

Takahashi, Y. and Iemura, H. (2000). Inelastic seismic performance of rc tall piers with hollow section. In *12th World Conference on Earthquake Engineering*, Auckland (New Zealand). Cited on page 66.

Taskari, O. and Sextos, A. (2015). Multi-angle, multi-damage fragility curves for seismic assessment of bridges. *Earthquake Engineering & Structural Dynamics*, 44:2281–2301. Cited on page 37.

Tzanetos, N., Elnashai, A., Hamdan, F., and Antoniou, S. (2000). Inelastic dynamic response of RC bridges subjected to spatial non-synchronous earthquake motion. *Advances in Structural Engineering*, 3:191–214. Cited on pages 25, 32, and 72.

Valdebenito, G. and Aparicio, Á. (2005). *Comportamiento sísmico de puentes atirantados y disipación de energía adicional; Un estado del conocimiento (in spanish)*. CIMNE. Universitat Politècnica de Catalunya, Barcelona (Spain). Monograph CIMNE IS-54. Cited on page 14.

Valdebenito, G. and Aparicio, Á. (2006). Seismic behaviour of cable-stayed bridges: A state-of-the-art review. In *Proceedings of the 4th International Conference on Earthquake Engineering*, Taipei (Taiwan). Cited on page 13.

Vamvatsikos, D. (2002). *SEISMIC PERFORMANCE, CAPACITY AND RELIABILITY OF STRUCTURES AS SEEN THROUGH INCREMENTAL DYNAMIC ANALYSIS*. PhD thesis, STANFORD UNIVERSITY. No cited.

Vamvatsikos, D. and Cornell, C. (2002). Incremental dynamic analysis. *Earthquake Engineering & Structural Dynamics*, 31:491–514. Cited on pages 160 and 168.

van Rossum, G. (1995). Python tutorial. Technical Report CS-R9526, Centrum voor Wiskunde en Informatica (CWI), Amsterdam. Cited on pages 4, 82, and 99.

Vanmarcke, E. (1983). *Random fields, analysis and synthesis*. MIT Press, Cambridge, MA. Cited on pages 16, 184, and 186.

Walther, R., Houriet, B., Isler, W., and Moïa, P. (1988). *Cable-stayed bridges*. Thomas Telford. Cited on pages vii, 10, 11, 13, 14, and 30.

Wang, J., Carr, A., Cooke, N., and Moss, P. (2003). Wave-passage effect on the seismic response of long bridges. In *2003 Pacific Conference on Earthquake Engineering*. Cited on pages 27 and 28.

Wang, J., Carr, A., Cooke, N., and Moss, P. (2009). The response of a 344 m long bridge to non uniform earthquake ground motions. *Engineering Structures*, 31:2554–2567. Cited on page 27.

Wolf, J. (1994). *Foundation vibration analysis using simple physical models*. Prentice Hall. Cited on page 35.

Xiong, Z., Feng, Y., Song, S., and Wang, J. (2013). Optimization design of large span cable-stayed bridge in high seismic risk zone. *Applied Mechanics and Materials*, 353-356:2015–2019. Cited on page 9.

Yang, C. and Cheung, M. (2011). Shake table test of cable-stayed bridge subjected to non-uniform excitation. *Procedia Engineering*, 14:931–938. Cited on page 30.

Yi, J. H., Kim, S. H., and Kushiyama, S. (2007). PDF interpolation technique for seismic fragility analysis of bridges. *Engineering Structures*, 29:1312–1322. Cited on page 164.

Zerva, A. (1990). Response of multi-span beams to spatially incoherent seismic ground motions. *Earthquake Engineering & Structural Dynamics*, 19:819–832. Cited on pages 25, 72, and 131.

Zerva, A. (1991). Effect of spatial variability and propagation of seismic ground motions on the response of multiply supported structures. *Probabilistic Engineering Mechanics*, 6:212–221. Cited on pages 15, 25, 27, and 28.

Zerva, A. (1992). Seismic loads predicted by spatial variability models. *Structural Safety*, 11:227–243. Cited on page 28.

Zerva, A. (2009). *Spatial variation of seismic ground motions: Modeling and engineering applications*. CRC Press, Boca Raton. Cited on pages 25, 29, 32, 81, 82, 87, 92, and 93.

Zerva, A. and Zervas, V. (2002). Spatial variation of seismic ground motions: An overview. *Applied Machanics Reviews*, 55:227–243. Cited on page 91.

Zheng, J. and Takeda, T. (1995). Effects of soil-structure interaction on seismic response of PC cable-stayed bridge. *Soil Dynamics and Earthquake Engineering*, 14:427–437. Cited on pages 36 and 95.

Zhong, J., Jeon, J.-S., Yuan, W., and DesRoches, R. (2017). Impact of spatial variability parameters on seismic fragilities of a cable-stayed bridge subjected to differential support motions. *Journal of Bridge Engineering*, 22(6). Cited on pages 31 and 166.